Localised Solar Energy Generation and Storage for EV Fleet Charging

María Núñez Muñoz

A thesis submitted in partial fulfilment of the requirements for the degree of

Doctor of Philosophy

The University of Sheffield

Faculty of Social Sciences

Management School

18th of August 2023

Abstract

The thesis explores the feasibility of using solar energy and battery energy storage systems (BESS) for electric vehicle (EV) fleet charging at commercial depots. It analyses the techno-economic impact of using such a system. Additionally, it evaluates the environmental impact of the emissions released from electricity production to charge the fleets, also known as Well-to-Tank (WTT) emissions.

The thesis adopts a modelling-based approach to developing a solar model and an energy management algorithm (EMA). These models have been used to investigate the environmental and techno-economic impact of charging an electric refuse collection vehicle (eRCV) fleet based at a waste management depot.

Results show a maximum cost reduction achieved with a BESS of 0.5MWh when the eRCV fleet is split and charged at 11:00h and 23:00h, and the power capacity connection on site is not constrained. It provides approximately £1M in savings over the system lifetime of 15 years. The maximum cost reduction for overnight charging is £530,000 with a BESS of 1MWh. Greenhouse gas (GHG) emissions are reduced by 41 tons CO_2 eq. per year with a BESS of 0.05 MWh. When the power capacity connection is constrained, and the fleet is charged overnight, a BESS of 10 MWh reduces the excess capacity charge incurred by the site from approximately £0.8M to zero. However, it is still not economically feasible due to the high cost of installing a BESS.

These findings contribute to establishing a body of literature that explores the use of solar energy and energy storage systems to reduce electricity costs and GHG emissions for electrifying road freight vehicle fleets. It explored the trade-offs between different PV energy systems, the building's energy demand, different fleet charging strategies and the installation of BESS.

The thesis also provides insights for transport fleet operators regarding EV charging management for maximising local solar energy generation and charging at a commercial depot. It supports operator and business decision making process regarding the installation of PV panels and BESS to charge an EV fleet, considering the system costs and benefits.

Publication list

Journal Articles

- **Nunez Munoz, M.**, Ballantyne, E.E.F. and Stone, D.A. (2022) 'Development and evaluation of empirical models for the estimation of hourly horizontal diffuse solar irradiance in the United Kingdom', *Energy*, 241. https://doi.org/10.1016/j.energy.2021.122820
- **Nunez Munoz, M.**, Ballantyne, E.E.F. and Stone, D.A. (2023) 'Assessing the Economic Impact of Introducing Localised PV Solar Energy Generation and Energy Storage for Fleet Electrification', *Energies*, 16(8), p. 3570. https://doi.org/10.3390/en16083570.

Conference Proceedings

- **Nunez Munoz, M.**, Ballantyne, E.E.F. and Stone, D.A. (2023) 'Using locally generated renewable energy to charge depot based electric freight fleets', in *World Conference on Transport Research (WCTR), Montreal, Canada, 17-21 July 2023*
- Naderi, M., Palmer, D., **Nunez Munoz, M.**, Al-Wreikat,Y., Smith, M., Fraser, E., Gladwin, D.T., Foster, M.P., Ballantyne, E.E.F. and Stone, D.A. (2023) 'Modelling and sizing sensitivity analysis of a fully renewable energy-based electric vehicle charging station microgrid', in *EVI: Charging Ahead Conference, Glasgow, UK, 14-17 November 2023.*
- **Nunez Munoz, M.**, Ballantyne, E.E.F. and Stone, D.A. (2022) 'Impact on annual electricity cost of introducing battery energy storage at a warehouse.', *Logistics Research Network (LRN) Conference, Aston University, UK, 7-9 September 2022*
- **Nunez Munoz, M.**, Ballantyne, E.E.F. and Stone, D.A. (2021) 'On-site PV generation to support local fleet vehicle charging.', *Logistics Research Network (LRN) Conference, University of Cardiff (Cardiff Business School), UK, 8-10 September 2021*

Conference Presentations

- **Nunez Munoz, M.**, Ballantyne, E.E.F. and Stone, D.A. (2023) 'Exploring the benefits of using locally generated solar energy, supported by a BESS, in reducing Well-to-Tank emissions associated with electric road freight fleets.', *10th International Workshop on Sustainable Road Freight Transport, The Centre For Sustainable Road Freight (SFR), Cambridge, UK, 4-5 December 2023*
- **Nunez Munoz, M.**, Ballantyne, E.E.F. and Stone, D.A. (2020) 'Exploring the feasibility of localised solar energy generation and storage for EV fleet mass charging at a commercial depot.', *Logistics Research Network (LRN) Conference, University of Cardiff (Cardiff Business School), UK, 9-11 September 2020*

Acknowledgments

"We will follow that trail! What trail? The trail that we blaze!" – My "Road to El Dorado" started four years ago and now it has come to an end.

I have been fortunate to have Dr. Erica Ballantyne and Prof. David Stone as my supervisors. And I would like to express my sincere gratitude for their support, invaluable guidance, and endless encouragement throughout my PhD journey. Their expertise, patience, and commitment have influenced both my research and personal growth during this time. I am immensely thankful for their insightful feedback, constructive criticism, and dedicated hours reviewing my work.

I would also like to express my sincere gratitude to M&S and Ashfield County Council for generously providing the invaluable data that formed the foundation of this research project.

To all my colleagues from the Doctoral Centre "DC", thank you for all the fun over the PhD journey and for letting me be part of the "PhDC" family. Also thanks to my friends. This journey has had many ups and downs, but we have celebrated success and navigated through the difficult moments of the PhD journey together. I will always be grateful for our friendship.

I want to make a special acknowledgement to my family. Dad and Mum, thank you for being so close while being so far. Thank you to my little niece and nephew, Maria, and Alvaro. Your sincere and pure love, who expects nothing in return but always guides me back home, is my greatest treasure.

Last but certainly not least, thank you to my partner, Marta for being with me throughout this intense part of my life. I have struggled with maintaining a work-life balance over the last months, so thank you for always being supportive, understanding and patient. I couldn't have done it without you!

Declaration

I, the author, confirm that the Thesis is my own work. I am aware of the University's Guidance on the Use of Unfair Means. This work has not been previously presented for an award at this, or any other, University.

María Núñez Muñoz

Table of Contents

ABSTRACT ..... **I**

PUBLICATION LIST ..... **II**

ACKNOWLEDGMENTS ..... **III**

DECLARATION ..... **IV**

ABBREVIATION LIST ..... **VII**

LIST OF FIGURES ..... **VIII**

1 INTRODUCTION **1**

1.1 ROAD FREIGHT TRANSPORT ELECTRIFICATION 4

1.2 RESEARCH AIMS & OBJECTIVES 7

1.3 RESEARCH METHODOLOGY 9

1.4 THESIS STRUCTURE 12

2 LITERATURE REVIEW **15**

2.1 GHG EMISSIONS FROM TRANSPORT 15

2.2 ELECTRIC FREIGHT FLEET CHARGING 24

2.3 ENERGY AND TRANSPORT SYSTEMS INTEGRATION TO FACILITATE THE ADOPTION OF EV FLEETS 32

2.4 SOLAR ENERGY AND ENERGY STORAGE FOR EV FLEET CHARGING 37

2.5 RESEARCH GAP 43

3 SOLAR IRRADIATION MODELLING FOR PHOTOVOLTAIC SOLAR ENERGY GENERATION IN THE UK **45**

3.1 INTRODUCTION 45

3.2 HORIZONTAL SOLAR IRRADIATION MODELLING 46

3.3 SOLAR MODELLING ON INCLINED SURFACES 75

3.4 FROM SOLAR IRRADIATION TO ENERGY GENERATION 82

3.5 SOLAR MODEL VALIDATION 82

3.6 CASE STUDY: LOCALLY GENERATED PV SOLAR ENERGY 89

3.7 SUMMARY 106

4 DEVELOPMENT OF AN ENERGY MANAGEMENT MODEL FOR THE EVALUATION OF BESS **107**

4.1 INTRODUCTION 107

4.2 LITERATURE REVIEW ON ENERGY MANAGEMENT SYSTEMS 108

4.3 METHODOLOGY 115

4.4 RESULTS: EVALUATION OF GRID RELIANCE, TOTAL COST AND GHG EMISSIONS USING BESS 137

4.5 DISCUSSION 170

4.6 SUMMARY 172

5 ELECTRIC FLEET ADOPTION 174

5.1 INTRODUCTION 174

5.2 METHODOLOGY 175

5.3 RESULTS 183

5.4 DISCUSSION 197

5.5 SUMMARY 199

6 TECHNICAL ASSESSMENT OF EV FLEET MASS CHARGING CONSIDERING POWER CAPACITY CONSTRAINTS 200

6.1 INTRODUCTION 200

6.2 METHODOLOGY 201

6.3 RESULTS 208

6.4 SUMMARY 221

7 CONCLUSIONS AND FUTURE WORK 223

7.1 OVERVIEW OF FINDINGS AND DISCUSSIONS 223

7.2 KEY FINDINGS AND WIDER APPLICABILITY 226

7.3 FUTURE WORK 227

8 REFERENCES 231

9 APPENDIX A 266

10 APPENDIX B 271

Abbreviation list

AC	Alternating current
ANN	Artificial neural network
AR	Autoregressive model
BCS	Base case scenario
BESS	Battery energy storage system
BEV	Battery electric vehicle
CAZ	Clean air zone
CCS	Carbon capture and storage
CEDA	Centre for environmental data analysis
CNG	Compressed natural gas
DC	Direct current
eHGV	Electric Heavy goods vehicle
eLCV	Electric Light commercial vehicle
eRCV	Electric refuse collection vehicle
EV	Electric vehicle
GDP	Gross domestic product
GHG	Greenhouse gas
HEV	Hybrid electric vehicle
HGV	Heavy goods vehicle
HVDC	High-voltage direct current
ICE	Internal combustion engine
LCV	Light commercial vehicle
LEZ	Low emission zone
LGV	Light good vehicle
LNG	Liquid natural gas
MIDAS	Met Office Integrated Data Archive System
NDCs	Nationally Determined Contributions
NOx	Nitrogen oxides
PHEV	Plug-in hybrid electric vehicle
PV	Photovoltaic
SoC	State of Charge
TCO	Total cost of ownership
TTW	Tank-to-Wheel
V2G	Vehicle-to-grid
WMD	Waste management depot
WTT	Well-to-Tank
WTW	Well-to-Wheel

List of Figures

FIGURE 1.1. WELL TO WHEEL (WTW) EMISSIONS BY FUEL TYPE FOR ROAD FREIGHT VEHICLES (OWN CREATION WITH DATA FROM KOLLAMTHODI *ET AL.* [23]).....3

FIGURE 1.2. TOTAL GHG EMISSIONS PER KWH BASED ON EACH ENERGY CARRIER INTRODUCED. (GRAPH ADAPTED FROM GUSTAFSSON *ET AL.* [35]).....6

FIGURE 1.3. OVERVIEW OF A DEPOT WITH ROOFTOP PV PANELS AND A BESS FOR EV FLEET CHARGING (MODIFIED PICTURE FROM [42]).....10

FIGURE 1.4. RESEARCH METHODOLOGY FLOWCHART.....11

FIGURE 2.1. GLOBAL CO_2 EMISSIONS BY SECTOR FROM 1970 TO 2021 (OWN CREATION WITH DATA FROM CRIPPA *ET AL.* [46]) ...16

FIGURE 2.2. GLOBAL TRANSPORT EMISSIONS IN MILLION METRIC TONS OF CO_2 AND PERCENTAGE CORRESPONDING TO 2021 (OWN CREATION WITH DATA FROM STATISTA [48]).....17

FIGURE 2.3. UK'S GHG EMISSIONS BY SECTOR FOR THE PAST 50 YEARS (OWN CREATION WITH DATA FROM CRIPPA *ET AL.* [46]. THE BLUE ARROW REPRESENTS THE TREND ACROSS THE YEARS.).....18

FIGURE 2.4. UK'S DOMESTIC GHG EMISSIONS BY TRANSPORT MODE IN 2020 (OWN CREATION WITH DATA FROM THE UK DEPARTMENT FOR TRANSPORT [7]). BORDERED SECTIONS HIGHLIGHT ROAD TRANSPORT MODES.....19

FIGURE 2.5. ROAD FREIGHT TRANSPORT EMISSIONS (DASHED LINES) COMPARED TO THE ANNUAL DISTANCE TRAVELLED (BLOCK CHARTS) FROM 1990 TO 2020 (OWN CREATION WITH DATA FROM THE UK DEPARTMENT FOR TRANSPORT [7,60]) 20

FIGURE 2.6. TOP GRAPH: GHG EMISSIONS RELEASED BY AN EV FLEET WHEN CHARGED FROM THE GRID (GREY BARS) AND FROM SOLAR ENERGY (YELLOW BARS). BOTTOM GRAPH: BREAKDOWN OF GRID ELECTRICITY SUPPLIED BY THE UK GRID NETWORK IN 2010, 2020 AND 2050 BY ENERGY SOURCE.....23

FIGURE 3.1 PROCESS FLOW APPLIED FOR THE CALCULATION OF LOCALISED PV SOLAR ENERGY (FIGURE OBTAINED FROM [175]). 46

FIGURE 3.2 "LOCATION OF MET OFFICE WEATHER STATIONS USED FOR THE STUDY" (FIGURE OBTAINED FROM [174]) 56

FIGURE 3.3 "COMPLETE PROCESS FLOW USED FOR THE EVALUATION OF THE EXISTING EMPIRICAL MODELS USING MEASURED DATA FROM SOUTH YORKSHIRE, NORFOLK, AND WEST SUSSEX" (FIGURE OBTAINED FROM [174]).....57

FIGURE 3.4."BOUNDARIES FOR CLEARNESS INDEX (kt) AND DIFFUSE FRACTION (kd) DEVELOPED BY MUNEER AND FAIROOZ [226], THAT HAVE BEEN APPLIED IN TEST 4 AS DESCRIBED IN TABLE 3.3" (FIGURE OBTAINED FROM [174]).....61

FIGURE 3.5 "THE COMPLETE PROCESS FLOW FOR THE DEVELOPMENT OF A NEW CORRELATION" (FIGURE OBTAINED FROM [174])...67

FIGURE 3.6. "HOURLY VALUES OF CLEARNESS INDEX (kt) AND DIFFUSE FRACTION (kd) (A) BEFORE AND (B) AFTER THE QUALITY PROCESS" (FIGURE OBTAINED FROM [174]).....67

FIGURE 3.7. "APPROACH TO SET INTERVALS FOR kt <0.2" (FIGURE OBTAINED FROM [174]) 68

FIGURE 3.8 "ERROR HISTOGRAM FOR THE SOUTH-YORKSHIRE CORRELATION" (FIGURE OBTAINED FROM [174]).....71

FIGURE 3.9. "ERROR HISTOGRAM FOR THE NORFOLK CORRELATION" (FIGURE OBTAINED FROM [174]). 71

FIGURE 3.10. "ERROR HISTOGRAM FOR THE WEST-SUSSEX CORRELATION" (FIGURE OBTAINED FROM [174]).....71

FIGURE 3.11. HOURLY RESULTS ON HORIZONTAL GLOBAL (GH), DIFFUSE (GD), AND DIRECT (GB) SOLAR IRRADIATION ON A WEEK IN (A) JANUARY AND (B) JULY.....74

FIGURE 3.12. HOURLY VALUES ON INCLINED TOTAL (GB), DIFFUSE (GDB), DIRECT (GBB) AND REFLECTED (GR) SOLAR IRRADIATION FOR A DAY IN JULY USING (A) HAY ANISOTROPIC MODEL, (B) WILLMOTT ANISOTROPIC MODEL AND (C) REINDL MODEL. 80

FIGURE 3.13. HOURLY RESULTS OBTAINED WHEN (A) REINDL ANISOTROPIC MODEL AND (B) WILLMOTT ANISOTROPIC MODEL ARE USED TO CALCULATE INCLINED DIFFUSE SOLAR IRRADIATION ON A DAY IN FEBRUARY. 81
FIGURE 3.14. COMPARISON OF HOURLY PV SOLAR ENERGY IN THE MONTH OF APRIL BETWEEN MEASURED DATA FROM SHEFFIELD IN 2018 (RED LINE) AND DATA MODELLED USING AVERAGED VALUES OF GH FROM FINNINGLEY BETWEEN 1982 AND 1995 (BLUE LINE). 83
FIGURE 3.15. COMPARISON OF HOURLY PV SOLAR ENERGY IN THE MONTH OF APRIL BETWEEN MEASURED DATA FROM SHEFFIELD IN 2018 (RED LINE) AND DATA MODELLED USING VALUES OF GH FROM WATNALL IN 2018 (BLUE LINE)..... 84
FIGURE 3.16. COMPARISON BETWEEN MEASURED MONTHLY VALUES IN SHEFFIELD (2012) AND MODELLED VALUES USING GROUND MEASUREMENTS FROM (A) SOUTH-YORKSHIRE FROM 1982 – 1995 AND FROM (B)NORTH-YORKSHIRE IN 2012..... 85
FIGURE 3.17. M&S YORK VANGARDE RETAIL PARK (IMAGE TAKEN FROM GOOGLE MAPS) 86
FIGURE 3.18. PV PANEL ROOFTOP INSTALLATION IN M&S YORK VANGARDE RETAIL PARK (IMAGE TAKEN FROM GOOGLE MAPS). .. 86
FIGURE 3.19. COMPARISON BETWEEN MODELLED DAILY PV ENERGY GENERATION (BLUE LINE) AND MEASURED DAILY PV ENERGY GENERATION (RED LINE) AT YORK VANGARDE RETAIL PARK (A) IN 2019 AND, (B) BETWEEN MARCH 2018 AND MARCH 2019. 87
FIGURE 3.20. MODELLED HOURLY PV ENERGY GENERATION (BLUE LINE) AND MEASURED HOURLY PV ENERGY GENERATION (ORANGE LINE) AT YORK VANGARDE RETAIL PARK IN (A)SEPTEMBER 20018 AND (B) DECEMBER 2018. 88
FIGURE 3.21. COMPANY PLANT FROM A BIRD'S EYE VIEW CORRESPONDING TO THE MAIN ROOF (BLUE) AND THE ATTACHED ROOF (RED) (IMAGE CREATED FROM THE AUTHOR USING GOOGLE MAPS VIEW). 91
FIGURE 3.22. ANNUAL ENERGY OUTPUT (COLOUR SCALE) ACHIEVED FOR EACH PANEL ORIENTATION AND TILT/ELEVATION ANGLE.... 93
FIGURE 3.23. COMPARISON BETWEEN ANNUAL SOLAR ENERGY GENERATION AND ACTUAL CONSUMPTION AT THE STUDIED COMPANY (GREY) ACCORDING TO THE DIFFERENT GENERATION SCENARIOS REFLECTED IN TABLE 3.19, TABLE 3.20 AND TABLE 3.21.... 97
FIGURE 3.24. MONTHLY SOLAR ENERGY GENERATION FOR EACH SCENARIO. SCENARIO DETAILS CAN BE FOUND IN TABLE 3.19, TABLE 3.20 AND TABLE 3.21. 98
FIGURE 3.25. ENERGY CONSUMPTION BREAKDOWN TO SHOW CONTRIBUTION FROM THE GRID AND FROM SOLAR FOR EACH SCENARIO. 99
FIGURE 3.26. COMPARISON OF THE ANNUAL GRID ENERGY COST PER YEAR WITH (SCENARIO 1, 2 AND 3) AND WITHOUT SOLAR ENERGY. 100
FIGURE 3.27. GLOBAL WARMING POTENTIAL FOR EACH OF THE SCENARIOS..... 104
FIGURE 4.1 HOURLY ENERGY DEMAND (ORANGE LINE) AND MODELLED PV SOLAR ENERGY GENERATION (YELLOW LINE) FOR THE WMD. THE POSITIVES VALUES STAND FOR ENERGY CONSUMPTION AND THE NEGATIVES INDICATE ENERGY GENERATION. ... 116
FIGURE 4.2. (A) MONTHLY ENERGY CONSUMPTION (ORANGE BLOCKS) AND MODELLED PV SOLAR ENERGY GENERATION (YELLOW BLOCKS) FOR THE WMD. (B) ENERGY BALANCE FOR THE WMD (THE POSITIVES VALUES STAND FOR ENERGY CONSUMPTION AND THE NEGATIVES INDICATE GENERATION). 116
FIGURE 4.3 HOURLY ENERGY CONSUMPTION AND MODELLED PV SOLAR ENERGY GENERATION FOR M&S RETAIL STORE. THE POSITIVES VALUES STAND FOR ENERGY CONSUMPTION AND THE NEGATIVES INDICATE GENERATION. 118
FIGURE 4.4 (A) MONTHLY CONSUMPTION AND MODELLED PV SOLAR ENERGY GENERATION FOR THE M&S RETAIL STORE. (B) ENERGY BALANCE FOR THE M&S RETAIL STORE. THE POSITIVES VALUES STAND FOR ENERGY CONSUMPTION AND THE NEGATIVES INDICATE GENERATION. 118

Figure 4.5 Hourly consumption and modelled PV solar energy generation for M&S retail store in May. 119
Figure 4.6 Energy flow diagram proposed for the Waste Management Depot. 120
Figure 4.7. Proposed energy management algorithm for the BESS charging/discharging process at WMD. 123
Figure 4.8. Diagram of the BESS when is charged. 124
Figure 4.9. Diagram of the BESS when is discharged. 125
Figure 4.10. Diagram of the BESS when is neither charged nor discharged. 125
Figure 4.11. Energy flow diagram proposed for the M&S retail store. 126
Figure 4.12. Proposed energy management algorithm for the BESS charging process at the M&S retail store. 128
Figure 4.13. "Assumed electricity price for small non-domestic sector from October 2022. The arrows represent the percentage increase between Q2 2022 and Q4 2022 (i.e., 80%) and between Q4 2022 and Q1 2023 (i.e., 20%)" (Figure obtained from [175]). 130
Figure 4.14. "Simulated electricity prices for one day of the year (from 00:00h to 23:00h) for WMD" (Figure obtained from [175]). 130
Figure 4.15. "Provided electricity prices for one day of the year (from 00:00h to 23:00h) for M&S retail store." 131
Figure 4.16. Simulation results for a week in (a) February and (b) July for the energy flow in the WMD assuming a BESS is not installed. 138
Figure 4.17. Simulation results when the energy management algorithm is applied in a week in (a) February and (b) July using a BESS with CBESS of 0.5 MWh for the WMD. It includes the State of Charge (SoC), modelled PV solar energy generation, energy demand from the WMD and energy purchased from the grid. 139
Figure 4.18. "Top graph (a): Hourly energy consumption from the grid assuming there is not a PV nor a BESS in place. Bottom graph (b): Hourly energy consumption from the grid assuming there PV panels and a BESS of 0.5 MWh installed at the WMD" (Figure obtained from [175]). 140
Figure 4.19. Monthly energy distribution at the WMD at different CBESS. The positives values on each graph represent the energy consumption from the grid, from solar and from the BESS. The negative values indicate solar energy generation and charging of the BESS. 142
Figure 4.20. A comparison of the hourly energy flow at the BESS at CBESS of 0.05MWh, 0.5 MWh and 5MWh. It includes the State of Charge (SoC), modelled PV solar energy generation, energy demand from the WMD and energy purchased from the grid. 143
Figure 4.21. Breakdown of energy used at different CBESS for the WMD, either covered by PV solar energy, from the BESS or from the grid. 144
Figure 4.22. Total cost over system lifetime at different CBESS for WMD. 145
Figure 4.23. Network consumption cost for red, amber, and green bands at different CBESS. 148
Figure 4.24. Capacity charge and excess capacity charge at different power connection capacities for (a) the base case scenario (system without BESS and PV panels) and (b) for a BESS with a capacity of 10 MWh. 149
Figure 4.25. Network costs (£) per year at different CBESS for a power connection capacity of 25 kW. 150
Figure 4.26. A comparison of the total cost over system lifetime between a power connection capacity of 150 kW (grey column) and 50 kW(orange column) at different battery capacities. 151
Figure 4.27. GHG emissions per year for the WMD at different CBESS. 152

FIGURE 4.28. SIMULATION RESULTS FOR A WEEK IN (A) JANUARY AND (B) JULY FOR THE ENERGY FLOW IN THE M&S RETAIL STORE ASSUMING THE BESS IS NOT INSTALLED. 154
FIGURE 4.29. SIMULATION RESULTS WHEN THE ENERGY MANAGEMENT ALGORITHM IS APPLIED IN A WEEK IN (A) JANUARY AND (B) JULY USING A BESS WITH A CAPACITY OF 0.5 MWH FOR THE M&S RETAIL STORE. 155
FIGURE 4.30. MONTHLY ENERGY DISTRIBUTION AT THE M&S RETAIL STORE AT DIFFERENT CBESS. THE POSITIVES VALUES STAND FOR ENERGY CONSUMPTION AND BESS DISCHARGING MODE WHILE THE NEGATIVES INDICATE ENERGY GENERATION AND CHARGING OF BESS. 157
FIGURE 4.31. A COMPARISON OF THE HOURLY ENERGY FLOW AT THE BESS AT DIFFERENT CBESS FOR THE M&S RETAIL STORE. .. 158
FIGURE 4.32. SIMULATION RESULTS WHEN THE ENERGY MANAGEMENT ALGORITHM IS APPLIED IN A WEEK IN (A) JANUARY AND (B) JULY USING A BESS WITH A CAPACITY OF 0.05 MWH FOR THE M&S RETAIL STORE. 159
FIGURE 4.33. SIMULATION RESULTS WHEN THE ENERGY MANAGEMENT ALGORITHM IS APPLIED IN A WEEK IN (A) JANUARY AND (B) JULY USING A BESS WITH A CAPACITY OF 5 MWH FOR THE M&S RETAIL STORE. 160
FIGURE 4.34. PERCENTAGE OF ENERGY USED FROM THE GRID AT DIFFERENT C_{BESS} FOR THE M&S RETAIL STORE (PURPLE SOLID LINE). AT 0.05 MWH AND 5 MWH, THE PIE CHARTS SHOW THE BREAKDOWN OF ENERGY COVERED BY THE GRID, SOLAR INSTALLATION, AND BESS (FURTHER BROKEN DOWN INTO ENERGY STORED FROM EXCESS SOLAR ENERGY OR THE GRID). 161
FIGURE 4.35. TOTAL COST OVER SYSTEM LIFETIME AT DIFFERENT CBESS FOR M&S RETAIL STORE. 162
FIGURE 4.36. TOTAL COST OVER SYSTEM LIFETIME AT DIFFERENT BATTERY CAPACITIES FOR M&S RETAIL STORE WHEN THE PEAK ELECTRICITY PRICE IS INCREASED. 164
FIGURE 4.37. NETWORK CONSUMPTION COST FOR RED, AMBER, AND GREEN BAND AT DIFFERENT CBESS FOR M&S RETAIL STORE. 166
FIGURE 4.38. CAPACITY CHARGE AND EXCESS CAPACITY CHARGE AT DIFFERENT POWER CONNECTION CAPACITIES FOR (A) THE BASE CASE SCENARIO (SYSTEM WITHOUT BESS AND PV PANELS) AND (B) FOR A BESS WITH A CAPACITY OF 10 MWH FOR M&S RETAIL STORE 167
FIGURE 4.39. CONSUMPTION COST PER YEAR FOR THE RED BAND AT DIFFERENT C_{BESS} AND $POWER_{CAPACITY}$ 168
FIGURE 4.40. CONSUMPTION COST PER YEAR FOR THE AMBER BAND AT DIFFERENT C_{BESS} AND $POWER_{CAPACITY}$ 168
FIGURE 4.41. CONSUMPTION COST PER YEAR FOR THE GREEN BAND AT DIFFERENT C_{BESS} AND $POWER_{CAPACITY}$ 168
FIGURE 4.42. GHG EMISSIONS PER YEAR FOR THE M&S RETAIL STORE AT DIFFERENT C_{BESS}. 170
FIGURE 5.1. TOTAL MONTHLY ENERGY CONSUMPTION AT THE WMD WITH A DIESEL RCV FLEET (GREY COLUMN); AND WITH AN ERCV FLEET (GREEN COLUMN). 178
FIGURE 5.2. ENERGY FLOW DIAGRAM PROPOSED FOR THE BCS 179
FIGURE 5.3. ENERGY FLOW DIAGRAM PROPOSED FOR THE BESS SCENARIO. 179
FIGURE 5.4. "FLOW CHART OF THE ENERGY MANAGEMENT ALGORITHM DEVELOPED FOR SCENARIO 2" (FIGURE OBTAINED FROM [175]). 180
FIGURE 5.5. SIMULATION RESULTS WHEN THE ERCV FLEET IS CHARGED AT 16:00H FOR A DAY IN (A) MARCH AND (B) JULY WITH A BESS OF 0.5MWH. 184
FIGURE 5.6. SIMULATION RESULTS WHEN THE ERCV FLEET IS CHARGED AT 16:00H FOR A DAY IN (A) MARCH AND (B) JULY WITH A BESS OF 5MWH. 185

Figure 5.7. Simulation results when the eRCV fleet is charged overnight for a day in (a) March and (b) July with a BESS of 0.5MWh. 186
Figure 5.8. Simulation results when the eRCV fleet is charged overnight for a day in (a) March and (b) July with a BESS of 5MWh. 187
Figure 5.9. Simulation results when the eRCV fleet is charged at 11:00h and 23:00h for a day in (a) March and (b) July with a BESS of 0.5MWh. 188
Figure 5.10. Simulation results when the eRCV fleet is charged at 11:00h and 23:00h for a day in (a) March and (b) July with a BESS of 5MWh. 189
Figure 5.11. Energy demand covered by the grid, solar energy or by the BESS for a capacity of 0.5 MWh and 5MWh for (a) charging scenario 1, (b) charging scenario 2 and, (c) charging scenario 3. 190
Figure 5.12. The total costs over the system lifetime for charging scenario 1. 192
Figure 5.13. The total costs over the system lifetime for charging scenario 2. 192
Figure 5.14. The total costs over the system lifetime for charging scenario 3. 193
Figure 5.15. Consumption band cost per year when for (a) scenario 1, (b) scenario 2, (c) scenario 3 195
Figure 5.16. Total GHG emissions for scenario 1. 196
Figure 5.17. eRCV fleet GHG emissions per year for the different charging scenarios. 197
Figure 6.1. "Energy flow diagram for (a) scenario 1, (b) scenario 2 and, (c) scenario3" (Figure obtained from [175]). 202
Figure 6.2. "Flow chart of the energy management algorithm developed for scenario 3" (Figure obtained from [175]). 205
Figure 6.3. "Monthly energy simulation results for scenario 2 using a BESS with a capacity of: (a) 0.5 MWh and (b) 5MWh. The positives values on each graph represent the energy consumption from the grid, from solar, either directly or via the BESS. The negative values indicate solar energy generation and energy storage in the BESS" (Figure obtained from [175]). 208
Figure 6.4. "Energy demand covered by the grid (purple line) for scenario 1 and scenario 2, and the breakdown of energy demand covered by the grid, by direct PV generation and by the solar via the BESS for CBESS of 0.5 MWh and 5MWh as examples (pie charts)" (Figure obtained from [175]). 209
Figure 6.5. "Hourly energy distribution for scenario 2 with a BESS capacity of 5MWh in a week in (a); February and (b) July" (Figure obtained from [175]). 211
Figure 6.6. "Total cost over system lifetime for scenario 1 and scenario 2" (Figure obtained from [175]). 212
Figure 6.7. "Network consumption cost per year for scenario 1 and scenario 2" (Figure obtained from [175]). 214
Figure 6.8. "Hourly energy distribution for scenario 3 with a BESS capacity of 5 MWh in a week in (a) February and (b) July" (Figure obtained from [175]). 216
Figure 6.9. "Hourly energy distribution for scenario 3 with a BESS capacity of 10 MWh in a week in (a) February and (b) July" (Figure obtained from [175]). 217
Figure 6.10. Top graph (a): Comparison of system's lifetime total cost between the three scenarios Bottom graph (b): Comparison of the network cost over system lifetime [175]. 220

List of Tables

TABLE 2.1. COMMERCIAL CLASSIFICATION OF CHARGER TYPES 29

TABLE 3.1. "DETAILED INFORMATION OF THE H-BASED MODELS ANALYSED AND CHOSEN FOR EVALUATION (MODEL 1 TO MODEL 6)" (TABLE OBTAINED FROM [174]) 54

TABLE 3.2. "DETAILS ON THE HOURLY HORIZONTAL GLOBAL AND DIFFUSE SOLAR IRRADIATION RAW DATA VALUES MEASURED AT EACH LOCATION UNDER STUDY" (TABLE OBTAINED FROM [174]). 55

TABLE 3.3. "NUMBER OF VALUES WITHIN THE REMAINING DATASETS AFTER EACH QUALITY TEST" (TABLE OBTAINED FROM [174]).. 62

TABLE 3.4. "STATISTICAL PERFORMANCE EVALUATION OF EXISTING EMPIRICAL MODELS BASED ON GROUND MEASURED DATA FOR SOUTH-YORKSHIRE, NORFOLK, AND WEST-SUSSEX" (TABLE OBTAINED FROM[174]). 65

TABLE 3.5. "DATASET USED TO DEVELOP AND VALIDATE THE CORRELATIONS AT EACH LOCATION" (TABLE OBTAINED FROM [174]).. 66

TABLE 3.6. "CORRELATIONS WITH BEST PERFORMANCE FOR DATA MEASURED IN EACH LOCATION" (TABLE OBTAINED FROM [174]).69

TABLE 3.7. "DETAILED INFORMATION OF THE DATASET USED AS COMPLETE, TRAINING AND VALIDATION DATASETS" (TABLE OBTAINED FROM [174]). 72

TABLE 3.8. "STATISTICAL ERROR METRICS OBTAINED FOR THE EXISTING EMPIRICAL MODELS USING DIFFERENT DATASETS" (TABLE OBTAINED FROM [174]) 72

TABLE 3.9. "ACCURACY EVALUATION OF DEVELOPED CORRELATION USING DIFFERENT DATASETS" [174] 73

TABLE 3.10. TOTAL AMOUNT OF SOLAR IRRADIATION PER YEAR IN AN INCLINED PV PANEL AT 25 DEGREES 81

TABLE 3.11. VALUES ASSUMED FOR THE CONVERSION BETWEEN ENERGY AND SOLAR IRRADIATION ON A PV INSTALLATION INCLINED. 82

TABLE 3.12. COMPARISON BETWEEN MEASURED VALUES AND MODELLED VALUES OF TOTAL SOLAR IRRADIATION RECEIVED FOR ONE PANEL INCLINED 25° IN THE REGION OF SOUTH-YORKSHIRE. 84

TABLE 3.13. DATA PROVIDED BY M&S FOR THE VALIDATION OF THE SOLAR MODEL 86

TABLE 3.14. VALUES ASSUMED FOR THE CALCULATION OF PV SOLAR ENERGY GENERATION AT YORK VANGARDE RETAIL PARK. 87

TABLE 3.15. COMPARISON BETWEEN MEASURED VALUES AND MODELLED VALUES OF TOTAL SOLAR GENERATION AT M&S YORK VANGARDE RETAIL PARK. 89

TABLE 3.16. VALUES ASSUMED FOR THE CONVERSION BETWEEN ENERGY AND SOLAR RADIATION ON AN PV INCLINED PANEL..... 90

TABLE 3.17. MAIN AND ATTACHED ROOF ORIENTATION AND ELEVATION ANGLES. 91

TABLE 3.18. NUMBER OF PV PANELS ASSUMED TO BE INSTALLED USING THE ACTUAL ROOF CONFIGURATION AND THE NEW ROOF CONFIGURATION (WITH 10% SKYLIGHTS). 92

TABLE 3.19. CHARACTERISTICS ASSUMED FOR THE ROOFS AND PV PANELS INSTALLED FOR SCENARIO 1. 92

TABLE 3.20: CHARACTERISTICS ASSUMED FOR THE ROOFS AND PV PANELS INSTALLED FOR SCENARIO 2. 93

TABLE 3.21. CHARACTERISTICS ASSUMED FOR THE ROOFS AND PV PANELS INSTALLED FOR SCENARIO 3. 94

TABLE 3.22. ANNUAL ENERGY CONSUMPTION IN THE STUDIED COMPANY AND THE ANNUAL ENERGY CONSUMED FROM SOLAR AND FROM THE GRID FOR EACH SCENARIO. 99

TABLE 3.23. BREAKDOWN OF ELECTRICITY COSTS PER SCENARIO. 101

TABLE 3.24: PAYBACK TIME BREAKDOWN BASED ON 2021 PRICES 102

TABLE 3.25 PAYBACK TIME BREAKDOWN BASED ON PRICES FROM 2023 103

TABLE 4.1. "NETWORK CHARGES FOR THE WMD" (TABLE OBTAINED FROM [175]). 133
TABLE 4.2. M&S RETAIL STORE NETWORK CHARGES. 133
TABLE 4.3. "TOTAL COST OF BESS FOR A LIFETIME OF 15 YEARS" (TABLE OBTAINED FROM [175]). 135
TABLE 4.4. "TOTAL COST OF PV INSTALLATION FOR A LIFETIME OF 15 YEARS FOR THE WMD" (TABLE OBTAINED FROM [175]). ..136
TABLE 4.5. TOTAL COST OF PV INSTALLATION FOR A LIFETIME OF 15 YEARS FOR THE M&S RETAIL STORE 136
TABLE 4.6 EMISSION CONVERSION FACTOR FOR THE ENERGY CONSUMED AT THE WMD. 137
TABLE 4.7. SYSTEM COST AT DIFFERENT BATTERY CAPACITIES FOR THE WMD. THE VALUES IN £ ARE INCLUDED IN APPENDIX A. ...146
TABLE 4.8 NETWORK COSTS ITEMISED AT DIFFERENT BATTERY CAPACITIES FOR THE WMD. THE VALUES IN £ ARE INCLUDED IN APPENDIX A. 147
TABLE 4.9. ANNUAL NETWORK COSTS (£) FOR ALL THE POWER CONNECTION CAPACITIES AT DIFFERENT BATTERY CAPACITIES 150
TABLE 4.10. SYSTEM COST AT DIFFERENT POWER CONNECTION CAPACITY FOR THE WMD. THE VALUES IN £ ARE INCLUDED IN APPENDIX A. 152
TABLE 4.11. SYSTEM COST FOR M&S RETAIL STORE. THE VALUES IN £ ARE INCLUDED IN APPENDIX A..... 163
TABLE 4.12. NETWORK COSTS FOR THE M&S RETAIL STORE 165
TABLE 4.13. SYSTEM COST AT DIFFERENT $POWER_{CAPACITY}$. THE VALUES IN £ ARE INCLUDED IN APPENDIX A. 169
TABLE 5.1. DETAILED INFORMATION OF EACH CHARGING SCENARIO. 177
TABLE 5.2. INITIAL COSTS ASSOCIATED WITH EV CHARGERS. 182
TABLE 6.1. "SUMMARY OF THE SCENARIOS STUDIED, AND THE APPROACH USED FOR THE COST ANALYSIS" (TABLE OBTAINED FROM [175]). 203
TABLE 6.2. SYSTEM COST AT DIFFERENT BATTERY CAPACITIES (CBESS) FOR SCENARIO 1 AND SCENARIO 2. THE VALUES IN £ ARE INCLUDED IN APPENDIX B. 213
TABLE 6.3. SYSTEM COST FOR SCENARIO 1 AND SCENARIO 3 (WITH A BESS OF 10 MWH). THE VALUES IN £ ARE INCLUDED IN APPENDIX B. 218
TABLE 9.1. SYSTEM COST AT DIFFERENT BATTERY CAPACITIES FOR THE WMD. 266
TABLE 9.2 NETWORK COSTS ITEMISED AT DIFFERENT BATTERY CAPACITIES FOR THE WMD. 267
TABLE 9.3. SYSTEM COST AT DIFFERENT POWER CONNECTION CAPACITY FOR THE WMD. 268
TABLE 9.4. SYSTEM COST FOR M&S RETAIL STORE. 269
TABLE 9.5. SYSTEM COST AT DIFFERENT $POWER_{CAPACITY}$. 270
TABLE 10.1. "SYSTEM COST AT DIFFERENT BATTERY CAPACITIES (CBESS) FOR SCENARIO 1 AND SCENARIO 2" (TABLE OBTAINED FROM [175]).. 271
TABLE 10.2. "SYSTEM COST FOR SCENARIO 1 AND SCENARIO 3 (WITH A BESS OF 10 MWH)" (TABLE OBTAINED FROM [175]). ..271

1 Introduction

The Nationally Determined Contributions (NDCs), which are a set of actions taken by each country under the Paris Agreement to reduce national emissions, have been proven inadequate. In fact, the current NDCs would lead to an increase on global average temperature around 3°C by 2100 if compared to pre-industrial levels [1]. This is 1.5°C above the temperature set, in the 2015 Paris Agreement treaty, to avoid more severe climate change impacts [2].

The urgency to minimise the negative effects of climate change is motivating a global demand towards decarbonisation policies. The UK has pledged by law (Climate Change Act 2008) "to ensure the net UK carbon account for the year 2050 is at least 100% lower than the 1990 baseline"[3]. For that to happen, decarbonisation of the transport sector is required. Now more than ever, the transport sector plays a crucial role in the UK's commitment to climate targets, overtaking the energy sector as the sector with the highest GHG emissions in the UK [4].

Despite the estimated impact that the coronavirus (COVID-19) pandemic has had on the reduction of GHG emissions, the transport sector continues to be the highest GHG emitter in the United Kingdom [4]. According to the latest available data, the transport sector emitted 109.5 $MtCO_2e$ in 2021, 91% of which came from road transportation [5]. In this particular framework, the significance of road freight transportation is noteworthy, not solely owing to its greenhouse gas (GHG) emissions but also due to its adverse influence on air quality. Approximately 46% of total road transport nitrogen oxide (NOx) emissions stem from heavy goods vehicles (HGVs) and light goods vehicles (LGVs) combined [6], despite these vehicle types accounting for merely 6% and 18% of total vehicle miles, respectively [7]. Freight transportation is an essential activity in our daily routine and a major contributor to the UK economy. This might be the reason why future predictions point out a further increase in freight transport demand linked to an increase in population and GDP [8]. More precisely, freight transport demand is expected to increase by 7% and 28% in 2030 and 2050 respectively, in relation to values from 2018 [8]. This would lead to an increase in GHG emissions if appropriate measures are not taken into consideration.

Efficiency measures have been adopted to reduce Tank-to-wheel (TTW) GHG emissions from the freight transport sector. According to Ballantyne and Heron [9], many of these efficiency measures (e.g., improve the fuel efficiency and driving and route optimisation) have been

implemented as a result of membership accreditation to a transport compliance scheme. Amongst others are the improvement of fuel efficiency [10], modal shift from road to rail [11,12] and logistics supply chain optimisation [13].

On one hand, fuel efficiency can be improved by reducing fuel consumption when the vehicle is at a standstill through "stop-start" technology, especially when applied to cars and LGVs. On the other hand, improving the engine efficiency can be achieved by means of smaller engines [10]. Ultimately, improvements on the vehicle aerodynamics have a positive effect on fuel efficiency [14]. According to the findings of The King Review[15], Leach *et al.*[10] and Madhusudhanan *et al.*[14], these measures could potentially reduce CO_2 emissions and fuel consumption by 30%. However, for the case of HGVs, the increase in freight transport demand has eclipsed the benefits achieved on fuel efficiency improvements and logistics [16].

Modal shift from road to rail has been explored as a measure to reduce TTW GHG emissions from road freight transport. In fact, freight mode shift has for a long time been the primary measure considered for decarbonisation of freight transport [17]. According to the report released by the Rail Partners [18], one single rail freight service could remove up to 129 HGVs from the road, reducing CO_2 emissions by 76%. However the shift from road to rail presents some challenges [17,19]. Geographically, rail networks have lower connectivity than road networks; and the movement of goods by rail is generally slower than by road. Moreover, rail infrastructure, and logistics and supply chain operations have to be adapted [19]. The Just in Time (JIT) model of supplying goods, characterised by moving small volumes at more frequent intervals, does not help with this transition [11]. Further investment would be needed on increasing and improving track gauge [18] to solve one of the main issues that restricts the rail freight movements in the UK [19]. Moreover, to maximise the shift from road to rail, railway decarbonisation would be required.

Optimisation of logistic supply chains is a complementary alternative to reduce GHG emissions and from freight transport too. Pan *et al.*[13] concluded that pooling supply chains reduces CO_2 emissions by 14%. On the other hand, a huge effort has been focused on data availability for logistics operations to enable an optimal use of vehicle capacity, which in turn reduces GHG emissions [17]. Despite the benefits obtained through reductions in GHG emissions, a combination of all these efficiency measures discussed would only reduce TTW GHG emissions by 29% and 20% in 2030 and 2050, respectively [8].

Due to this limited reduction in GHG emissions, it is imperative to find ways to fully decarbonise the freight transport sector to achieve the net zero target by 2050. In this regard, local authorities are taking leadership by introducing policies to establish Clean Air Zones (CAZ) and Low Emission Zones (LEZ) in major UK towns and cities [20]. CAZ and LEZ policies are designed to promote the adoption of vehicles with reduced emissions (i.e., alternatives to petroleum-based conventional fuels, electric or hybrid vehicles), and road freight transport fleets are the main target under those policies. Many of these policies impose a fee on those vehicles entering the CAZ that do not meet emission standards [21].

In the short term, alternatives to petroleum-based conventional fuels (i.e., diesel/petrol) have been extensively explored as a measure to reduce further TTW GHG emissions on road freight transport. However, it is difficult for these to compete against conventional fuels, due to the high energy density and availability of conventional fuels [17]. In fact, petroleum-based conventional fuel consumption increased for road transport between 2020 and 2021 [22], and they are still the main source of energy to power freight road vehicles [10]. Kollamthodi *et al.*[23] calculated Well to Wheel (WTW) GHG emissions by fuel type (i.e., petrol/diesel, biomethane and natural gas) for different road freight transport vehicles. The data from [23] is illustrated in Figure 1.1.

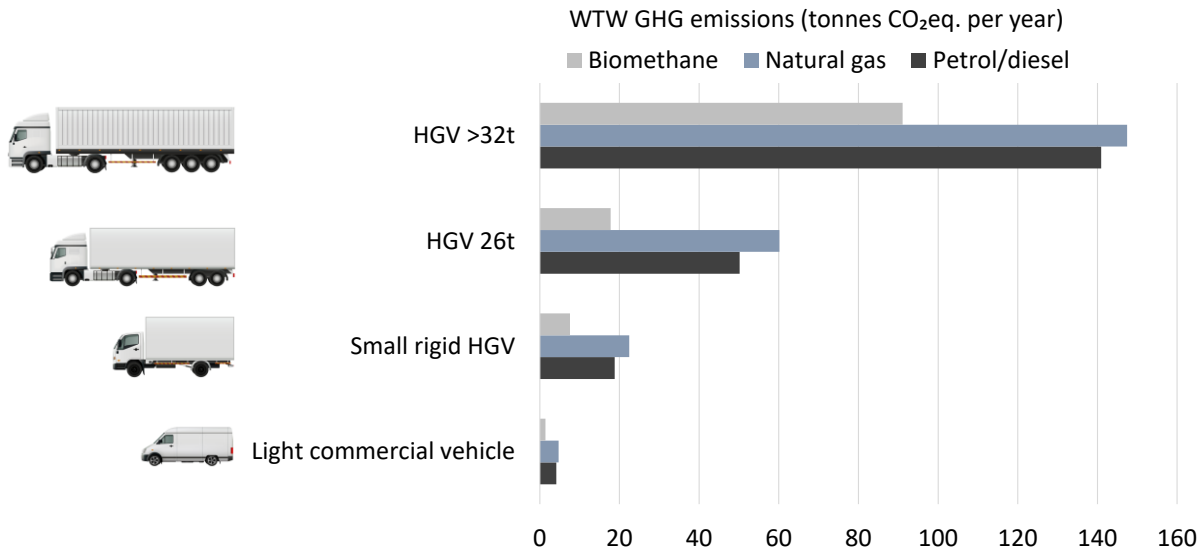

Figure 1.1. Well to Wheel (WTW) emissions by fuel type for road freight vehicles (own creation with data from Kollamthodi *et al.* [23]).

Compressed and liquid natural gas (CNG and LNG) is one of the "transitional fuel" towards zero carbon alternatives. It has less carbon content than conventional fuels and emits lower

quantities of nitrogen oxide (NOx) and particulate matter (PM) per unit of energy. However, despite the benefits associated with air pollution in the short term, it would never achieve the level of decarbonisation needed in the long term [23]. A recent study from Langshaw *et al.*[24] estimates a 13% reduction on GHG emissions only if the LNG powered vehicles are as efficient as their equivalents powered by diesel. Moreover, the leakage of methane in the stages of gas supply and vehicle refuelling reduces considerably the benefits of using CNG and LNG to power road freight transport fleets [25].

However, the use of biofuels (i.e., biomethane) in road freight transport present a potential alternative to fossil fuels with a performance comparable to conventional vehicles, although there are still methane leakages associated with the vehicle use. The main disadvantage when discussing its capability is the availability of suitable feedstock and their sustainability, especially concerning indirect land use changes [17,23,26].

Road freight transport decarbonisation is not easy and presents significant challenges. Moreover, the alternatives explored at this point ease GHG emissions reduction in the short term [26], especially if driving range or storage density is of primary concern [27]. They alone cannot achieve the significant decarbonisation required in the long run [28]. One of the most promising solutions to decarbonise transport is electrification.

1.1 Road freight transport electrification

Electrified powertrains are a promising solution because they not only help to reduce air pollution as they are zero emission at the tailpipe, but also they minimise the noise associated with transportation, which is particularly attractive in the context of city logistics [29]. Further, road freight transport fleets can be electrified using different energy vectors, for example hydrogen or electricity.

Hydrogen is a chemical energy carrier and thus its potential role in energy systems shares some similarities with that of electricity. It is in fact a promising alternative in the long term to the path of net zero. Proof of that is the rise in demand around the world [30] and the increase in new policies adopted by many countries to promote the investment in hydrogen [30,31], some of them relying on the potential of carbon capture and storage (CCS) and green hydrogen. However, there is a controversial debate about its suitability as a clean fuel. The majority of hydrogen is currently produced from natural gas by means of steam reformation of methane, or from coal gasification [17,30]. These forms of hydrogen are known as grey and black

hydrogen respectively, and, as a consequence of being produced from fossil fuels, emit huge quantities of GHGs during their production. In order to make it a cleaner fuel, both grey and black hydrogen production relies on CCS technology to sequestrate the carbon released to the atmosphere. However, a cleaner version of hydrogen can be achieved if it is produced by electrolysis. Electrolysis only requires the use of water and electrical energy to produce hydrogen, however only 0.1% of total hydrogen produced around the world is done through electrolysis [30]. This way of producing hydrogen is not exempt from controversy around its suitability as a clean fuel, mainly due to its efficiency [32,33]. According to Bossel [32], only between 20% and 25% of the energy used for the electrolysis is converted into vehicle motion. Moreover, if the hydrogen is liquefied, the energy loss is further reduced by up to 81% [17]. However, hydrogen is seen as a promising alternative to conventional diesel fuel to be used in heavy, long-haul trucks due to its high energy density if compared to battery electric vehicles (BEV), and hence ease of storage for mobile applications.

BEVs are a potential solution not only for the long term but also in the short term to reduce GHG emissions from road freight transport. Furthermore, if compared with hydrogen fuel cells, batteries are a relatively mature technology. The infrastructure required for delivering electricity is currently well-established although it needs to be upgraded to handle the required increase in power demand to electrify road transport. According to the Office for National Statistics [34], the uptake of BEVs has increased by approximately 80% between 2020 and 2021 and is gaining importance amongst businesses as an action to reduce business carbon emissions.

A combination of a transport model and an energy model, developed by Rosenberg *et al.*[28] was used to simulate the interaction between the energy system and road freight transport, and it was found that for small trucks (i.e., up to 50 tonnes) and large trucks operating in a route smaller than 300 km/day, BEVs will be the dominant technology due to their efficiency, maturity and lower costs when compared to hydrogen powered vehicles.

BEVs have zero tailpipe emissions, that means no GHG emissions, particulates, NOx, or ground level ozone are released. However, BEVs can still emit important quantities of GHG emissions if the electrical energy used to charge them comes from fossil fuels such as coal, oil, or natural gas. The total GHG emissions per kWh for an HGV powered by diesel, electricity, green hydrogen (H_2 electrolysis), grey hydrogen (H_2 Steam Methane Reformation), compressed natural gas (CNG) and biomethane can be seen in Figure 1.2. The graph has been

adapted from Gustafsson *et al.*[35]. The GHG emissions in Figure 1.2 are itemised by emissions produced as a result of direct fuel combustion (TTW-Combustion) and upstream emissions released for the production of energy (WTT-electricity) or fuel (WTT -other), also known as Well-to-Tank (WTT) emissions. Considering the use of an electricity grid mix with a carbon intensity similar to the average in the EU (i.e., 269 g CO_2eq. per kWh), the WTT impact is so high as to almost negate the advantage of replacing fossil fuels entirely. Simply transitioning to hydrogen powered vehicles or BEVs alone won't be sufficient to diminish the environmental impact of the road freight transport unless the carbon intensity of the electricity grid mix is reduced to zero [17]. In this regard, it has been demonstrated that the most efficient pathway for the use of renewable energies when it comes to transport electrification is through battery electric vehicles [36].

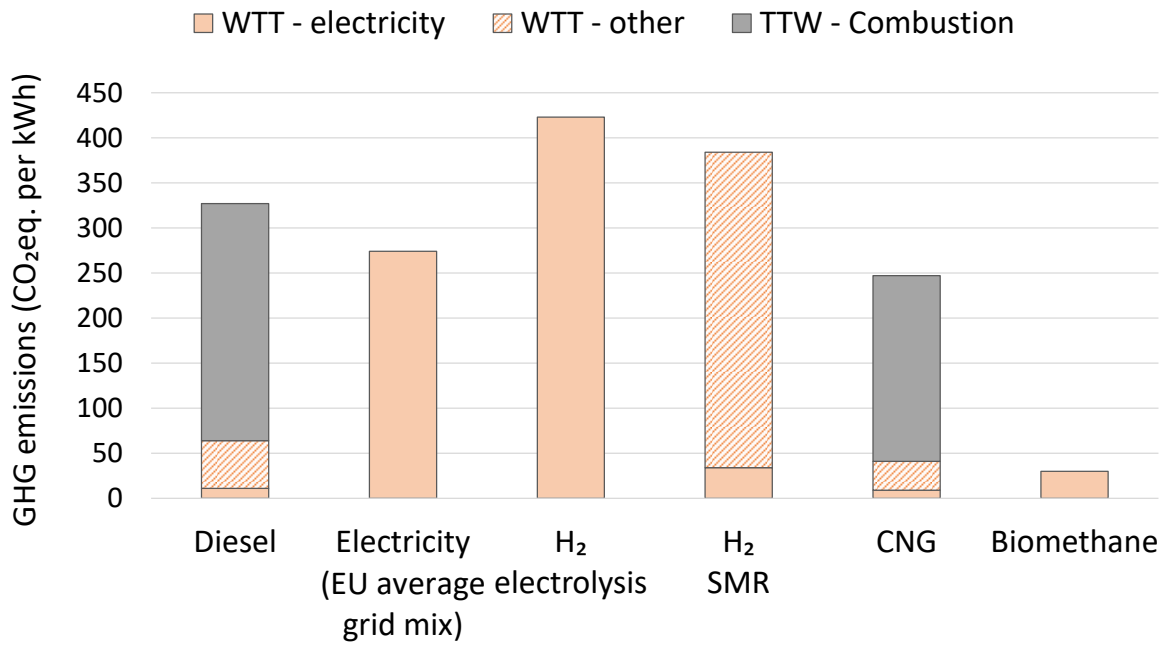

Figure 1.2. Total GHG emissions per kWh based on each energy carrier introduced. (graph adapted from Gustafsson *et al.* [35])

The European Commission's new strategy involves increasing the target for reducing GHG emissions from 40% to 55% by 2030 (if compared to 1990 levels), aimed at making Europe the world's first climate-neutral continent by 2050 [37]. To accomplish the mentioned goal, a hastened electrification in sectors that rely on fossil fuels is needed at the same time as the deployment of renewable energy generation increases. In the UK specifically, the aim is to reduce emissions by up to 76% and 85% from the power sector by 2030 and 2035 respectively, compared to 2019 levels [38].

The power and transport sector therefore go hand in hand on the path towards a net zero future. However, as the power sector continues to decarbonise, the use of renewable energies in transportation becomes a priority to maximise the environmental benefits of transport electrification.

1.2 Research Aims & Objectives

This study is focused on identifying whether the barriers associated with the WTT emissions from electric vehicle fleets associated with the grid mix could be addressed in a way that ensures the benefits of road freight transport electrification are maximised. The approach is therefore to perform a systematic analysis of how on-site solar energy generation and energy storage could be used to unlock additional reductions in GHG emissions.

The adoption of on-site solar energy generation supported by battery energy storage systems is explored for two different premises, a retail store, and a waste management site, considering the energy consumption and logistic operations carried out at each site. A fleet of electric refuse collection vehicles (eRCV) is explored as a representative example of fleet energy consumption and the impact this has on the power connection capacity.

Overall, the thesis aims to explore the feasibility of using on-site solar generated energy and battery energy storage for EV fleet charging, considering operational and technical constraints. The operational constraints reflect realistic vehicle operating and charging times. On the other hand, technical constraints refer to challenges associated with the power connection capacity issues when a fleet is electrified in a depot, as well as the balance between energy consumption and on-site generation. The analysis is performed considering the impact on grid dependency, GHG emissions and system lifetime costs.

Broadly, the research aims and objectives of the thesis are:

1) **Research Aim 1** – To understand the scientific context and the current status and identify current research gaps in freight transportation. In particular, its environmental impact and, more in depth, the challenges associated with its electrification, not only from a logistic point of view but also from a more technical perspective that combines the transport and energy systems.

a) **Objective 1a** – To conduct a literature review on road freight transport focused on its environmental impact and the emissions associated with each type of road freight vehicle (i.e., heavy goods vehicle and light commercial vehicles).
b) **Objective 1b** – To conduct a literature review on road freight transport electrification, particularly past and recent developments in charging infrastructure and strategies.
c) **Objective 1c** – To conduct a literature review regarding the interaction between the energy and transport sectors when it comes to fleet electrification, including integrating renewable energy and energy storage systems with an electrified fleet.

2) **Research Aim 2** – To examine the energy potential that a PV solar installation would have in logistic and commercial sites, such as a warehouse or a store.
   a) **Objective 2a** – To develop a new empirical solar model capable of estimating the solar energy generation at different locations in the UK, using solar radiation datasets and information of the specific site (i.e., latitude/longitude, available area for the PV installation).
   b) **Objective 2b** – To validate and test the model appropriately by comparing the model output with real-life recorded values from different PV installations.
3) **Research Aim 3** – To assess the potential benefits of implementing a BESS on a logistic or commercial site connected to the grid considering that the site has a PV solar installation on-site.
   a) **Objective 3a** – To develop a tailored energy management algorithm that facilitates the integration of all the system components (i.e., PV solar installation, a BESS, and the system demand load) for the correct energy distribution.
   b) **Objective 3b** – To apply the energy management algorithm to different commercial buildings in regard to operations and energy consumption characteristics.
   c) **Objective 3c** – To examine the impact that a combination of solar energy and energy storage has on such commercial building in regard to total costs, grid dependency and GHG emissions, considering the following variables:
      - ✓ Battery capacity.
      - ✓ Power connection capacity.
4) **Research Aim 4** – To assess the feasibility of charging an electric fleet in a commercial depot by using localised solar energy and battery energy storage system (BESS) considering operational (i.e., operating and charging times) and technical constraints (i.e., power capacity connection).

a) **Objective 4a** – To update the energy management algorithm developed for the Research Aim 3 to add the electric fleet as an extra energy demand at specific hours in each day.
b) **Objective 4b** – To apply the updated energy management algorithm in a commercial depot considering different charging scenarios.
c) **Objective 4c** – To evaluate the output obtained regarding grid dependency, total costs and GHG emissions and compare the results with the output obtained for a base case scenario (BCS) in which the fleet is electrified but the energy demand from the depot and the fleet is entirely covered from the grid mix.
d) **Objective 4d** – To develop a new algorithm that mitigates the need for potential power infrastructure upgrades that might arise from transitioning from a conventional fleet to an electric one.
e) **Objective 4e** – To evaluate to what extent solar energy and BESS can ease the power capacity constraint when it comes to fleet electrification on a commercial depot.

1.3 Research methodology

This thesis adopts a pragmatic philosophical position to address the research aims of the thesis and the subsequent research objectives, based on the gaps found in literature that are presented in the following chapter. As highlighted by the works of various scholars [39–41] pragmatism evaluates the concept of truth through the lens of its impact, results, and applicability. This perspective allows researchers to embrace methodologies or suitable techniques for achieving pragmatic solutions and tangible outcomes.

1.3.1 Modelling and simulation-based methodology

In alignment with the research aims and the philosophical standpoint, the methodology followed in this thesis adopts a modelling and simulation based strategy, capable of providing valuable data when it comes to electrifying a fleet with the help of renewable energy generation and an energy storage system. The simulation tools and models are designed to calculate solar energy generation and to manage the energy flow of a system formed by a PV installation, battery energy storage system (BESS), an EV fleet and the grid network. Figure 1.3 illustrates an example overview of such system.

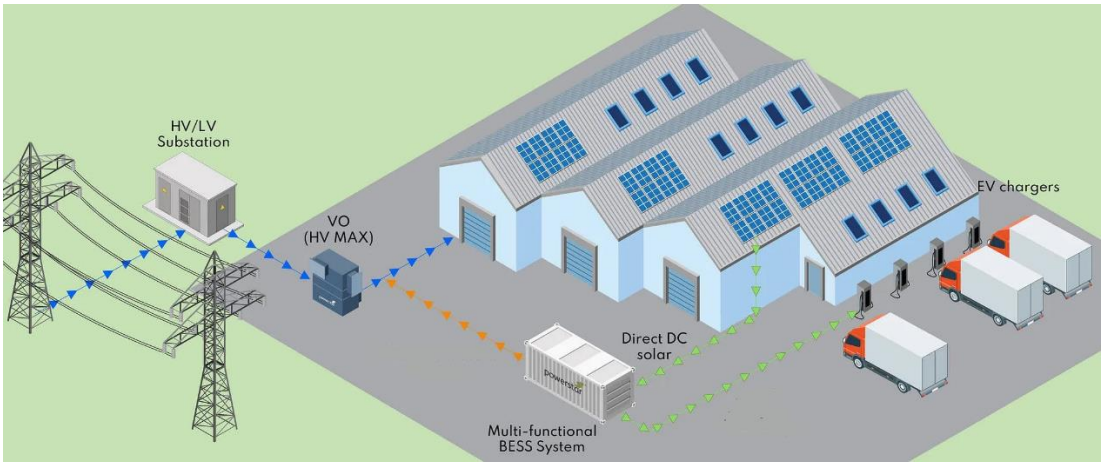

Figure 1.3. Overview of a depot with rooftop PV panels and a BESS for EV fleet charging (modified picture from [42])

A research methodology flowchart is presented in Figure 1.4 to show how the various modelling elements combine.

Initially, the available solar energy generation at the specific location (e.g., depot or warehouse) is estimated by a solar model. A detailed explanation of the solar model development and validation can be found in Chapter 3. The input data used for the development of the solar model, in the form of ground-based measurements of horizontal solar irradiation, were obtained from the Centre for Environmental Data Analysis (CEDA) Archive. The CEDA Archive is a reliable source of climatological and atmospheric measurements based in the UK.

The BESS is another aspect of the system (see Figure 1.3) that has been modelled. The output from the model refers to the State of Charge (SoC) of the BESS. The simulations were carried out with data on energy demand supplied by commercial partners interested in the project. The data utilised in this research project were provided by industrial partners under conditions of confidentiality, prohibiting their publication or sharing with any third parties following the terms stipulated by the sponsors.

Knowing the available solar energy generated by the PV solar installation, how the BESS behaves and the demand from the depot or warehouse, the energy flow of the system is controlled by an energy management system. Chapter 4 contains a detailed methodology for developing the BESS model and the energy management algorithm.

The output obtained from the energy management algorithm is evaluated in Chapter 4, in two commercial premises, a waste management depot and an M&S retail store. That initial

evaluation aimed to understand how commercial and logistics premises function with PV panels and BESS, and considered the technical and economic impact. The outcome of the evaluation allowed the selection of the case study based on the energy requirements of both premises. The waste management depot was selected as the commercial premises to evaluate the introduction of an EV fleet based on the potential benefits achieved when the PV panels and BESS are installed.

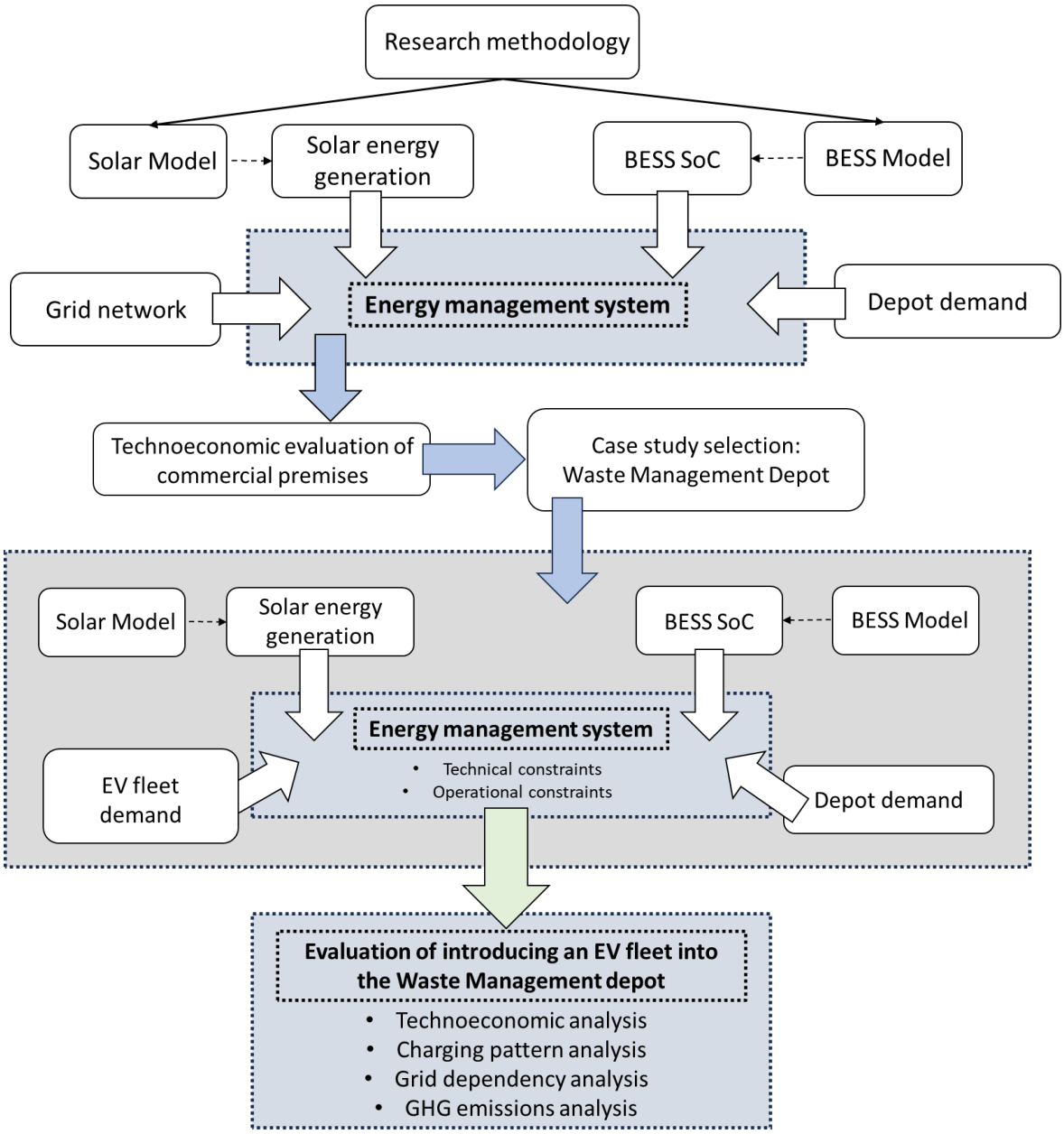

Figure 1.4. Research methodology flowchart

The second part of the research methodology focuses on evaluating the introduction of an EV fleet into the commercial waste depot. An energy management system is created with specific

algorithms considering technical and operational constraints such as power connection capacity and EV charging patterns. This part of the thesis is explained in detail in Chapter 5 and Chapter 6.

MATLAB software and Simulink, a MATLAB-based graphical programming environment, are used to develop the models and energy management algorithms. MATLAB software has been chosen for being a high-level industry-standard programming language capable of handling a significant amount of data. It is accessible and supported by the University of Sheffield.

The study is focused on the UK, and the empirical solar correlations are developed for locations within the UK. Nevertheless, the methodology presented in the study could be considered a framework to assess the feasibility of using on-site solar-generated energy and energy storage for EV fleet charging in other countries. In other locations, alternative solar irradiation data, energy consumption and EV fleet charging demand could still be processed by the model and simulation tools presented in the study.

1.4 Thesis structure

Chapter 2 provides a literature review that contextualises the issue associated with road freight transport emissions and explores the issues and peculiarities of road freight transport electrification, such as charging infrastructure and charging patterns. The review shows that charging EV fleets from renewable energy sources is of paramount importance for achieving a sustainable transportation system. However, research into the technicalities of depot-based EV fleet charging using renewable energy generation and energy storage is still in need of exploration taking into consideration the operational and logistic requirements of road freight transport fleets.

Considering that renewable energy is the centrepiece to maximise the benefits that electrification of transport has on GHG emissions, in Chapter 3 a new solar model is developed for the estimation of solar energy availability at specific sites within the UK. For that purpose and considering the scarcity of ground level data on diffuse solar irradiation in the UK, and the relevance that this data has when applied to different empirical solar models, site specific empirical solar correlations are developed. The accuracy and validity of the results obtained from the newly developed solar model were compared against measured data from two different PV installations, one located in a private household, and another placed at the Marks

and Spencer (M&S) York Vangarde Retail Park store rooftop. The newly developed solar model can be used as a tool for supporting commercial and logistics companies on their decision to improve sustainability by providing valuable and accurate information on local availability of solar energy. At the end of the chapter, the solar model is applied to a case study performed for a company in the industrial sector [43].

Chapter 4 explores the impact of introducing a BESS, from both a technical and economic standpoint, on the overall energy use of the system. The system considers the energy demand from the commercial or logistic site, the energy generation from the PV solar installation, the energy store by the BESS and the energy from the grid network. The final aim of the thesis is to explore the feasibility of using PV solar energy generated on site together with local energy storage for EV fleet charging. Understanding how different commercial premises respond to the introduction of a BESS regarding costs, grid dependency and GHG emissions, is essential to progress with the study. To that end, the approach has been demonstrated at two different example premises, a waste management depot (WMD) and a M&S retail store. The reason behind the selection of these two sites relies on their differences in the operational and technical characteristics (e.g., activity developed on the site or their site specific energy consumption) with the aim of providing a broader set of results. To perform the investigation, an energy management model is developed based on a rule-based energy management algorithm in the form of “if” / ”else” and “then” statements. The algorithm manages the energy flows between the premises, the PV solar installation, the BESS, and the grid. The results obtained from the model, were analysed and it was found that the introduction of the BESS together with the PV solar system reduces the grid dependency, the total costs and the GHG emissions if compared to the base case scenario for the WMD. On the contrary, the installation of a BESS in premises with similar characteristics to the M&S retail store, is only economically justified for a certain gap between off-peak and peak electricity prices. Moreover, in premises like M&S retail store, where the on-site solar energy generated proves inadequate even for fulfilling their internal energy requirements, justifying the use of solar energy for EV fleet charging seems challenging.

In Chapter 5, the electrification of a fleet of refuse collection vehicles is examined, at the waste management depot (WMD) introduced in the previous chapter. The aim of the chapter is to explore the potential benefits, if any, of the integration of PV solar panels, a BESS and an eRCV fleet against a given base case scenario (BCS). The BCS refers to a hypothetical scenario

in which the WMD does not have PV solar panels installed nor a BESS but wishes to switch its refuse collection vehicles to an electrically powered eRCV fleet. In this BCS, the eRCV fleet and the depot's demand are to be entirely covered from the grid mix. Additionally, in order to have a broader knowledge of how the use of PV panels and a BESS could impact on fleet electrification, three different charging patterns are assessed. Based on the results, it is found that the introduction of PV panels and a BESS reduces the grid dependency of the overall facility, system's lifetime total cost for certain BESS capacities, and the overall GHG emissions. Depending on the charging pattern, the benefits of on-site PV panels and a BESS can be further maximised.

Chapter 6 addresses the issue of the site network power connection capacity when it comes to fleet charging at depot based stations. For that purpose, a new ruled-based control strategy that avoids increasing the power connection capacity is developed for the energy management algorithm. For the analysis, different scenarios are compared assuming the eRCV fleet is charged overnight (i.e., from 21:00h). The objective of making such a comparison is to determine, in the case that there is the option, what is the most feasible way forward. Either to keep the network power connection capacity at the same level as it was prior to the adoption of the eRCV fleet or upgrade the network power connection to add more flexibility regarding the charging time and dependency from the grid at lower electricity and network connection costs. The findings indicate that greater cost reduction flexibility exists when the power connection upgrade is not constrained. If the upgrade of the network power connection is not an option, a 10 MWh BESS, in this case, effectively fulfils energy requirements without surpassing the contracted grid connection power capacity. However, other strategies, such as smart charging, must be implemented with the BESS to make it an economically viable option.

Finally, the findings of the thesis are summarised in Chapter 7. Also, an extensive analysis regarding the research limitations and future research opportunities raised from the PhD thesis, are outlined.

2 Literature Review

As discussed in the introduction chapter, the different energy carriers explored will be needed to ease the climate impact associated with road freight transport in the pathway towards net-zero carbon in 2050. In the long-term scenario towards net-zero carbon, road freight transport electrification is seen as a promising solution.

This chapter presents a comprehensive literature review on road freight transport electrification. In the beginning, the chapter aims to contextualise the topic by describing the past, current, and future predictions on emissions associated with road transport globally and, more in-depth, the emissions related to road freight transportation in the UK. Additionally, due to the relevance of the Well-to-Tank (WTT) emissions (i.e., upstream emissions released for the production of energy), and the impact associated with the carbon intensity of the electricity grid mix when electrifying a fleet, a review of the literature in this topic is performed as part of the contextualisation stage of this chapter. The following sections focus on reviewing the technicalities presented in literature published on electric freight fleet charging (i.e., infrastructure and strategies) and the synergy between energy and transportation in facilitating road freight transport electrification. In this regard, the literature shows that energy storage systems have been proven to be a potential technology towards integrating energy and transport systems when it comes to fleet electrification, particularly if the energy system is powered by renewable energies.

Overall, throughout the literature, it is shown that charging EV freight fleets with renewable energy sources is paramount for achieving a sustainable transportation system. However, research into the feasibility of using renewable energy sources to charge EV fleets while considering the logistic and operational constraints that may arise is still needed. The outcomes of such a study will align the objectives of transportation and logistics companies with the sustainability needs of the local and national government agenda around the decarbonisation of transport. Moreover, it will contribute to knowledge on the feasibility of using renewable energy for freight fleet electrification and the potential future research on this topic.

2.1 GHG emissions from transport

The onset of the late 18th-century Industrial Revolution marked the commencement of amplified anthropogenic emissions. These emissions, encompassing greenhouse gases (GHGs) like carbon dioxide (CO_2), methane (CH_4) and nitrous oxide (N_2O), arising from fossil fuel

combustion and deforestation, have escalated over time owing to continued population and economic growth [44]. While global governments strive to curtail the repercussions of this surge in GHG emissions within the mid-term, it has been stated that the impact of anthropogenic emissions will spread and have consequences beyond 2100 [45].

Figure 2.1 shows global CO_2 emissions by sector for the past half century. The global trend for those 50 years suggests that transport is the sector which experienced the most significant increase in CO_2 emissions, second to electricity [46]. As shown in Figure 2.1, there have been a few episodes when global CO_2 emissions from transport have decreased. However, the most significant reduction corresponds to the period between 2019 and 2020. This decrease in emissions was largely a result of the eruption of policy measures adopted and implemented during the Covid-19 pandemic. However, once those measures were lifted the year after, in 2021, the global transport emissions increased again to almost pre-pandemic levels [47].

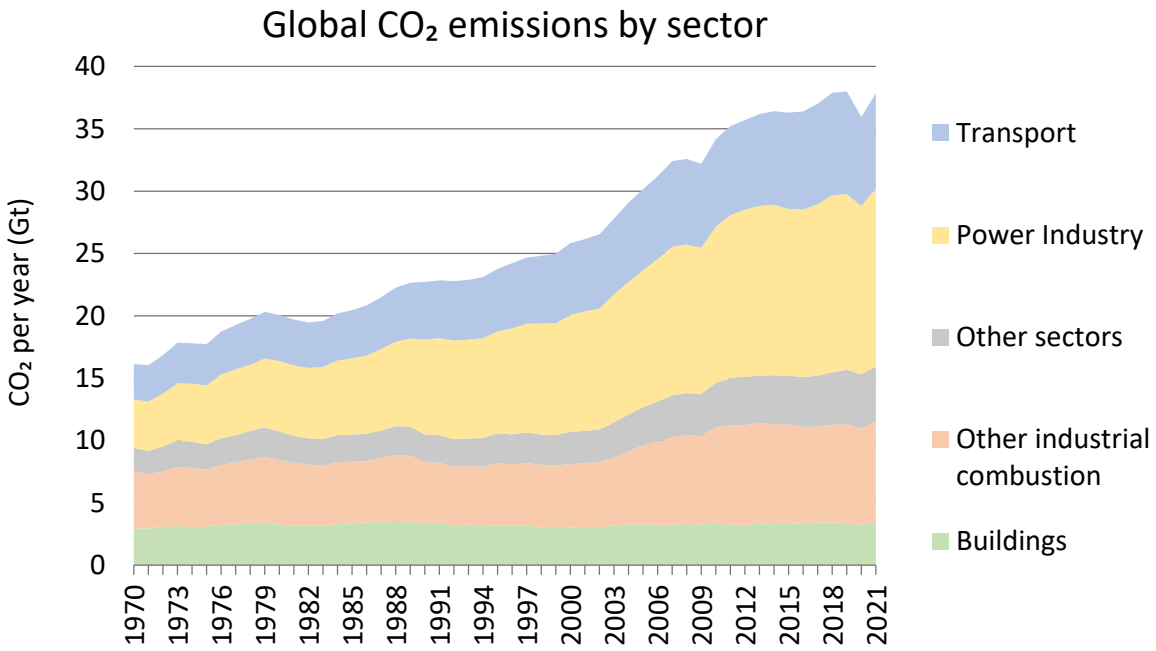

Figure 2.1. Global CO_2 emissions by sector from 1970 to 2021 (own creation with data from Crippa *et al.* [46])

In 2021, worldwide total CO_2 emissions accounted for almost 38 Gt, of which approximately 21% came from the transport sector (Figure 2.1).

The share of global CO_2 emissions from the transport sector corresponding to 2021 can be seen in Figure 2.2, created with data from Statista [48]. According to Figure 2.2, Asia and Oceania were the biggest emitters of CO_2 emissions from transportation (i.e., 2,490 million metric tons

of CO_2), followed by North America, Europe, Central and South America and Africa. However, looking at CO_2 emissions at the country level, The United States of America (USA) is the biggest emitter of CO_2 emissions globally, surpassing all other countries [46]. In 2021, the United States emitted 1,647 million metric tons of CO_2 [46]. On the other hand, China was responsible for almost a 40 % of total CO_2 emissions from Asia and Oceania (i.e., 0.955 million metric tons of CO_2) [46]. In Europe, Germany was the most significant contributor to CO_2 emissions from transport, followed by Czechia and the UK (i.e., 0.143, 0.114 and 0.107 million metric tons of CO_2, respectively) [7,46].

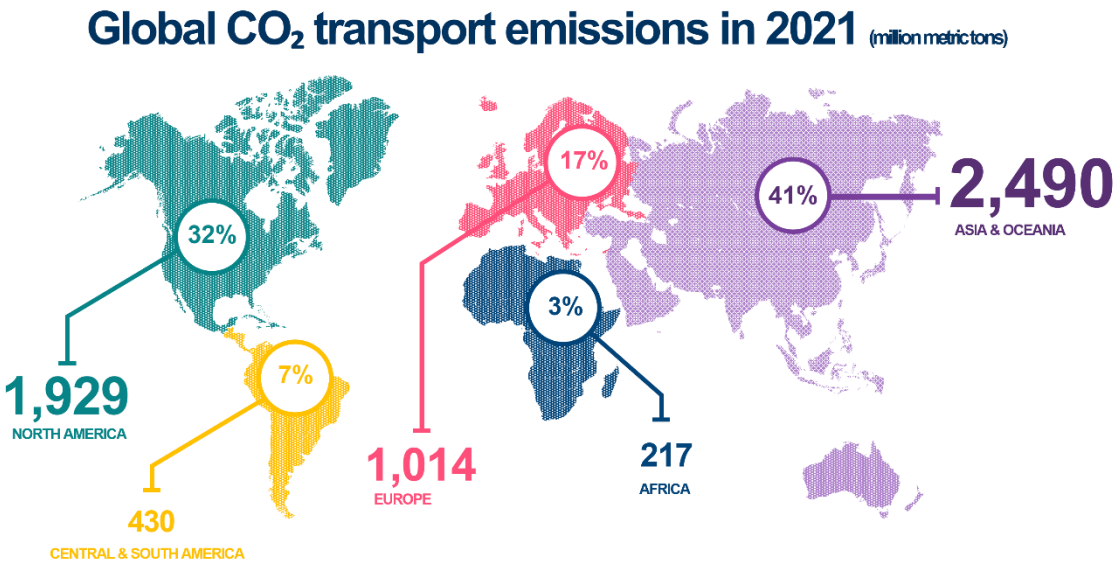

Figure 2.2. Global transport emissions in million metric tons of CO_2 and percentage corresponding to 2021 (own creation with data from Statista [48]).

Road transportation has gradually gained importance and has become responsible for the most significant proportion of GHG emissions within the transport sector [49]. In Europe, road transport is attributable to approximately 77% of total GHG emissions from transportation [50]. Multiple factors underlie the surge in GHG emissions within the road transport domain. Notably, the rapid pace of industrialisation and urbanisation has substantially influenced passenger and freight transportation density, thereby amplifying mileage [51]. Consequently, this has led to a noticeable escalation in traffic congestion, emerging as a pivotal driver of GHG emissions in road transportation [52]. Rothengatter [53] affirmed that the upsurge in vehicle numbers, driven by income growth in developed nations, has significantly impacted emissions from passenger transport. For instance, the car fleet in the UK expanded from ten cars per one thousand citizens around 1960 to more than 400 over four decades [49]. Moreover, road

infrastructure improvements have facilitated road freight transport's growth due to its flexibility compared to trains or ships [49].

The escalation GHG emissions from road transport has produced severe consequences on air quality. According to the World Health Organisation, 90% of the global population is exposed to air pollution, and it is the cause of 7 million deaths every year [54]. In Europe, transport is the only sector where emissions remain higher than in 1990. As a response, European Union (EU) policies have strategically shifted toward addressing air quality concerns, predominantly through incentivising the adoption of low-carbon emission vehicles [55]. For instance, large European cities such as Paris, Madrid, Berlin, Brussels, and London have been introducing drastic policies to curtail emissions and enhance traffic flow and accessibility to urban areas by establishing Low Emission Zones (LEZ).

In the UK, transport is the only sector where GHG emissions remain higher than in 1970, as can be seen in Figure 2.3 and it has only reduced its emissions by 4% since 1990 [4].

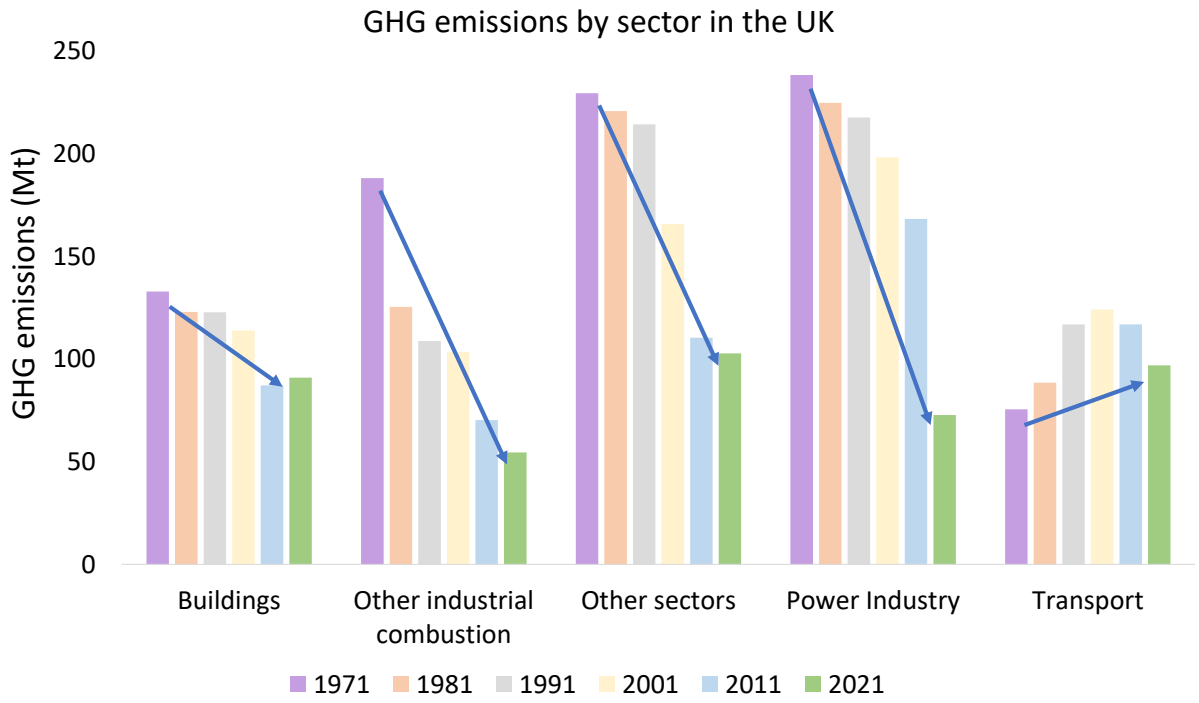

Figure 2.3. UK's GHG emissions by sector for the past 50 years (own creation with data from Crippa *et al.* [46]. The blue arrow represents the trend across the years.)

2.1.1 Road freight transport emissions in the UK

The most recent data on GHG emission by transport mode, in the UK, corresponds to the year 2020. As it is shown in Figure 2.4, in that year, the total GHG transport emissions in the UK were 99 $MtCO_2eq$. In 2021, when the restrictions from Covid-19 were lifted, the GHG emissions increased to 105 $MtCO_2eq$ [34].

The majority of GHG emissions (i.e., 89.6%) came from road vehicles. The biggest contributors to this were cars and taxis, which made up 52% of the emissions from domestic transport (51.8 $MtCO_2eq.$), Heavy Goods Vehicles (HGVs) (19% of domestic transport emissions, 18.6 $MtCO_2eq.$) and Light Commercial Vehicles (LCV) (16% of emissions, 16 $MtCO_2eq.$) [7].

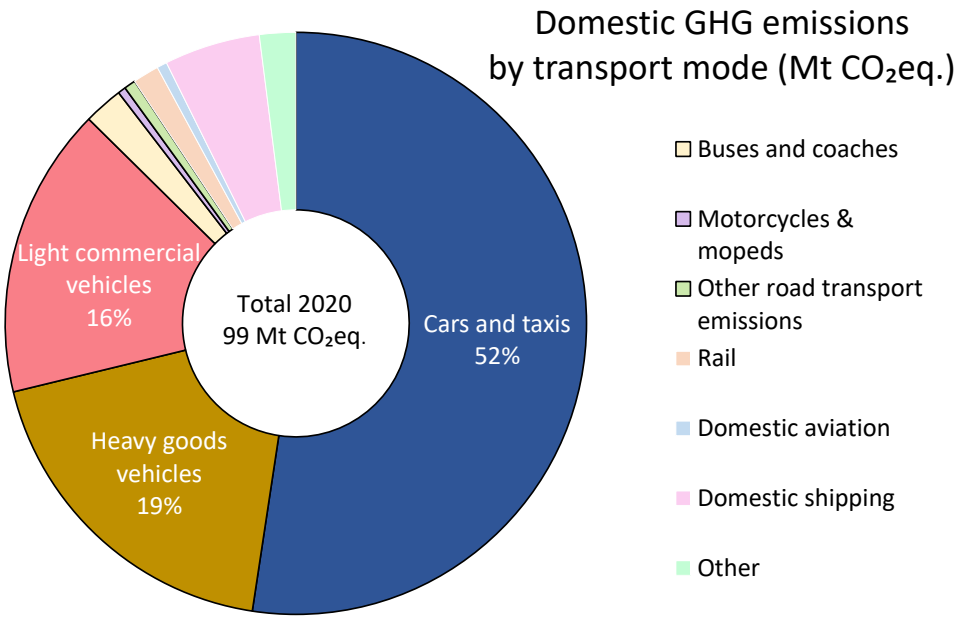

Figure 2.4. UK's domestic GHG emissions by transport mode in 2020 (own creation with data from the UK Department for Transport [7]). Bordered sections highlight road transport modes.

Road is the most popular mode of freight transport due to its flexibility and ease of access along the supply chain, door-to-door and last-mile delivery. In 2020, it accounted for 77% of all domestic freight moved in the UK [56]. However, freight transportation has a massive impact on air quality [7,8]. Whilst road freight transport is the main target under LEZ policies [57], it is also the sector that provides significant benefit to the country's economy. It contributes £13.6 billion to the UK economy and employs over 289,000 individuals [58].

LCVs are the only road-type freight vehicle that has increased GHG emissions since 1990 [7]. Partly because the number of licensed LCVs has almost doubled [7]. The increase in GHG emissions and distance travelled by this mode of road freight transport can be seen in Figure 2.5. The expansion of this mode of transportation can be attributed to the rise in online retail home deliveries and the flourishing sectors reliant on van utilisation[59], and this is expected to continue growing in the following years. Currently, vans are essential for many SMEs (Small and medium-sized enterprises) and are used daily. In fact, due to its impact on urban air quality, the van sector has been one of the main targets under LEZ policies to reduce emissions [9]. LEZs have already been imposed in many UK towns and cities, pushing the van sector towards electrification.

On the other hand, emissions from HGVs present an almost flattened trend, although overall the emissions have been reduced from 21.2 $MtCO_2eq.$ to 18.6 $MtCO_2eq.$ since 1990. As it is shown in Figure 2.5 and contrary to LCVs, the distance travelled by HGVs has been constant over time. However, the relation between GHG emissions and distance travelled by both modes of road freight transportation is significant. In comparison, HGV emissions are disproportionally higher when compared with miles travelled. The main reason for this is that smaller vehicles tend to have better fuel efficiency and, HGVs usually transport heavier goods over longer distances [7].

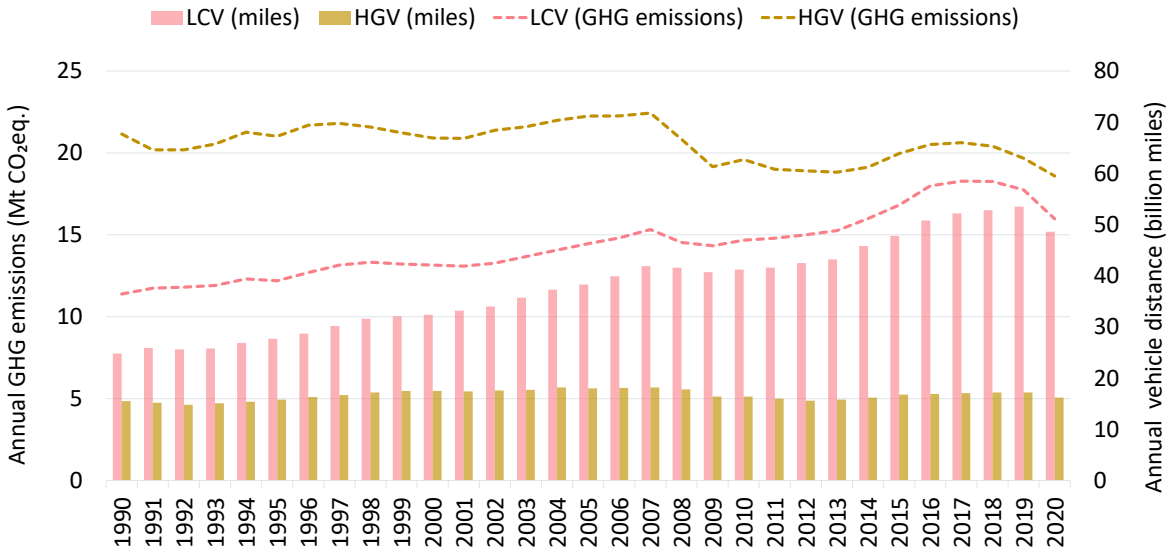

Figure 2.5. Road freight transport emissions (dashed lines) compared to the annual distance travelled (block charts) from 1990 to 2020 (own creation with data from the UK Department for Transport [7,60])

2.1.2 Impact of the carbon intensity of the electricity grid mix on the transport electrification.

The uplift of Covid-19 pandemic restrictions entailed a significant increase in GHG emissions in 2021 compared with 2020 due to increased emissions from road transport, energy and residential sectors [4]. However, when compared to 1990's levels, emissions have been reduced in the UK by 47.6%, according to the last statistical data released corresponding to 2021 [4]. The comprehensive decline can be ascribed to the diminished coal and gas electricity generation, accompanied by the heightened adoption of renewable energy sources within the power sector. Notably, the distribution of electricity generation across various fuel categories has undergone substantial shifts over the past decade. Renewables-based electricity generation has surged by 30%, aligning with a commensurate 28% reduction in coal, oil, and gas-based generation [61]. The UK aims to continue to decrease the emissions from the energy sector. Precisely, expectations based on the net zero target point to a reduction of emissions by up to 76% by 2030 and 85% by 2035, compared to 2019 levels [38].

Whereas the power sector reduces the share of electricity supplied by fossil fuels, the uptake of electric vehicles has been snowballing in the past years. Amidst the Covid-19 pandemic, 2021 saw a worldwide new EV registration record of 6.6 million [62]. Moreover, it is estimated that by 2030, the total number of EVs in circulation worldwide will soar to 145 million [62]. According to predictions, this number could represent around 30% of the total vehicles sold globally by 2030. However, it must still catch up to the 60% needed by 2030 to achieve net zero worldwide by 2050 [62]. From the road freight transport perspective, EV market penetration is progressing more slowly than expected [63]. In fact, the market for BEVs (battery electric vehicles) has shown a lack of growth in most established automotive markets [64] with some exceptions such as Norway and the Netherlands [65]. China and Europe are in the lead on sales of electric light commercial vehicles (LCV) that in 2021 increased by over 70%. On the other hand, 4% of the global fleet of buses and only 0.1% of heavy goods vehicles (HGV) are electric [62].

In the UK, the number of battery electric HGVs (eHGV) and electric LCVs (eLCV) registered for the first time has increased noticeably between 2020 and 2021. Concretely, eHGVs new registrations have increased by 800%, from 16 registered in 2020 to 145 in 2021 [66]. Similarly, eLCVs new registrations increased from 2020 to 2021 although to a lesser extent by 129%; from 5,707 new registrations in 2020 to 13,048 in 2021 [66]. Despite the remarkable

increased in eHGVs and eLCVs, these vehicles only account for 0.07% and 6% of all new road battery electric vehicles registered in 2021, respectively [66]. While it is true that the electrification of road freight transport is happening at a slower pace when compared to private cars, a substantial increase in EV adoption from road freight transport is expected in the coming years as a result of net zero policies.

However, as it was discussed in the introduction chapter, simply transitioning to BEVs alone won't be sufficient to diminish the environmental impact of the road freight transport unless the carbon intensity of the electricity grid mix is reduced to zero [17]. In this regard, different authors have been exploring the impact of charging the EVs from different energy sources. A study conducted by Saber *et al.* [67] demonstrated that utilising wind and solar energy instead of conventional power resulted in an 8 tonnes reduction in annual GHG emissions per electric vehicle (EV). A case study based on 15 food retailing companies in the city of Berlin showed that GHG emission would be reduced approximately 96% if EVs are charged completely with renewable energies, as opposed to from energy sourced from the grid network, where the reduction is around 26%, when compared to conventional vehicles [68]. Acha *et al.* [69] conducted a comparative analysis of various vehicle types, encompassing ICE (internal combustion engine), HEV (hybrid electric vehicle), PHEV (Plug-in hybrid), and BEV (battery electric vehicle). The study assessed the environmental impact of using petrol to power ICE and HEV vehicles versus employing coal to generate electricity to charge PHEVs and BEVs. The findings underscored that EVs, and PHEVs can exhibit adverse environmental effects when charged with non-renewable energy sources. The study further emphasised the necessity for the UK grid mix to curtail its carbon footprint and proactively promote renewable energy sources to substantiate the viability of EVs as a sustainable alternative for minimising CO_2 emissions.

Figure 2.6 compares the impact on GHG emissions when an EV fleet is charged from the grid and when it is charged using only solar energy in the UK. For that purpose, the breakdown of electricity supplied by the grid network is presented for 2010, 2020 and 2050 at the bottom of Figure 2.6. The share of electricity supplied by the grid mix in 2010 and 2020 has been obtained from the Department for Business, Energy & Industrial Strategy (BEIS) [61]. Whereas the breakdown of electricity from the grid for the year 2050 has been calculated assuming complete decarbonisation of the power sector. In accordance, the UK carbon intensity from the grid mix

and solar energy in 2050 has been calculated considering the predictions on emissions from the power sector [38] and on electricity demand [70].

The GHG emissions associated with the charging of an EV fleet can be seen at the top of Figure 2.6 in grey colour, when the fleet is charged from the grid at each specific year and, in yellow colour when it is charged from solar energy. The GHG conversion factors to estimate GHG emissions from the grid mix in 2010 and 2020 have been obtained from the UK Government [71]. The conversion factors to estimate GHG emissions from the solar energy generation has been obtained from Stamford *et al.*[72] for 2010 and, from GaBi LCA Database documentation [73] for emissions in 2020. The reduction in GHG emissions from charging an EV fleet with solar energy between 2010 and 2020 corresponds to a reduction in emissions associated with the energy consumed in PV panels manufacturing [74].

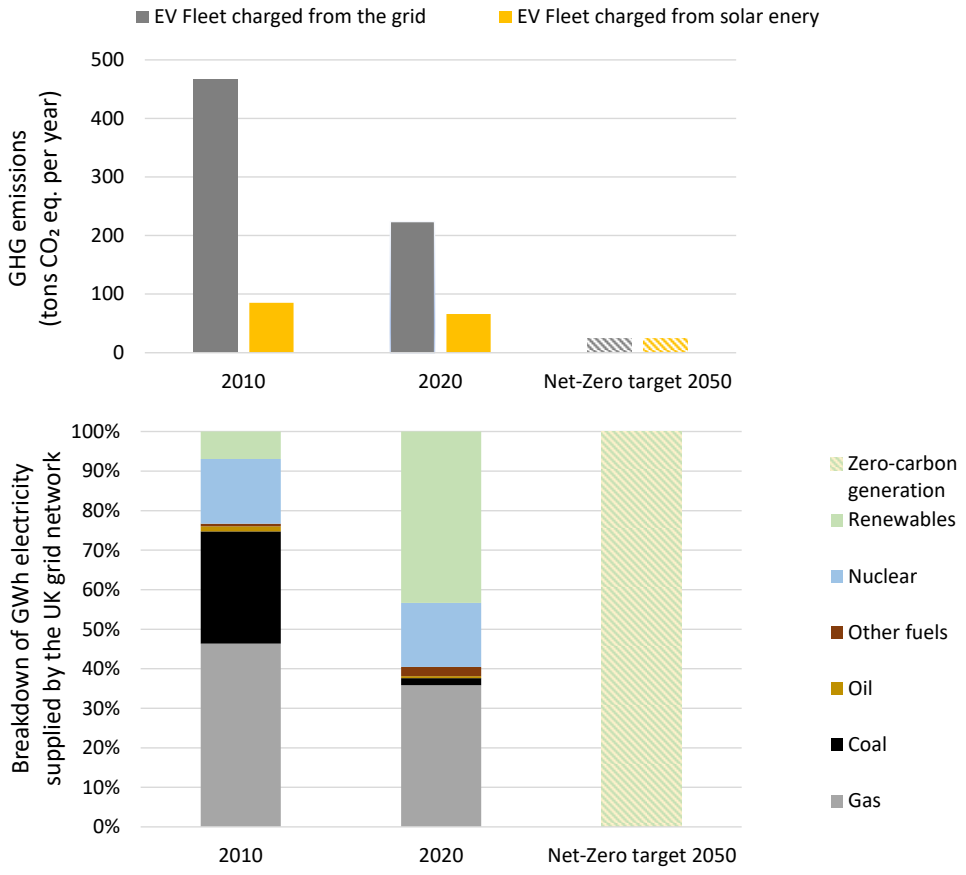

Figure 2.6. Top graph: GHG emissions released by an EV fleet when charged from the grid (grey bars) and from solar energy (yellow bars). Bottom graph: Breakdown of grid electricity supplied by the UK grid network in 2010, 2020 and 2050 by energy source.

The analysis assumes that the GHG impact in 2050 will be similar in both scenarios (i.e., grid mix and solar installation), assuming complete decarbonisation of the power sector. Until then,

the differences in GHG emissions when the EV fleet is charged from solar energy are remarkable. In 2010, when the grid mix distribution was governed by using fossil fuels to generate electricity, charging an EV fleet from the grid mix meant almost five hundred tons of CO_2eq. per year released to the atmosphere, whereas charging the same fleet from solar energy emitted less than one hundred tons of CO_2eq. per year. Despite the increased use of low-carbon sources in the grid mix in 2020, there is still a 70% reduction in GHG emissions when the EV fleet is charged with solar energy. The GHG emissions an EV fleet releases are highly dependent on the energy generation mix when charging [75].In light of this, it is essential to prioritise the use of renewable energies to maximise the benefits of transport electrification.

Despite the increased number of policies in Europe and the UK encouraging the electrification of short-haul HGV fleets, insufficient research has been done to explore strategies for planning the electrification of HGVs, according to some authors such as Danese *et al.*[76] and Borlaug *et al.*[77]. However, despite the need for more research in this field, some authors have demonstrated the feasibility of HGVs fleet electrification [78]. Large logistic companies will be the early adopters in the short term due to their greater capacity to invest in innovative technologies. However, in the long term, small companies are expected to electrify their fleet to comply with net-zero policies.

2.2 Electric freight fleet charging

The proportion of EVs globally for freight transportation is relatively modest compared to private cars, and one reason for that is the availability of charging infrastructure [79]. Fleet operators have mentioned that the greatest challenges they face in fleet electrification are associated with grid capacity, connection upgrading, associated infrastructure costs, and planning permission issues on leasehold properties [80]. So consequently, it is necessary to perform an extensive review of the literature available on EV fleet charging, considering the environmental benefits of using renewable energies for charging and the current challenges that fleet and transport operators face regarding road freight electrification.

2.2.1 Charging infrastructure

For electric freight fleets to become competitive with other alternatives, it is crucial to consider their charging infrastructure [81]. However, provision of charging infrasture is a complicated task that involves various stakeholders [82]. These stakeholders include those in the energy

supply sector, who are responsible for distribution infrastructure and selling electricity, as well as those who facilitate charging services for end-users [83].

In their investigation, Skippon *et al.* [84] interviewed car and van fleet operators in the UK, specifically focusing on sectors like waste management and property refurbishment. The primary objective was to assess the likelihood of companies embracing electric vehicles (EVs) and their envisaged charging approach. The study findings revealed that, in the event of a fleet transition to EVs, a home-based charging infrastructure would be imperative. This observation highlights the interplay between business nature and the viability of depot-based charging. When the workplace is based on a distributed set of locations, it complicates depot-based charging opportunities [84].

Generally, the lack of available charging infrastructure is a disincentive for the uptake of EVs [64,85]. This was highlighted by Amazon's Director of Global Fleet and Products who emphasised the challenges associated with EV charging infrastructure in the company's decarbonisation strategy [86] as it strives to achieve a 50% reduction in net carbon emissions for all shipments by 2030 [87]. Likewise, the capital investment required [65], mainly when the current power connections are inadequate to meet the EV fleet's charging needs during off-peak hours at the depot, and companies are obligated to upgrade their utility grid connections themselves [88,89] further discourages EV adoption. In fact, the adoption of electric fleets implies an increase in demand [90] on the depot's electricity supply [91], that in-turn requires in many cases an upgrade of the network connection to ensure this demand is met [92].

Pelletier *et al.* [93] discusses different options for EV fleet charging infrastructure, within the commercial sector. They evaluate the combination of charging at the depot, at the customer location or at a public charging station as feasible ways forward for EV fleet charging. Public charging stations are essential for deploying eLCV and eHGV fleets, especially for fleets that perform frequent long-distance trips [94]. According to a study performed by Topsector Logistiek [95], 17,000 charging points consisting of a combination of home charging, depot charging, public charging and customer location charging points would be needed to support the electrification of road freight transport in the city of Amsterdam alone. Along the same line, the European Automobile Manufacturers' Association (ACEA) [96] estimated that approximately 300,000 charging points (i.e., private and public) would be required by 2030 to support the EU's electric freight fleets market.

Many authors have assessed the electrification potential of road freight fleets using public charging. The results obtained by Liimatainen *et al.*[97] confirmed the hypothesis related to the importance of having access to on-road fast-charging infrastructure to increase the potential electrification of road freight trucks. Regarding short-distance trips, most short-haul electric truck charging is expected to be carried out at depots. Nevertheless, a network of public charging stations is still required to support the adequate function of the road freight fleet. Powar *et al.*[98] focused the study on HGVs that perform short-distance routes (i.e., up to 200 miles). The authors focused deeply on the benefits of using DC networks to accomplish the charging, using PV panels and battery energy storage systems (BESS), instead of traditional AC networks. The authors assumed the fleet would arrive at the charging station with a 30% state of charge (SoC) and leave with up to 80%. The HGVs were assumed to be charged using extra-fast chargers, assuming it would take 40-70 minutes to charge the battery fully.

Whitehead *et al.*[79] found that a modest number of public charging stations would be enough to facilitate the operations of electric trucks in the South-East Queensland region of Australia. In addition, the availability of public and on-road charging stations reduces driver range anxiety by providing emergency charging opportunities. Thus, increased public charging stations could boost market confidence in road freight transport electrification.

The routing issues have been investigated, especially for those EV fleets with limited autonomy that would benefit from recharging at public stations at different points along the route. Felipe *et al.* [99] proposed heuristic algorithms to analyse technologies and energy savings on en-route charging. Schneider *et al.*[100] research study proposed an algorithm and also incorporated operational and logistic constraints into the routing problem, such as limited freight capacities and customer time windows. Along the same lines, Goeke *et al.*[101] considered technicalities such as speed, gradient and cargo distribution to create an energy consumption model to achieve accurate outputs on routing optimisation. Hiermann *et al.* [102] included the customer location as an en-route charging point and found that an optimised route could be achieved if a fleet mix of freight vehicles is considered. More recent studies on en route optimisation based on public charging include the work by Montoya *et al.*[103], Pelletier *et al.*[104], Schiffer *et al.*[78], Raeesi *et al.*[105], or Erdelić *et al.*[106], amongst others.

The routing problem has received extensive attention over the past decade for the electrification of freight fleets. On the contrary, the issue of depot charging and its scheduling has received less attention [29]. Despite this, depot charging is still reported as the preferred location to

charge an EV freight fleet [107–109] due to operational barriers such as the risk of queuing and the possible cargo security concerns associated with public charging stations [29,65]. Depot charging serves as the prevailing charging approach for EV commercial fleets delivering in urban areas or electric trucks with short-range routes (<300 km/day), often overnight if it is compatible with freight operations, as it reduces electricity costs [62,93,108]. The results obtained from Betz *et al.*[108] show that depot charging is the preferred location for urban commercial fleets performing deliveries in and around the city mainly because the EVs battery capacity provides enough range for the fleet to return to the depot to be charged at the end of the shift due to the proximity between the area of operation and the company depot. In addition, charging EV fleets at the depot during designated times of the day could lead to reduced energy expenses by taking advantage of discounted commercial off-peak electricity rates. However, implementing charging points at commercial depot sites is still far behind expectations, even considering the positive opportunities associated with EVs for the commercial sector due to barriers such as power connection upgrade costs [110].

Easy access to depot charging infrastructure is vital to prevent delivery disruptions associated with EVs, which can hinder electric freight fleet adoption and their sustained usage [111]. Despite the challenges associated with EV charging infrastructure for freight operations, such as initial high costs, deploying adequate charging infrastructure will be essential in achieving a sustainable and inclusive electrification of road freight transport [76].

Rosenberg *et al.*[28] studied the integration of different electric road freight vehicles with the grid and its trend based on future scenarios (i.e., 2030 and 2050). The authors assumed that HGVs would be charged overnight, whereas small trucks were assumed to be charged in shorter periods using fast chargers. Furthermore, these events were assumed to occur in time windows of between 45-90 minutes due to alignment with mandatory breaks for HGV drivers [112].

Borlaug *et al.* [77] explored the electrification for HGVs that perform routes shorter than 200 miles assuming that vehicles would be charged at a depot. The authors found that, for the three freight fleets studied, electrification is feasible through depot charging alone and at power levels lower than 100 kW per vehicle. Moreover, Borlaug *et al.* [77] found that fleets characterised for having regular operating schedules and extended periods of downtime could benefit the most from structuring the charging pattern to reduce energy costs at the same time the impact on the grid is minimised.

However, according to Teoh [81], relying solely on pre-planned charging schedules, typically at depot locations, poses a significant risk. He suggests to also incorporate charging strategies based on last-minute charging decisions made by drivers, to avoid issues related to range anxiety or inadequate battery capacity in the presence of congestion or long queues at customer sites. However, logistic operations are typically defined by the existence of planned routes and schedules. While drivers may make spontaneous decisions, it is unlikely that they would need to charge the eHGV or eLCV during the route if the EV battery capacity is sufficient to allow for a round trip from the depot, even in the event of unexpected issues or delays along the way.

2.2.2 Charging strategies

Some advantages to planning HGVs electrification, particularly in short or mid-haul, are the well-established demand patterns that can be reliably forecast over an extended period [78,113]. However, planning HGVs electrification is sometimes a difficult task when customer demand doesn't remain stable over a near-term planning horizon [78]. Furthermore, the time required to charge HGVs, assuming a battery size bigger than 300 kWh, is another major obstacle to their electrification [76] that could sometimes result in lost revenue [114]. Deciding between using a heavier battery to increase range freedom while decreasing cargo weight [77], or opting for a lighter battery presents a trade-off that must be carefully considered [114]. In this regard, the charging strategy plays a key role, and finding a reliable charging strategy is of paramount importance, and is one of the major concerns for transport operators when they decide to electrify their fleet [109]. Ideally, a good charging strategy would ensure that their daily operations are meet while also minimising costs [95].

The charging pattern needs to be tailored to meet the economic and operational needs of the transport operation. Specifically, in terms of operations, the charging strategy will impact the daily driving distance and the operational timetable [81]. Part of that strategy relies on the charging time that its dependant on the type of charger. The commercial classification of charger types are as follows Table 2.1:

Table 2.1. Commercial classification of charger types

Type	Connector type	Power rating (kW)	Average charging time
Slow charging	AC type 1 & 2	3	12 hours
		7	6-8 hours
		22	3 hours
Rapid charging	DC CHAdeMO	50-100	40 mins
Ultra-rapid charging	CCS	50-350	20 mins

In [81], the author divides the charging strategies into three categories: downtime charging also known as overnight charging, opportunity charging, and intrusive charging.

Downtime charging is one of the most widespread charging strategies that take place outside of the fleet's operating hours and, compared to other strategies, is relatively simple to implement [81]. The ability to charge the fleet during periods of inactivity enables longer charging times, making it easier to reduce the power required to charge the fleet fully. In this case, slow charging modes are used with chargers rated at 22 kW. However, the timings and durations of the downtime charging are dependent on the logistic and operational requirements. In this regard, it is very common to charge the fleet overnight at the depot [115]. Moreover, overnight depot charging takes advantage of lower electricity prices from the grid compared to using public chargers, and simplifies the route planning [109]. Overall, as long as the daily operations of the company can be accomplished within the driving range of the EV battery, overnight charging has been proven to be the most economically efficient charging strategy [95].

On the other hand, opportunity charging entails the fundamental principle that the requirement to charge the vehicle does not alter the operational requirements. It is expected that the charging activity takes place while the driver is performing the required transportation tasks (i.e., loading, unloading or having a break) [81] and subsequently using high-capacity chargers (i.e., 50 kW or higher) [109] that allows the vehicle to be charged en-route in a shorter time. One of the main disadvantages of opportunity charging is the higher electricity costs compared to the downtime charging strategy and the difficulties in integrating charging on daily routes without negatively impacting operational requirements [109]. However, opportunity charging might be

worthwhile to implement in routes that exceed the EV battery range (i.e., long-haul transport fleets) [63,109]. The study Taefi *et al.* [116] presented could serve as an example of opportunity charging. The author assumes the vehicle is charged simultaneously with goods being loaded/unloaded or during driver breaks. Implicit to such assumptions is the required availability of fast charging at customer locations or parking, and the consequences that fast charging has on EV battery degradation [117]. Moreover, there are some possibilities to have available spaces for fast charging in public charging stations specially for freight vehicles [65]. According to Nicolaides *et al.* [33], electric refuse collection vehicles (eRCV) could benefit from opportunity charging; in a period of 30 minutes, while unloading, the eRCV could be fully charged using a 50 kW charging station. Kin *et al.*[109] extensively explored opportunity charging and its feasibility as an alternative to facilitate freight transport electrification. For that purpose, the authors explored vehicle fleets with different operational profiles with an average daily distance between 107 km for large vans, 135 km for small trucks and 121 km for small vans. Some of the key insights from the study were that opportunity charging is easier to implement in companies with LCV fleets, as for this type of freight fleet, there is more availability of high-capacity charging stations than for HGV fleets. Fleets operating within rural areas also find it challenging to adhere to the opportunity charging strategy because of the difficulty of finding high-capacity charging stations. If high capacity charging stations are available, opportunity charging is a more profitable strategy for HGV fleets due to the remarkable difference in cost between smaller and bigger EV batteries. Authors conclude that opportunity charging has to be well integrated. It has to come with high-capacity charging stations and a reservation system at charging points to avoid queuing.

As opposed to opportunity charging, intrusive charging interrupts transport operations to facilitate charging events [81]. One of the main disadvantages of intrusive charging is the queuing time on public charging stations that is worsened by the limited availability of charging stations and the extended time required to charge the vehicle [65]. So, whereas the range time can be increased using this charging strategy, the operational efficiency is reduced.

There are different strategies for EV fleet charging, compatible with different operational and logistic requirements. Moreover, the charging strategy selected impacts on when and how much charging is required, and consequently, this has consequences on infrastructure availability [65,118] or grid infrastructure constraints [114]. In fact, the growing adoption of EVs and the resulting increase in demand for charging could potentially compromise the

stability and dependability of the power system. Smart charging or vehicle-to-grid (V2G) strategies have been used extensively to ease the penetration of EV fleets. Smart charging seeks to provide technical benefits (i.e., avoiding the saturations of transformers) and economic benefits (i.e., minimising electricity costs) by optimising charging [119]. Thus, smart charging becomes unavoidable when there is high penetration of EV fleets [75,118]. V2G on the other hand, has been extensively used to balance the grid demand or peak shaving due to the flexibility EVs have to offer [120]. However, one of its disadvantages is the degradation of batteries and the energy losses during their operation [119,121]. EVs have also been used as a mass energy storage system to mitigate intermittent renewable energy generation, allowing the EV fleets better integrate the transport and power systems. [121–123]

Over the last decade, many of the smart charging algorithms proposed by the scientific community explore the economics of electrification and aim to maximise economic benefits of fleet electrification [75,113,119]. For example, by adapting the charging time to the lowest electricity prices [120] to reduce overall cost of charging a vehicle. An example of those algorithms can be found in [124] and [125]. CO_2 emission reduction is another popular reason for using smart charging; Hoehne *et al.*[126] study provides an example. Their findings suggested that EV emissions associated with charging could be noteacebly reduced by adjusting user's charging behaviour. For example, by charging the EVs at time when the grid's carbon intensity is reduced (i.e., charging during day hours instead of at night time). However, in agreement with Tortós *et al.* [121], Hoehne *et al.*[126] stated that encouraging EV fleet transport operators or drivers to modify their charging behaviour would probably involve providing subsidies to energy generators or the users themselves. Smart charging is also used to mitigate grid power issues when it comes to EV fleet electrification [127,128]. In fact, EV fleets can be used to provide frequency response services [120]. According to Blatiak *et al.* [120] frequency response seems to preserve the battery life of an EV better than when compared to V2G services. Moreover, in one of their studies, Blatiak *et al.* [120] compared the outcomes of different charging strategies, using smart charging strategies (i.e., charge the commercial fleet at low electricity prices), and frequency response. The study demonstrated that fleets with adaptable routes that take part in frequency response services could potentially boost their profits by as much as 38% during the summer and 12% during the winter. The benefits in profits of introducing optimal charging in summer compared to winter is due to the increase of solar output.

Somehow, EVs could serve as a link to connect transport and energy sectors. In fact, the correct operation between both sectors is crucial to facilitate the adoption of EVs.

2.3 Energy and transport systems integration to facilitate the adoption of EV fleets

The energy and transport sectors share the same objective towards a net zero future, complete system decarbonisation, yet they are not well coordinated [129]. Considering the predictions from industry analysts on the increase in number of LCVs and consequently, their requirements for charging points, the power supply grid and the transport systems need to be well coordinated since EV charging connects them both.

EVs have been researched extensively across various domains and viewpoints. In terms of their interface with the power grid, two established areas of study have emerged: power systems stability / availability, and transportation studies. However, as transport becomes increasingly electrified, it is essential to consider the synergies and conflicts between the power system and the transportation requirements. In fact, when exploring the use of V2G, the majority of studies focus on the power system perspective, and most lack consideration of operational and logistic constraints. Similarly, a different area of study exists that deals with the same concerns but excludes important aspects of power system, the vehicle routing problem. The vehicle routing problem is tailored to EVs and is concerned with EV usage efficiency based on different driving patterns, with the focus on finding the optimal route rather than determining the most effective charging strategy, which is observed on power system related studies. This means that EV charging electrification is either explored from the power system operation perspective (i.e., power system research field) or from the logistic and operations perspective as seen in the transport studies field.

In their study to understand the interconnection between transport and power sectors, Quirós-Tortós *et al.* [121] estimate that by 2030, approximately 10% of EVs will be available daily through V2G to help the grid to maintain the balance between demand and generation. The authors concluded that the extent to which EVs can potentially provide grid services would be directly linked to EV users' benefits. In this regard, EV charging management is required to ensure effective and safe use of the power grid. However, certain practices to solve technical issues might cause rapid degradation of the EV battery. For example, in [121], the EVs are disconnected from the electricity source when the modelled system detects a thermal or voltage problem on the grid. Then, the EVs are connected again when it is technically safe. For that to happen, the management system first disconnects the EVs that have been connected for longer

times, assuming the more prolonged the connection time, the higher the SoC of the EV battery. On the other hand, the EVs that have been disconnected for longer times have the priority to be connected to the network once it is technically safe to do so. The experiment results showed that this approach effectively mitigated network issues; however, to avoid rapid degradation and thus preserve a good state of the EV's battery health, the EV should be connected to a minimum uninterrupted charging time of 15 minutes before disconnection occurs.

The different charging patterns scenarios, considering when and how the fleets are charged, impact the power grid. In a pioneering study accomplished in the UK to understand the EV fleet's impact on the grid, authors found that uncontrolled charging could lead to extra pressure on the power system [121]. Moreover, it was found that the transformer capacity would likely be exceeded with an EV penetration of 40%. In the event of a higher EV penetration (i.e., 90%), the low-voltage network might face voltage constraints, which in-turn would impact charging. Therefore, effective management of EV charging seems necessary to ensure the adequate integration of transport and power systems. However, further consideration is required regarding charging constraints by, for example, asking EV users to charge the EVs during off-peak hours as it might affect EV adoption [98].

Rosenberg *et al.*[28] tried to connect both sectors (i.e., transport and power) through a combination of models for energy supply and road freight transport. The authors used the output from the combination of models to analyse road freight transport's impacts on the power system on the path towards net zero. As a result, the authors concluded that the electrification of road freight transport is feasible in Norway and would not trigger a negative impact on the power system.

Bradley *et al.*[114] explored the electrification of HGVs in southern California to determine optimum charging station placement and provide suggestions to policymakers to encourage the adoption of electric trucks amongst transport operators and fleet managers. The results indicate that charging overnight would be the most optimal solution because it meets the HGVs' charging needs and prevents the fleet from wasting time in the middle of the operation. Moreover, authors concluded that the grid capacity is a constraint to replacing conventional with electric HGVs due to each vehicle's energy requirements.

Many authors have flagged the issue associated with the power connection capacity at the charging station. Schmidt *et al.*[63] addressed the feasibility of commercial fleet electrification

while taking into account the technical constraints of the vehicles themselves (such as driving range) and the charging infrastructure (including factors like charging capacity and station availability). The aim of the study [63] was to offer insights into the types of fleet mobility patterns that could derive advantages from different charging scheduling strategies to extrapolate these findings to a broader spectrum of commercial fleet applications. Results showed that commercial fleet electrification is technically feasible. For example, fleets with routes higher than 81 km successfully managed to keep the minimal power capacity connection required to provide continuous operation by first charging vehicles with the lowest SOC. However, this approach would require on-site personnel to allocate the vehicles to the charging stations unless the system is automated. On the other hand, results show that 73% of the studied fleets benefit from a predicted or planned charging event, compared to a first-come-first-served charging strategy, as it increases the number of successful trips. The results are in line with the conclusions presented by Kin *et al.*[109] if opportunity charging is the strategy selected by transport fleet operators; planned charging events that facilitates a slot reservation at charging points is essential.

Despite the valuable outcomes, the study of Schmidt *et al.*[63] it does have certain limitations. Regarding power connection capacity, the authors' approach involved utilising the minimum necessary power connection capacity to ensure uninterrupted operations. Consequently, the study's findings apply to commercial or logistic companies involving light commercial vehicles. However, the applicability becomes constrained when considering heavy-duty vehicles with larger battery capacities (i.e., those used for waste management), as the power required would be higher, owing to the need for higher power chargers.

Kin *et al.*[109] explored the techno-operational and financial feasibility for fleet electrification for a wider variety of commercial vehicles. Amongst others, the study investigated the feasibility of electrifying small trucks with a 200 kWh battery capacity. It is pertinent to note that detailed technical specifications concerning power connection were omitted, given the specific focus on case study insights. Nonetheless, the authors drew attention to the concern of power connection capacity within the local grid, particularly in charging heavy-duty vehicles (HGVs) at depot facilities.

A more technically orientated research paper by Pelletier *et al.* [29] on EV fleet charging strategies aims at providing an optimisation tool for depot charge scheduling considering different constraints such as maximum power retrieved from the grid to charge the vehicles.

Two maximum powers are considered, 20 kW and 500 kW. The latter allows the fleet of 5, 10 and 15 medium duty electric trucks to be charged. Although the authors of the study do not specify, the tonnage associated with medium duty electric trucks is between 4 to 12 tonnes. When the power connection capacity is reduced, the fleet size has to be limited to five vehicles otherwise, the charging power required would surpass the maximum allowable (i.e., 20 kW). Moreover, results indicate that introducing power grid limitations renders fleet charging unviable for one of the scenarios. The authors concluded that limiting the power grid connection capacity could lead to a substantial rise in energy costs under certain circumstances.

The studies analysed are examples of research papers advising of the consequences or implications that a limitation on the grid power connection would have when it comes to electrify a fleet. Moreover, there are some uncertainties regarding HGV charging requiring more power and concentrated loads. Therefore, it is unclear what would be the costs and lead times associated with distribution system upgrades related to HGVs charging. Borlaug *et al.*[77] summarise available information from public and private reports on the cost incurred on power distribution system upgrades required for depot charging based in the United States. As a result of data gathering on costs, the authors found that as the charging demands rise, the probability of upgrades being needed at higher points in the distribution system (i.e., distribution feeders or substations) also increases. Moreover, as EV adoption continues to grow, fast charging demand is expected to increase, and it will become necessary to establish sub-transmission and transmission-level interconnections for specific stations. Hence, upgrades at both the transmission and distribution levels will likely be needed [98].

Numerous solutions investigated in existing literature have centred around two key areas: smart charging [90] and load/demand management [130]. These strategies have long been a subject of scholarly inquiry, complementing each approach. Within the realm of smart charging, the integration of load management algorithms smoothens the load profile by effectively coordinating vehicle charging processes [131]. It is worth noting that, in tandem, these approaches yield a reduction in charging costs [132,133]. These methodologies are collectively acknowledged as pivotal in curtailing costs associated with adopting electric fleets. In [77] authors found that freight fleets with consistent operating schedules and lengthy off-shift periods stand to gain the flexibility to arrange charging periods when energy prices are at their lowest (i.e., overnight). At the same time, the impacts on the grid network are reduced. Moreover, extending the charging time overnight allows for flattening the power required by

keeping a constant minimum power and reduces the peak demand by more than 80%. By doing so, the authors concluded that approximately 90% of the substations studied would be able to manage the penetration of 100 electric HGVs without the need for a distribution system upgrade. Therefore, managing charging scenarios efficiently is crucial.

2.3.1 Energy storage systems.

A complementary solution is energy storage. Energy storage has demonstrated its potential as a technology contributing towards integrating energy and transport systems when it comes to fleet electrification, particularly if renewable energies power the energy system [134]. The potential advantages of combining energy storage with renewable energy generation depend highly on the localised energy management approach. It gains importance when EV fleets are included in the system due to their operational schedules and the available charging infrastructure on their planned routes [135]. Researchers have extensively investigated energy management from various perspectives, aiming to attain improved efficiency across the distribution network, such as minimising losses in distribution systems [136,137], reducing costs by controlling the energy sources and controllable loads [135], or mitigating GHG emissions [138,139].

Betz and Lienkamp [107] developed an energy management system to evaluate the advantages of incorporating EV fleets within commercial premises. They aimed to seamlessly integrate three key technologies—PV solar energy, energy storage, and EV fleets—to curtail the total cost of ownership (TCO) and CO_2 emissions. When running the simulations, authors assumed the EV is available at the commercial site and can be used as a battery to store PV surplus solar energy. This approach eliminates the need to sell excess PV solar energy to the grid, indirectly increasing its self-consumption and making it profitable.

Compared to the overnight grid-based charging proposed by Borlaug *et al.*[77], Powar *et al.*[98] aimed at creating a grid-independent DC connection to charge an electric HGV fleet using solar energy and energy storage. The authors [98] were motivated to develop such electric architecture to alleviate the backlogs in clean energy approvals in the United States and avoid large curtailments within the traditional AC grid due to a poor transmission grid infrastructure. The charging stations were assumed to be located in urban areas with limited space for PV installations. Hence, the authors considered a remote PV installation that already exists at a distance of between 150 km and 400 km with respect to the charging station. The PV

installation was designed to balance solar generation and EV fleet demand, and the BESS was then used to supply energy at peak hours of demand during the night. The remote PV and BESS are connected to a high-voltage direct current (HVDC) transmission bus by a low-voltage direct current (LVDC) to HVDC converter station. The generated DC power is transmited with HVDC transmission and converted to medium-voltage direct current (MVDC). MVDC power is distributed to the charging stations and converted to LVDC. The results show a reduction in power loss at low, medium and high voltage levels when the proposed DC system is used, when compared to the traditional AC grid power system. The authors concluded that switching to DC networks could increase the efficiency of the power system in the event of increased demand for fast charging stations.

Pietracho *et al.*[92] assess the integration of electric vehicles into the commercial sector considering economic and environmental factors compared to conventional fleets. The study's findings indicated that, compared to conventional fleets, electric fleets report a higher Total Cost of Ownership (TCO), primarily attributed to the infrastructure investment required for charging stations. Energy storage technology can reduce costs by decreasing the consumption from the grid at peak prices. However, in some cases, this approach is not an option if the system requires a grid connection upgrade to provide energy at lower prices. In fact, when it comes to adopting EV fleets, the network upgrade is presented as a serious issue by many logistics companies [140]. Moreover, considering that the energy consumption and peak power loading from the introduction of EVs will increase significantly in commercial locations [141], it is worth exploring alternatives to reduce the costs over the system lifetime, to better suit the needs of logistics companies who are expected to charge multiple vehicles at any given time. In this regard, the electrification of transport requires a linkage between electricity and fleet operators to conduct research together to understand the practicalities of integrating fleet charging demands on the power grid, considering that both the power and transport sectors will be more interconnected as the electrification of transport increases [28,142].

Battery energy storage systems (BESS) play a vital role in the energy transition of transport and power systems. Moreover, improvements in technology and large-scale manufacturing have resulted in lithium-ion batteries becoming a worthwhile option for energy storage [98].

2.4 Solar energy and energy storage for EV fleet charging

The current energy security issues together with the environmental concerns have motivated and opened up a new push for investment in electrification and renewable energies [143]. In

fact, governments and companies looking into reducing carbon impact and oil and gas dependency, are adopting policies and guidelines that prioritise the use of renewable energies, such as REPowerEU plan [143] or the British Energy Security Strategy [144]. For the transport sector to fully decarbonise is essential the use of renewable energies. However, there are still many questions that require an answer that concerns logistic and transport operators.

Battery Energy Storage Systems (BESS) are a key technology in the transition towards sustainable energy systems. According to recent projections [145], battery energy storage in particular, is set to take centre stage as the fastest growing source to assist the power system on increasing its efficiency and resilience. In a scenario based on the use of renewable energies to charge EV fleets, the use of energy storage systems is a requirement. They not only provide reliable regulation of active and reactive power and frequency, but also overcome problems related to interruptions of transmission or distribution systems [146]. Additionally, BESS can enhance the self-sufficiency and self-consumption indicators, and increase the overall flexibility of the grid [147]. It has the potential to reduce the energy bills by purchasing power from the grid during the off-peak hours and selling it back to the network during the peak demand hours. Due to the volatile nature of renewable energies, energy storage systems enhance their integration by levelling their output fluctuations and balancing the power flow [146]. With its ability to store excess energy generated from renewable sources and discharge during peak demand, battery storage offers versatile and reliable solution not only to balancing the grid, but also increasing the potential to use renewable energies to charge EV fleets.

Several researchers have evaluated the integration of EVs and PV systems, highlighting the potential advantages arising from a synchronized charging approach that harnesses the synergies between these technologies within the grid network [148–152]. From both technical and economic standpoints, it is evident that an uncoordinated EV/PV system could lead to elevated demand during peak periods, consequently imposing additional burdens on power grids due to congestion and potential over-voltage challenges. The "duck curve" can explain it; PV generation peaks during low demand while decreasing during high demand periods. Consequently, utility companies must increase production to fill this gap, often over-stressing the grid. To that extent, a significant penetration of EVs with uncoordinated charging (i.e., charging in the evening) would increase this effect [152,153]. Chaouachi *et al.* [149] proposed a more decentralized energy grid to mitigate these adverse techno-economic repercussions. Powar *et al.*[98] proposed a grid-independent DC connection for EV fleet fast charging using

solar energy and BESS to avoid large curtailments within the traditional AC grid due to a poor transmission grid infrastructure. The proposed infrastructure solved the issue by storing the curtailed surplus energy.

Some authors have been examined the integration of localised solar energy and EV fleet charging for specific scenarios. For instance, Alvaro-Hermana *et al.* [154] presented a case wherein an EV shuttle fleet comprising four vehicles was employed to commute between an intermodal exchange station and a conference venue in Madrid. Notably, this operation strategically harnessed locally generated solar energy. The EV shuttle fleet exhibited specific driving patterns, covering approximately 3 km during the morning (from 08:00h to 09:00h) and traversing the reverse route in the evening (from 19:00h to 20:00h), with predetermined routes for both directions. The total number of trips performed was 20. All these operational requirements enabled the EV shuttle fleet to be fully charged while parked (from 09:00h until 19:00h) considering that the total energy fleet demand (i.e., 19.08 kWh) is lower than the solar energy generated (i.e., 47.3 kWh). Tulpule [148] delved into the economic and environmental aspects of EV charging at the workplace using on-site PV solar energy. The study adopted a comprehensive charging timeframe for EVs (from 06:00h to 20:00h) and integrated parking fees from EV users into the model, thereby contributing to a reduction in the PV payback period. With this approach, it was demonstrated that an optimal PV installation capacity reduces payback time, so there is no need to increase the number of PV panels to achieve maximum benefits.

Mouli *et al*, [155] developed a model for PV power installation tailored to EV charging in a workplace. The authors included energy storage systems to mitigate reliance on the grid during simultaneous EV charging instances. An evaluation of different storage capacities revealed that grid dependence ceased to decline at a specific capacity. It is noteworthy that this investigation was conducted in Norway, where substantial seasonal disparity exists between summer and winter sunlight, distinct from regions not located in the far northern latitudes. While previous studies predominantly focused on workplace EV charging during daylight hours, it is essential to recognise that commercial settings often entail overnight charging when the fleet is not operating. Consequently, when designing the PV model, charging schedule and EV range planning pertinent to commercial fleets should be considered. EV charging has been implemented at workstations, capitalising on daylight hours when the EV is parked and benefiting from sun exposure [156,157].

Clairand *et al.* [158] proposes an EV charging strategy for isolated power systems with a high penetration of renewable generation. The strategy aims on one hand to reduce the impact on the power system when a fleet of EVs are being charged and, on the other hand, to maximise the use of renewable energy. The authors based the charging strategy on mechanisms to incentivise EV owners to charge the fleet during period of low demand and high renewable generation. The study assesses different charging scenarios considering power capacity constraints. Due to the fact that energy storage is not used in this study, excess renewable energy is not used by the EV fleets. Thus, authors concluded that the addition of energy storage is needed to facilitate the integration of renewable energies by levelling their output fluctuations and balancing the power flow.

Domínguez-Navarro *et al.* [159] explore the integration of EV fleet charging with renewable energies (i.e., solar and wind) but consider adding energy storage. The authors highlight the potential benefit of integrating renewable energy and storage system in EV charging infrastructure to reduce the impact on the grid. However, the type of EVs studied were private cars and vans. Thus it is not easy to extrapolate these results to road freight fleets, which are characterised by specific operational requirements.

In the current literature, there is a lack of publications addressing the implications of using renewable energy and energy storage for EV fleet charging based on freight transport fleets (i.e., eRCV). Part of the literature reviewed addressed the use of renewable energy and energy storage focused on the implications that it has on the power system [98] using public charging stations. Others, discussed the electrification of freight vehicles using renewable energy and energy storage for depot fleet charging with certain limitations regarding technical constraints (i.e., power capacity) [63].

2.4.1 Electric Refuse Collection Vehicle (eRCV) Fleets.

In the United Kingdom, the Environmental Protection Act of 1990 mandates waste collection authorities (WCAs), typically comprising district, metropolitan, or city councils, to organize and oversee household waste collection within their respective jurisdictions [160,161]. Central to this responsibility is the establishment of collection schedules and routes, with a prevalent approach being alternate weekly collection (AWC) systems, wherein recyclable and residual waste are collected on alternating week [162,163]. Adopting such systems aims to optimize

operational efficiency while accommodating variations in external factors such as traffic flow and adverse weather conditions [162].

Waste management encompasses various processes, including collection, transportation, processing, recycling, and disposal of waste materials [164]. Central to the effectiveness of waste management systems is the optimization of vehicle tours, which play a pivotal role in facilitating waste movement from collection points to processing or disposal facilities [165]. Precisely, the logistics of waste management involves the generation of fleet tours that originate from the depot, traverse designated pickup locations to collect waste materials, make deliveries at disposal sites such as landfills or recycling centres, and ultimately return to the depot [166]. Managing waste collection fleets, particularly in the context of electric refuse collection vehicles (eRCVs), constitutes a critical aspect of modern urban waste management systems.

In recent years, there has been a notable shift towards integrating eRCVs into waste collection fleets, driven by imperatives for sustainability and environmental stewardship [167,168]. Despite the potential benefits of eRCVs in mitigating noise pollution and reducing carbon emissions, their widespread adoption poses logistical challenges, particularly concerning range limitations and charging infrastructure [168,169]. For instance, while eRCVs are equipped with oversized batteries to extend operational range and facilitate prolonged service hours, the consequent increase in energy consumption and procurement costs warrants careful consideration [169].

The operational dynamics of eRCVs differ substantially from their diesel-powered counterparts, necessitating nuanced approaches to route planning and scheduling [167,168]. In [167] authors explored the Waste Collection Vehicle Routing Problem with Time Windows (WCVRPTW) for a plug-in hybrid electric refuse collection fleet (compressed natural gas (CNG) + battery). Assumptions considered the start point of the route at the depot followed by the waste collection from customers until the vehicle is full. By then, the vehicle must go to a landfill or to a recycling point to empty its waste. After unloading, the refuse vehicle returns to its duty. In addressing this problem, authors found that plug-in hybrid electric waste collection vehicles introduce new logistical intricacies due to their limited battery or compressed natural gas (CNG) capacities, resulting in shorter driving ranges than traditional internal combustion engine (ICE) vehicles. Furthermore, the scarcity of irregular distribution of refuelling stations worsened the challenge of planning efficient routing solutions [168]. Waste management

companies must develop comprehensive strategies for route optimization and charging infrastructure deployment to ensure the viability and efficiency of eRCV operations [167,168].

Furthermore, empirical studies underscore the importance of contextual factors such as population density (e.g., city centres or rural settlements) and waste composition in shaping the operational parameters of eRCV fleets [168,169]. Variations in waste compacting cycles and energy consumption patterns highlight the need for tailored approaches to route planning [168,169]. Especially in diverse urban and rural settings, for example with high occupancy domestic flats, single-family houses distributed over a large area or clinical waste collections that require higher frequency collections. Consequently, effective waste collection management necessitates a holistic understanding of the interplay between technological capabilities, operational constraints, and environmental considerations.

A study by Ewert *et al.* [166] employs a multi-agent-based simulation methodology to assess the technical feasibility and potential economic and environmental consequences of transitioning to fully electric refuse collection vehicle (eRCV) fleets. Despite advancements in electric vehicle (EV) technology, questions persist regarding the ability of eRCVs to withstand real-world working conditions and the optimal system design parameters, including battery capacity, type, and charging technology. Central to the discussion is the critical role of battery capacity in shaping eRCV performance and cost-effectiveness. Larger batteries offer extended ranges but come with increased costs and reduced payload capacity. The selection of electric municipal vehicles must carefully balance energy consumption considerations, accounting for driving consumption and auxiliary energy usage under specific working conditions. Findings of [166] underscore the technical feasibility of electrified waste collection in urban areas and highlight opportunities to optimize battery capacity and charging strategies to enhance cost-effectiveness. By leveraging a combination of small and large battery-equipped vehicles supplemented with fast charging options, waste management operators can mitigate range limitations and maximize operational efficiency. On the other hand, the environmental benefits of eRCVs are substantial, with significant GHG emission reductions compared to internal combustion engine vehicles (ICEVs) [166].

Integrating on-site solar energy generation for EV charging remains underutilised in the waste management sector, primarily due to the obstacles impeding its development and implementation. A noteworthy challenge arises from the inherent unpredictability of renewable energy sources [170]. Specifically, solar energy, reliant on weather patterns, exhibits a

constrained timeframe of peak power production, often concentrated around midday [171,172]. Moreover, a fleet's charging strategy and operational times have an economic impact interconnected to the solar energy generation on-site. According to Nunez Munoz *et al.*[173] splitting the charging of an eRCV fleet into two-time windows (i.e., 9 out of 19 eRCVs are charged at 11:00h and the other 10 eRCVs at 23:00h) reduces the grid dependency, the total cost and the GHG emissions, when compared to overnight charging, due to the increase in solar energy usage. However, charging the fleet across two time periods affects logistics operations and vehicle scheduling. The eRCVs that are charged at 11:00h operate between 06:00h and 10:00h and then from 18:00h to 22:00h, whereas the other 10 operate within the expected pattern [162] (i.e., between 06:00h and 14:00h). It would require a change in vehicle availability, if compared to the current operations [162] where the RCVs operates continuously in the morning and are parked at the depot at night. On the other hand, modifying logistics operations due to the charging requirements might open the option for better optimization of fleet usage and route planning.

In summary, integrating eRCVs into waste collection fleets represents a pivotal advancement in sustainable urban waste management. However, realizing the full potential of eRCVs requires proactive measures to address logistical challenges, optimize operational practices, and ensure alignment with broader sustainability objectives.

2.5 Research gap

Throughout the revision of the literature, it was shown that charging EV fleets with renewable energy sources is of paramount importance for achieving a sustainable transportation system. With the increasing adoption of EVs for road transportation and, in particular of eLCVs and eHGVs within the freight transport sector, there is a pressing need to shift away from traditional fossil fuel based charging systems towards cleaner and more efficient alternatives. By using renewable energy sources such as solar power to charge EV fleets, GHG and CO_2 emissions can be significantly reduced over the short and long term.

While electrification of road freight transport has been demonstrated as achievable, there remains a gap in the literature regarding the feasibility and potential benefits of using renewable energy sources to charge EV fleets, while considering the logistic and operational constraints that may arise. As such, further research is needed to explore the practicality of integrating renewable energy into the charging infrastructure of EV fleets, considering factors such as fleet schedule, charging time, energy demand and solar energy generation and network power

constraints. Addressing these issues and supporting decision making with technical knowledge to facilitate the adoption of EV fleets within fleet and transport operators, is essential for the transition towards more sustainable road freight transportation.

Based on this review of the literature, the following research questions have been identified:

I. What are the environmental and economic benefits of using solar energy and BESS to charge an electric freight fleet when logistic and operational constraints are considered?
II. When using solar energy and BESS, what are the implications on the grid dependency and consequently GHG emissions, when different charging strategies are applied?
III. To what extent, solar energy and BESS can ease the power capacity constraints when it comes to EV fleet electrification?

The following chapters will address these questions. Chapters 3 and 4 will build the foundation to be able to answer research questions I and II in Chapter 5. In Chapter 6, research question III will be answered. To start to address these questions it is essential to be able to determine how much solar energy is available at a given location. To this end, chapter 3 addresses the modelling of solar PV generation such that the results may inform the investigations in the later chapters.

3 Solar irradiation modelling for photovoltaic solar energy generation in the UK

3.1 Introduction

Nowadays, it is almost impossible to imagine a transition to EV transportation without considering renewable energies. In Chapter 2 the environmental impact of transitioning to electric vehicles (EVs) has been discussed, assuming that those EVs were charged with electricity derived from fossil fuels. This thesis explores the feasibility of using localised solar energy generation and energy storage to charge an EV fleet at a depot. For that purpose, in this chapter a new empirical solar model is proposed for the estimation of solar energy generation at different locations in the UK. The model is developed using MATLAB. The development and results section, corresponding to the diffuse horizontal solar irradiation modelling, have been published in the journal Energy in 2022[1] [174]. The methodology developed in this chapter to convert horizontal solar radiation into solar energy generation has been previously published in the Energies journal in 2023[2] [175].

Typically, solar energy systems are installed on tilted surfaces, such as depot rooftops, where the solar irradiance received encompasses the direct ($G_{b\beta}$), diffuse ($G_{d\beta}$), and reflected (G_r) irradiation components on tilted surfaces. When estimating or forecasting solar energy availability, these three elements can be derived from the global horizontal solar irradiation (G_H) and its components, the diffuse horizontal solar irradiation (G_d) and the direct horizontal irradiation (G_b).

This chapter describes the solar model developed to determine the PV solar energy generated locally in different locations in the UK, as shown in Figure 3.1. The chapter first focuses on the global horizontal solar irradiation (G_H) and its two components (i.e. G_d and G_b). A review of the literature on horizontal solar irradiation modelling is introduced followed by the methodology applied to calculate the estimated diffuse horizontal solar irradiation ($G_{d,est}$) and G_b. Results are presented and validated against real data on PV solar generation in two different

[1] Part of this chapter has been used for publication at the Energy journal as Nunez Munoz M, Ballantyne EEF, Stone DA. Development and evaluation of empirical models for the estimation of hourly horizontal diffuse solar irradiance in the United Kingdom. Energy 2022;241. https://doi.org/10.1016/j.energy.2021.122820

[2] Nunez Munoz M, Ballantyne EEF, Stone DA. Assessing the Economic Impact of Introducing Localised PV Solar Energy Generation and Energy Storage for Fleet Electrification. Energies 2023;16:3570. https://doi.org/10.3390/en16083570

installations; a private house located in Sheffield and at M&S York Vangarde Retail Park. Finally, one of the case studies where the solar model was applied is presented. The case study was developed for The Translational Energy Research Centre (TERC) and funded by the European Regional Development Fund [43].

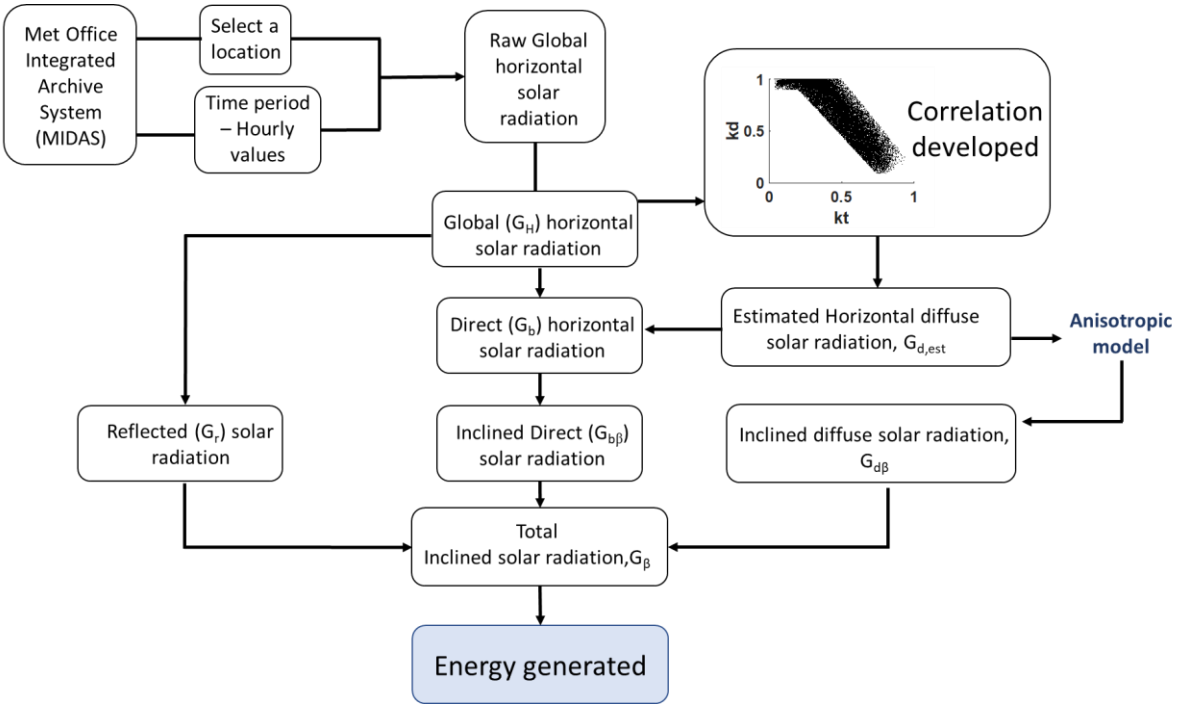

Figure 3.1 Process flow applied for the calculation of localised PV solar energy (Figure obtained from [175]).

3.2 Horizontal solar irradiation modelling

Horizontal solar irradiance is the radiation incident on a horizontal surface, parallel to the ground. Global horizontal solar irradiation (G_H) is the total horizontal irradiation received and is the sum of direct horizontal solar irradiation (G_b) and diffuse horizontal solar irradiation (G_d) as follows.

$$G_H = G_b + G_d$$

Equation 3.1

3.2.1 Global horizontal solar irradiation (G_H)

Global horizontal solar irradiation (G_H) can be assessed through satellite technology or ground-based pyranometer/pyrheliometer devices. While satellite measurements offer a more extensive dataset [176], ground-level measurements are deemed superior in precision, mainly attributed to their diminished occurrence of significant systematic errors [177]. Addressing and

mitigating these errors necessitate a crucial procedure involving a comparative analysis of satellite and ground-based data [178–180]. However, it is noteworthy that acquiring ground-level measurements for diffuse and direct horizontal irradiation involves substantial costs [181,182] and is complicated to measure [183]. Consequently, ground-level solar radiation measurements are limited, particularly in developing countries [184,185].

In the United Kingdom, global horizontal solar irradiation records cover the period from 1947 to 2018 and remain the country's most frequently collected solar irradiation data. Weather stations situated in Greater London have been monitoring horizontal global irradiation data from 1958 and 2018. Likewise, the documented records for horizontal global irradiation in West Sussex encompass the interval between 1992 and 2018. Additionally, data from Norfolk is available for the years 1981 to 2006. While several other locations across the UK have conducted measurements of horizontal global irradiation, these records are generally over a much shorter timeframe (for example, South Yorkshire from 1982 to 1995). Due to the reasonable amount of global horizontal solar irradiation data in the UK, for the development of the solar model, the G_H data values are obtained through the open data archive of Met Office Integrated Data Archive System (MIDAS). More details about the dataset information is included in Section 3.2.2.

3.2.2 Diffuse horizontal solar irradiation (G_d)

The diffuse horizontal solar irradiation is the portion of the global solar irradiation that reaches the Earth's surface after being scattered by air molecules and particles in the atmosphere [186]. Conversely, ground horizontal diffuse irradiation values are very scarce. In fact, the latest available data on G_d was measured at the London weather station back in 2005.

In the absence of horizontal diffuse solar irradiation data, different types of diffuse solar models have been developed to estimate horizontal diffuse solar irradiation. There is not a universal classification of the different types of solar models used to predict solar radiation values, they can be grouped differently depending on the parameters considered. De Simón-Martín *et al.* [187] classify the models in two main groups; models that require climate variables to predict solar radiation and models that use spatial interpolation to obtain solar radiation data. Noia *et al.* [188] refer to physical models as an approach that describe the physical process of scattering and absorption that occurs between the earth and the atmosphere in the solar radiation transfer. The authors identify the other type of solar models as statistical [189] where statistical

regressions between satellite and ground solar radiation measurements are made for a specific area. On the other hand, Hay [190] divides the solar models in two different types; theoretically based approaches (defined as physical models by Noia *et al.* [188]) and empirically based approaches [191]. For the purpose of this section, two different approaches have been identified to calculate solar radiation values: using machine learning techniques or empirical solar models.

Machine learning techniques

Machine learning techniques have many applications to predict values of solar radiation [185]. Essentially, the algorithms learn from input data and create a model that produces output data for pattern recognition or forecasting problems [192]. The use of machine learning techniques to model solar radiation has been shown in recent years to be a very promising method [193,194]. In fact, different authors have been evaluating and estimating solar radiation values using machine learning algorithms, especially models based on artificial neural networks (ANNs).

Martín *et al.* [195] predicts values of solar irradiance in a time scale of 3 days ahead by using autoregressive models (AR) and neural networks in different cities in Spain. Lou *et al.* [196] determined diffuse horizontal irradiance using a machine learning algorithm (Boosted Regression Tree) in Hong-Kong. Amrouche and Le Pivert [197] obtained values of daily global horizontal irradiance in two locations in France using daily weather forecast as input data for the ANNs model. Alzahrani *et al.* [198] estimate hourly solar radiation data using neural networks with three, five and six inputs variables (hour, azimuth, zenith angle, temperature, wind speed and wind direction). In essence, the parameters used as input data together with relative humidity, sunshine hours or evaporation are more accessible [199].

Overall, one of the advantages of using machine learning techniques is the ability to predict solar radiation values. Accuracy [200] is another advantage of using these techniques although, on the other hand, the machine learning techniques have high computational costs and are time consuming if compared to empirical models [185].

Empirical solar models

Empirical solar models have seen widespread use in accurately forecasting diffuse irradiance in areas where solar radiation data is either unavailable or not measured [201]. These models

establish correlations between diffuse fraction (kd) or diffuse transmittance with other available variables. Li *et al.* [202] classified empirical models in two groups. The first group includes models that predict horizontal diffuse irradiance from global horizontal irradiation (H-based models). In contrast, the second group consists of models that rely on various weather variables (non H- based models) such as air temperature, relative humidity, or ratio of sunshine duration. Non H- based models have better accuracy than H- based models in places where there is limited information on solar radiation data [202]. Nonetheless, the prevailing method to acquire values for horizontal diffuse solar irradiance involves the utilisation of H- based models, specifically, by establishing a correlation between the diffuse fraction (kd) and the clearness index (kt) [196,202].

- Non H-based models

Non H- based models are also classified as parametric models [203,204]. As mentioned previously, these models require more detailed information on weather and atmospheric conditions. The main characteristic of these models is that they are able to predict values of horizontal diffuse solar radiation (G_d) without having values of global horizontal solar radiation (G_H).

Iqbal [205] developed an empirical equation to estimate diffuse transmittance from the ratio of sunshine fraction (SF) using measured data from three different locations in Canada. Hussain [206] established a correlation to evaluate the horizontal diffuse radiation for locations of North and Central India with SF and water vapour (W_v) content in the atmosphere. Coppolino [207] recommended an equation for any place in Italy which correlates horizontal diffuse radiation with SF and solar altitude angle (γ_s). Bashahu [184] studied different correlations from previous authors (e.g. Iqbal [205], Coppolino [207]) to developed nine equations to obtain values of horizontal diffuse solar radiation in Dakar, Senegal. The author correlated diffuse fraction and diffuse transmittance with SF, W_v, and clearness index. Li *et al.* [208] developed two correlations. Firstly, values of diffuse transmittance were obtained using SF, the ambient temperature, and relative humidity and secondly, the values of diffuse radiation were obtained using the already mentioned weather variables and clearness index. The correlations were validated using measured data from Guangzhou station in China.

- H-based models

Due to their simplicity and accuracy, these H- based empirical models are integrated into specialised software for solar energy applications and forecasting [209]. H- based models estimate horizontal diffuse solar radiation empirically using measured global horizontal solar radiation. The correlation of diffuse fraction (kd) and clearness index (kt) allows for the calculation of the diffuse solar radiation [182].

Diffuse fraction (kd) is the ratio between horizontal diffuse solar irradiation (G_d) and the global horizontal solar irradiation (G_H) [210].

$$kd = \frac{G_d}{G_H}$$

Equation 3.2

Clearness index (kt) is defined as the ratio between G_H and the extra-atmospheric irradiance (G) [210].

$$kt = \frac{G_H}{G}$$

Equation 3.3

Liu and Jordan [211] pioneered the empirical model for predicting G_d from G_H. Subsequently, numerous researchers have been investigating and refining this correlation to suit various geographical locations.

Erbs *et al.* [212] formulated the diffuse fraction correlation by analysing ground solar radiation data for four cities in the United States between 1961 and 1976. The resulting correlation was validated using measured values from Highett, Australia between 1966 and 1969. Reindl *et al.* [213] established a correlation between the diffuse fraction and clearness index by examining solar irradiation measurements obtained from two U.S. cities from 1979 to 1982. Additionally, one year's worth of data from each of three European cities were used. De Miguel *et al.* [214] established a correlation model utilising ground-based hourly measurements of global and diffuse solar irradiation on horizontal surfaces across Greece, Portugal, France, and Spain. The ground measurements took place in a different period of time for each location between 1978 and 1996.

Muneer and Saluja [215] formulated a series of regression models tailored to various UK locations, including East Hampstead, Aberporth, Aldergrove, Eskdalemuir, and Lerwick. The models correlated the value of diffuse fraction with clearness index, and they were validated using measured values, at ground level, of hourly global and diffuse solar radiation from 1981, 1982 and 1983. The authors found the clearness index the most relevant parameter for the estimation of horizontal diffuse solar irradiance. Ruiz-Arias *et al.*[181] devised a sigmoid function employing kt as a predictor for computing kd, drawing upon data from 21 distinct locations spanning Europe and the United States.

While the previously discussed models centre on establishing a correlation between the diffuse fraction (kd) and the clearness index (kt), a concurrent avenue of research has explored the influence of additional predictors in diffuse solar irradiance computation. Reindl *et al.* [213] identified that various predictors, including kt, ambient temperature, relative humidity, and solar altitude, held greater significance in estimating diffuse solar radiation when compared to the remaining 24 predictors.

Muneer and Munawwar [216] argued in favour of adding other predictors for estimating the diffuse solar radiation. The models developed were used to calculate values of hourly diffuse radiation. The data used to develop the correlations were based on nine worldwide locations. The study's findings indicated that the integration of additional parameters such as sunshine fraction (SF), cloud cover and air mass (m) leads to an improvement in the correlation between kd and kt. A parallel outcome was observed in Tamanrasset (Algeria) where Salhi *et al.* [201] assessed eighty empirical models and found that the most accurate model established a correlation between kd, kt and SF.

Gopinathan and Soler [217] studied different correlations to better determine how many parameters had to be considered for a highly accurate estimation of diffuse radiation values. The study employed ground measurements of solar radiation values from 1980-1990 in four different locations around Spain. The results showed a higher accuracy when, in addition to kt, sunshine fraction (SF) and solar altitude angle (γ_s) are also considered.

The correlation from the study of De Miguel *et al.* [214] was introduced previously in this section of the literature review. The authors only correlate the diffuse fraction with kt, but important findings were revealed from this research. The authors identified an increased error percentage in the correlation in summer periods for lower latitudes and they pointed out that

solar latitude should be considered to minimise the error. On the other hand, De Miguel *et al.* [214] also found the influence that the air mass has on the diffuse solar component due to the scattering effect of this parameter at lower solar latitudes. An extended explanation on the effect of the air mass as a function of solar latitude in diffuse solar radiation can be found in Vazquez *et al.* [218].

Irrespective of the count of predictors employed, many authors have underscored the empirical models' reliance on the dataset's location used to develop the correlation [212,214,216]. Consequently, due to the significant importance of estimating horizontal diffuse solar irradiance in solar energy projects, numerous researchers worldwide are formulating empirical correlations to obtained accurate values tailored to specific locations.

Tapakis *et al.* [209] undertook a comparative analysis encompassing twenty-three pre-existing models established in various countries and novel correlations formulated based on Athalassa (Cyprus) datasets. The study unveiled that, among the assessed pre-existing models, those originated in cities sharing akin climatological conditions with Athalassa exhibited superior performance. Notwithstanding, the newly developed correlations achieved the utmost accuracy in estimating diffuse horizontal solar irradiance.

Bailek *et al.* [219] formulated a suite of empirical correlations to predict the monthly average daily diffuse horizontal solar radiation within the Algerian Sahara. Notably, the authors demonstrated that one newly developed correlation yielded precise results when juxtaposed with established models created in different geographical contexts.

In a recent study, Berrizbeitia *et al.* [176] found that employing a singular correlation for all 19 global locations studied was unfeasible. Consequently, the authors arrange each site in an ascending order of latitude and developed three monthly-averaged hourly correlations. Among these correlations, one explicitly spans the entire UK.

The literature review above has shown some of the most relevant correlations and models used to estimate diffuse solar radiation and what parameters should be considered when developing said models. Its accuracy characterises the machine learning techniques; however, the author of the thesis discards the learning techniques for their application on predicting diffuse horizontal solar irradiation due to their high computational costs and time-consuming. On the other hand, empirical models characterise by their accuracy and straightforward application. However, the literature review highlights the importance of using local datasets when

developing empirical correlations due to the location dependency of such models (i.e., latitude and weather conditions). In this regard, there is a gap in the literature concerning the availability of empirical models developed in the UK that could be accurately applied to this thesis. Amongst all the empirical models reviewed from the literature, only some have been selected based on the dataset location to be as near as possible to the UK. Table 3.1 shows a summary of such models.

Therefore, considering the location dependency of empirical models and the scarcity of empirical models that predicts hourly values of diffuse horizontal solar irradiation in the UK, the objectives of section 3.2.2 are:

1) To assess the performance of the empirical solar models outlined in Table 3.1 across diverse regions within the United Kingdom to ascertain the most suitable fit for estimating horizontal diffuse solar irradiation (G_d).
2) To formulate distinct site-specific correlations for each UK region under investigation, tailored for the estimation of horizontal diffuse solar irradiation (G_d), followed by a rigorous evaluation of their accuracy compared to the existing models presented in Table 3.1.

Table 3.1. “Detailed information of the H-based models analysed and chosen for evaluation (Model 1 to Model 6)” (Table obtained from [174])

Model		**Location (see note below)**	**Predictors**	**Correlation**	
Model 1	**Torre’s model** [220]	Spain (1)	kt	$kt \leq 0.225$ $0.225 < kt < 0.755$ $kt > 0.755$	$kd = 0.9943 - 0.1165 \cdot kt$ $kd = 1.4101 - 2.9918kt + 6.4599kt^2 - 10.329kt^3 + 5.514kt^4$ $kd = 0.18$
Model 2	**De Miguel’s model** [214]	France (3), Portugal (4), and Spain (1)	kt	$kt \leq 0.21$ $0.21 < kt < 0.76$ $kt > 0.76$	$kd = 0.995 - 0.081 \cdot kt$ $kd = 0.724 + 2.738kt - 8.32kt^2 + 4.967kt^3$ $kd = 0.180$
Model 3	**Reindl’s model (1)** [213]	Denmark (1), Germany (1), Ireland (1) and U.S.A(2)	kt	$kt \leq 0.3$ $0.3 < kt < 0.78$ $kt > 0.78$	$kd = 1.020 - 0.248 \cdot kt$ $kd = 1.45 - 1.67kt$ $kd = 0.147$
Model 4	**Muneer’s model (1)** [215]	United Kingdom (5)	kt	$kt > 0.2$	$kd = 0.687 + 2.932kt - 8.546kt^2 + 5.227kt^3$
Model 5	**Reindl’s model (2)** [213]	Denmark (1), Germany (1), Ireland (1) and United States (2)	kt and γ_S	$kt \leq 0.3$ $0.3 < kt < 0.78$ $kt > 0.78$	$kd = 1.020 - 0.254 \cdot kt + 0.0123 \sin(\gamma_S)$ $kd = 1.4 - 1.749kt + 0.177 \sin(\gamma_S)$ $kd = 0.486kt - 0.182 \sin(\gamma_S)$
Model 6	**Muneer’s model (2)** [221]	United Kingdom (2)	kt, SF and m	-	$kd = (0.899 - 0.683SF + 0.648SF^2 + 0.028m - 0.002m^2) + (0.880 - 0.666SF - 0.314SF^2 - 0.158m + 0.003m^2)kt + (-1.751 + 2.786SF - 1.924SF^2 + 0.044m + 0.012m^2)kt^2$

**The numeric value enclosed within parentheses in the "location" column indicates the number of cities scrutinized within each location to formulate the correlation.*

3.2.2.1 **Methodology for assessing and developing H- based models to estimate horizontal diffuse solar irradiation (G_d).**

Information regarding the dataset and climatological conditions at the weather stations.

The datasets used for the present study were obtained from The Centre for Environmental Data Analysis (CEDA) Archive. It serves as the UK's national data centre for atmospheric and earth observation research. The Archive provides access to horizontal solar irradiation data from the open data version of Met Office Integrated Data Archive System (MIDAS) [222,223].

The datasets comprise hourly recordings of horizontal global and diffuse solar irradiation measured in kJ/m^2. These recordings indicate the solar irradiance received during the hour ending at a specific time. Following Gueymard [224], this study considers at least three years' worth of data for each location to assess and validate solar radiation models. Table 3.2 shows detailed information regarding the weather station locations, the measurement period, and the number of recorded measurements for each location.

Table 3.2. "Details on the hourly horizontal global and diffuse solar irradiation raw data values measured at each location under study" (Table obtained from [174]).

Location	Latitude [degrees]	Period of measurements	Number of values recorded
Finningley (South-Yorkshire)	53.4845	1982-1995	113,154
Hemsby (Norfolk)	52.6953	1982-1999	134,605
Crawley (West Sussex)	51.1059	1982-1992	91,529

As depicted in Figure 3.2, the weather stations of Finningley, Hemsby, and Crawley are situated in three distinct regional areas within the UK - the North East, the East of England, and the South, respectively [225].

The North East region, where the Finningley station is located [225], experiences cool temperatures throughout the year than other parts of England. During the chilliest month, which falls in January, temperatures range from -0.5°C to approximately 2°C. Conversely, in the peak warmth of July and August, temperatures range between 17°C and 21.5°C. As we move further south, the average temperatures for the coldest and warmest months progressively increase.

In the climate of the eastern region [225], the average temperatures range from 0°C to 2°C during winter and from 20°C -23°C during summer. Moreover, this area is among the driest in the country, with an average annual rainfall of 700 mm.

Moving on to the southern England climate, temperatures vary from approximately 0.5°C to about 3°C in January and from 21°C -23.5°C in July [225]. The southern region boasts the sunniest locations in mainland UK, enjoying an average annual sunshine duration ranging from 1,550 to 1,600 hours.

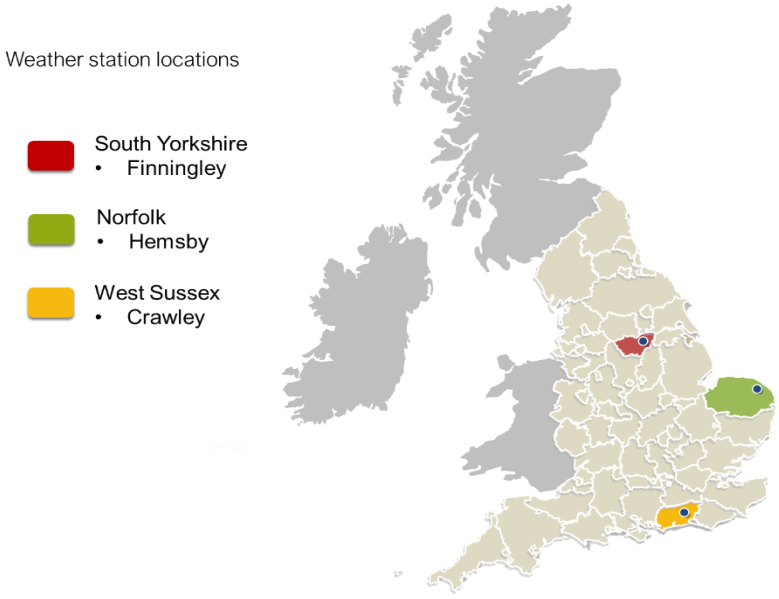

Figure 3.2 “Location of Met Office weather stations used for the study” (Figure obtained from [174])

Data pre-processing

Several pre-processing steps are undertaken to make the raw data usable. These steps are explained below and depicted in Figure 3.3. The raw datasets from Table 3.2 underwent a pre-processing phase to eliminate extraneous data points, notably invalid values recorded at 23:59, corresponding to daily irradiation readings. Scrutiny of the raw data unveiled intervals of data absence resulting from equipment errors, operational issues, or errors in diffuse irradiation data processing [226]. These identified gaps were also excluded from the datasets.

Following the raw data pre-processing, the next step corresponded to calculating the astronomical parameters in a time period of one minute. The computation of astronomical parameters plays a critical role in determining the hourly horizontal extra-atmospheric

irradiation (G), the unknown variable in Equation 3.3, and thus to progress with the comparative study and development of new correlations.

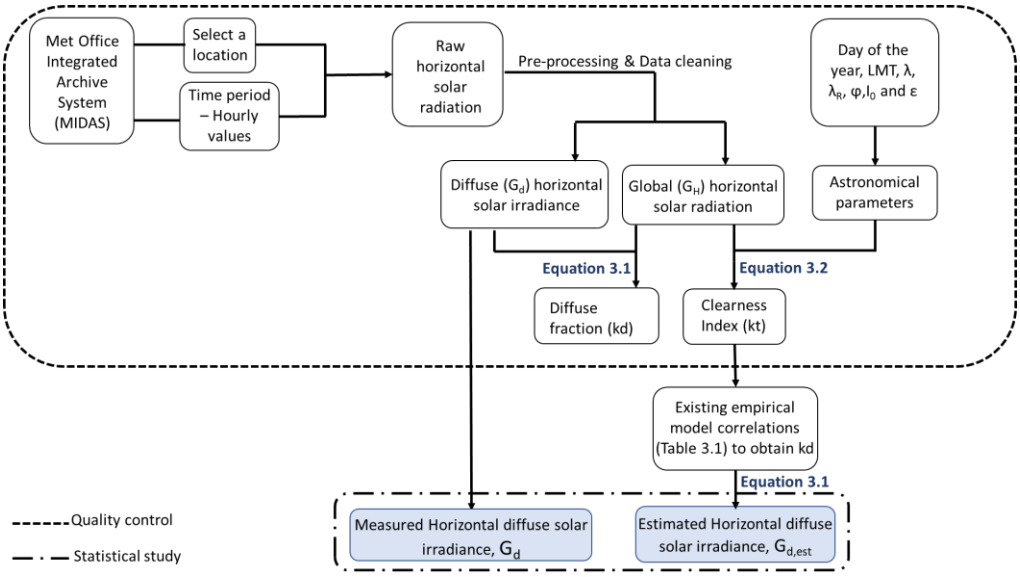

Figure 3.3 "Complete process flow used for the evaluation of the existing empirical models using measured data from South Yorkshire, Norfolk, and West Sussex" (Figure obtained from [174]).

The computation of the horizontal e-atmospheric irradiance (G_0) is executed using Equation 3.4 [227]:

$$G_0 = I_0 \cdot \left(1 + 0.033 \cdot \cos\left(\frac{360 \cdot DOY}{365}\right)\right) \cdot \sin \gamma_s \left[\frac{W}{m^2}\right]$$

Equation 3.4

Which involves the following parameters: I_0 is the solar constant with a fixed value of 1,367 W/m^2 [227]. The variable DOY denotes day-of-year, representing the nth day of the year (e.g. January 1st corresponds to DOY =1; February 1st to DOY =32, March 1st to DOY =60, etc. Note that leap years are excluded). γ_s denotes the solar altitude angle.

With the aim of maintaining coherence in solar angle measurements, the Standardised ISO system has been used for this study. [228]. The ISO system adopts a north orientated reference frame, where angles are calculated clockwise (0°-360°). Following that system, γ_s is calculated as in Equation 3.5 [228]:

$$\gamma_s = \text{asin}\left(\sin\varphi \cdot \sin\delta - \cos\varphi \cdot \cos\delta \cdot \cos\omega\right) \quad [\text{degrees}]$$

Equation 3.5

where φ is the latitude, δ is the declination angle and ω is the hour angle. δ is defined by [227], following the approximate equation of Cooper (1969) [229], and it can be seen in Equation 3.6:

$$\delta = 23.45 \cdot \sin\left[360 \cdot \frac{(\mathrm{DOY} + 284)}{365}\right] \ [\mathrm{degrees}]$$

Equation 3.6

The calculation of the hour angle ω, accounting for a north orientated system, is mathematically derived as presented in Equation 3.7 [228]:

$$\omega = \mathrm{t} \cdot 15° \ [\mathrm{degrees}]$$

Equation 3.7

where t represents the local solar time. Consistent with Sunter's findings [230], the UK observations employ Universal Time Coordinated (UTC) as the standard time, without incorporating daylight savings adjustments. Therefore, the estimation of t is determined following the methodology outlined in [231] as ;

$$\mathrm{t} = \mathrm{LMT} + \frac{\lambda - \lambda_R}{15} + \mathrm{EOT} \quad [\mathrm{hours}]$$

Equation 3.8

In the context of Equation 3.8, LMT denotes the local mean time or civil time. The variable "λ" represents the longitude of the standard time meridian, while "λ_R" is the longitude of the specific location. Additionally, EOT stands for the equation of time [227]. The calculation of EOT can be estimated using Equation 3.9:

$$\mathrm{EOT} = 229.2 \cdot (0.000075 + 0.001868 \cdot \cos \mathrm{B} - 0.032077 \cdot \sin \mathrm{B} - 0.014615 \cdot \cos 2\mathrm{B} - 0.04089 \cdot \sin 2\mathrm{B}) \ [\mathrm{minutes}]$$

Equation 3.9

where B is a coefficient calculated by [227] following Equation 3.10;

$$\mathrm{B} = (\mathrm{DOY} - 1) \cdot \frac{360}{365}$$

Equation 3.10

After determining all astronomical parameters, the horizontal e- atmospheric irradiance (G_0) was computed at one minute intervals. For consistency with hourly dataset measurements, G_0 values were subsequently averaged every 60 minutes, yielding an hourly value denoted as G [kW/m^2]. Furthermore, the dataset's hourly irradiation measurements in kJ/m^2 were transformed into hourly irradiance measurements in kW/m^2. This transformation enabled the calculation of the clearness index (kt) through Equation 3.3, and the estimation of the diffuse fraction (kd) using Equation 3.2

In the context of Model 6 (as listed in Table 3.1), two additional parameters were derived to facilitate the calculation of the diffuse fraction (kd).

- The sunshine fraction (SF) denotes the proportion of sunshine duration relative to the total day length [177]. The CEDA archive furnished daily sunshine duration data for each location from 1982 to 1999. The day length can be determined using Equation 3.11 [231]:

$$\text{Day length} = \frac{2}{15} \cdot \cos^{-1}(-\tan\varphi \cdot \tan\delta) \quad [\text{hours}]$$

Equation 3.11

- The calculation of air mass (m) followed the procedure outlined by [216], as detailed in Equation 3.12:

$$m = [\sin\gamma_s + 0.50572(\gamma_s + 6.07995)^{1.6364}]^{-1}$$

Equation 3.12

Quality control

Following the pre-processing of the raw data, a quality control procedure was executed to ensure data accuracy and reliability. The quality control process encompassed four distinct tests, with three of these tests established by Younes *et al.* [232] while the fourth test was introduced by Muneer and Fairooz [226].

The initial test involved the exclusion of solar altitude values (γ_s) below 7°. This step aimed to eliminate data influenced by the cosine effect, effectively addressing errors arising from the sensor's response to radiation angles during sunrise and sunset.

The second test implemented a logical evaluation to ensure that values for both kt and kd remained within the range of zero to one [181], maintaining data consistency and validity.

$$0< kt <1$$

$$0< kd <1$$

The third test involved the computation of diffuse horizontal irradiance values for clear ($G_{d,c}$) and overcast ($G_{d,oc}$) sky conditions. The objective of this test was to ascertain that the observed horizontal diffuse irradiance (G_d) remained within the range defined by $G_{d,c}$ and $G_{d,oc}$ [232].

$$G_{d,oc} \leq G_d \leq G_{d,c}$$

To determine $G_{d,c}$ and $G_{d,oc}$, the approach employed by Younes *et al.* [232] leveraged the Page model, utilising Equation 3.13 for overcast sky conditions and Equation 3.14 for clear sky conditions. This ensured a comprehensive evaluation of the diffuse horizontal radiation under varying atmospheric scenarios.

$$G_{d,oc} = 572 \cdot \gamma_s$$

Equation 3.13

$$G_{d,c} = kd \cdot T_{rd} \cdot F(\gamma_s)$$

Equation 3.14

Where T_{rd} is the theoretical diffuse irradiance on a horizontal surface when the sun is at the zenith [232]. Its computation adheres to Equation 3.15, as expressed below:

$$T_{rd} = -21.657 + 41.752 \cdot T_L + 0.51905 \cdot T_L^2$$

Equation 3.15

Here T_L stands for the Linke turbidity factor, indicating aerosol concentration within the atmosphere and reflecting the interplay of atmospheric scattering and absorption [233]. A higher concentration of aerosols leads to increased atmospheric scattering.

Remund *et al.* [234] compiled an extensive global T_L database encompassing data from seven distinct cities in the United Kingdom. The turbidity factor values employed within this study were derived from monthly measurements conducted in Aughton, London, and Brooms Barn (United Kingdom) between 1981 and 1990. Notably, an average value between September and

November was utilised to address this gap since the T_L value for October was missing in the database for all UK locations.

$F(\gamma_s)$ is the solar elevation function, calculated by Younes *et al.* [232] following Equation 3.16:

$$F(\gamma_s) = 3.8175 \cdot 10^{-2} + 1.5458 \cdot \sin\ (\gamma_s)\ - 0.59980 \cdot \sin\ (\gamma_s)^{\,2}$$

Equation 3.16

Furthermore, an additional assessment was incorporated to ensure the quality of the retained data. This evaluation, as outlined by Muneer *et al.* [226], introduces a boundary condition based on the ratio between the clearness index (kt) and the diffuse fraction (kd). A representation of these boundaries is depicted in Figure 3.4.

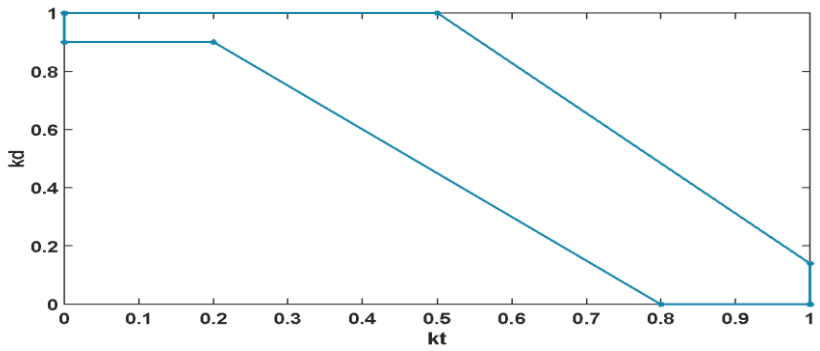

Figure 3.4."Boundaries for clearness index (kt) and diffuse fraction (kd) developed by Muneer and Fairooz [226], that have been applied in test 4 as described in Table 3.3" (Figure obtained from [174])

The number of values within the remaining datasets after each quality test are shown in Table 3.3 for each of the study locations. Test 1, focused on rectifying equipment errors, notably exhibits the most significant influence on the quality control process. Specifically, Test 1 resulted in an approximate reduction of 57% in the data points under consideration for each location. Conversely, the outcomes of Test 2, Test 3 and Test 4 indicate a comparatively lesser impact on the quality control of each dataset. These tests ensure coherence among various solar radiation values (e.g. G_d cannot surpass G) [235].

Table 3.3. "Number of values within the remaining datasets after each quality test" (Table obtained from [174]).

		South-Yorkshire		Norfolk		West-Sussex	
Test	**Condition applied**	**Before test**	**After test**	**Before test**	**After test**	**Before test**	**After test**
Pre-processing	Deletion of 23:59 data and values of zero solar radiation	113,154	108,016	134,605	130,145	91,529	91,519
Test 1	Solar altitude<7°	108,324	46,053	130,145	54,419	91,519	39,664
Test 2	0< kd <1 0< kt <1	46,053	41,337	54,419	53,037	39,664	32,825
Test 3	$G_{d,oc} \leq G_d \leq G_{d,c}$	41,337	40,316	53,037	52,174	32,825	32,108
Test 4	Boundaries kd and kt	40,316	35,397	52,174	45,627	32,108	27,497

Statistical error metrics for the evaluation of empirical H- based models

Statistical error metrics have been used extensively in literature to evaluate the performance of empirical solar models. For instance, Tapakis *et al.* [209] examined empirical models aimed at estimating hourly diffuse fraction for the Nicosia region (Cyprus) through the utilisation of mean bias error (MBE), root mean square error (RMSE), and the coefficient of determination (r^2). Similarly, in the evaluation of empirical models correlating diffuse solar radiation and clearness index for the Kerman region (Iran), Khorasanizadeh *et al.* [236] used mean absolute percentage error (MAPE), mean absolute bias error (MABE), RMSE, relative standard error (RSE), and correlation coefficient (r). The assessment of a solar model's capacity to compute diffuse solar radiation was conducted by Hofmann *et al.* [237], using the RMSE metric. Additionally, Yao *et al.* [238] appraised daily diffuse solar radiation models for various Chinese regions through statistical analysis, encompassing metrics such as MBE, RMSE and r. In estimating hourly diffuse solar irradiation under all sky conditions, Ruiz-Arias *et al.* [181] introduced a regressive model validated by metrics such as r^2, MBE and RMSE.

To evaluate the performance of the empirical models developed within this study, three widely used statistical error metrics [239,240] have been selected; MBE, RMSE and r^2. Both the MBE and RMSE maintain the units of the variables (kW/m^2).

The MBE metric is a prevalent method employed for assessing the performance of solar models [241,242]. It quantifies the arithmetic mean of the discrepancies between estimated and measured values of hourly diffuse horizontal irradiance, and its formulation is provided in Equation 3.17 as:

$$\mathrm{MBE} = \frac{\sum_{i}^{n}(G_{d,est,i} - G_{d,meas,i})}{n}$$

Equation 3.17

Where $G_{d,est,i}$ represents the estimated hourly diffuse horizontal irradiance (kW/m^2), $G_{d,meas,i}$ denotes the measured hourly diffuse horizontal irradiance (kW/m^2) and n is the total number of data points.

Negative or positive MBE values indicate under-prediction or over-prediction by the model, respectively. For this study, MBE is chosen to offer a comprehensive assessment of model accuracy. A MBE nearest to zero is desired.

The RMSE stands out as the most widely adopted statistical error metric when gauging the reliability and precision of a solar model [243,244]. Specifically, the RMSE metric facilitates a point-by-point evaluation of the differences between estimated and measured values [245]. The calculation of RMSE is outlined in Equation 3.18:

$$\mathrm{RMSE} = \sqrt{\frac{\sum_{i}^{n}(G_{d,est,i} - G_{d,meas,i})^2}{n}}$$

Equation 3.18

RMSE metric gives more weight to the largest errors [239] often stemming from the cosine effect [246]. However, this study effectively mitigates such errors through the initial quality control test. A lower absolute RMSE corresponds to enhanced model accuracy.

Lastly, the coefficient of determination (r^2) is chosen to evaluate the degree of linearity between the measured values and those acquired through the models' correlations (as expressed in Equation 3.19).

$$r^2 = \frac{\left[\sum(G_{d,est} - \overline{G_{d,est}}) \cdot (G_{d,meas} - \overline{G_{d,meas}})\right]^2}{\sum(G_{d,est} - \overline{G_{d,est}})^2 \cdot \sum(G_{d,meas} - \overline{G_{d,meas}})^2}$$

Equation 3.19

Where $\overline{G_{d,est}}$ and $\overline{G_{d,meas}}$ represent the mean estimated and measured hourly diffuse solar irradiance, respectively. The r^2 values span between 0 and 1, with the latter indicating a perfect linear relationship.

3.2.2.2 Results

Analysis and evaluation of existing empirical H- based models applied to the UK

In this section, the six empirical correlations introduced at the beginning and presented in Table 3.1 are chosen to estimate hourly horizontal diffuse solar irradiance. These correlations were selected based on the location of its datasets, ensuring similarity to the climatological conditions of the three regions studied (South Yorkshire, Norfolk, and West Sussex). The objective was to assess and identify the most appropriate model for estimating values of horizontal diffuse irradiance (G_d). The valuation process for the existing empirical models is shown in Figure 3.3.

Following the quality control procedure, the obtained clearness index (kt) values were used to compute the diffuse fraction (kd) using the correlations detailed in Table 3.1 for each model. Next, using the measured global horizontal solar irradiance (G_H) in conjunction with Equation 3.2, the values of estimated horizontal diffuse solar irradiance ($G_{d,est}$) were obtained and compared against the actual G_d values. The comprehensive statistical outcomes for each model are provided Table 3.4. The outcomes presented in Table 3.4 corresponds to the three studied regions: South Yorkshire, Norfolk, and West Sussex. In general, the correlations employing multiple predictors (Model 5 and Model 6) did not yield better outcomes when contrasted with correlations relying solely on kt as the predictor across all studied locations. Nonetheless, a notable distinction in the statistical errors emerged between Model 5 and Model 6. The findings indicate that the inclusion of solar altitude (γ_s), in Model 5 influences the results more than a combination of solar altitude (γ_s), SF and m as used in Model 6. For the three locations, Model 5 achieved higher values of r^2 and lower values of MBE and RMSE than Model 6. The variations in MBE and RMSE values remain relatively modest compared to the differences highlighted by r^2.

The results obtained by using Model 1, Model 2 and Model 3 exhibit a consistent pattern of r^2, MBE and RMSE across all investigated sites. None of the models outperforms the others in all three statistical indicators. Model 1 achieves the highest value of r^2, while the lowest MBE and RMSE values are associated with Model 3 and Model 2. With Model 4, r^2 value ranges from 0.77-0.79, depending on location. This result aligns closely with the findings presented by [215]. It is worth noting that this correlation was designed to cover values of kt >0.2. However, when the correlation is applied across the complete kt range for each dataset, Model 4 emerges

as the top performer for all studied locations. Muneer's model (Model 4) returns the highest r^2 values and the lowest MBE and RMSE values among the models considered.

As previously indicated, the empirical models rely on distinct datasets associated with various geographical locations, rendering them non-universal correlations. Consequently, Muneer's model correlation, developed explicitly for the United Kingdom through a regressed equation, would exhibit a better fit with the measured values compared to other models for the selected locations. Generally, for South Yorkshire, Norfolk, and West Sussex, each model's MBE and RMSE values show minor fluctuations. However, the values of r^2 exhibit a decline in each model as latitude decreases.

Table 3.4. "Statistical performance evaluation of existing empirical models based on ground measured data for South-Yorkshire, Norfolk, and West-Sussex" (Table obtained from[174]).

South-Yorkshire

	r^2	MBE	RMSE
Predictors: **kt**			
Model 1	0.863	-0.022	0.045
Model 2	0.856	-0.013	0.040
Model 3	0.861	-0.015	0.041
Model 4	0.770	-0.0016	0.048
Predictors: **kt**, $\boldsymbol{\gamma_s}$, SF and m			
Model 5	0.858	-0.0097	0.039
Model 6	0.778	0.027	0.065

Norfolk

	r^2	MBE	RMSE
Predictors: **kt**			
Model 1	0.839	-0.023	0.048
Model 2	0.836	-0.015	0.044
Model 3	0.837	-0.017	0.044
Model 4	0.789	-0.001	0.039
Predictors: **kt**, $\boldsymbol{\gamma_s}$, SF and m			
Model 5	0.826	-0.0098	0.043
Model 6	0.732	0.031	0.071

West-Sussex

	r^2	MBE	RMSE
Predictors: **kt**			
Model 1	0.829	-0.026	0.051
Model 2	0.823	-0.017	0.047
Model 3	0.825	-0.018	0.047
Model 4	0.771	-0.001	0.041
Predictors: **kt**, $\boldsymbol{\gamma_s}$, SF and m			
Model 5	0.819	-0.01	0.045
Model 6	0.734	0.035	0.075

Development and evaluation of new empirical H- based models at different locations in the UK

Following the comparative analysis of empirical models and their performance against measured data at the three designated locations, a new model has been formulated to enhance the accuracy of horizontal diffuse irradiance prediction. This section aims to establish specific correlations for each site that closely match the measured data. According to the findings presented in Table 3.4, it is evident that among the empirical models, those incorporating kt as a predictor exhibited the most significant influence on result accuracy. Consequently, the correlations developed in this study rely on a single predictor, the clearness index, (kt).

As highlighted in the study by Vignola *et al.* [178], employing identical datasets for model development and validation is discouraged. Therefore, a certain portion of the datasets, used to develop the correlation, will be referred to as "training datasets" and, the portion of the datasets used to validate the model will be called "validation datasets" [181]. Detailed information regarding the years allocated for the training and validation datasets for each location is presented in Table 3.5.

Table 3.5. "Dataset used to develop and validate the correlations at each location" (Table obtained from [174])

	Training dataset	**Validation dataset**
South-Yorkshire	1982-1989	1990-1995
Norfolk	1982-1993	1994-1999
West-Sussex	1982-1987	1988-1992

The process employed to formulate a novel correlation is visually depicted in Figure 3.5 as a diagram and will be elaborated next.

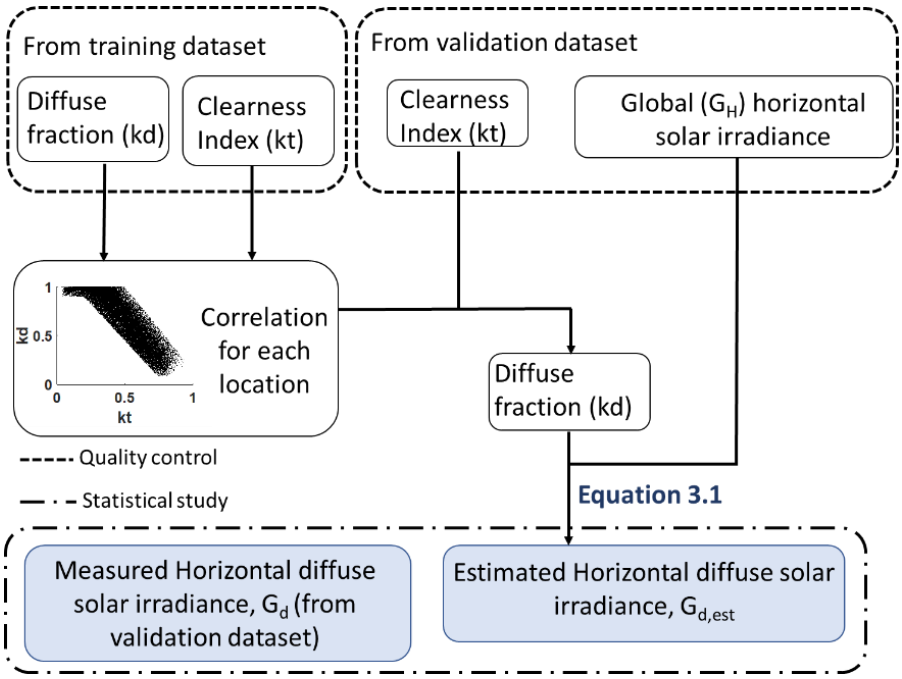

Figure 3.5 "The complete process flow for the development of a new correlation" (Figure obtained from [174])

The quality control process was executed on both datasets for each respective region. Figure 3.6 provides a visual representation of the hourly measurements of the clearness index (kt) and diffuse fraction (kd) before and after the quality procedures in the context of the South Yorkshire region.

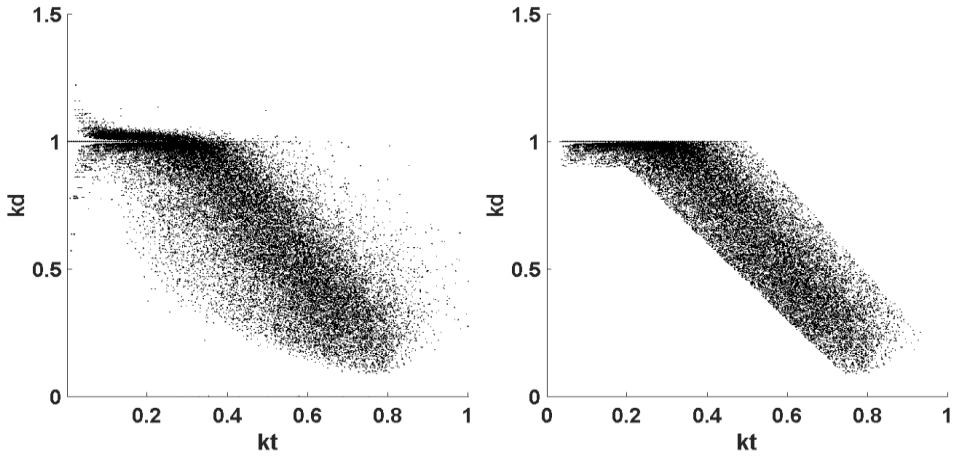

(a) (b)

Figure 3.6. "Hourly values of clearness index (kt) and diffuse fraction (kd) (a) before and (b) after the quality process" (Figure obtained from [174]).

Figure 3.6 displays values of kd and kt from the “training dataset” to create a correlation for each location.

The dataset was divided into segments to facilitate a more tailored fitting of correlations for each section. In the case of the initial kt values, the determination of interval lengths followed the methodology established by Muneer *et al.* [215]. Within the 0≤ kt ≤0.3 range, kd values were averaged in 0.05 increments and plotted. This section of data points exhibited a linear pattern for kt values ranging from 0 to 0.2, as depicted in Figure 3.7. Consequently, a linear regression was applied to values falling below 0.2

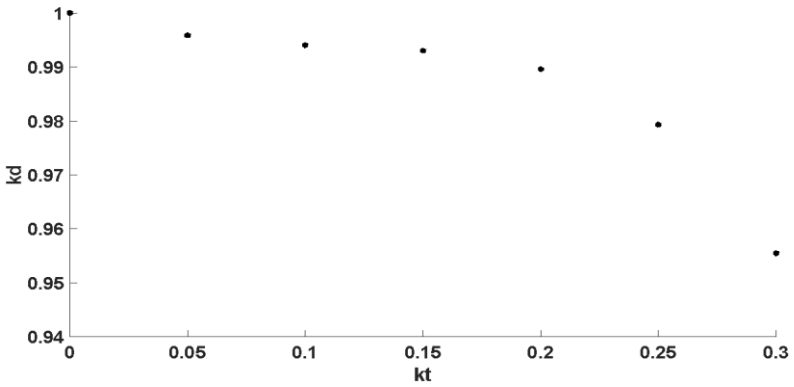

Figure 3.7. “Approach to set intervals for kt <0.2” (Figure obtained from [174])

For kt values exceeding 0.2, the correlations that yielded better performance were a 4th order polynomial for South-Yorkshire and Norfolk and a cubic correlation for West-Sussex. Although higher-order polynomial equations and correlations with intervals between 0.2 and 0.8 or 0.9 were explored for all locations, they did not demonstrate significant improvement in model accuracy, so they were discarded.

Following the formulation of the correlations, the validation process involved incorporating clearness index (kt) values from the designated "validation dataset" into each correlation. Subsequently, the obtained diffuse fraction (kd) was combined with global horizontal solar irradiance (G_H) to compute the hourly estimates of horizontal diffuse solar irradiance ($G_{d,est}$) using Equation 3.2. A comparative analysis was conducted between these values and G_d measurements from the “validation dataset” and the statistical evaluation was performed. The detailed equations and the statistical error metrics for South-Yorkshire, Norfolk and West-Sussex are shown in Table 3.6.

Table 3.6. "Correlations with best performance for data measured in each location" (Table obtained from [174]).

	Correlation for South-Yorkshire (Ground measurements 1990-1995)	r^2	**MBE**	**RMSE**
kt <0.2	**kd** =0.9982-0.0473**kt**	0.872	0.0015	0.027
kt >0.2	**kd** =0.7392+2.428**kt** -6.739kt^2+2.626 $\mathbf{kt}^3$+1.366 $\mathbf{kt}^4$			
	Correlation for Norfolk (Ground measurements 1994-1999)			
kt <0.2	**kd** =0.9996-0.0497**kt**	0.840	0.004	0.04
kt >0.2	**kd** =0.6671+3.76**kt** -8.078$\mathbf{kt}^2$+5.231$\mathbf{kt}^3$+0.05306$\mathbf{kt}^4$			
	Correlation for West-Sussex (Ground measurements 1988-1992)			
kt <0.2	**kd** =1.0011-0.075**kt**	0.830	0.003	0.03
kt >0.2	**kd** =0.01898+7.117**kt** -16.54$\mathbf{kt}^2$+10.07$\mathbf{kt}^3$			

In the context of South Yorkshire, a comparative analysis of the newly developed correlation with the empirical models examined in Table 3.4 reveals a distinct enhancement in terms of statistical errors. When compared to Model 4, which previously exhibited the most accurate predictions within the limits of the correlation, the new correlation exhibits significant improvements across various metrics. Specifically, there is a marked increase in r^2, a slight enhancement in MBE, and a noteworthy reduction in RMSE.

Similarly, for the Norfolk region, the novel correlation model showcases improvements over existing empirical models, particularly regarding MBE values. Although the gains in r^2 and RMSE more modest, they improve predictive accuracy. While the magnitude of improvement is less pronounced than that observed in South Yorkshire, it is nevertheless noteworthy.

Finally, the new correlation model created for the region of West-Sussex yields remarkable changes when contrasted with existing empirical models. The RMSE has experienced a significant reduction, ranging from an average of 0.051 to 0.03. Furthermore, the improvements in MBE relative to Model 3, Model 1 and Model 2 are evident. Most notably, the enhancement in r^2 compared to Model 4, is substantial.

Though the advancement in Norfolk may not match that of South Yorkshire and West-Sussex, the novel correlation still contributes to enhanced outcomes when evaluated against existing models (as displayed in Table 3.4).

3.2.2.3 Empirical H- based model validation

Upon the establishment of the novel correlations, the model had to be validated. The accuracy of each new correlation was tested by error histograms and by comparison with different datasets.

Error histograms

Each data point of $G_{d,est}$ calculated with the new correlation, was compared to the measured values of G_d. The errors were calculated keeping the same units as $G_{d,est}$ and G_d (kWh/m^2) as follows:

$$\text{Error} = G_{d,est} - G_d$$

Equation 3.20

The error histograms for South-Yorkshire, Norfolk and West-Sussex are presented in Figure 3.8, Figure 3.9, and Figure 3.10, respectively.

An accurate correlation of horizontal diffuse solar irradiance is characterized by most estimates having minimal or no errors, with errors exhibiting a symmetrical distribution centred around 0. The error distribution is entirely symmetrical for all three correlations, indicating high accuracy of the results and therefore validating the developed correlations. Moreover, the correlation for South Yorkshire shows that 53% of the estimates fall within the intervals of [-0.01 0.01] kWh/m^2, while the corresponding percentages for Norfolk and West Sussex are 51% and 41%, respectively.

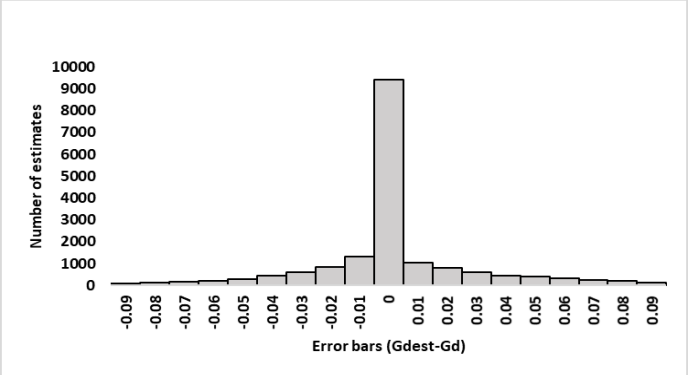

Figure 3.8 "Error histogram for the South-Yorkshire correlation" (Figure obtained from [174]).

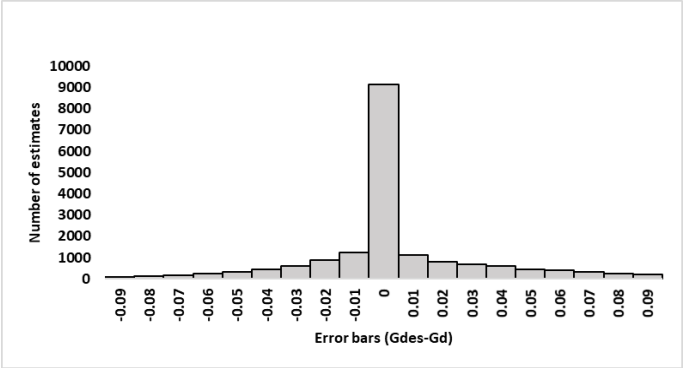

Figure 3.9. "Error histogram for the Norfolk correlation" (Figure obtained from [174]).

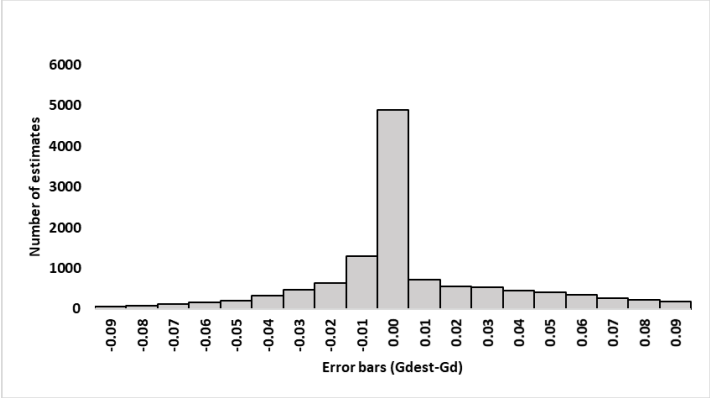

Figure 3.10. "Error histogram for the West-Sussex correlation" (Figure obtained from [174]).

Comparison between different datasets

A complementary test has been carried out to evaluate the accuracy of the new correlations developed for South-Yorkshire, Norfolk, and West-Sussex. Three distinct datasets were employed for each location to verify the robustness of the outcomes. The underlying expectation was that the statistical error metrics should exhibit negligible fluctuations across these datasets. This would imply that the correlations can be used to accurately predict the

horizontal diffuse solar irradiance at the specific location. To study the accuracy of the developed correlations, first, the existing empirical models have been evaluated with three different datasets. This makes it possible to compare the existing models and the new correlations. Table 3.7 provides information on the years used for complete, training and validation datasets for each location.

Table 3.7. "Detailed information of the dataset used as complete, training and validation datasets" (Table obtained from [174]).

	Complete dataset	**Training dataset**	**Validation dataset**
South-Yorkshire	1982-1995	1982-1989	1990-1995
Norfolk	1982-1999	1982-1993	1994-1999
West-Sussex	1982-1992	1982-1987	1988-1992

Table 3.8 presents the outcomes of the current empirical models for the three locations. The results obtained from these models showed minor variations between the datasets.

Table 3.8. "Statistical error metrics obtained for the existing empirical models using different datasets" (Table obtained from [174])

South Yorkshire									
	Complete dataset			Training dataset			Validation dataset		
	r^2	MBE	RMSE	r^2	MBE	RMSE	r^2	MBE	RMSE
Model 1	0.86	-0.022	0.045	0.862	-0.023	0.046	0.863	-0.0215	0.044
Model 2	0.856	-0.013	0.040	0.857	-0.014	0.041	0.859	-0.0129	0.039
Model 3	0.861	-0.015	0.041	0.859	-0.015	0.042	0.860	-0.0142	0.040
Model 4	0.770	-0.0016	0.048	0.769	-0.002	0.040	0.77	-0.0018	0.040
Norfolk									
	Complete dataset			Training dataset			Validation dataset		
	r^2	MBE	RMSE	r^2	MBE	RMSE	r^2	MBE	RMSE
Model 1	0.839	-0.023	0.048	0.842	-0.024	0.049	0.836	-0.022	0.048
Model 2	0.836	-0.015	0.044	0.838	-0.016	0.044	0.833	-0.014	0.044
Model 3	0.837	-0.017	0.044	0.839	-0.017	0.045	0.833	-0.016	0.044
Model 4	0.789	-0.001	0.039	0.797	-0.002	0.038	0.778	-0.0002	0.039
West Sussex									
	Complete dataset			Training dataset			Validation dataset		
	r^2	MBE	RMSE	r^2	MBE	RMSE	r^2	MBE	RMSE
Model 1	0.829	-0.026	0.051	0.826	-0.019	0.048	0.827	-0.0108	0.033
Model 2	0.823	-0.017	0.047	0.823	-0.018	0.048	0.822	-0.0148	0.045
Model 3	0.825	-0.018	0.047	0.826	-0.019	0.048	0.824	-0.0161	0.045
Model 4	0.771	-0.001	0.041	0.783	-0.003	0.045	0.757	0.00146	0.045

Table 3.9 displays the differences between the training dataset and the validation dataset for the newly developed correlations. Overall, the performance indicators exhibit minimal variations between both datasets, indicating the accuracy of the correlations in determining values of horizontal diffuse solar irradiance for the studied locations. To conclude, the new correlations present an improvement if compared with existing models for the regions studied.

Table 3.9. "Accuracy evaluation of developed correlation using different datasets" [174]

	Training dataset			**Validation dataset**		
	r^2	MBE	RMSE	r^2	MBE	RMSE
South-Yorkshire	0.877	0.001	0.025	0.872	0.0015	0.027
Norfolk	0.85	0.002	0.033	0.840	0.004	0.04
West-Sussex	0.844	0.002	0.04	0.830	0.003	0.03

3.2.3 Direct horizontal solar irradiance (G_b)

Direct horizontal solar radiation, also called beam radiation, is the portion of the global radiation that arrives at the Earth's surface directly from the sun [186]. And it can be accurately calculated using Equation 3.1 with the knowledge of global and diffuse horizontal solar radiation values.

3.2.4 Results

Values of horizontal global solar irradiation (G_H), horizontal diffuse solar irradiation (G_d) and horizontal direct solar irradiation (G_b) are presented in Figure 3.11 modelled for the city of Sheffield.

The value of G_H corresponds to ground measurements obtained in a weather station closed to Watnall (Nottinghamshire) in 2018. G_d have been estimated by using the diffuse horizontal correlation based in South Yorkshire. Finally, G_b has been calculated using Equation 3.1.

Figure 3.11 shows the hourly results on horizontal global, diffuse, and direct solar irradiation for a week in January (Figure 3.11a), and a week in July (Figure 3.11b). Horizontal solar irradiation values received in January are lower than those received in July. Mainly due to the amount of horizontal direct irradiation that arrives at the horizontal surface. In July, there is more hours of sun and the sky tend to be clear most of the time, so the majority of the solar

irradiation received is direct. On the contrary, in winter and autumn, the sky is covered by clouds and the radiation received is mostly diffuse.

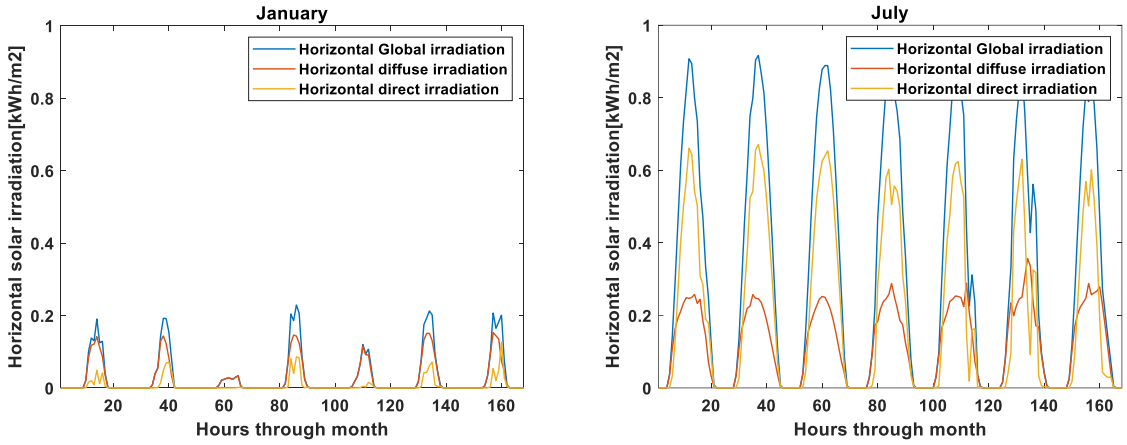

(a) (b)

Figure 3.11. Hourly results on horizontal global (G_H), diffuse (G_d), and direct (G_b) solar irradiation on a week in (a) January and (b) July.

The results obtained on horizontal solar irradiation are used in the next section, following Figure 3.1, for the estimation of solar irradiation on inclined surfaces.

3.3 Solar modelling on inclined surfaces

In section 3.2, the importance of knowing accurate values of horizontal solar irradiation was highlighted and values of horizontal global (G_H), diffuse (G_d), and direct (G_b) solar irradiation were estimated. Those are essential parameters for the estimation of irradiation on inclined/tilted surfaces. PV solar systems are generally mounted on inclined surfaces and orientated to maximize the amount of available irradiation incident. Consequently, the solar irradiation incident on a tilted surface has to be determined by converting solar radiation from horizontal surface to the tilted surface of interest [247].

Inclined solar radiation (G_β) is the irradiation incident on an inclined surface to the ground. The calculation of solar radiation on inclined surfaces, as described by Equation 3.21, is the addition of the beam component from direct inclined radiation ($G_{b\beta}$), diffuse inclined radiation ($G_{d\beta}$), and reflected radiation (G_r).

$$G_\beta = G_{b\beta} + G_{d\beta} + G_r$$

Equation 3.21

3.3.1 Direct beam solar radiation on inclined surfaces ($G_{b\beta}$)

The direct irradiation on inclined surfaces *(*$G_{b\beta}$*)* can be computed using geometrical relationships (i.e. angle of incidence, zenith angle) between the horizontal and inclined surfaces, according to the following equation:

$$G_{b\beta} = G_{bN} \cdot \cos(\theta) = \frac{G_b}{\cos(\theta_z)} \cdot \cos(\theta) = \frac{G_b}{\sin(\gamma_s)} \cdot \cos(\theta) = G_b \cdot r_b$$

Equation 3.22

The zenith angle (θ_z) is the complement to the solar altitude γ_s. G_{bN} is the beam component of the direct irradiation and G_b is the horizontal direct solar irradiation on a horizontal surface. r_b is the ratio of hourly radiation received by a tilted surface to that of a horizontal surface outside the earth's atmosphere. The solar incidence angle (θ) allows the prediction of the amount of radiation received on a solar panel at a specific time and location [248]. It is the angle between the sun rays and the normal on a surface. Together with zenith angle allows for the conversion of direct solar irradiance between horizontal and inclined surfaces. Following equation from Mcevoy *et al.* [248] θ is calculated as:

$$\cos\theta = (\cos\gamma_s \cdot \cos(\alpha_S - \alpha) \cdot \sin\beta) + (\cos\beta \cdot \sin\gamma_s)$$

Equation 3.23

where α is the angle at which the panel is orientated, in degrees from 0° to 360°, β is the inclination angle of the panel, and α_S is the azimuth angle.

Solar azimuth (α_S) is the angle between the projection of sun's centre onto the horizontal plane and due north considering a north orientated system. The azimuth angle calculation follows the equation below [228,249].For morning hours, $t \leq 12$

$$\text{For } \omega \leq 180,\ \cos\alpha_s = \left(\frac{\sin\delta \cdot \cos\varphi + \sin\varphi \cdot \cos\delta \cdot \cos\omega}{\cos\gamma_S}\right)$$

Equation 3.24

The afternoon azimuth for $t > 12$

$$\text{For } \omega > 180,\ \cos\alpha_s = 360 - \left(\frac{\sin\delta \cdot \cos\varphi + \sin\varphi \cdot \cos\delta \cdot \cos\omega}{\cos\gamma_S}\right)$$

Equation 3.25

where φ is the latitude, δ is the declination angle, ω is the hour angle and γ_s is the solar altitude angle, all of them introduced in Section 3.2.2.1.

3.3.2 Reflected solar radiation (G_r)

The estimation of reflected irradiation (G_r) requires values of the global horizontal solar irradiation (G_H) and the albedo. The conventional method for modelling reflected radiation assumes that the reflected rays are diffuse and the coefficients of reflection of the beam and diffuse rays are identical [247]. The reflected radiation is calculated as follows:

$$G_r = G_H \cdot \rho \cdot \left(\frac{1 - \cos\beta}{2}\right)$$

Equation 3.26

Where ρ is the albedo and and β is the inclination angle of the panel.

The albedo represents the ground's reflectance of solar radiation. Liu and Jordan [250] determined a value of albedo equal to 0.2 -0.7(with snow). In a study by Gul *et al*. [251] various

surfaces and sky conditions were compared to determine their impact on the albedo. The authors concluded that the albedo value remained relatively constant for overcast skies. For this study, concrete was assumed as the surface material with an albedo value of 0.2.

3.3.3 Diffuse solar radiation on inclined surfaces ($G_{d\beta}$)

It is not possible, on the other hand, to calculate diffuse irradiation on inclined surfaces ($G_{d\beta}$) by geometrical relationship because the diffuse component comes from all points of the sky [252,253].

Many authors have been testing the most appropriate diffuse radiation model on inclined surfaces. In literature, those have been divided in isotropic and anisotropic models [204]. Isotropic models are simple models that assumes that the sky distribution of the diffuse irradiation is uniform over the sky dome. Thus, the diffuse component resulting from the solar radiation scattering and the horizon brightening component area assumed to be zero [252]. On the other hand, the anisotropic models are more complex. Those models assumed not only the isotropic diffuse component but also the anisotropic effect of the diffuse sky radiation [254]. According to Reindl *et al*. [255] isotropic models are not recommended for calculating diffuse solar radiation on tilted surfaces across various locations in the United States.

Noorian *et al.* [254] investigated twelve distinct models for diffuse radiation to determine the model that best matched actual data from Iran. The authors found that depending on the orientation of the panel, some models adjusted better than other ones, but they concluded that anisotropic models, in both scenarios, were the best fits to real data. El-Sebaii *et al*. [256] compared isotropic and anisotropic models in Saudi Arabia. The findings revealed that the anisotropic model accurately estimated solar radiation on inclined surfaces. Demain *et al*. [252] made an extensive comparison between 14 different isotropic and anisotropic models. The authors evaluated the models with measured solar irradiation data from Belgium. The results from the statistical analysis showed that the performance of each model is clearly influenced by the sky conditions. Moreover, none of the models analysed performed well for all the sky conditions. To overcome this limitation, the author combined three anisotropic models that resulted to be better for the estimation of the global irradiation on inclined surfaces.

Maleki *et at*., [204] conducted a comprehensive review of various studies that examined the most suitable models for calculating solar radiation on tilted surfaces across different locations.

The authors highlighted that both isotropic and anisotropic models can provide accurate results, depending on the location. However, for the present study, only the models highlighted by Maleki *et at.,* [204] with highest accuracy for different locations around the world has been selected for the calculation of diffuse solar irradiation on inclined surfaces. The models selected corresponds to Hay's (1979) [257], Willmott's (1982)[258] and Reindl's (1990) models [255].

- Hay's model:

$$G_{d\beta} = G_d \cdot \left[F_{Hay} \cdot r_b + (1 - F_{Hay})\left(\frac{1 + \cos\ \beta}{2}\right)\right]$$

Equation 3.27

Where G_d is the horizontal diffuse solar irradiance, r_b is the ratio of hourly radiation received by a tilted surface to that of a horizontal surface outside the earth's atmosphere, β is the inclination angle of the panel and F_{Hay} is an anisotropic index used by Hay and can be obtained following Equation 3.27.

$$F_{Hay} = \frac{G_b}{G}$$

Equation 3.28

Where G_b is the horizontal direct solar irradiance and G is the hourly horizontal extra-atmospheric irradiance.

- Willmott's model:

$$G_{d\beta} = G_d \cdot \left[\frac{G_{bN} \cdot r_b}{I_0} + C_\beta\left(1 - \frac{G_{bN}}{I_0}\right)\right]$$

Equation 3.29

where I_0 is the solar constant, G_d is the horizontal diffuse solar irradiance, r_b is the ratio of hourly radiation received by a tilted surface to that of a horizontal surface outside the earth's atmosphere, G_{bN} is the beam component of the direct irradiation and C_β can be calculated as followed:

$$C_\beta = 1.0115 - 0.20293\beta - 0.080823\beta^2 \text{ [}\beta\text{ is in radians]}$$

Equation 3.30

- Reindl's model:

$$G_{d\beta} = G_d \cdot \left[F_{Hay} \cdot r_b + (1 - F_{Hay})\left(\frac{1 + \cos\beta}{2}\right)\left(1 + f_R \sin^3\left(\frac{\beta}{2}\right)\right)\right]$$

Equation 3.31

All the parameters have been introduced in the previous model except the modulating function f_R, that accounts for the impact of increasing overcast sky on diffuse radiation intensity, that can be calculated following Equation 3.32

$$f_R = \sqrt{\frac{G_b}{G_H}}$$

Equation 3.32

The anisotropic models have been applied to estimate the diffuse solar irradiation on inclined surfaces and the hourly results can be seen in Figure 3.12a (Hay's model), Figure 3.12b (Willmott's model) and, Figure 3.12c (Reindl's model). Additionally, Figure 3.12 shows hourly values of reflected and direct solar irradiation on inclined surfaces and the total solar irradiation received in an inclined surface (Equation 3.21). The reflected and direct solar irradiation on inclined surfaces have the same values for the three different graphs on Figure 3.12, as its output does not depend on the anisotropic model used. The diffuse inclined solar irradiation changes with the anisotropic models applied.

Both Willmott's model and Reindl's model were developed based on Hay's model. When Hay's model and Reindl's model are used, inclined diffuse solar irradiation ($G_{d\beta}$) is almost identical for both models. Reindl's model is a modification on Hay's model. It introduces an index that takes into consideration the horizon brightening diffuse radiation [255]. The values are slightly higher than those for Hay's model because are considering the horizon brightening proportion of the diffuse irradiation. However, this portion of the diffuse irradiation does not seem to be relevant for the location studied [259].

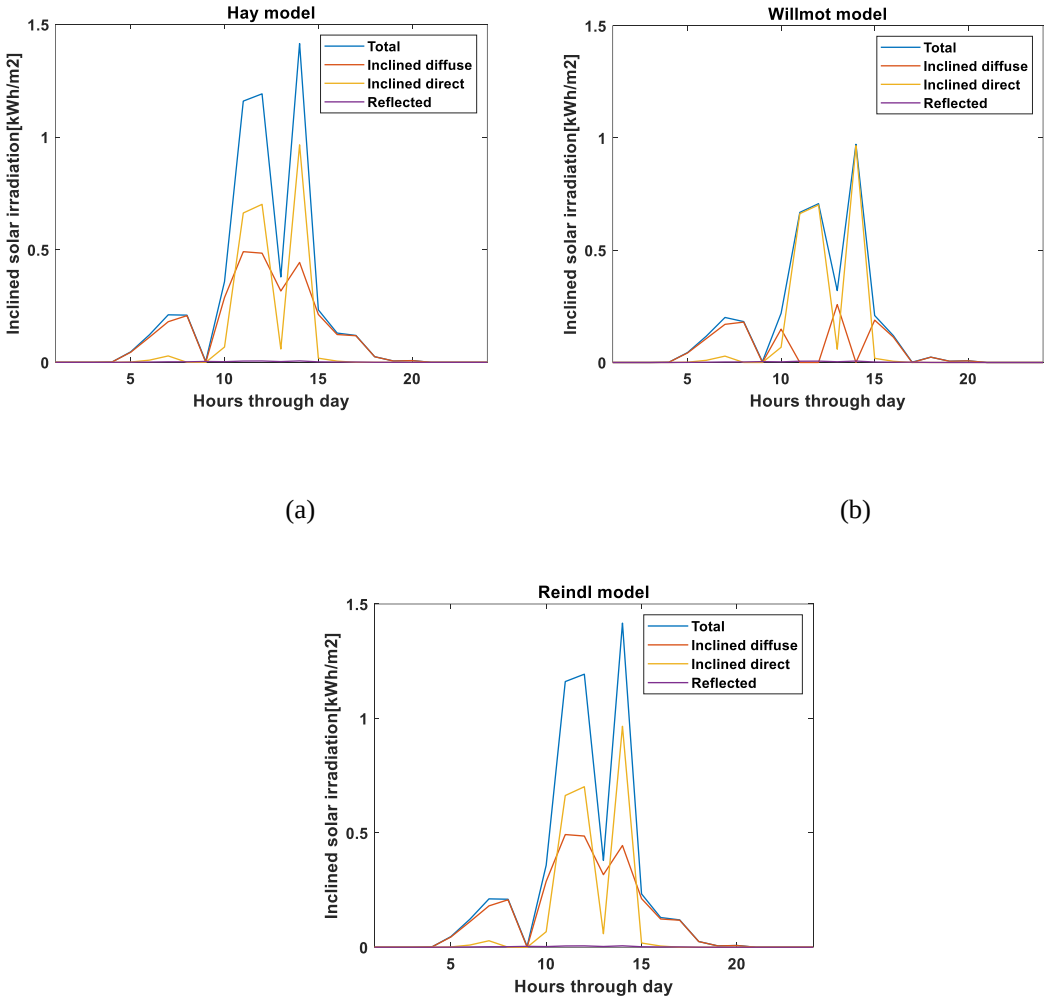

Figure 3.12. Hourly values on inclined total (G_{β}), diffuse ($G_{d\beta}$), direct ($G_{b\beta}$) and reflected (G_{r}) solar irradiation for a day in July using (a) Hay anisotropic model, (b) Willmott anisotropic model and (c) Reindl model.

On the contrary, the results obtained for $G_{d\beta}$ when Willmott's model is applied, differ from the other two. Willmott's model introduces a new anisotropic index and modified Hay's model. As it can be seen in Figure 3.12, the model under predicts values of diffuse solar irradiation on inclined surfaces on clear hours (i.e.at 11:00h, 12:00h, and 14:00h when there is higher amount of direct irradiation hitting the surface). This can be seen better in Figure 3.13. The results were calculated for a day in February. The sky is covered by clouds predominantly, and the inclined diffuse solar irradiation reported by both, Reindl's anisotropic model (see Figure 3.13a) and Willmott's anisotropic model (see Figure 3.13b) is the same.

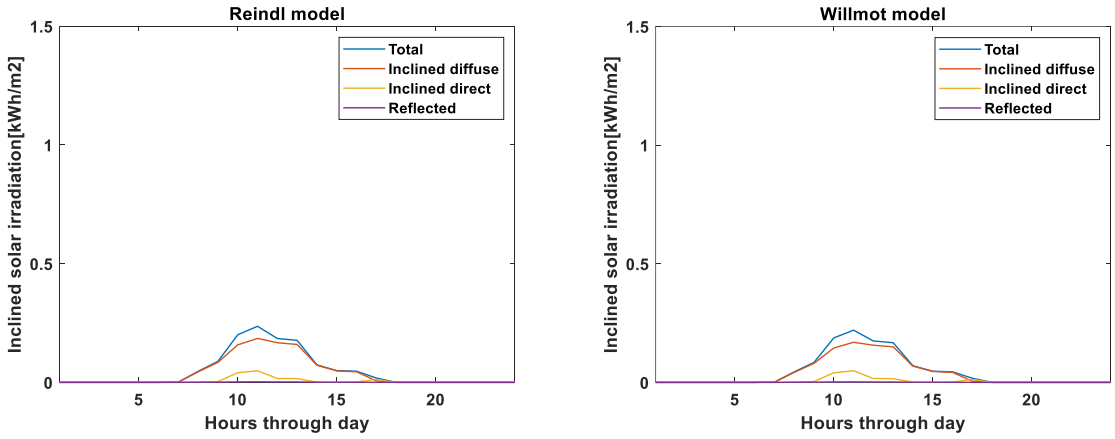

(a) (b)

Figure 3.13. Hourly results obtained when (a) Reindl anisotropic model and (b) Willmott anisotropic model are used to calculate inclined diffuse solar irradiation on a day in February.

When the total amount (i.e. over a year) of irradiation received by a PV panel inclined 25° for the region of South-Yorkshire is calculated, the differences between the three models analysed is almost negligible as it can be seen in Table 3.10. However, for the purpose of the study, the model selected to calculate diffuse solar irradiation on an inclined surface and to progress with the estimation of PV solar energy generation is Hay's model. The model has been selected because the one that better fits solar irradiation values received on a surface studied in Sheffield.

Table 3.10. Total amount of solar irradiation per year in an inclined PV panel at 25 degrees

Total amount of solar irradiation received per year (kWh/m^2)		
Reindl's model	**Hay's model**	**Willmott's model**
1,066	1,064	1,038

Details on how the solar model has been validated are included in Section 3.5.

3.4 From solar irradiation to energy generation

The solar model predicts solar irradiation received on an inclined surface. However, the most interesting parameter for the implementation of solar system is the energy generation. Thus, the model developed in this study converts the computed solar irradiation into energy generation by considering inverter efficiency (ηi), panel efficiency (ηp) and panel dimensions and total number of panels following Equation 3.33.

$$\text{Energy generated (kWh)} = G_\beta \left(\frac{\text{kWh}}{\text{m}^2}\right) \cdot \eta i \cdot \eta p \cdot \text{panel dimenssions } (\text{m}^2) \cdot \text{n°ofpanels}$$

Equation 3.33

3.5 Solar model validation

The solar model as been validated against a private household PV installation and a PV installation located in one of the M&S rooftop stores.

3.5.1 Private household PV solar energy installation

In order to validate the model, measured solar energy generation from a PV solar installation in Sheffield (South-Yorkshire) has been used. The system for the measured data collection is made for 16 solar panels which are south orientated with a tilt angle of 30 degrees. The data was measured as hourly energy generation (kWh) for the period of March 2018 to December 2018.

Inclined solar irradiation values (G_β) were transformed into energy generation values by applying Equation 3.33. The values assumed to transform solar irradiation on inclined surfaces (kWh/m^2) into PV solar energy generation (kWh) are introduced in Table 3.11.

Table 3.11. Values assumed for the conversion between energy and solar irradiation on a PV installation inclined.

Parameter	Value
Inverter efficiency (%)	0.8
Panel efficiency (%)	0.14
Panel dimensions (m^2)	1.64
Number of panels	16

It was discussed throughout the literature review, and it has been confirmed during the validation process that the location of solar radiation weather stations and the year of measurements used for the input data to the model, impact the hourly modelled output significantly. Figure 3.14 shows the measured hourly values of total PV solar energy generated in the installation studied in Sheffield for the month of April (orange). Whilst values of modelled PV solar energy using Hay's anisotropic model can be seen for the month of April (blue). The input data to the model corresponds to averaged ground measurements of global horizontal solar irradiation (G_H) from the region of South-Yorkshire. Precisely, ground measurements values were taken in the weather station of Finningley between 1982 and 1995. On the other hand, measured and modelled values of hourly PV solar energy generation has been compared in Figure 3.15 using different values of G_H. The ground measurements of G_H took place in a weather station located in Watnall (Nottinghamshire) in 2018. If both figures are compared (Figure 3.14 and Figure 3.15), it can be seen that the model adjusts better to measured values of PV solar energy generation when the ground measurements of G_H are taken on the same year as the measured values of solar energy generation.

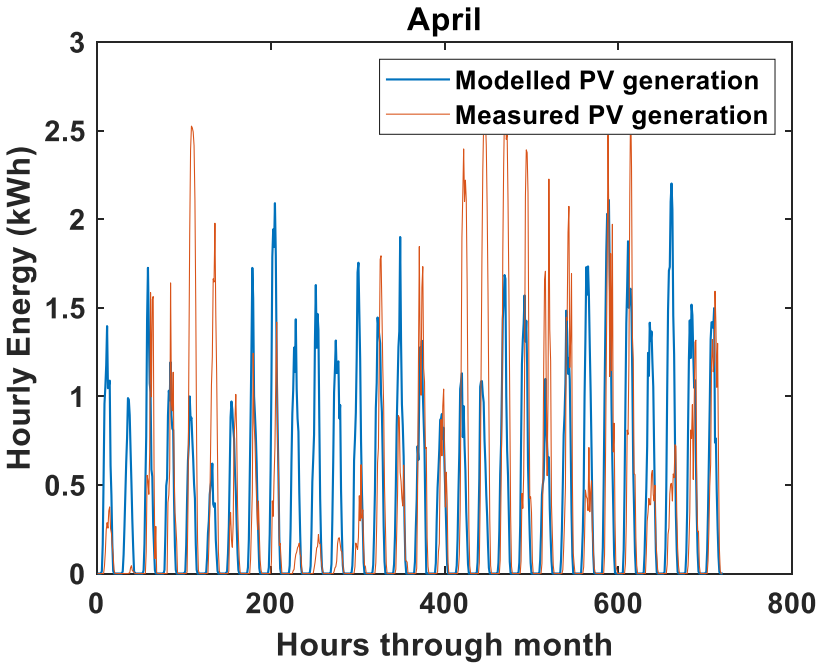

Figure 3.14. Comparison of hourly PV solar energy in the month of April between measured data from Sheffield in 2018 (red line) and data modelled using averaged values of G_H from Finningley between 1982 and 1995 (blue line).

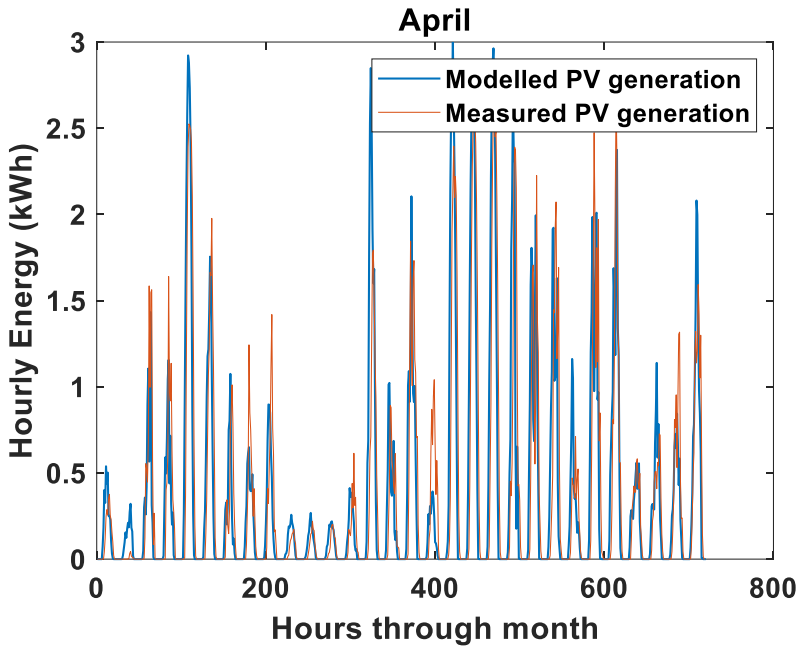

Figure 3.15. Comparison of hourly PV solar energy in the month of April between measured data from Sheffield in 2018 (red line) and data modelled using values of G_H from Watnall in 2018 (blue line).

The total amount of PV solar energy generated has been obtained for both, the measured and the modelled values. The results can be seen in Table 3.12. The difference between measured and modelled values has been calculated following Equation 3.34.

$$\%\ \text{error} = \left|\frac{\text{model value} - \text{measured data}}{\text{measured data}}\right| \cdot 100$$

Equation 3.34

As it can be seen in Table 3.12, the percentage error between measured and modelled PV solar energy generation values are below 10%. Furthermore, when the input data used for the model (G_H) corresponds to ground measurements from just 2018 (the year of the validation measurements), the model gives lower errors (7% error) than when input data of averaged values between 1982 and 1995 is used (9.5% error).

Table 3.12. Comparison between measured values and modelled values of total solar irradiation received for one panel inclined 25° in the region of South-Yorkshire.

	Total PV solar energy generation	
Measured values in Sheffield (kWh)	2,826	
Modelled values (kWh)	Input data South- Yorkshire (Averaged 1982-1995)	Input data Nottinghamshire (2018)
	2,558	3,041
Error difference (%)	**9.5**	**7**

Monthly comparisons have also been carried out between measured and modelled values as it can be seen in Figure 3.16. For the purpose of this comparison, monthly values of solar irradiation (G_β) have been calculated to be compared with measured monthly values of solar irradiation. The monthly values have been estimated by adding every hour of the month for the modelled values. In case of the measured values, daily measurements from the same installation in Sheffield in 2012 have been added for each month. The modelled data have been created using values of global horizontal solar irradiation from South-Yorkshire measured between 1982-1995 (Figure 3.16a) and from North-Yorkshire measured in 2012 (Figure 3.16b).

The model adjusts better when the input data (i.e., ground measurements of global horizontal solar irradiation) corresponds to values taken the same year as the measured values (Figure 3.16b). The weather conditions change every year, and this impacts the solar irradiation received at a certain location and needs to be remembered when the model is being validated. When the model is being used to predict average possible generation from a location, averaged input data (G_H) from across a number of years is a better input to the model

Therefore, it can be concluded that the higher the precision on input data, the better the approach from the model to measured values. The percentage error has been calculated for all the input data measurements (i.e. South-Yorkshire, North-Yorkshire, and Nottinghamshire) being the percentage error below a 10% for all of them.

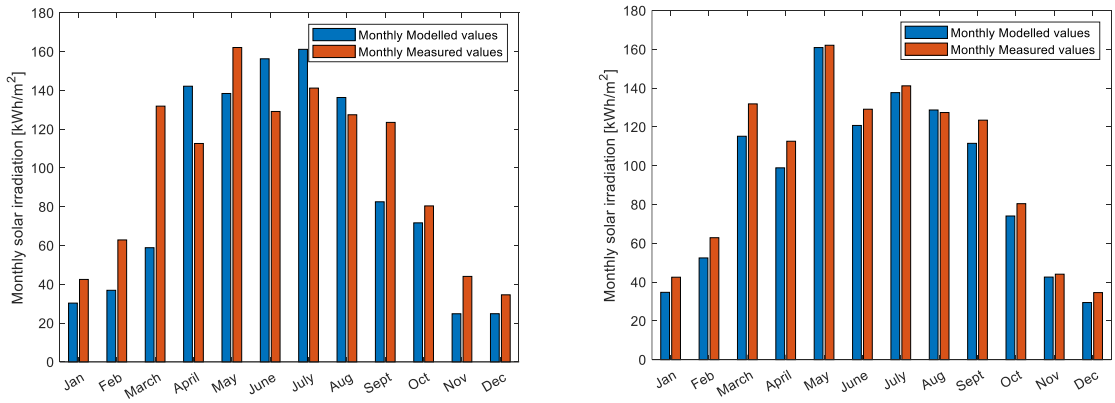

(a) (b)

Figure 3.16. Comparison between measured monthly values in Sheffield (2012) and modelled values using ground measurements from (a) South-Yorkshire from 1982 – 1995 and from (b)North-Yorkshire in 2012.

3.5.2 PV solar energy installation in a M&S store

M&S has provided data of PV solar energy generation at the store located in Vangarde Retail Park in York. The store has 600 PV panels installed (see Figure 3.17).

Figure 3.17. M&S York Vangarde Retail Park (image taken from Google maps)

Part of the roof is inclined towards the south and part inclined towards north. The majority of the solar panels are installed over the roof inclined towards south. Panels installed in the north-face part of the roof, are tilted towards the south as well (Figure 3.18). It has been estimated that the PV panels are tilted 10° to the horizontal.

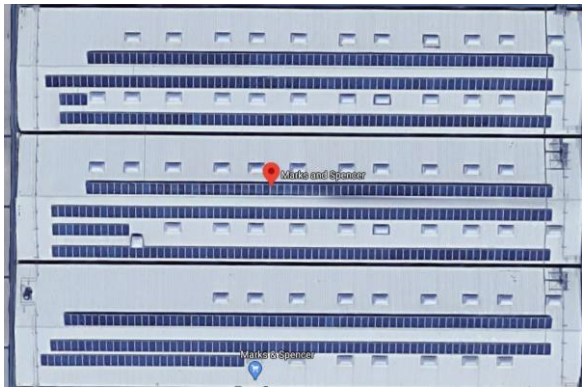

Figure 3.18. PV panel rooftop installation in M&S York Vangarde Retail Park (image taken from Google maps).

The time period and the frequency of measurements provided for the PV installation are shown in detail in Table 3.13.

Table 3.13. Data provided by M&S for the validation of the solar model

Type	Time period	Frequency
PV generation	31/03/2018 - 31/03/2019	Half hourly energy values (kWh)
	01/01/2019 - 31/12/2019	Daily energy values (kWh)

For the validation of the solar model, the half hourly values provided by M&S have been added to get hourly and daily measurements of PV solar energy generation. Modelled values of PV solar energy generation has been estimated considering the assumptions included in Table 3.14.

Table 3.14. Values assumed for the calculation of PV solar energy generation at York Vangarde Retail Park.

Parameter	Value
Inverter efficiency (%)	0.8
PV panel efficiency (%)	0.14
PV panel dimensions (m^2)	1.64
Number of PV panels	600
PV panel tilt angle (degrees)	10
PV panel orientation (degrees)	180

The total annual PV energy generation at York Vangarde Retail Park for 2019 was 138,276 kWh whereas for the period from March 2018 to March 2019 the PV solar energy generation was 93,764 kWh. The difference between both datasets can be seen Figure 3.19 in detail.

More precisely, Figure 3.19 shows daily PV solar energy output together with the modelled PV energy generation for measured values in 2019 (see Figure 3.19a) and, for measured values from March 2018 to March 2019 (see Figure 3.19b).

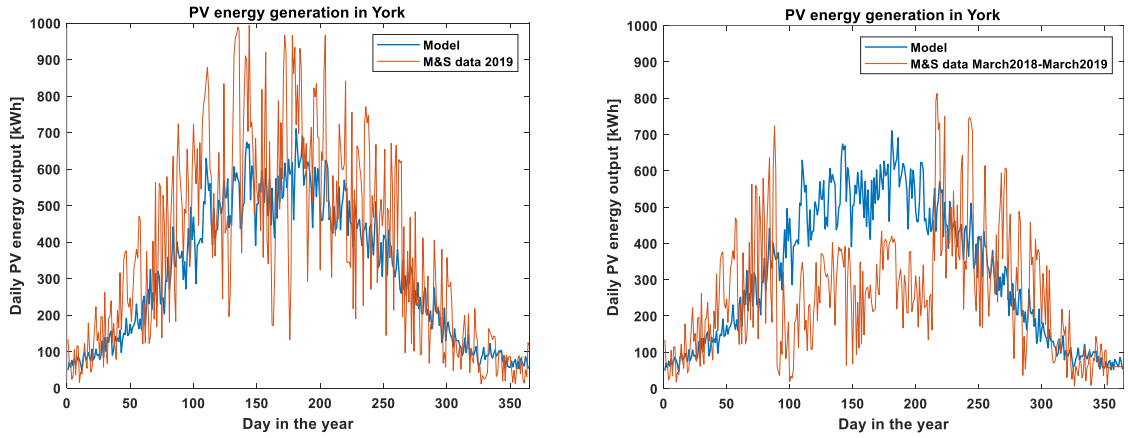

(a) (b)

Figure 3.19. Comparison between modelled daily PV energy generation (blue line) and measured daily PV energy generation (red line) at York Vangarde Retail Park (a) in 2019 and, (b) between March 2018 and March 2019.

The drop in PV solar energy generation at M&S York Vangarde in spring and summer when data was taken between March 2018 and March 2019 (Figure 3.19b) is related to a suspected error in measurements. For the modelled data (blue line) in Figure 3.19b, the PV energy

generation increases during spring-summer (April-July), when normally the skies are clear, and the weather achieves higher temperatures and decreases in autumn and winter months (February-September) when overcast skies prevail. On the contrary in Figure 3.19b, measurements from M&S York Vangarde store (orange line) report a higher PV energy output in autumn-winter season than in spring-summer season.

Some of the error measurements from values taken between March 2018 and March 2019 can be seen in detail in Figure 3.20 when hourly measured and modelled hourly energy generation values are plotted for a month in September (Figure 3.20a) and, for a month in December (Figure 3.20b). Specifically, for certain hours on the 11th of September (see Figure 3.20a) or during the last days of December (Figure 3.20b).

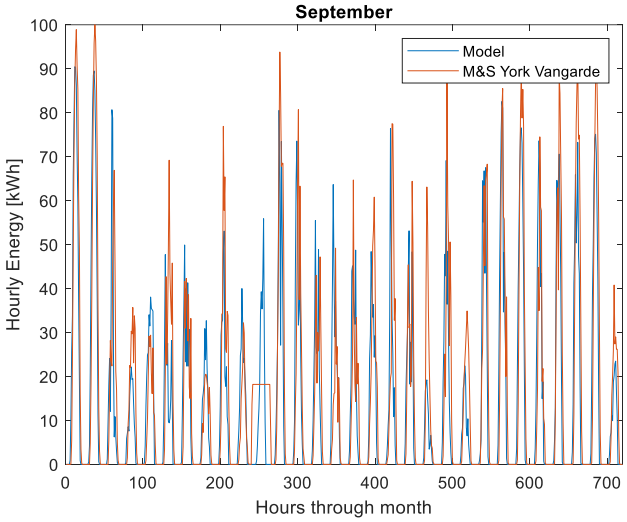

(a)

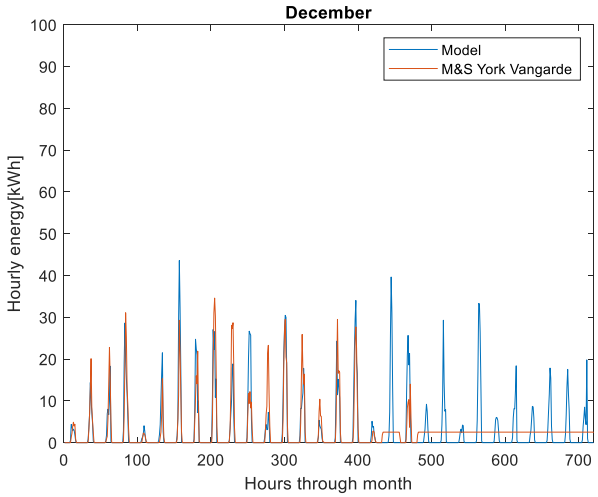

(b)

Figure 3.20. Modelled hourly PV energy generation (blue line) and measured hourly PV energy generation (orange line) at York Vangarde Retail Park in (a)September 20018 and (b) December 2018.

Due to the differences in PV energy output between the data provided and the error in measurements, the data used for the validation of the model corresponds to daily measurements of energy values from January 2019 to December 2019. The total energy generation for that period at York Vangarde Retail Park was 138,276 kWh. Whereas the total modelled PV solar generation obtained was 120,860 kWh. The error difference between both values can be seen in Table 3.15.

Table 3.15. Comparison between measured values and modelled values of total solar generation at M&S York Vangarde Retail Park.

	Total PV solar energy generation
Measured values at M&S York Vangarde (kWh)	138,276
Modelled values (kWh)	120,860
Error difference (%)	**12.6**

3.6 Case study: Locally generated PV solar energy

After its validation, the solar model was used to estimate PV solar generation at different locations within the UK for different companies. As an example, one of the case studies is presented in this section. The case study was developed for The Translational Energy Research Centre (TERC) and funded by the European Regional Development Fund [43].

The study aimed to support the company's decision to improve sustainability within its business by providing valuable information regarding a possible transition towards locally produced solar energy. For this purpose, the study evaluated the feasibility of a PV installation to offset some of the current energy use within the buildings with the help of the PV solar model developed and introduced in the previous sections. Additionally, the report explored relevant parameters per the main aim, such as estimated energy savings and electricity bill reduction, payback time and emission reductions.

3.6.1 Input data used for the solar model

The global horizontal solar irradiation (G_H) values used as input data to the solar model were obtained from a weather station at Watnall (Nottinghamshire) as an average of measurements taken between 2009 and 2019. The values assumed to transform solar irradiation (kWh/m2) into solar energy generation (kWh), following Equation 3.33, are included in Table 3.16.

Table 3.16. Values assumed for the conversion between energy and solar radiation on an PV inclined panel

Parameter	Value
Inverter efficiency (%)	0.80
Panel efficiency (%)	0.20
Panel dimensions (m^2)	1.67
Number of panels	
Scenario 1	596
Scenario 2	596
Scenario 3	1,136

The assumptions regarding PV panel dimensions and PV panel and inverters efficiency are based on the PV panel and inverter datasheet included in Appendix 1 and Appendix 2, respectively. The maximum efficiency achievable by the inverter is around 98-99%; however, a more conservative assumption has been made, using an average inverter efficiency of 80% due to the operation of the inverter typically not being at the optimum operating point for most of the operational cycle. For example, when operating below its rated power, the inverter still has some fixed losses, which reduce its operating efficiency. As can be seen in Table 3.16, the number of PV panels is different for the three scenarios explored. Detailed information on each scenario under study is provided in the following section.

3.6.2 Case study data

The case study was performed for a company in the industry sector. When this study was performed, the company depended entirely on the grid to cover the energy demand. The energy consumption, provided by the company as an hourly average value, was equal to 47.6 kWh. The company in Sheffield comprises several buildings; however, only two have been considered for installing PV panels. Each roof has been assigned a different name (the main roof - highlighted in blue in Figure 3.21, and the attached roof - highlighted in red in Figure 3.21).

The characteristics of the roofs have been estimated using Google Maps and are summarise in Table 3.17. The main roof has an area of approximately 1,600 m². Part of the roof is orientated towards the southeast, and the other part faces the northwest. The angle of orientation towards the southeast is approximated at 125 °, and the other half of the roof is assumed to be oriented 305 ° northwest. The elevation of the roof is assumed to be 20°. In this case, both halves of the main roof have the same roof elevation. The attached roof has an area of approximately 792 m². The orientation of the attached roof is the same assumed for the main roof. The elevation

of the roof has been set as 5° from estimates provided by the company. Both sections of the attached roof have the same tilt angle.

Table 3.17. Main and attached roof orientation and elevation angles.

	Main roof		**Attached roof**	
Roof elevation	20°		5°	
Roof orientation	South east	North west	South east	North west
	125°	305°	125°	305°

Based on roof characteristics assumptions and the portion of the roof available for PV panel installation, the PV panels in the main roof and attached roof would likely be distributed as shown in Figure 3.21. The criteria considered for the installation of the PV panels was to keep the existing skylights unobstructed.

Figure 3.21. Company plant from a bird's eye view corresponding to the main roof (blue) and the attached roof (red) (image created from the author using Google maps view).

Roof refurbishment project

The company asked to explore a new scenario for the PV installation based on the refurbishment of both roofs. For the new roofs, the area available for panels was now taken as a fraction of the total area. Due to the configuration of the rooftops, with fewer physical hurdles, it was assumed that 80% of the total area would be available for PV installation [260]. Within the 20% off, it is assumed that 10% of the area is covered by skylights and an additional 10% is restricted as a maintenance area and area covered by electrical equipment. Taking 20% off

each roof area, the maximum available space for installing PV panels in the main roof would be 1,280 m². The available area for the attached roof would equal 634 m².

The number of PV panels selected for each orientation of the rooftop, according to the actual and the refurbished roof, are summarised in Table 3.18.

Table 3.18. Number of PV panels assumed to be installed using the actual roof configuration and the new roof configuration (with 10% skylights).

Number of PV panels installed					
		Main roof		Attached roof	
	Total	South-east	North-west	South-east	North-west
Actual roof	596	216	212	102	66
New roof (refurbished)	1,136	380	380	263	113

3.6.2.1 Scenarios studied

This case study defines three scenarios for analysing and evaluating introducing PV solar panels into the company. The study estimates the hourly, monthly, and annual solar energy generation values for the three scenarios. Additionally, it gives detailed information on estimated energy and electricity bill savings, emission reductions and payback time.

Scenario 1

Scenario 1 is built upon the characteristics of the actual roofs. Detailed information on Scenario 1 is included in Table 3.19.

Table 3.19. Characteristics assumed for the roofs and PV panels installed for Scenario 1.

	Roof orientation		Roof elevation		Number of PV panels		PV panel orientation		PV panel elevation	
	South east	North west	South east	North west	South east	North west	South east	North west	South east	North west
Main roof	125°	305°	20°		216	212	125°	305°	20°	
Attached roof			5°		102	66			5°	

Scenario 2

In Scenario 2, PV panels are installed at the optimum PV panel tilt/elevation according to the roof orientation. The optimum PV panel elevation or tilt is the one that gives the highest annual energy generation on each roof. Thus, expectations are that the annual energy output will be

higher than in Scenario 1. However, the installation cost will also be higher, as frames will be required to hold the panels at the optimum angle, increasing the installation costs.

The optimum panel tilt/elevation angle has been calculated using the PV solar model. Figure 3.22 shows the annual energy output for different panel orientations and tilt/elevation angles. Yellow indicates the highest energy output values, and purple indicates the lower output achieved. Considering the orientation of the roofs of the company studied, the optimum panel tilt/elevation angle when the roof is orientated 125 ° southeast would be approximately 22°. For the roof section orientated at 305 ° northwest, the optimum panel tilt/elevation angle equals 0°.

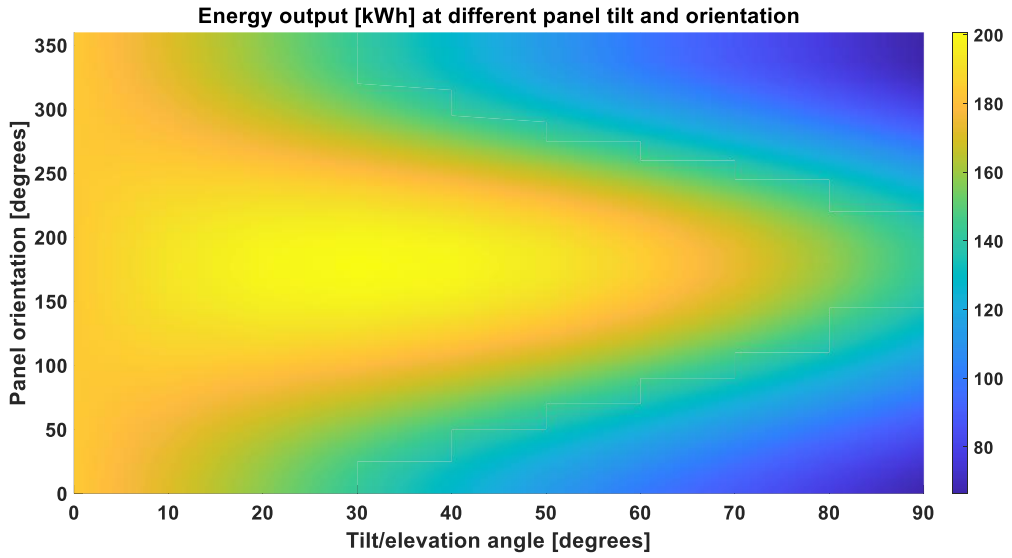

Figure 3.22. Annual energy output (colour scale) achieved for each panel orientation and tilt/elevation angle.

The specifications and assumptions made for the Scenario 2 are included in detail in Table 3.20.

Table 3.20: Characteristics assumed for the roofs and PV panels installed for Scenario 2.

	Main roof		Attached roof	
Roof elevation	20°		5°	
PV panel tilt	22°		0°	
Roof orientation	South east	North west	South east	North west
	125°	305°	125°	305°
Number of PV panels	216	212	102	66

Scenario 3

Scenario 3 is built upon the roof refurbishment project. Therefore, the number of PV panels in Scenario 3 is higher than in Scenario 1 and Scenario 2, so a higher energy annual output would be expected. Detailed information about the characteristics and assumptions for Scenario 3 is shown in Table 3.21.

Table 3.21. Characteristics assumed for the roofs and PV panels installed for Scenario 3.

	Main roof		Attached roof	
Roof elevation	20°		5°	
PV panel tilt	20°		5°	
Roof orientation	South east	North west	South east	North west
	125°	305°	125°	305°
Number of PV panels	380	380	263	113

3.6.2.2 Parameters analysed

The analysis of energy savings, emission reductions and payback time is supported by the assumption of prioritising the use of solar energy whenever available. If solar generation does not meet the demand at each hour, the plant will also draw energy from the grid. On the contrary, when solar generation exceeds the demand, the surplus is sold to the grid.

Energy savings

Energy savings are estimated considering values of energy consumption and solar energy generation. For the energy consumption, the hourly average value provided by the company, and equal to 47.6 kWh, was used. The solar energy generation values used were calculated hourly. The difference between the generation and consumption was calculated as well as the energy that would come from the grid, from solar energy and the surplus solar energy sold to the grid.

To estimate the cost of the energy from the grid, the total amount of the energy consumption from the grid was split between two different unit rates. According to the information provided by the company regarding the forecast consumption and energy cost, approximately 92% of the total consumption will lie in the unit rate between 07:00-24:00 (12.528 pence per kWh) while the remaining 8% will correspond to the unit rate between 00:00-07:00 (10.896 pence per kWh). The total cost of the electricity corresponds to the cost of the energy consumed from

the grid minus the surplus sold to the grid (value assumed equal to 5 pence per kWh)[3] [261,262].

$$\text{Total cost of electricity} = \text{Cost of energy from the grid} - \text{Surplus earnings}$$

Equation 3.35

GHG emission reductions

The GHG impact factors considered for the calculation of GHG emissions are the following:

- 233 gCO_2eq/kWh from the UK grid mix [263].
- 68.6 gCO_2eq/kWh from photovoltaics obtained from Gabi Software model[4].

The estimated annual GHG emissions have been obtained following Equation 3.36 for the emissions associated with energy grid consumption and, Equation 3.37 for the emissions associated with the solar energy consumption, respectively.

$$\text{Grid impact} = \text{Energy from grid (kWh)} * 233\ \frac{gCO_2}{kWh}$$

Equation 3.36

$$\text{PV installation impact} = \text{Solar energy consumption (kWh)} * 68.6\ \frac{gCO_2}{kWh}$$

Equation 3.37

The surplus energy is sold to the grid, where it displaces the need to generate electricity by higher-carbon sources, because of this it receives a credit equivalent to that of the grid mix impact (Equation 3.38).

$$\text{Surplus impact} = \text{Surplus(kWh)} * 68.6\frac{gCO_2}{kWh} - \text{Surplus(kWh)} * 233\ \frac{gCO_2}{kWh}$$

Equation 3.38

[3] An approximate value corresponding to the Smart Export Guarantee (SEG) tariff offered by electricity suppliers (i.e. British gas: 3.2 pence per kWh, Bulb: 5.57 pence per kWh) in 2019.

[4] The photovoltaic model is based on the global average market mix of photovoltaic technologies installed: Mono-Silicon 42 %, Multi-Silicon 47 %, Cadmium-Telluride (CdTe) 7 % and Copper-Indium-Gallium-Diselenide 4 %.

Payback time

The payback time for each scenario has been calculated following Equation 3.39.

$$\text{Payback time (years)} = \frac{\text{Total capital cost}}{\text{Annual savings} - \text{Annual maintenance}}$$

Equation 3.39

The capital cost includes the PV panels, inverters, and installation costs. The assumptions considered for the calculation of the payback time are as follows:

- The cost per panel is assumed to be £179 [264].
- The cost for a typical inverter of 150 kW is £9,100, for an inverter of 50 kW is £5,400 and for an inverter of 30 kW, the cost would be approximately around £2,400 [264].
- The installation costs are assumed to be 20 pence per W [265].
- To ensure an optimum performance of the PV panels, it is recommended to make a basic cleaning maintenance at least one a year. The cost of the maintenance has been assumed to be £7 per panel [266]. The cost has been calculated considering that the cleaning cost of 20 PV panels is between £100-£150.

Finally, the annual savings corresponds to the difference between electricity costs without solar and the electricity cost with solar, also considering the surplus energy sold to the grid.

All the results for the three scenarios analysed in this study are explained in the next section.

3.6.2.3 Results obtained for the case study

Solar energy output

In this section, the annual and monthly solar energy output will be displayed for the three different scenarios.

Figure 3.23 displays the annual energy consumption at the studied company (grey column) and the annual solar energy generation for all the scenarios. The annual energy generation obtained for the scenarios analysed, does not exceed the annual consumption although it could reduce the dependency from the grid to a greater or lesser extent. A detailed discussion about this is introduced in the next section.

In Scenario 2, the optimum PV panel tilt/elevation angle is used to maximise the capture of direct solar radiation, especially in months when the overcast weather prevails over clear skies. However, in this particular study, elevating the panel to its optimum angle (Scenario 2) does not report a notable change when compared to the annual generation achieved if the panels are installed at the roof elevation (Scenario 1). The results of annual energy output obtained for Scenario 3 shows a large increase when compared to Scenario 1 and Scenario 2 due to the large increase in the amount of PV panels accommodated on the roofs.

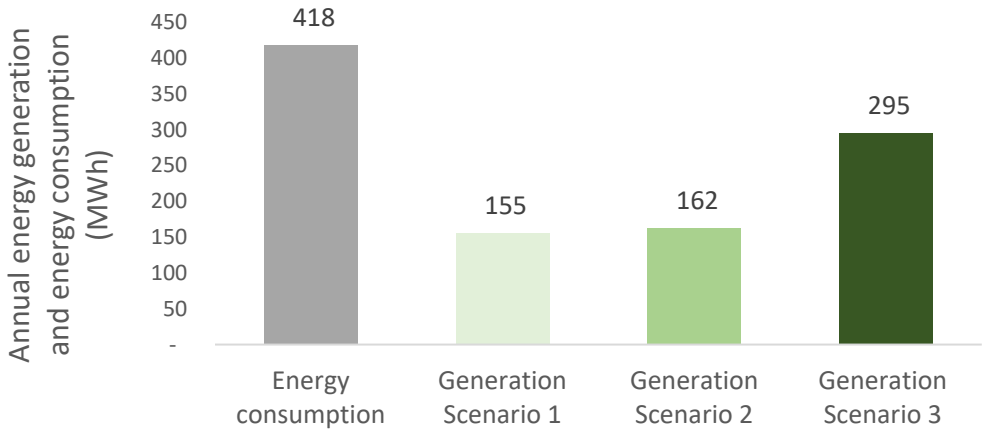

Figure 3.23. Comparison between annual solar energy generation and actual consumption at the studied company (grey) according to the different generation scenarios reflected in Table 3.19, Table 3.20 and Table 3.21.

When looking at the monthly breakdown shown in Figure 3.24, it can be observed that between Scenario 1 and Scenario 2, the higher differences in monthly energy output corresponds to the spring and autumn seasons. This is due to the increase in direct solar radiation achieved by elevating the PV panels to its optimum value. The peak production is achieved in summer season.

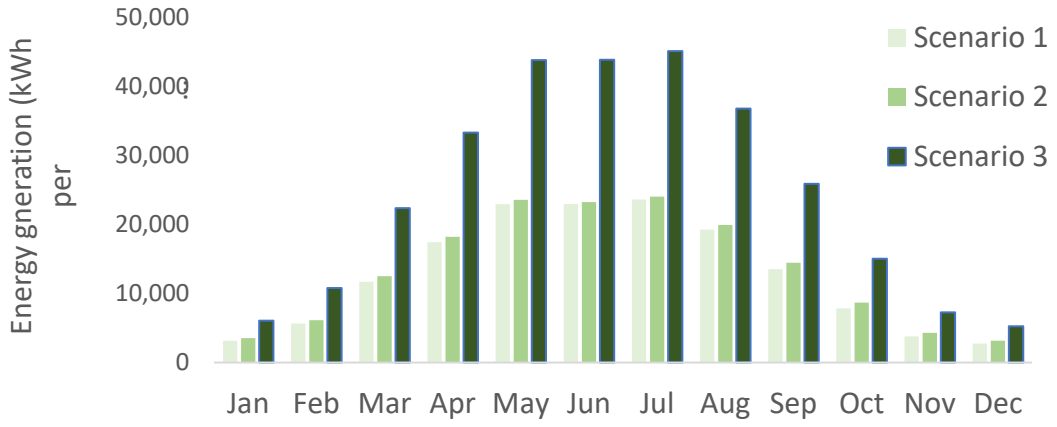

Figure 3.24. Monthly solar energy generation for each scenario. Scenario details can be found in Table 3.19, Table 3.20 and Table 3.21.

Another important difference to be mentioned between the scenarios is the contribution of each roof (main and attached) to the annual solar energy output. The percentage contribution of the attached roof (29%) is significantly lower than the contribution attributed to the main roof (71%) for all the scenarios. This is due to the area of the attached roof being smaller than the area of the main roof and thus, a lower number of PV panels can be accommodated.

Annual energy savings

The annual energy consumption at the studied company is shown in Table 3.22 in addition to the energy consumed from the grid and from solar generation. As the annual solar energy generation increases, the dependency from the grid decreases.

Scenario 1 would reduce the consumption of energy from the grid by approximately 30% (i.e., from 418,071 kWh to 291,130 kWh), while Scenario 2 would reduce consumption by 31% (i.e., from 418,071 kWh to 289,520 kWh). On the other hand, in Scenario 3 the annual energy savings account for 38%, due to the increase in the number of PV panels installed (i.e., from 418,071 kWh to 258,259 kWh).

Table 3.22. Annual energy consumption in the studied company and the annual energy consumed from solar and from the grid for each scenario.

Annual energy consumption (kWh)		**418,071**	
Annual energy supply (kWh)	Scenario 1	Scenario 2	Scenario 3
From solar	126,941	128,551	159,812
From the grid	291,130	289,520	258,259

These percentage differences are visualised in Figure 3.25.

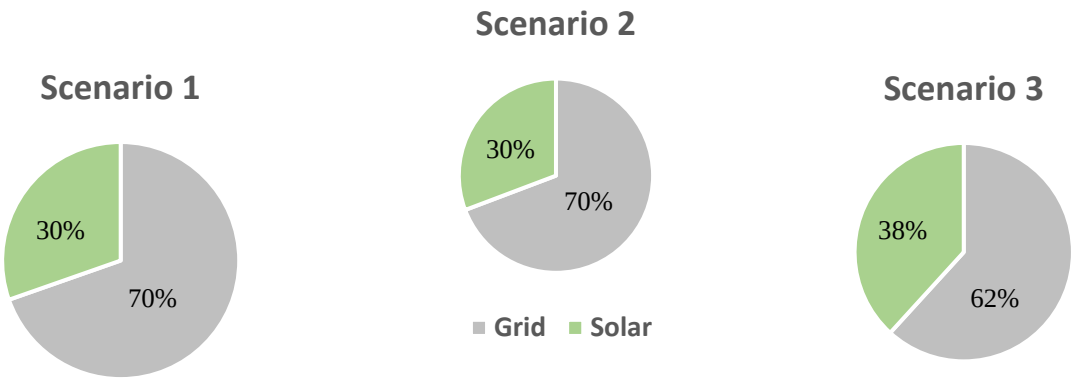

Figure 3.25. Energy consumption breakdown to show contribution from the grid and from solar for each scenario.

Suppose the solar energy generation data from Figure 3.23 is compared with the annual energy supplied from solar, shown in Table 3.22. In that case, it can be observed that the company does not use part of the solar energy generated. Solar energy generation surpasses the energy demand at certain times of the year (i.e., summer). According to the results, there would be potential to reduce further the dependency on the grid if all the surplus solar energy is stored for later use when the PV installation is not generating by for example, using an energy storage system.

Considering the fact that the difference in energy savings between Scenario 1 and Scenario 2 is not large, only a difference of 1%, it is necessary to estimate what the electricity bill savings and the payback time are, to determine if the use of the optimum tilt/elevation PV panel is worth the cost.

Electricity bill savings

The estimated annual electricity bill for the company analysed is shown in Figure 3.26 (i.e., no solar), together with the grid energy cost for each scenario. Detailed calculations to estimate the cost of electricity can be seen in Table 3.23.

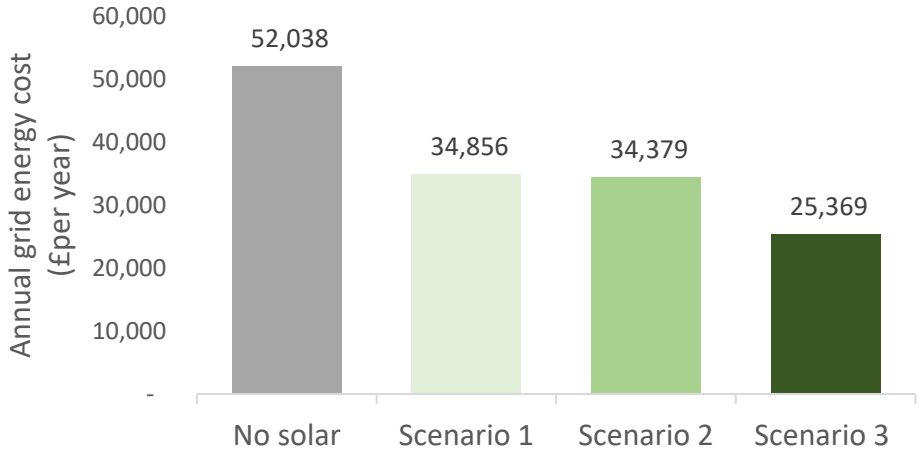

Figure 3.26. Comparison of the annual grid energy cost per year with (Scenario 1, 2 and 3) and without solar energy.

The electricity cost in Scenario 1 and Scenario 2 is reduced by approximately 33% and 34%. However, for Scenario 3, the reduction achieves a 51% if compared to the cost of electricity without solar. The higher reduction in energy cost for Scenario 3 is a consequence of the higher amount of solar surplus energy sold to the grid than for Scenario 1 and Scenario 2, as seen in Table 3.23.

Table 3.23. Breakdown of electricity costs per scenario.

		Without solar installation	
Unit rate		Energy consumption from grid (kWh)	Energy cost (£)
	07:00-24:00	384,625	48,394
	00:00-07:00	33,446	3,644
	Total	418,071	
		Total cost	**52,038**
		Scenario 1	
Unit rate		Energy consumption from grid (kWh)	Energy cost (£)
	07:00-24:00	267,839	33,700
	00:00-07:00	23,290	2,538
	Total	291,130	36,237
		Solar energy consumption (kWh)	
		126,941	
		Solar surplus (kWh)	Surplus earnings (£)
		27,626	1,381
		Total cost	**34,856**
		Scenario 2	
Unit rate		Energy consumption from grid (kWh)	Energy cost (£)
	07:00-24:00	266,358	33,513
	00:00-07:00	23,162	2,524
	Total	289,520	36,037
		Solar energy consumption (kWh)	
		128,551	
		Solar surplus (kWh)	Surplus earnings (£)
		33,168	1,658
		Total cost	**34,379**
		Scenario 3	
Unit rate		Energy consumption from grid (kWh)	Energy cost (£)
	07:00-24:00	237,598	29,895
	00:00-07:00	20,661	2,251
	Total	258,259	32,146
		Solar energy consumption (kWh)	
		159,812	
		Solar surplus (kWh)	Surplus earnings (£)
		135,543	6,777
		Total cost	**25,369**

Payback time

In this section, the payback time for the three different scenarios is estimated. The result for each scenario can be seen in Table 3.24.

Scenario 1 presents the lower payback time, 12.5 years. Scenario 2, on the other hand, increases the payback time by 4 years when compared to Scenario 1. The difference for the payback time between Scenario 1 and Scenario 2, considering both have the same number of PV panels,

relies on the extra cost associated to the installation needed to elevate the PV panels to the optimum collection angle (i.e., installation costs), which is approximately £50,000[5] [267]. The total payback time for Scenario 2 is 16 years. In Scenario 3, the increase in the payback time, when compared to Scenario 1, is due to the increased size of the PV system, despite producing more energy.

Table 3.24: Payback time breakdown based on 2021 prices

	PV system size (kW)	PV panel cost	Inverter cost	Installation cost	Annual maintenance cost	Annual savings	**Payback time (Years)**
Scenario 1	200	£106,684	£14,500	£40,000	£4,172	£17,182	**12.5**
Scenario 2	200	£106,684	£14,500	£90,000 (extra cost due to the frame installation)	£4,172	£17,659	**16**
Scenario 3	380	£203,344	£26,000	£76,000	£7,952	£26,669	**16**

However, it is worth noting that prices change and vary over time and between the components chosen. Therefore, these figures are only indicative of potential cost savings. The results shown in Table 3.24 were calculated based on energy costs in 2021, and they did not reflect the economic impact of the Russian invasion of Ukraine on the UK's energy and gas prices [268].

With the aim of reflecting the changes in energy prices, a new payback time has been estimated. The assumptions for the calculations are as follows:

- Increase of almost 200% in electricity prices between December 2021 and March 2023. A detailed explanation about the estimate can be found in chapter 4, section 4.3.3.
- The cost per panel is assumed to be £220 [264].
- The cost for a typical inverter of 150 kW is £11,800, for an inverter of 50 kW is £6,680 and for an inverter of 30 kW, the cost would be approximately around £2,925 [264].
- The installation costs are assumed to be 20 pence per W [265].

[5] The price includes a cost per frame between £50-£115 and an extra cost to install the frames. The cost is illustrative, and it might not reflect actual installation costs for a specific installation.

- To ensure an optimum performance of the PV panels, it is recommended to make a basic cleaning maintenance at least one a year. The cost of the maintenance has been assumed to be £7 per panel [266][6].

The results obtained for the new payback time are shown in Table 3.25.

As shown in Table 3.25, the payback time has been reduced by 8 years for Scenario 1, 11 years for Scenario 2 and 10 years for Scenario 3, approximately, if compared to the estimations shown in Table 3.24. The rise in electricity prices incentivises the adoption of a PV system, as they yield substantial annual energy savings that counterbalance the initial investment in PV panels and inverters.

Table 3.25 Payback time breakdown based on prices from 2023

	PV system size (kW)	PV panel cost	Inverter cost	Installation cost	Annual maintenance cost	Annual savings	**Payback time (Years)**
Scenario 1	200	£131,120	£18,480	£40,000	£4,172	£48,612	**4.2**
Scenario 2	200	£131,120	£18,480	£90,000 (extra cost due to the frame installation)	£4,172	£49,488	**5.3**
Scenario 3	380	£249,920	£33,205	£76,000	£7,952	£66,238	**6**

Emission reductions

This section analyses the emissions reductions for each scenario when compared to the actual consumption without solar energy. As it can be seen in Figure 3.27, almost 50% emission reductions are achievable when Scenario 3 is used. Scenario 1 and Scenario 2 reduce the actual emissions by 26% and 27%, respectively. The major difference in emission reductions between Scenario 3 compared with Scenario 1 and 2 is due to the reduction in the dependency from the grid and the surplus solar energy that contributes to a reduction of energy production in the grid.

[6] Approximate value calculated considering that the cleaning cost of 20 PV panels cost between £100-£150.

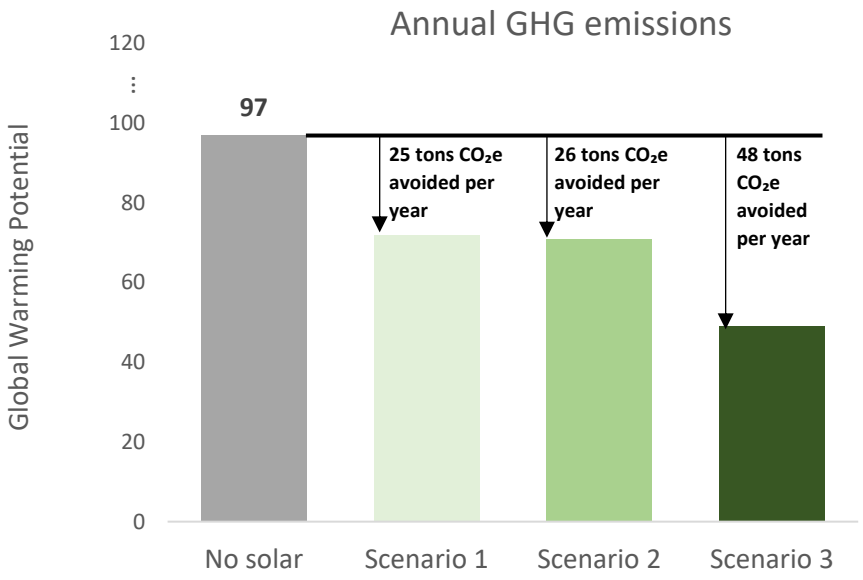

Figure 3.27. Global Warming Potential for each of the scenarios.

Equivalent over system lifetime (20 years) to:

- Lifetime emissions savings equivalent to 71-137 typical households in the UK[7].
- Lifetime emissions captured by 1000-1920 English oak trees[8], approximately 10 km² of woodland in the Peak District.

3.6.2.4 Conclusion & Recommendations

The key points obtained from the results are as follows:

1. Energy output: Scenario 1 reports the lowest solar energy output followed by Scenario 2 and Scenario 3. The final output can be increased by elevating the PV panels to its optimum angle (Scenario 2) or by increasing the number of PV panels installed (Scenario 3). However, to decide what is the most appropriate PV installation, it is suggested to consider other parameters such as energy cost, emission reductions or payback time.

[7] Committee on Climate Change (assuming the average UK home's carbon footprint is 7 tons CO_2) – The Fifth Carbon Budget

[8] Imperial College London (assuming an oak tree can absorb 500 kg CO_2) – Is planting trees the answer to climate change?

2. Dependency on the grid: The higher the solar energy generation, the lower the dependency on the grid. Scenario 1 reduces the energy consumption from the grid by 30%, followed by Scenario 2 with 31%, and Scenario 3 achieving the highest energy consumption reduction of approximately 38%.
3. Electricity bill: The electricity bill cost is reduced by 51% in Scenario 3 if compared to the cost of electricity without solar. This is driven by the increased number of PV panels. Although in terms of the reduction of energy dependency from the grid there is not a big difference between Scenario 3 and Scenario 1 and 2, the electricity bill cost results show a more significant difference due to the solar surplus energy sold to the grid.
4. Payback time: Based on the initial 2021 results, payback time is the same for Scenario 2 (optimum angle) and Scenario 3 (increased number of panels), 16 years. Scenario 1 requires a lower payback time, 12.5 years. The installation cost required to elevate the PV panels to its optimum configuration increases the payback time. However, when the electricity costs are updated to 2023 prices, the benefits achieved from the increase on the energy annual savings minimise the incurred extra costs on installation reducing the payback time between 8 and 11 years.
5. Emissions reduction: The scenario most favourable considering the reduction of emissions is Scenario 3, this scenario achieves a reduction of 50% in comparison to the actual plant. If the system lifetime is assumed to be 20 years, the emission reductions would be equivalent to the total amount of emissions captured by 1920 English oak trees, approximately and extension of 10 km^2 of woodland in the Peak District.

Throughout the study, the implications, and opportunities of using solar energy at the company studied have been analysed. It has been demonstrated that the introduction of solar energy generation technology would report positive benefits in many aspects for the business. However, the adequacy of a specific PV panel installation has to be evaluated using different parameters (i.e. payback time, emission reductions or energy cost). If the limiting factor is the payback time, an installation similar to Scenario 1 would be recommended. However, if emission reductions or electricity bill savings are considered, a Scenario 3 type of installation would be the best choice.

The estimates made in the report are based on standard approaches to PV generation modelling and may not reflect actual installation costs and savings for a specific installation.

3.7 Summary

Throughout the review of existing literature, one can understand the importance of having accurate information on solar irradiation for horizontal surfaces. However, due to the scarcity of those measurements, different types of modelling have been adopted by researchers to estimate values of horizontal solar irradiation, specially, diffuse horizontal solar irradiation. In this study, the models have been divided between machine learning techniques and empirical solar models. The latter are extensively used in absence of horizontal solar radiation data, particularly horizontal diffuse solar radiation. In this chapter, three different solar empirical models have been developed to estimate values of horizontal diffuse solar radiation in the UK.

A summary of different models to obtain solar irradiation on inclined surfaces from values of solar irradiation on horizontal surfaces have been introduced. In reality, PV solar systems are generally mounted on inclined surfaces and so it is important to develop a model that estimates values of irradiation on inclined surfaces. The estimation of the direct and reflected components of solar irradiation on inclined surfaces are relatively simple. The diffuse component of the solar irradiation on an inclined surface can be evaluated following isotropic or anisotropic models. In this chapter, results suggest Hay's model as the one that better adjusts to real measurements for the estimation of diffuse solar radiation on inclined surfaces.

The results obtained on energy generation from the developed solar model, have been validated against real values of PV solar energy generation in two different premises, a household, and a store. The percentage error was no higher than 10%.

Finally, the solar model was applied in a case study to evaluate the feasibility of a PV installation to offset some of the current energy use within the buildings studied.

Following the development and validation of the solar model, the next chapter focuses on developing an energy management model to evaluate a system formed by a PV installation and a battery energy storage system (BESS). Understanding how different commercial premises react to introducing a BESS is essential to explore the feasibility of using solar generated energy and energy storage for EV fleet charging.

4 Development of an energy management model for the evaluation of BESS

4.1 Introduction

There are numerous benefits to implementing a Battery Energy Storage System (BESS) and localised solar energy generation within a system. In Chapter 3, a model was developed and validated to estimate the available solar energy generation at different locations in the UK. The addition of a BESS can provide several benefits, it can help balance the system energy requirements from the grid and maximise utilisation of the energy available from renewable sources. These benefits were explored in Chapter 2 in the literature review covering energy storage systems.

This chapter aims to evaluate the impact of introducing a BESS on the energy use of the system from both a technical and economic standpoint. The system considers the energy demand from the commercial or logistic site, the energy generation from the PV solar installation, the energy store by the BESS and the energy consumed from the grid. For that purpose, this chapter focuses on developing an energy management model capable of controlling the energy flows between the premises, the PV solar installation, the BESS, and the grid through an algorithm implemented in a MATLAB model. Different energy management approaches have been considered for the model and are discussed in section 4.2, giving special attention to the energy storage model. The outcome of an energy management model depends on the energy characteristics of the system under study, such as energy consumption and energy generation. In this regard, the model was developed and applied in two different commercial sites: a waste management depot (WMD) and a M&S retail store, to reflect the different outcomes obtained. Moreover, the selection of these two sites relies on their differences in the operational and technical characteristics (e.g., activity developed on the site or the energy consumption) to provide a broader set of results. The energy consumption data for both commercial sites was measured on an hourly basis over a year with data supplied by commercial partners interested in the project. The hourly PV solar energy generation was estimated through the solar model developed in Chapter 3. The results obtained from the energy management model are analysed at the end of this chapter, considering the technical and economic aspects, and the potential greenhouse gas (GHG) emissions released/saved by this approach. Part of the methodology

described in this chapter for the WMD has been previously published in the Energies journal in 2023[9] [175].

4.2 Literature review on energy management systems

The potential benefits of integrating a BESS in a system powered by renewable generation depend highly on the energy management approach within the system [134].

Energy management has been the subject of comprehensive research by scholars for various objectives, including enhancing efficiency throughout the distribution network (e.g., minimising losses in distribution systems) [136,137], optimising cost savings by maximising utilisation of "green" energy sources and controllable loads, and reducing greenhouse gas (GHG) emissions [138,139,269–272].

Energy management is now more relevant than ever, as we face an energy crisis. Within this context, energy analyst experts suggest the best way to move forward is by accelerating the clean energy transition [145]. As was discussed in Chapter 2, the clean energy transition has to be supported by the introduction of other technologies able to manage energy consumption/generation without relying on the use of fossil fuel based power plants. Energy storage has emerged as a key technology to provide flexibility to the power systems, in particular battery energy storage [145].

The use of energy management techniques for the integration of renewable energies and BESS has been also explored by some authors [273–275]. The management of these systems is a challenge due to the difficulties caused when all the components (i.e. demand load, renewable sources and BESS) need to be coordinated [276,277]. To optimise said systems, precise energy management is required to make use of the energy storage effectively and safely [278], thus the modelling of the BESS is one of the most important components of the energy management system [134].

The energy storage models are classified and analysed differently by authors, depending on the application and the optimisation technique applied. Byrne *et al.* [278] categorised energy

[9] Nunez Munoz M, Ballantyne EEF, Stone DA. Assessing the Economic Impact of Introducing Localised PV Solar Energy Generation and Energy Storage for Fleet Electrification. Energies 2023;16:3570. https://doi.org/10.3390/en16083570

storage models as dynamic models, energy flow models, physics-based models, and black box models. The energy storage is defined in the study as an asset to maintain stability in the grid network. Dynamic models reflect the dynamics of the battery and are used for time scales of milliseconds to minutes. Energy flow models are classed as the best choice when the aim is to perform a techno-economic assessment and operate within timeframes spanning minutes to hours. Such energy flow model also considers conversion efficiencies. Physics-based models are developed considering the physics associated with each energy storage technology (i.e., mechanical storage, electrochemical storage, etc.) and black box models only considers the inputs and outputs of the battery.

Yang *et al.* [134] classify BESS models as either generic and dynamic models and identifies different timeframes for each. The dynamic model, as per Byrne *et al.* [278], considers the changes in the battery storage as a consequence of the dynamics of the battery, the current and voltage characteristics. These differences in the dynamics of the BESS are controlled by differential equations. On the other hand, the generic model, according to Yang *et al.* [134] is the most widely used out of the two models. Contrary to the dynamic model, it assumes that any voltage or current change is achievable with changes in the state of charge (SoC). The SoC is the level of charge of the battery relative to its capacity and it fluctuates according to the energy flowing in or out of the battery. This generic model is what Byrne *et al.* [278] categorised as an energy flow model and it is run in the range of minutes to hours. The process of charging/discharging the battery following the generic model is expressed mathematically as follows [134]:

$$\mathrm{SoC}_{(t+\Delta t)} = \mathrm{SoC}_{(t)} + \frac{{\mathrm{P}_{\mathrm{BESS(t)}}}^{+} \cdot \mathrm{BESS}_{\mathrm{ceff}} \cdot \Delta t}{\mathrm{C}_{\mathrm{BESS}}}, \text{when charging}$$

Equation 4.1

$$\mathrm{SoC}_{(t+\Delta t)} = \mathrm{SoC}_{(t)} + \frac{{\mathrm{P}_{\mathrm{BESS(t)}}}^{-} \cdot \Delta t}{\mathrm{BESS}_{\mathrm{deff}} \cdot \mathrm{C}_{\mathrm{BESS}}}, \text{when discharging}$$

Equation 4.2

Where C_{BESS} is the capacity of the battery (kWh), $BESS_{ceff}$ is the charging battery efficiency, $BESS_{deff}$ is the discharging battery efficiency, and $P_{BESS(t)}^{+}$ and $P_{BESS(t)}^{-}$ are the charging/discharging power of the BESS, respectively. Δt is the time increment.

The SoC is the most frequent parameter used to evaluate the energy status of the battery. Rosewater *et al.* [279] categorised battery models according to the units used to describe the SoC. Energy reservoir models define capacity in units of energy (kWh), charge reservoir models express it as unit of charge (Ah) and concentration-based models simulates the SoC with units of concentration (mol/L) of the active materials of the electrodes (i.e., lead-acid batteries). Rosewater *et al.* [279] defined the charging/discharging process of the battery for the energy reservoir model as:

$$C_{BESS} \cdot \frac{\partial SoC}{\partial t} = BESS_{rteff} \cdot P_{BESS(t)}{}^{+} + P_{BESS(t)}{}^{-}$$

Equation 4.3

Where $BESS_{rteff}$ is the battery round trip efficiency and $\frac{\partial SoC}{\partial t}$ is the rate of change of SoC.

The energy flow model described by Byrne *et al.* [278], the generic model by Yang *et al.* [134] and the energy reservoir model of Rosewater *et al.* [279] all model the battery considering the charging/discharging processes as changes in the SoC, without considering the dynamics of the BESS.

The same approach has been followed by authors focused on the techno-economic assessment of the hybrid system (combining a BESS and renewable energy generation). Moradi *et al.* [139] followed the same approach to represent the battery behaviour in a system formed by a PV solar installation, a wind turbine, a BESS, a diesel generator, fuel cells and a gas turbine. The aim of the study was to use the renewable energy (i.e. solar and wind) more efficiently and to reduce the energy costs and emissions. The energy storage system constraints (i.e. power output and SoC constraints) were set in place to ensure the correct use of the battery, and the SoC at time "t" was calculated following Equation 4.1 and Equation 4.2. The study showed an improvement in energy utilisation efficiency and cost savings when introducing a BESS in the system.

Carli *et al.*[280] studied a system composed by a small port area, a PV installation and a BESS. The BESS was optimised to store energy from the PV installation and use it when needed. The BESS energy model considers the charging/discharging battery efficiencies in a discrete time model as follows:

$$Soc_{(t)} = SoC_{(t-1)} + \mathrm{BESS_{ceff}} \cdot \mathrm{E_{BESS(t)}}^{+} - {\mathrm{E_{BESS(t)}}^{+}}/{\mathrm{BESS_{deff}}}$$

Equation 4.4

Where $\mathrm{E_{BESS(t)}}^{+}$ and $\mathrm{E_{BESS(t)}}^{-}$ is the energy stored and released from the BESS, respectively. $\mathrm{BESS_{ceff}}$ is the charging battery efficiency and $\mathrm{BESS_{deff}}$ is the discharging battery efficiency.

The authors [280] developed a model predictive control to achieve the optimum distribution between the demand loads from the port, the BESS, and the grid. The aim behind the algorithm was to maximise the use of PV solar energy and minimise the energy cost by optimally buying and selling the energy from/to the grid. The efficiency of this algorithm was measured based on the effects on total energy cost, self-supply, and energy independence. When compared with the output obtained when applying a naïve algorithm, results showed that the implementation of a model predictive control to optimise the energy flow would likely yield annual savings for the system to 8.2%.

Babacan *et al.*[281] developed an algorithm to minimise the energy costs in four different scenarios, all of them including the use of energy storage. The energy storage system was modelled considering the fluctuation of the SoC based on the charge/discharge energy flow as follows:

$$SoC_{(t)} = SoC_{(t=t0)} - \sum_{t=1}^{s} \mathrm{P_{BESS(t)}} \cdot \Delta \mathrm{t}$$

Equation 4.5

Where $SoC_{(t=t0)}$ is the initial SoC and $\mathrm{P_{BESS(t)}}$ is the power. The algorithm was applied to 53 residential premises and results successfully reported a reduction in peak net demand, power fluctuations and reliance on the grid.

From a more technical point of view, Puranen *et al.* [282] examined the feasibility of an off-grid residential building using PV solar energy with a BESS and hydrogen storage in Finland. The battery was modelled in this study considering a limited BESS capacity (i.e. C_{BESS}) but unlimited charge/discharge power. The SoC is the parameter used to determine the energy flow in and out of the battery. The battery charging and discharging power are obtained by following Equation 4.6 and Equation 4.7,respectively.

$$P_{BESS(t)} = -\min\left\{BESS_{ceff} \cdot P_{IN(t)} \cdot \left(1 - SoC_{(t-1)}\right) \cdot C_{BESS} \Big/ \Delta t\right\}$$

Equation 4.6

$$P_{BESS(t)} = -\min\left\{P_{OUT(t)} \cdot SoC_{(t-1)} \cdot BESS_{deff} \cdot C_{BESS} \Big/ \Delta t\right\}$$

Equation 4.7

Here, $P_{IN(t)}$ and $P_{OUT(t)}$ is the power in and out of the battery, before considering the efficiency of the battery. The results showed the need of having a system capable of storing energy, both short term and seasonally due to the variations on renewable energy generation throughout the year. The hydrogen storage was used as a seasonal storage system and the BESS was used as a short-term energy storage. Based on the simulations, authors concluded that both forms of storage would be needed together to make the off-grid operation technically feasible in the residential building studied. The exclusive use of the battery would make the BESS capacity impractically large to meet the demand load in winter when there is limited solar energy generation. On the other hand, relying only on hydrogen storage would be wasteful due to its poor round trip efficiency and the volume required for the physical storage of hydrogen.

The approach used by Moradi *et al.* [139], Carli *et al.* [280], Babacan *et al.*[281] and, Puranen *et al.* [282] to describe the behaviour of the energy storage system, has been proven to be an effective approach to assess the techno-economic aspects of a system formed by the energy storage, demand load and a renewable energy source.

The integration of the energy storage and the distribution of the energy within the system has been accomplished by many authors with the help of an algorithm. Their chosen algorithm is a set of mathematical instructions or rules implemented in a computational programme for solving, in that particular case, energy management problems [273,283,284]. The diverse range of algorithms found in literature for the energy managament of a system is justified considering the different forms of energy storage used and the design criteria followed on each system studied [283].

There are technically oriented algortihms developed to serve as a tool to manage the energy flow of a system. The work done by Chakir *et al.* [274] serves as an example of this. On the cited study, Chakir *et al.* [274] developed an energy management algorithm to determine the energy used by each source in a grid connected PV-BESS system in a residential building. The

algorithm determines the energy flow according to a ranking of priorities. In the first instance, the priority is the consumption of instantaneous PV solar energy, secondly, the storage of PV energy at the BESS and finally the use of the energy from the grid (or sale of energy to the grid in case of excess energy). The algorithm dictates the power variations in time slots (i.e. hour slots), and as a result, the battery power is the average consumption per hour of charge. The authors highlighted the simplicity and low cost implementation of the algorithm that was developed and simulated using MATLAB/SIMULINK. The study by Chapaloglou *et al.* [285] could be used as another example of a more technically oriented algorithm. The authors created an algorithm capable of managing the energy flow to counteract the peak demand load values. The energy management algorithm created was a combination of a forecasting model (i.e. to forecast consumption values) and a power optimisation model able to provide real time control of the BESS. The results based on the algorithm proved the benefits an energy management system has on controlling BESS energy flow for peak demand shaving.

On the other hand, authors have also developed algorithms more focused on the techno-economic aspect of the energy system. Iliadis *et al.* [275] used Python and Modelica to simulate a system composed by diesel generators, PV solar panels and a wind turbine. The authors of the study accomplished a techno-economic analysis of a system where a BESS was used to level out the consumption from the fossil-based sources (i.e. diesel and heavy oil generators) thus enabling higher renewable energy penetration levels. To achieve this, the authors developed an algorithm designed to operate a BESS that applies a load levelling approach to the system. It predicts the operation of the BESS based on a daily forecast of hourly demand load consumption and PV-wind energy generation. Contrary to the algorithm developed by Chakir *et al.* [274] and Chapaloglou *et al.* [285], the algorithm proposed by Iliadis *et al.* [275] was run once a day without considering possible intra-day changes.

Different algorithms try to optimise different qualities for the system. Flexibility and rapid response are the characteristics that better describe the algorithm developed by Moradi *et al.* [139]. As for the case of Iliadis *et al.* [275], the algorithm is developed by using day-ahead data although it incorporates the flexibility to better reflect intra-day and intra-hour changes. The algorithm is created from a set of constraints that aim to reflect the optimal distribution of energy in a microgrid, formed by renewable and non renewable sources, to reduce operation and maintenance costs, and emissions. Optimal load scheduling, efficiency energy consumption or emission and cost reductions were amongst others, the objectives that Wasif

Ali *et al.* [277] pursued to develop the energy management algorithm. The authors analysed the outcome from three different types of algorithms to determine which of them would be closer to the optimum solution. The algorithms where applied into a virtual power plant formed by a decentralised power system, power consumers and energy storage.

Commercial buildings have extensively been used to validate the electricity cost savings from using energy management algorithms and optimising the consumption at the lowest electricity price [286]. The reduction in network costs by peak shaving were examined by Tiemann *et al.* [287] for more than 5,000 companies from diverse sectors when energy storage was used. The authors evaluated the payback time considering different energy storage technologies and different network fees. Sepúlveda-Mora *et al.* [288] studied the economic benefits of adopting energy storage based on different energy tarifs using an energy dispatch algorithm from HOMER. They compared three different commercial buildings to account for the differences in energy demand. The study concluded that when a Time of Use (TOU) tariff is in place, the economic benefits of introducing energy storage into the system are similar for the three commercial buildings analysed regardless of the energy demand. McLaren *et al.* [289] explored the economics of adopting PV solar and energy storage technology at commercial buildings using NREL's Renewable Energy Optimisation modeling. They found a direct correlation between an increase in electricity price, an increase in PV solar energy generation on-site and the costs savings. The largest savings were related to the reduced energy costs, instead of demand costs (paid monthly based on the peak power required by the building).

When evaluating the potential benefits that a BESS has in a commercial building, there are important factors that vary from site to site. The relation between the energy demand and on-site renewable generation is important, as are the operational or technical constraints. These factors influence the outcome obtained when an energy management algorithm is applied at different sites. For the purpose of this chapter, a rule-based algorithm has been developed [290] to be integrated within the energy management system. Rule-based control strategy algorithms offer the advantage of straightforward integration [291]. Moreover, they have been successfully applied to systems formed by photovoltaic panels and battery energy storage systems by other authors [290,292,293].

In this chapter, two different premises are studied, a waste management depot and a M&S retail store to assess the potential benefits of implementing a BESS considering that these premises already have a PV installation on -site.

4.3 Methodology

In this section, the two case studies are introduced: a waste management depot and a M&S retail store. The energy consumption from the buildings and the modelled PV solar energy generation are compared to identify the most appropriate use of a BESS. Then, for each system, a tailored energy management algorithm is developed. Finally, the techno-economic analysis is completed.

4.3.1 Description of the buildings under study

Waste management depot

For the purpose of the study, a local authority waste management depot (WMD) in Nottinghamshire, UK, has been examined. The facility encompasses two different buildings, each with a floor area of 2,445 m² and 2,361 m² respectively. Currently, the company relies entirely on the grid to meet the energy demand of these buildings. No PV panels or a BESS are installed on the site, and the existing refuse collection vehicles at the depot are powered by conventional fuels (i.e., diesel or petrol). The local authority provided hourly energy consumption data for the depot from 1st of April 2021 to 31st of March 2022. The total energy consumption for the depot during this period was 234 MWh.

The PV solar energy generation for both buildings has been determined using the solar model described in Chapter 3. The input data used as hourly solar irradiation data for this study was obtained through the CEDA archive. Hourly data was collected from a weather station situated in Walnatt (Nottinghamshire, UK) for the period between 2009 and 2019, measured in kJ/m^2. The values of global solar irradiation were then averaged and transformed into kWh/m^2 to be used as input to the solar model. The PV installation was assumed to consist of 946 PV panels on one building and 918 PV panels on the other, commensurate with the available roof size of the existing depot buildings. The PV panels are assumed to be tilted at the existing roof inclination angle, 30 degrees, and orientated towards the south-east (140 degrees) and the north-west (320 degrees), aligned with the existing buildings. Based on this configuration, the total modelled PV solar energy generation from April 2021 until end of March 2022 was 328 MWh. Hourly modelled PV solar energy generation, and energy consumption corresponding to the local authority waste management buildings are plotted in Figure 4.1.

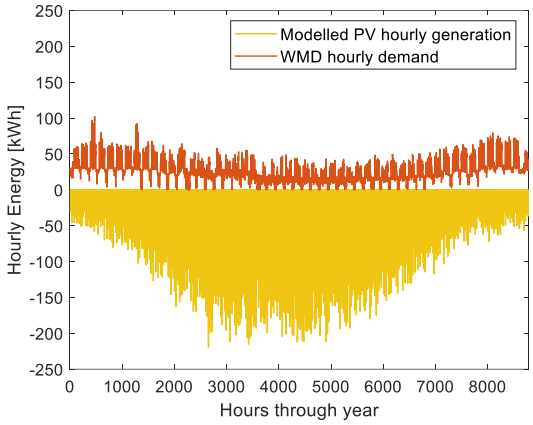

Figure 4.1 Hourly energy demand (orange line) and modelled PV solar energy generation (yellow line) for the WMD. The positives values stand for energy consumption and the negatives indicate energy generation.

The energy demand from the WMD increases as winter approaches and decreases during the summer months. The PV solar panels generate the most energy in May, June, and July. It is during these months when a higher portion of the solar radiation hits the surface in the UK. However, during the autumn and winter months the PV solar energy generation is minimal due to the reduced solar radiation received, as can be seen in Figure 4.2a.

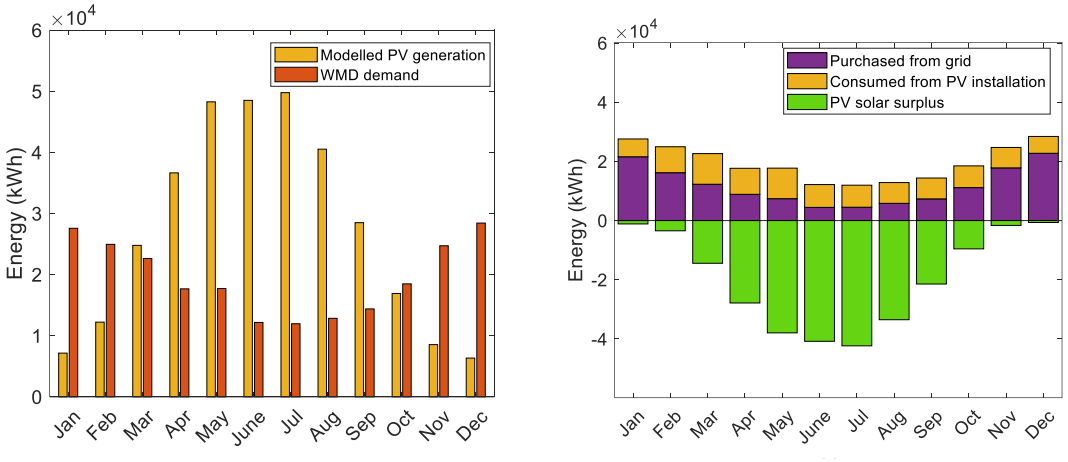

(a) (b)

Figure 4.2. (a) Monthly energy consumption (orange blocks) and modelled PV solar energy generation (yellow blocks) for the WMD. (b) Energy balance for the WMD (The positives values stand for energy consumption and the negatives indicate generation).

For the WMD, the modelled PV solar energy generation and the energy demand follow opposite trends throughout the year. This significantly impacts the self-consumption potential of the site. Self-consumption (Sc) is defined by Luthander *et al.* [294] as the percentage of the PV solar energy consumed directly (PV_d) relative to the total PV solar energy generation (PV_T) (Equation 4.8)

$$\text{Sc}\ (\%) = \frac{\text{PV}_\text{d}}{\text{PV}_\text{T}} \times 100$$

Equation 4.8

In the case of the WMD, the self-consumption value is 28% because most of the PV solar energy generated is not used instantaneously, as shown in Figure 4.2b. In order to increase the self-consumption of the site, a similar trend in energy consumption and solar energy generation would be beneficial (i.e., increase the energy consumption in summer and decrease it in winter). However, due to the operational characteristics of each commercial site, it is only sometimes an option. Alternatively, introducing a BESS could improve the site's energy performance by storing a portion of the PV surplus solar energy for later use when the PV panels are not producing. In this regard, the benefits and impacts of introducing a BESS for the WMD are explored in detail in section 4.4.1

M&S retail store

The second case study corresponds to one of the many M&S retail stores that includes a food section, located in the UK. The chosen store has a floor area of approximately 12,000 m². Currently, the store is fully dependent on the grid to cover the energy demand with an annual consumption of around 1,700 MWh. M&S provided hourly energy consumption data from 1st of April 2021 to 31st of March 2022 for this study.

As for the WMD introduced previously, the PV solar energy generation for the store has been modelled using the solar model described in Chapter 3. The input data used for the model was measured in kJ/m^2 between 2012 and 2019 in a weather station located in London. The values of global solar irradiation were then averaged and transformed into kWh/m^2 to be used as input to the solar model.

It has been estimated that the PV installation could have 2,528 PV panels, half of them orientated towards the south-east (150 degrees) and the other half towards the north-west (330 degrees), aligned to the existing building. Additionally, it is assumed that the PV panels are tilted to the existing roof elevation angle, 10 degrees. Based on this configuration, the total modelled PV solar energy generation from April 2021 until end of March 2022 was 484 MWh. The modelled PV solar energy generation, and the hourly energy consumption corresponding to the M&S retail store are plotted in Figure 4.3.

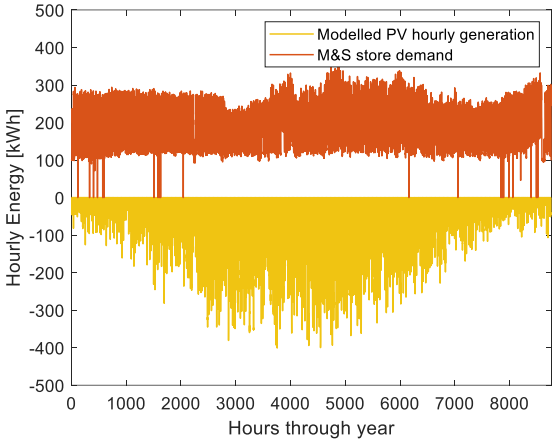

Figure 4.3 Hourly energy consumption and modelled PV solar energy generation for M&S retail store. The positives values stand for energy consumption and the negatives indicate generation.

If comparing the energy consumption of the M&S retail store and that of the WMD, the energy consumption at the M&S retail store is between 6 and 10 times higher than the consumption of the depot. This is visible when comparing Figure 4.3 with Figure 4.1. Possible reasons for that could be the intensive use of refrigeration units across the shop floor, air conditioning use over summer season and lights within the building.

In contrast to the depot, the energy consumption at the M&S retail store is relatively stable throughout the year. In most cases, the energy consumption is higher than the PV solar energy generated, as shown in Figure 4.4a.

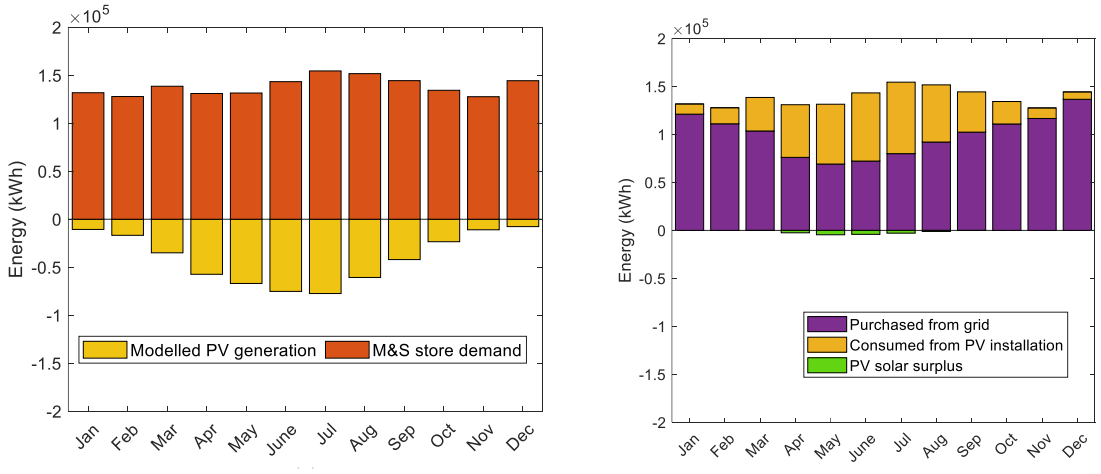

(a) (b)

Figure 4.4 (a) Monthly consumption and modelled PV solar energy generation for the M&S retail store. (b) Energy balance for the M&S retail store. The positives values stand for energy consumption and the negatives indicate generation.

Only during a few hours from April to August, the PV solar energy generation surpasses the store consumption, as can be seen in Figure 4.4b and in detail in Figure 4.5 using May as example.

Following Equation 4.8, the self-consumption value for the M&S retail store is 97%. In that case, most of the PV solar energy generated is instantly used by the store.

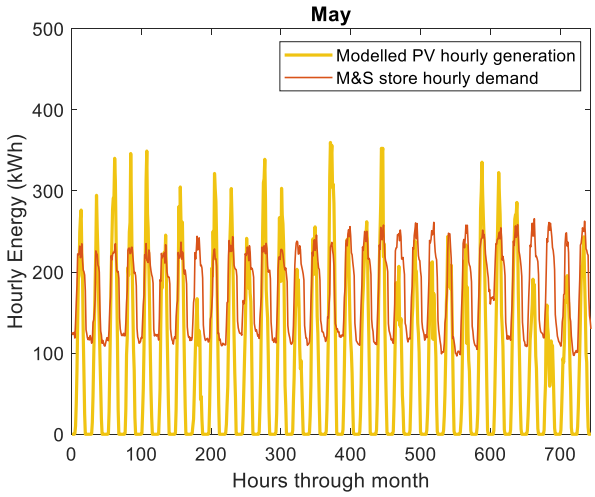

Figure 4.5 Hourly consumption and modelled PV solar energy generation for M&S retail store in May.

The optimum use of the BESS for the premises described above is dependent on the relationship between consumption and generation. For the WMD, there is significantly more PV solar energy available to be stored than for the M&S retail store. This enables the integration of the BESS at the WMD to maximise the use of PV solar energy and reduce the dependency on the grid and electricity cost. In contrast, the M&S retail store is more likely to use the PV solar energy instantaneously without the need of a BESS. The use of the BESS at this store to increase the PV solar energy consumption is only justified for a handful of days in the year. Considering these differences between both sites, the BESS would have to be used very differently at each location. In the next section, the BESS model and the energy management algorithms are explained.

4.3.2 Energy management algorithm

Waste management depot

The main objective when developing the energy management algorithm for this location was to prioritise the use of PV solar energy whenever possible. As has been introduced previously, each location studied shows differences in terms of consumption and PV solar energy generation that determine some aspects of the required energy management.

The energy management algorithm developed for the WMD considers the connections between the system formed by the PV installation, the proposed BESS, the depot, and the grid. The goal is to maximise the use of the PV solar energy and reduce the depot dependency on the grid. This will, at the same time, contribute to reducing the electricity cost and the environmental impact. For this purpose, the proposed energy flow diagram for the WMD is presented in Figure 4.6. The depot is assumed to be equipped with rooftop PV panels and a BESS (with a round-trip efficiency of 90% [146]). The depot's and the eRCV fleet energy demand are firstly supplied by solar energy followed by energy stored in the BESS, and lastly by the grid if needed. If, at any time, there is surplus solar energy after fulfilling the total energy demand, the excess is stored in the BESS for later use.

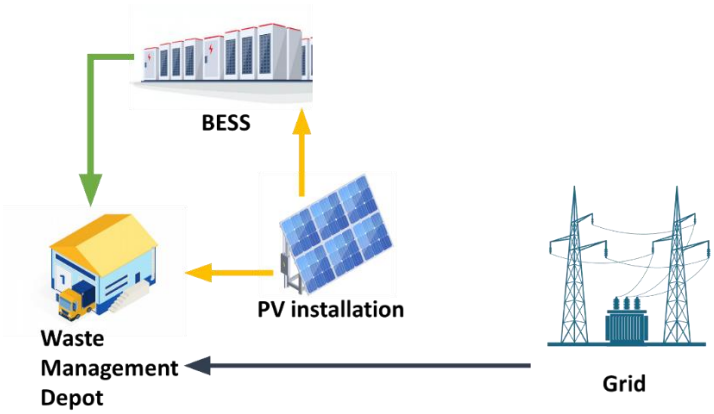

Figure 4.6 Energy flow diagram proposed for the Waste Management Depot.

For the development of the algorithm, some constraints have been considered.

- The BESS is restricted to not being charged and discharged during the same hourly time step (t) and it will only operate within a pre-set state of charge ($SoC_{(t)}$) range that is assumed to be 20% (SoC_{min}) and 90% (SoC_{max}) of the total battery capacity

(Equation 4.9). These SoC limits were selected as reasonable values for typical battery system operations without being specific to any particular equipment [279].

$$\mathrm{SoC_{min}} \leq \mathrm{SoC_{(t)}} \leq \mathrm{SoC_{max}}$$

Equation 4.9

- The battery has a constraint for charging and discharging, limiting the maximum charging power to $2\mathrm{C_{BESS}}$, where $\mathrm{C_{BESS}}$ is the capacity of the battery (Equation 4.10). This limitation aligns with the recommendations provided in various Lithium-based cell datasheets to prevent rapid cell degradation. As such, it is only advisable to operate up to $2\mathrm{C_{BESS}}$. Self-discharge of the battery is assumed to be negligible.

$$\text{BESS max. power[kW]} = 2 \cdot \mathrm{C_{BESS}}$$

Equation 4.10

- The BESS is modelled using an energy flow model according to Byrne *et al.* [278]. The BESS is modelled assuming that any voltage or current change is achievable with changes in SoC [134,278,279] following Equation 4.11 [279].

$$\mathrm{C_{BESS}} \cdot {}^{\partial \mathrm{SoC}}/_{\partial \mathrm{t}} = \mathrm{BESS_{rteff}} \cdot \mathrm{P_{BESS(t)}}^{+} + \mathrm{P_{BESS(t)}}^{-}$$

Equation 4.11

- The algorithm is run 8,784 times as this corresponds to the total number of hours per year. When the algorithm ends at time step 8784, the BESS energy balance must be 0. The energy balance is calculated following Equation 4.12. Where "Total energy in" and "Total energy out" is the sum of hourly values of energy coming in and out of the BESS for the whole year (i.e., from t=1 to t=8784), respectively. "$\mathrm{Energy_{(t=0)}}$" refers to the energy store at the BESS at t=0 (i.e., $\mathrm{SoC_{min}}$) and "$\mathrm{Energy_{(t=8784)}}$" is the energy store at the BESS at t=8784.

$$\begin{aligned}\text{BESS energy balance (kWh)} &= (\text{Total energy in} - \text{Total energy out}) - (\mathrm{Energy_{(t=0)}} \\ &\quad - \mathrm{Energy_{(t=8784)}})\end{aligned}$$

Equation 4.12

- The amount of power available ($\text{Power}_{(t)}$) from the grid is the maximum power connection capacity ($\text{Power}_{\text{max.capacity}}$) (Equation 4.13).

$$\text{Power}_{(t)} = \text{Power}_{\text{max.capacity}}$$

Equation 4.13

The algorithm used for charging and discharging the BESS is introduced in this section and is shown in Figure 4.7.

The charging process only takes place when the PV generation (PV_{gen}) is higher than the WMD energy demand ($\text{Depot}_{\text{demand}}$). The PV surplus solar energy ($\text{PV}_{\text{surplus}}$) stored at the BESS in any given time interval will depend on the available capacity in the battery to store energy ($\text{BESS}_{\text{available}}$) in the previous interval. (Figure 4.8).

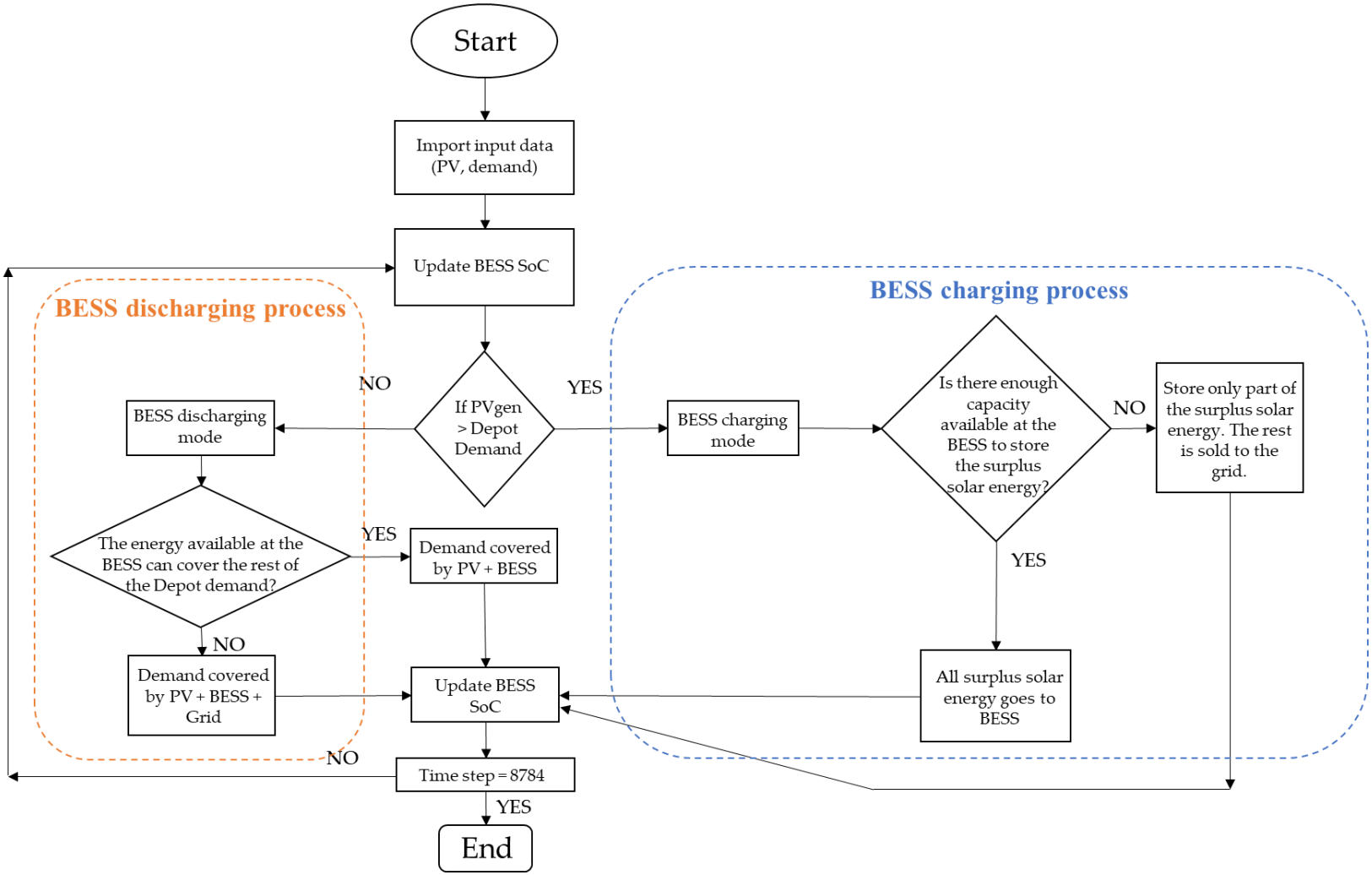

Figure 4.7. Proposed energy management algorithm for the BESS charging/discharging process at WMD.

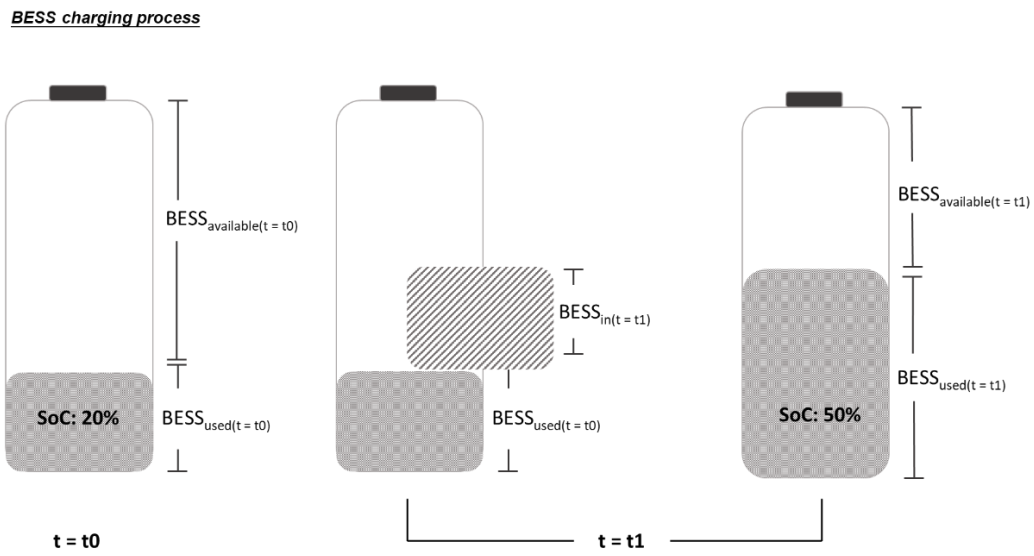

Figure 4.8. Diagram of the BESS when is charged.

When the algorithm is initialised at t=t0, the SoC of the bank of batteries is at its minimum (SoC_{min}) thus the portion of the BESS capacity (C_{BESS}) that has been used $(BESS_{used})_{t=t0}$ corresponds to the 20% of the C_{BESS}. At t=t1, the available capacity at the BESS $(BESS_{available})_{(t=t1)}$ corresponds to the difference between the maximum percentage of the BESS capacity that can be used ($BESS_{max.cap}$) (i.e. at SoC_{max}) and the portion of the BESS capacity that is used ($BESS_{used}$) at t=t1 following Equation 4.14.

$$(BESS_{available})_{t=t1} = BESS_{max.cap} - (BESS_{used})_{t=t1}$$

Equation 4.14

At=t1, the BESS capacity that has been used ($(BESS_{used})_{t=t0}$) can be calculated as in Equation 4.15:

$$(BESS_{used})_{t=t1} = (BESS_{used})_{t=t0} + ((BESS_{in})_{t=t1} \cdot BESS_{rteff})$$

Equation 4.15

Where $BESS_{rteff}$ is the round trip battery efficiency and $(BESS_{in})_{(t=t1)}$ is the amount of energy store at the corresponding time step (i.e., t=t1). The algorithm considers the SoC of the BESS for the previous time period (t=t0), i.e. $(BESS_{used})_{t=t0}$, as a base for the energy that is stored at t=t1 (i.e. $((BESS_{in})_{t=t1})$.

On the other hand, the battery is discharged when there is not enough PV solar energy to meet the energy demand of the depot, as it is shown in Figure 4.7.

The energy discharged from the battery ($BESS_{out\ (t=t2)}$), will depend on the available energy stored at the battery from the previous time period, ($BESS_{used}$) $_{t=t1}$, as it can be seen in Figure 4.9.

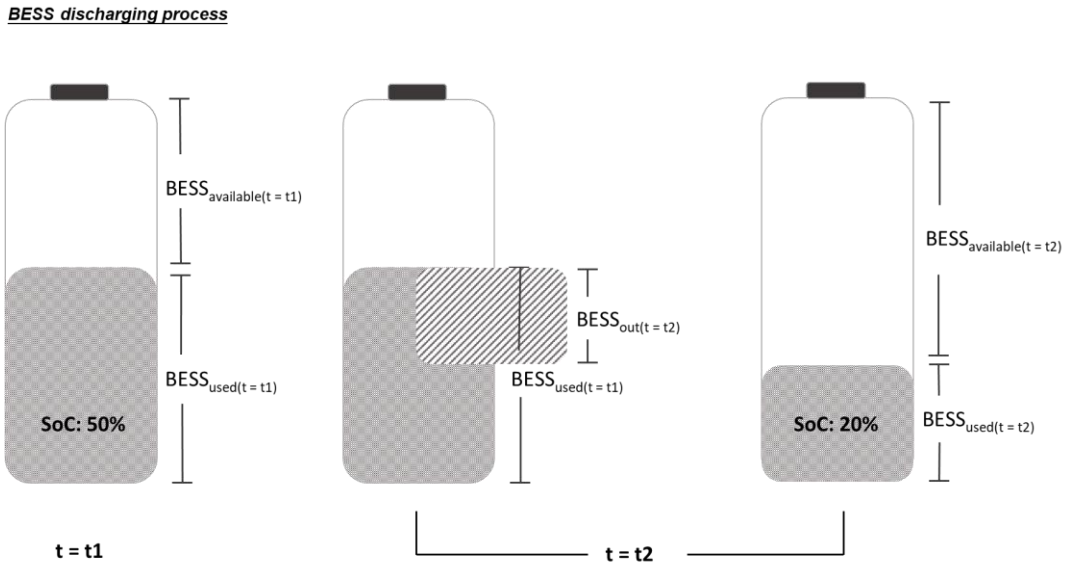

Figure 4.9. Diagram of the BESS when is discharged.

When the BESS is discharged up to the minimum SoC in t=t2, the BESS can't be further discharged at t=t3 (Figure 4.10). So, at t=t3 if the energy demand has not been covered by the instantaneous PV solar energy, the grid is required to support the energy demand from the depot.

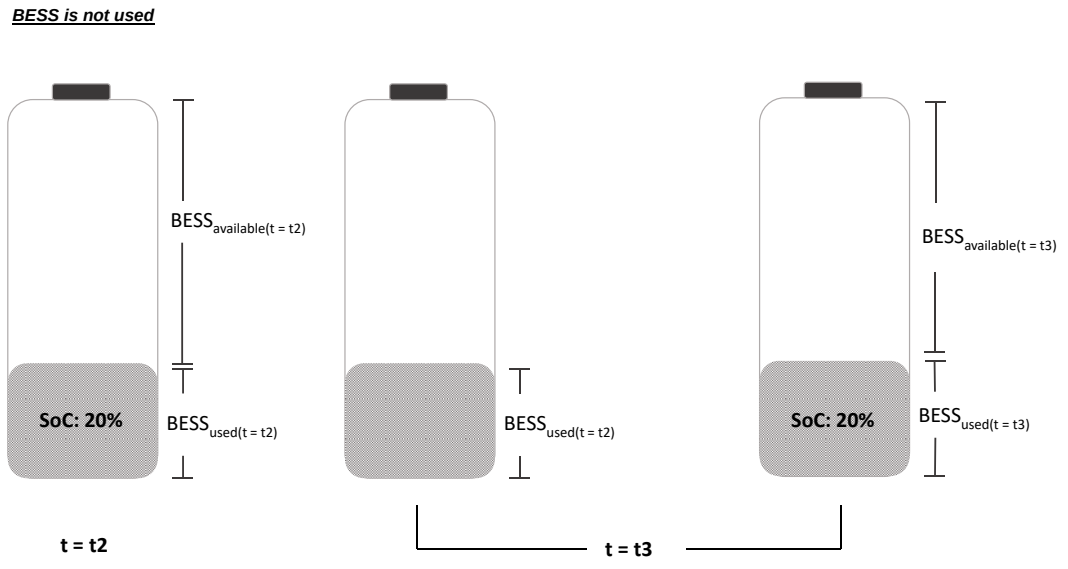

Figure 4.10. Diagram of the BESS when is neither charged nor discharged.

M&S retail store

As shown in the previous section (section 4.3.1), at the M&S retail store, the installation of a BESS won't significantly increase the use of PV solar energy. According to data shown in Figure 4.4b, most of the PV solar energy generated would be used directly by the store.

Taking this into consideration, the main objective of the energy management algorithm is to minimise the costs from the electricity bought from the grid, and this is achieved following an arbitrage strategy. The energy management algorithm developed for the M&S retail store connects the system formed by the PV solar installation, the BESS, and the store with the grid as shown in Figure 4.11. The only difference with the algorithm developed for the WMD is that the grid is also connected to the BESS. This allows the system to take advantage of electricity price differences throughout the day.

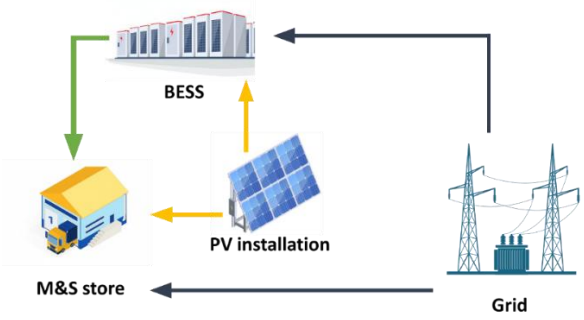

Figure 4.11. Energy flow diagram proposed for the M&S retail store.

For this purpose, a threshold price is used so the BESS is charged from the grid when electricity prices are below the threshold and discharged when the prices are above the threshold. According to Byrne *et al.* [278], the ratio between high prices (H_{PRICE}) and low prices (L_{PRICE}) for arbitrage to be profitable, would be related to the round trip efficiency as in Equation 4.16:

$$\frac{H_{PRICE}}{L_{PRICE}} \geq \frac{1}{BESS_{rteff}}$$

Equation 4.16

A further priority is to maximise the performance of the PV solar installation. Thus, the energy demand is first covered with PV solar energy, and surplus solar energy is stored in the BESS if available.

For the development of the algorithm, the BESS constraints used correspond to the same constraints introduced for the WMD (see Equation 4.9 to Equation 4.13). SoC_{min} and SoC_{max} are assumed to be 20% and 90% of the total battery capacity, respectively. $BESS_{rteff}$ is 90%.

The algorithm used for the BESS charging/discharging process at the M&S retail store can be seen in Figure 4.12.

When there is surplus solar energy, the BESS can be charged not only from the PV panels but also from the grid as long as the electricity price stays below the threshold price and the power constraint is not surpassed (Figure 4.12). When the energy demand can't be entirely covered by the solar energy, the same rule applies. The BESS can be charged from the grid, once the energy demand has been met, if the electricity price is below the threshold price and the power constraint is not surpassed.

As opposed to the algorithm created for the WMD, the BESS is not always discharged when the energy demand can't be met by the solar energy. For the BESS to be discharged, the electricity price must be higher than the threshold price. Otherwise, the demand is covered with solar energy and with energy from the grid.

In the following section, the electricity prices assumed for the WMD are introduced. In the case of the M&S store, the electricity price was provided by the company at the time of the study and is also discussed.

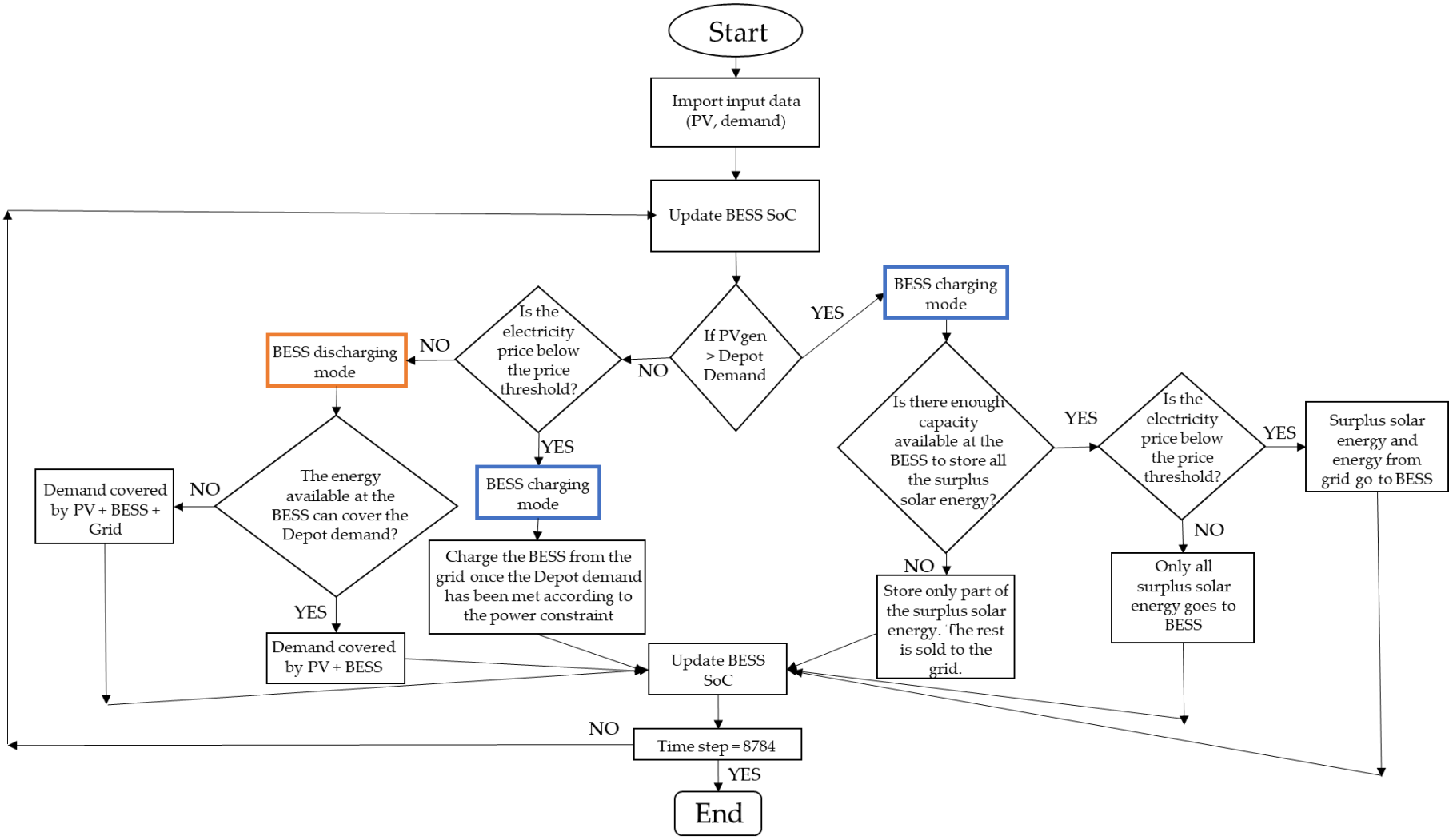

Figure 4.12. Proposed energy management algorithm for the BESS charging process at the M&S retail store.

4.3.3 Electricity price profile

Waste management depot

The electricity price paid at the WMD had to be assumed, considering the available data from the UK government.

Since 2021, there has been a significant surge in electricity prices, and over the last year (2022/23), global gas and wholesale electricity prices have quadrupled. To estimate the cost of electricity for the WMD, the average electricity price in the non-domestic sector published by BEIS [295] has been considered. BEIS provides average quarterly and annual electricity prices based on surveys conducted for energy suppliers and non-domestic consumers. The depot under study falls into the small consumption band, according to BEIS classification. This band's electricity price escalated by 63% to 25p/kWh between Q3 2021 and Q3 2022.

Forecasts indicate a persistent price escalation during the winter period. Unfortunately, the available data for the non-domestic sector has not been updated since Q3 2022, just before the implementation of the Ofgem price cap (1st October -31st December 2022). Since then, the Ofgem price cap has been updated twice. Thus, the change for electricity prices for non-domestic consumers has been extrapolated from the percentage change corresponding to each Ofgem price cap. The latest report on domestic energy prices indicates an 80% escalation in the price cap from April 2022 to October 2022 [296] followed by a 20% uptick from October 2022 to January 2023 [297].

Figure 4.13 displays the electricity pricing dynamics within the small consumption band of the non-domestic sector. The figure includes publicly disclosed prices (in purple) and projected estimates (in orange). For Q4 2022, the electricity rate of 37.80 p/kWh was considered to experience an 80% surge compared to Q2 2022 (21.04 p/kWh). In Q1 2023 a further 20% increase was applied to estimate the electricity price (i.e. 45.40 p/kWh).

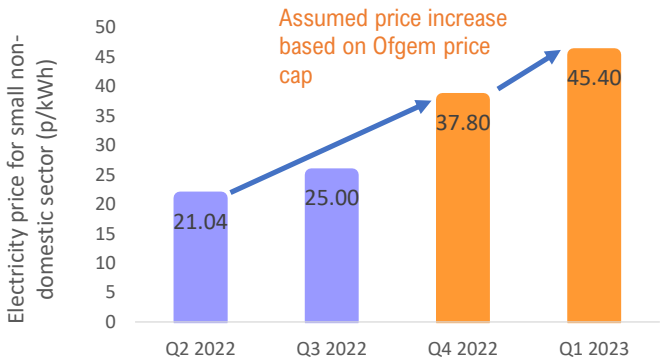

Figure 4.13. "Assumed electricity price for small non-domestic sector from October 2022. The arrows represent the percentage increase between Q2 2022 and Q4 2022 (i.e., 80%) and between Q4 2022 and Q1 2023 (i.e., 20%)" (Figure obtained from [175]).

Considering the price volatility and continuous increases, the study has adopted the average price assumed for Q1 2023 which is 45.4 p/kWh.

The WMD operates with a variable tariff contract, so the electricity price fluctuates hourly. In order to create a price profile throughout a typical day based on the average price assumed (i.e. 45.4 p/kWh), the study has simulated the shape of the price profile, using wholesale electricity prices from the Nord Pool website for the UK [298]. Nord Pool is in the EU Regulation on Wholesale Energy Market Integrity and Transparency framework for power trading across Europe.

As an example, Figure 4.14 shows the electricity prices assumed for the WMD for one day of the year. There are two peak times when the electricity cost is at its highest value (between 6am and 10am, and 4pm-8pm).

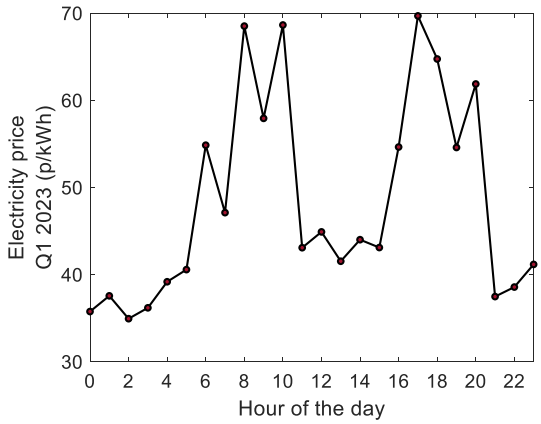

Figure 4.14. "Simulated electricity prices for one day of the year (from 00:00h to 23:00h) for WMD" (Figure obtained from [175]).

M&S retail store

The electricity tariff at the M&S retail store was provided and it is based in two consumption bands (i.e., economy 7 tariff). These types of tariffs are characterised for offering lower electricity prices at off-peak times and higher prices at peak times. The electricity tariffs are as follows:

- Day band: Corresponds to the band from 08:00h to 23:00h in which the electricity price is at 10.76 p/kWh.
- Night band: It represents the time of the day when the electricity price is set at 7.15p/kWh (i.e. between 00:00h and 07:00h).

A representative price profile is shown in Figure 4.15.

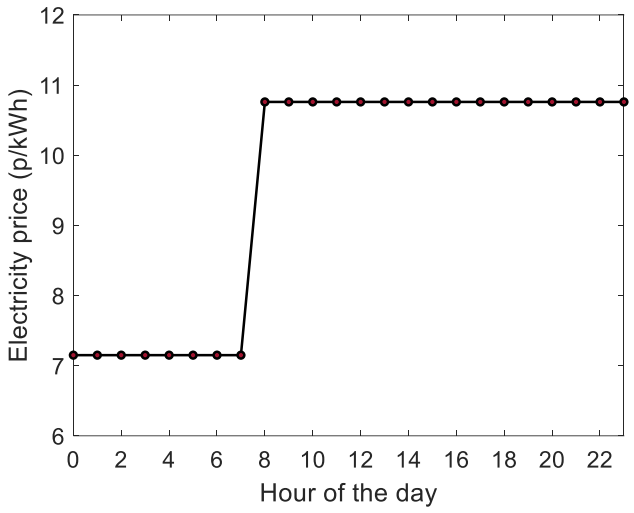

Figure 4.15. "Provided electricity prices for one day of the year (from 00:00h to 23:00h) for M&S retail store."

4.3.4 System cost analysis

The economic analysis for the two different sites has been quantified considering the costs of energy from the grid (E_c), network costs (N_c), cost of the BESS ($BESS_c$), cost of the PV installation (PV_c) and the revenue obtained from the sale of surplus solar energy (Rev_c) following Equation 4.17.

$$\text{Total costs over system lifetime} = E_c + N_c + BESS_c + PV_c - Rev_c$$

Equation 4.17

A detailed description of each cost from Equation 4.17, is introduced next.

Cost of energy (E_c):

The cost of energy refers to the cost of electricity purchased from the grid and is calculated following Equation 4.18.

$$\text{Cost of energy} = \text{Electricity price } \left(\frac{\text{p}}{\text{kWh}}\right) \cdot \text{Energy consumption (kWh)}$$

Equation 4.18

Network charges (N_c):

The network cost components include the contracted power connection capacity costs and the cost for utilising the network distribution system that is charged by the energy supplier. The total network cost (N_c) is the sum of the capacity cost (C_c), exceeded capacity cost (ExC_c), fixed cost (F_c) and consumption band cost ($Consmp_c$) (Equation 4.19)

$$N_c = C_c + ExC_c + F_c + Consmp_c$$

Equation 4.19

Capacity cost (C_c) pertains to the contracted power connection capacity. If the power connection capacity is exceeded, additional costs will be incurred (i.e., exceeded capacity costs). Meanwhile, the consumption band cost ($Consmp_c$) represents the fee for network utilisation during specific periods throughout the day, segmented into three distinct bands:

- The amber band rate is charged between 07:00h-16:00h and 19:00h-21:00.
- The red band rate spans from 16:00h to 19:00h.
- The green band rate is from 00:00h to 07:00h and from 21:00h to 24:00h.

For the Waste management depot (WMD), the network charges were selected based on the price from Western Power Distribution Network in the UK for a LV Site-Specific Band 1 [299]. The network charges can be seen in Table 4.1.

Table 4.1. “Network charges for the WMD” (Table obtained from [175]).

Network charges	Price	Unit of measure
Capacity charge	2.91	p/kVA/day
Exceeded capacity charge	5.73	p/kVA/day
Fixed charge	297	p/day
Consumption band:		
Amber charge	0.737	
Red charge	4.301	p/kWh
Green charge	0.054	

On the other hand, the network charges for the M&S retail store have been provided by the company and can be seen in Table 4.2.

Table 4.2. M&S retail store network charges.

Network charges	Price	Unit of measure
Capacity charge	4.44	p/kVA/day
Exceeded capacity charge	5.73	p/kVA/day
Fixed charge	4,718	p/day
Consumption band:		
Amber charge	0.202	
Red charge	4.922	p/kWh
Green charge	0.026	

The capacity cost is calculated in Equation 4.20.

$$C_c(£/\text{year}) = \frac{\frac{\text{Power}_{\text{capacity}}(\text{kW})}{\text{PF}\left(\frac{\text{kW}}{\text{kVA}}\right)} \cdot \frac{\text{Capacity charge}\,\frac{\text{p}}{\text{kVA}}}{\text{day}} \cdot 365\ \text{days}}{100\ \text{p}/£}$$

Equation 4.20

PF is the power factor. Considering the active and reactive power of the electrical devices of both sites analysed, a PF of 0.9 has been selected.

The total exceeded capacity cost (ExC_c) is calculated as the sum of the excess power capacity multiplied by the exceeded capacity charge each day following Equation 4.21.

$$\mathrm{ExC_c}(£/\mathrm{year}) = \sum_{i=1}^{n} \left(\frac{\left(\frac{\text{Excess power}_{\text{capacity}}(\mathrm{kW})}{\mathrm{PF}\left(\frac{\mathrm{kW}}{\mathrm{kVA}}\right)} \right)_i \cdot \frac{\text{Exceeded capacity charge} \frac{\mathrm{p}}{\mathrm{kVA}}}{\text{day}}}{100 \frac{\mathrm{p}}{£}} \right)$$

Equation 4.21

The fixed costs ($\mathrm{F_c}$) per year are obtained applying Equation 4.22.

$$\mathrm{F_c}\left(\frac{£}{\mathrm{year}}\right) = \frac{\text{Fixed charge } \left(\frac{\mathrm{p}}{\mathrm{day}}\right)}{100 \frac{\mathrm{p}}{£}} \cdot 365 \text{ days}$$

Equation 4.22

Ultimately, consumption band costs ($\mathrm{Consmp_c}$) are estimated by calculating the energy consumption at each band time multiplied by the corresponding band charge as expressed in Equation 4.23:

$$\mathrm{Consmp_c}\left(\frac{£}{\mathrm{year}}\right) = \frac{\text{Energy consumption (kWh)} \cdot \text{consumption band charge } (\frac{\mathrm{p}}{\mathrm{kWh}})}{100 \frac{\mathrm{p}}{£}}$$

Equation 4.23

Cost of BESS ($\mathrm{BESS_c}$**)**:

For the cost of the BESS, a capital cost of £245/kWh [300] and £2.5/kWh-year in Operation and Maintenance (O&M) costs [301] have been used. The BESS capital costs are obtained using Equation 4.24

$$\mathrm{BESS_{Cc}}(£) = \mathrm{C_{BESS}}\ (\mathrm{MWh}) \cdot \frac{1{,}000\ \mathrm{kWh}}{1\ \mathrm{MWh}} \cdot 254 \frac{£}{\mathrm{kWh}}$$

Equation 4.24

The O&M cost of the BESS has been calculated in Equation 4.25.

$$\mathrm{BESS_{OMc}}(£) = \mathrm{C_{BESS}}\ (\mathrm{MWh}) \cdot \frac{1{,}000\ \mathrm{kWh}}{1\ \mathrm{MWh}} \cdot 2.5 \frac{£}{\mathrm{kWh\ per\ year}} \cdot \text{BESS lifetime (years)}$$

Equation 4.25

BESS lifetime has been assumed to be 15 years [300,301]. In Table 4.3, the total cost of the BESS ($BESS_c$) has been calculated for each BESS capacity (C_{BESS}) as the addition of $BESS_{Cc}$ and $BESS_{OMc}$.

Table 4.3. "Total cost of BESS for a lifetime of 15 years" (Table obtained from [175]).

BESS capacity (MWh)	Capital cost (£)	O&M cost (£)	Total cost (£) in 15 years
0.05	12,700	1,875	14,575
0.1	25,400	3,750	29,150
0.5	127,000	18,750	145,750
1	254,000	37,500	291,500
5	1,270,000	187,500	1,457,500
10	2,540,000	375,000	2,915,000

Cost of PV panels (PV_c):

The capital cost assumed for the PV system is £1.25/W_{DC} and the O&M cost is £17.92 / kWp-year [302]. The capital and O&M costs consider the costs associated with the inverter [302]. The PV panel capital costs are obtained using Equation 4.26.

$$PV_{Cc}(£) = \text{Number of PV panels} \cdot \text{PV panel power output (W)} \cdot 1.25 \frac{£}{W_{DC}}$$

Equation 4.26

The O&M cost of the PV installation has been calculated in Equation 4.27.

$$PV_{OMc}(£) = \text{Number of PV panels} \cdot \text{PV panel power output (W)} \cdot \frac{1\text{kW}}{1{,}000\ \text{W}} \cdot 17.92 \frac{£}{\text{kWp per year}} \cdot \text{PV lifetime (years)}$$

Equation 4.27

Table 4.4 and Table 4.5 show the total cost for the PV installation with a lifetime of 15 years, as the addition of PV_{Cc} and PV_{OMc}, for the WMD and for the M&S retail store, respectively.

Table 4.4. "Total cost of PV installation for a lifetime of 15 years for the WMD" (Table obtained from [175]).

Number of PV panels installed in the depots	PV panel power output, STC (W)	PV system size (MW)	Capital cost (£)	O&M costs (£)	Total cost (£) in 15 years
1,864	270	0.5	629,100	135,282	764,382

Table 4.5. Total cost of PV installation for a lifetime of 15 years for the M&S retail store

Number of PV panels installed in the depots	PV panel power output, STC (W)	PV system size (MW)	Capital cost (£)	O&M costs (£)	Total cost (£) in 15 years
2,528	270	0.68	853,000	183,472	1,036,672

Revenue from the sale of PV surplus solar energy ($\mathrm{Rev_c}$):

For both sites, it is assumed that the PV surplus solar energy is sold back to the grid, and it generates an annual revenue that is considered in the calculations of total costs (Equation 4.28). In the UK, the revenue from the sale of surplus solar energy is regulated by the Smart Export Guarantee scheme [261]. However, there is not a unique rate and rates vary amongst the different electricity suppliers and the type of tariffs. For a fixed tariff, a typical price is between 3 to 7 pence per kWh [303,304]. Variable tariffs can offer prices up to 15 pence per kWh [305]. According to the differences in rates, a sale price of 5 pence per kWh has been used for this study.

$$\mathrm{Rev_c}(£/\mathrm{year}) = \frac{\text{Sale price } \left(\frac{\mathrm{p}}{\mathrm{kWh}}\right) \cdot \text{surplus solar energy(kWh)}}{100\ \mathrm{p}/£}$$

Equation 4.28

4.3.5 Greenhouse gas (GHG) emissions analysis

The estimated annual GHG emissions have been calculated to analyse the impact that introducing a PV installation and a BESS has on both sites. The GHG emissions have been calculated following this equation:

$$\text{GHG emissions (tons } \mathrm{CO_2eq.}) = \text{Energy (kWh)} \cdot \mathrm{ECF}\left(\frac{\mathrm{kg\ CO_2eq.}}{\mathrm{kWh}}\right) \cdot 10^{-6}\left(\frac{\mathrm{tons}}{\mathrm{kg}}\right)$$

Equation 4.29

Where ECF stands for Emission Conversion Factor. The emission conversion factors used in this study are shown in Table 4.6. The emission conversion factor for electricity generated from the grid have been obtained from the UK Government GHG Conversion Factors for Company Reporting [306]. The conversion factor for emissions resulting from the consumption of PV solar energy have been obtained from Gabi database [73]. The PV emission factor is based on the global average of photovoltaic technologies installed: Mono-Silicon 42 %, Multi-Silicon 47 %, Cadmium-Telluride (CdTe) 7 % and Copper-Indium-Gallium-Diselenide 4 %.

Table 4.6 Emission conversion factor for the energy consumed at the WMD.

	Emission conversion factor (kg CO_2 eq. per kWh)
Electricity generated from photovoltaic	0.0686
Electricity generated from grid mix	0.19338

The GHG emissions related to the surplus solar energy sold to the grid are calculated considering not only the impact generated from the PV solar energy but also the saved emissions that would be generated if that energy would come from the grid mix. The equation used to express the impact from the surplus solar energy is Equation 4.30.

$$GHG\ \text{emissions}\ (\text{tons}\ CO_2\text{eq.}) = \left(\text{PV surplus energy(kWh)} \cdot 0.0686 \left(\frac{\text{kg}\ CO_2\text{eq.}}{\text{kWh}}\right) \cdot 10^{-6} \left(\frac{\text{tons}}{\text{kg}}\right)\right) - \left(\text{PV surplus energy(kWh)} \cdot 0.19338 \left(\frac{\text{kg}\ CO_2\text{eq.}}{\text{kWh}}\right) \cdot 10^{-6} \left(\frac{\text{tons}}{\text{kg}}\right)\right)$$

Equation 4.30

4.4 Results: Evaluation of grid reliance, total cost and GHG emissions using BESS

4.4.1 Waste management depot

Section 4.3.1 introduced the hypothetical PV installation at the WMD and the self-consumption percentage. Figure 4.16 shows the hourly energy flow corresponding to the WMD, assuming that PV panels were installed but not a BESS. A week in February (Figure 4.16a) and a week in July (Figure 4.16b) have been plotted as an example. Each vertical line in Figure 4.16 marks the hour 24:00h, the beginning of a new day.

The WMD is reliant on the energy from the grid all year round. During winter, the dependency on the grid expands for longer hours than in summer, due to the lower solar energy generation. If a BESS were installed, the PV surplus solar energy could be used to reduce the dependency from the grid still further, predominantly at night. The impacts of adding a BESS to the system are explored next for the WMD. The energy management algorithm is applied assuming a range of batteries with different capacities.

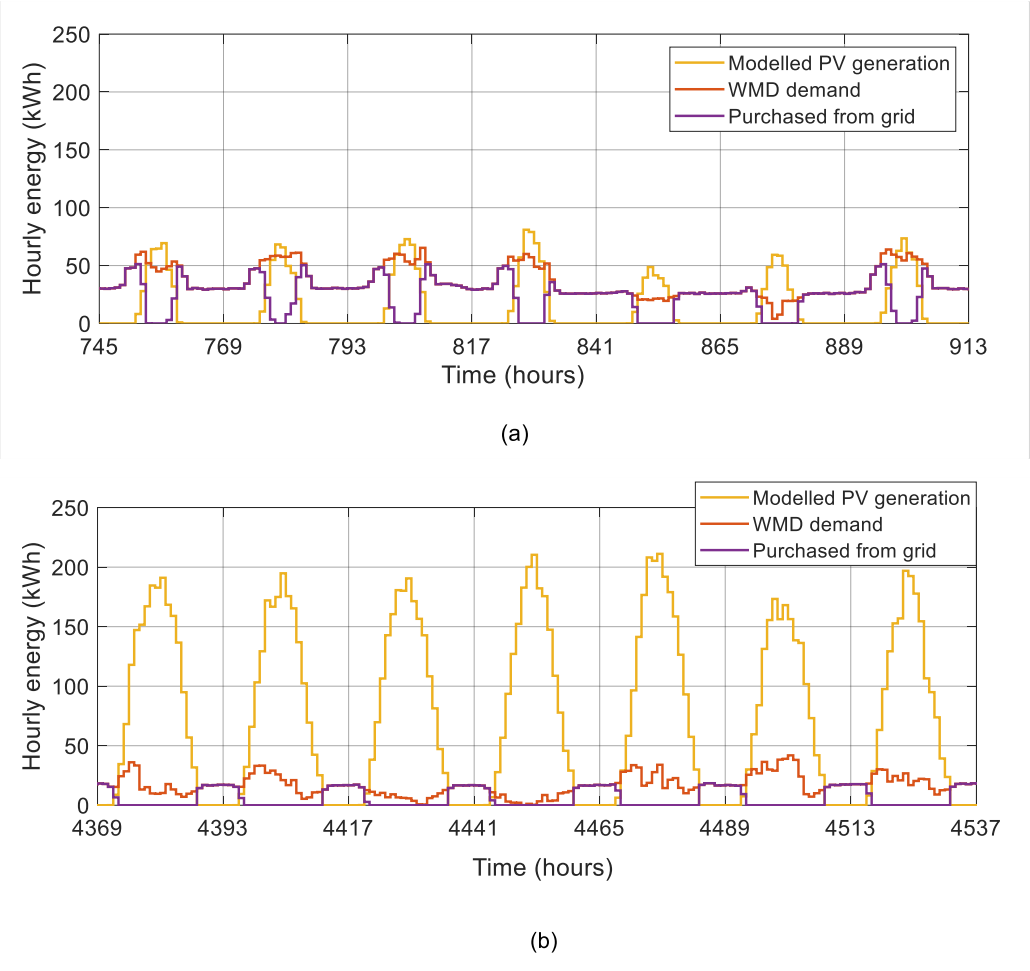

Figure 4.16. Simulation results for a week in (a) February and (b) July for the energy flow in the WMD assuming a BESS is not installed.

Impact of the BESS capacity (C_{BESS})

A simulation is carried out by applying the energy management algorithm to the WMD. The results can be seen in Figure 4.17 for a BESS with a capacity (i.e. C_{BESS}) of 0.5 MWh. Figure 4.17a shows how energy flows hourly within the system in a week in February as a representation of the system's energy flow during winter months (each vertical line of Figure 4.17 marks the beginning of another day). Solar energy is used to cover the WMD's energy

demand whenever possible. During winter, the system is dependent on the grid due to insufficient PV solar energy generation.

On the other hand, Figure 4.17b shows a week during July as a representative example of how energy is distributed during summer. Figure 4.17b can be compared with

b when no BESS was implemented. At this time of the year, the system is independent of the grid during the day when the BESS is in place. The energy demand is covered entirely by instantaneous PV solar energy during the day and stored PV solar energy being used at night.

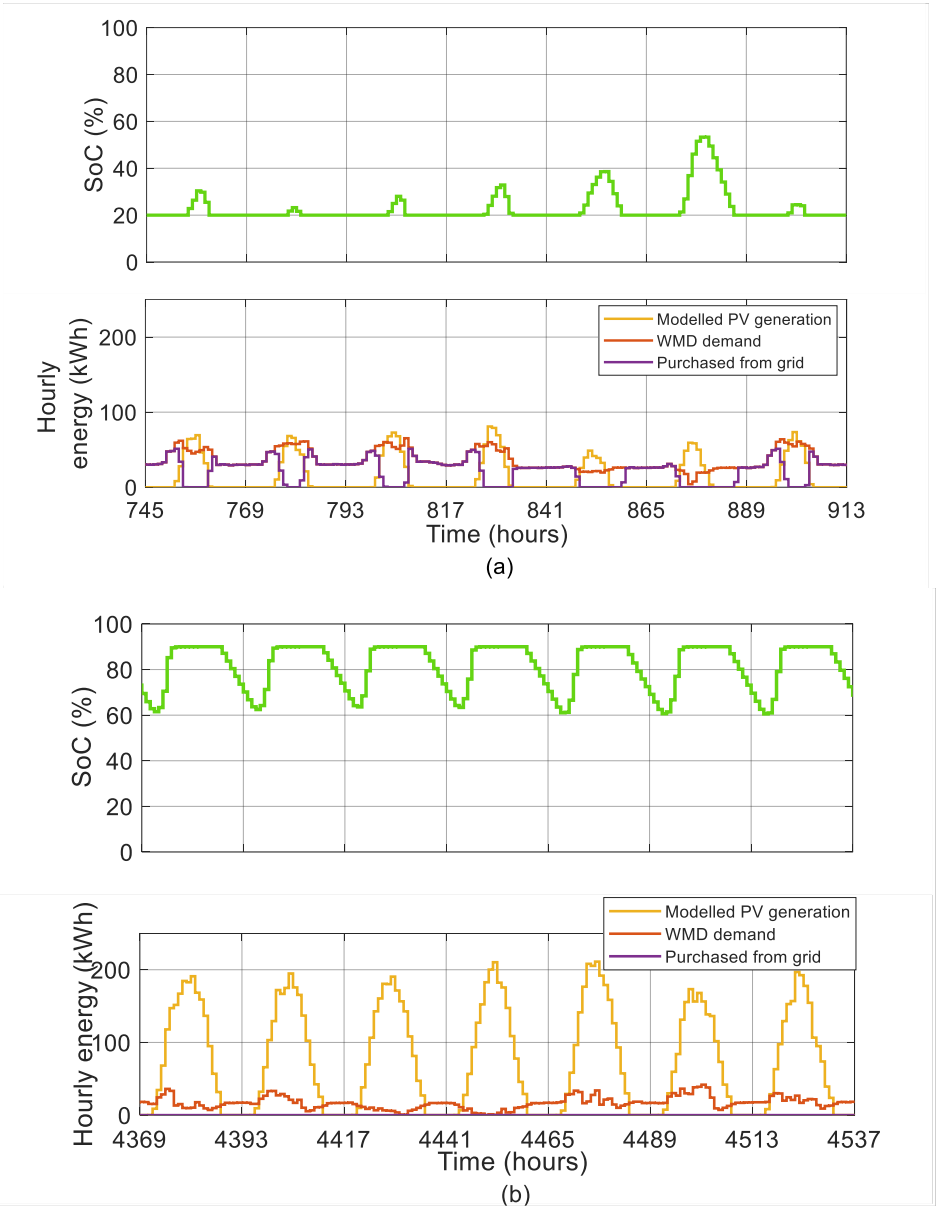

Figure 4.17. Simulation results when the energy management algorithm is applied in a week in (a) February and (b) July using a BESS with CBESS of 0.5 MWh for the WMD. It includes the State of Charge (SoC), modelled PV solar energy generation, energy demand from the WMD and energy purchased from the grid.

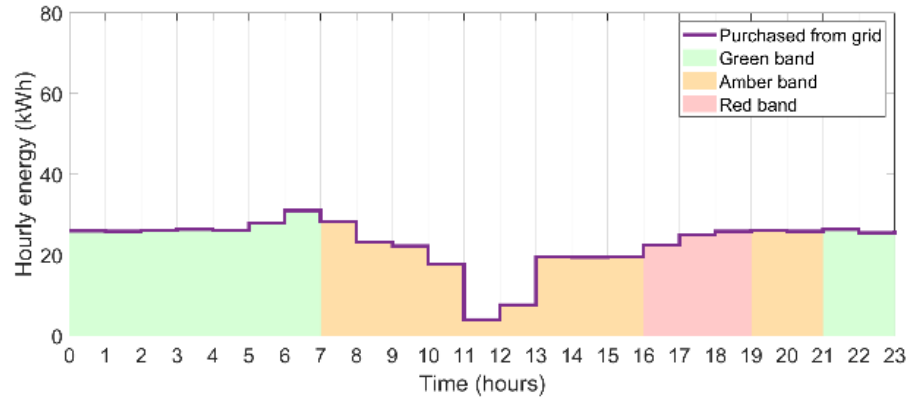

(a)

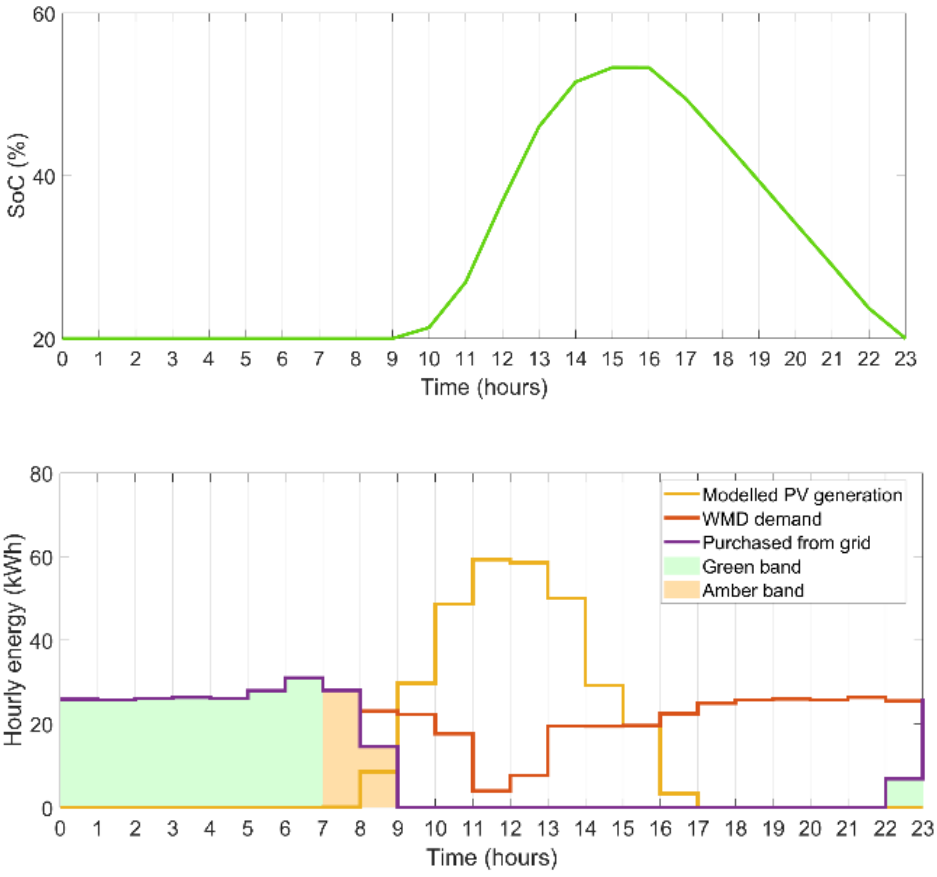

(b)

Figure 4.18. "Top graph (a): Hourly energy consumption from the grid assuming there is not a PV nor a BESS in place. Bottom graph (b): Hourly energy consumption from the grid assuming there PV panels and a BESS of 0.5 MWh installed at the WMD" (Figure obtained from [175]).

The impact of introducing a BESS can be seen for a day in February in Figure 4.18. Figure 4.18a shows the hourly energy distribution assuming the BESS is not installed. On the other hand, Figure 4.18b, shows results for the same day with a BESS of 0.5 MWh. The shaded colour area represents the consumption time bands at which the energy is purchased from the

grid. During this day, the WMD energy demand is relatively lower, and a higher surplus solar energy can be stored at the BESS. The stored energy is discharged from the BESS when no solar energy is available to meet the WMD energy demand, allowing the system to be independent from the grid for a longer period of time if compared to the same day when the BESS is not in place.

Figure 4.19 shows monthly results from the energy management algorithm at different battery capacities (i.e. C_{BESS}). The positive values on each graph represent the energy consumption from the grid, from solar and from the BESS. The negative values indicate solar energy generation and charging of the BESS. The energy consumption at the WMD is covered from the grid (i.e. Purchased from grid), directly from the solar panels (i.e. Consumed from PV) or from the surplus solar energy stored at the BESS (i.e. From BESS). The fraction of solar energy that is not directly consumed, is stored at the BESS (i.e. To BESS) or sold to the grid as surplus solar energy (i.e. PV solar surplus). When the BESS with capacities equal or higher than 0.5 MWh is in place, the grid is not used for over 5 months to cover the energy demand.

As shown in Figure 4.19, the larger the BESS capacity, the more surplus solar energy can be stored after the WMD energy demand has been met. It is important to consider that the energy in and out of the BESS is balanced yearly, and not monthly. For that reason, for capacities higher than 0.1 MWh, in March and April the monthly energy charged into the BESS is higher than the energy discharged from the BESS. In contrast, from September to November, the monthly energy charged into the BESS is lower than the energy discharged from the BESS. This can be explained because from March, the monthly solar energy generation is higher than the monthly WMD energy demand (see Figure 4.2a). Therefore, the BESS is used to store the surplus solar energy and the overall energy discharged from the BESS is lower than the energy stored over the month. When the solar energy generation starts to decrease in October (see Figure 4.2a), the surplus energy stored in the BESS is lower than the overall monthly requirements on the BESS.

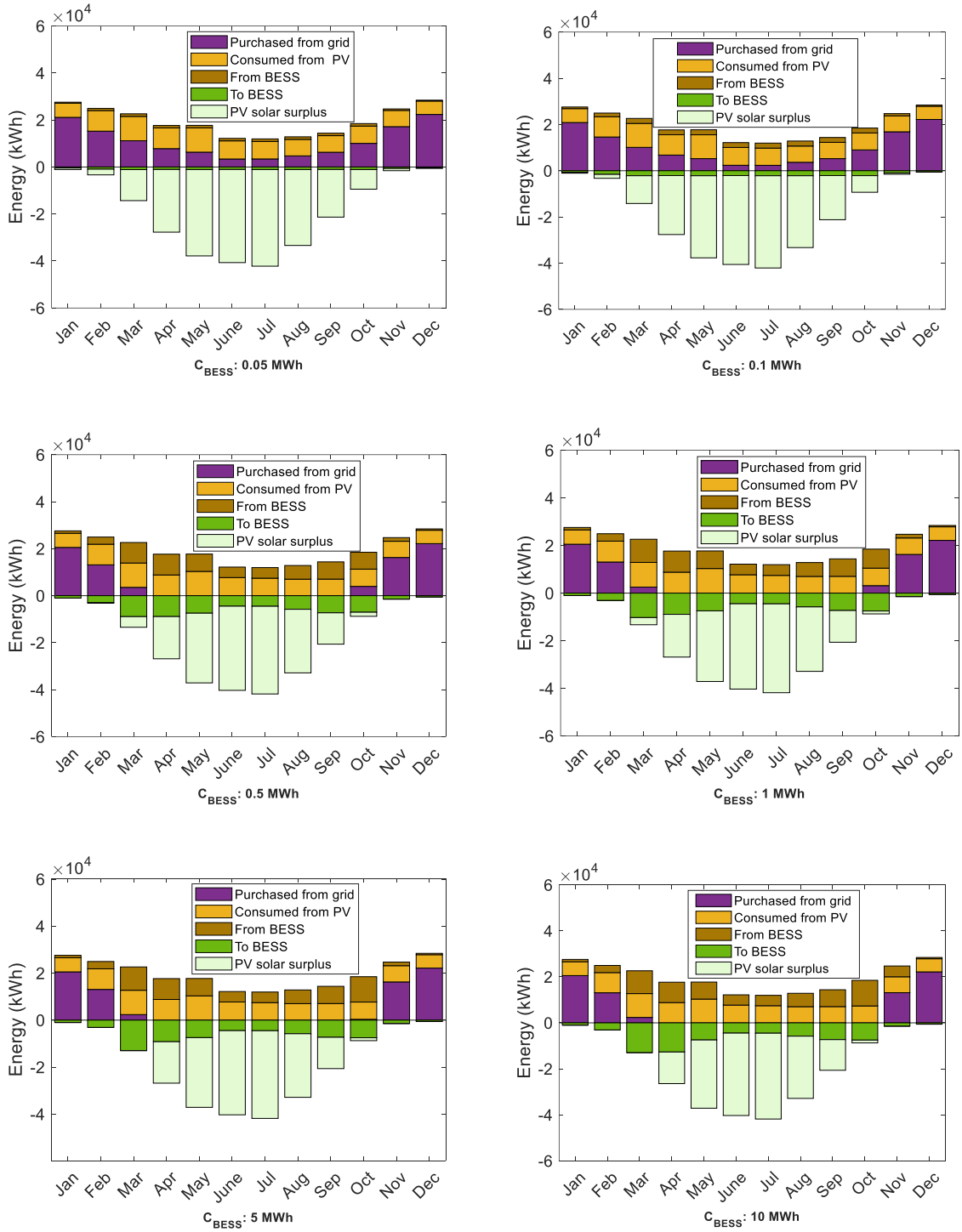

Figure 4.19. Monthly energy distribution at the WMD at different CBESS. The positives values on each graph represent the energy consumption from the grid, from solar and from the BESS. The negative values indicate solar energy generation and charging of the BESS.

The energy flow within the BESS can be seen for different battery capacities (C_{BESS}) on Figure 4.20. For a BESS with a relatively small capacity of 0.05 MWh and 0.1 MWh, the battery can be fully charged in the morning and discharged in the afternoon every day, from spring until

autumn. In the evening, the system relies on the energy from the grid. In winter, because there is less solar energy available to be stored, the BESS completes only a few cycles.

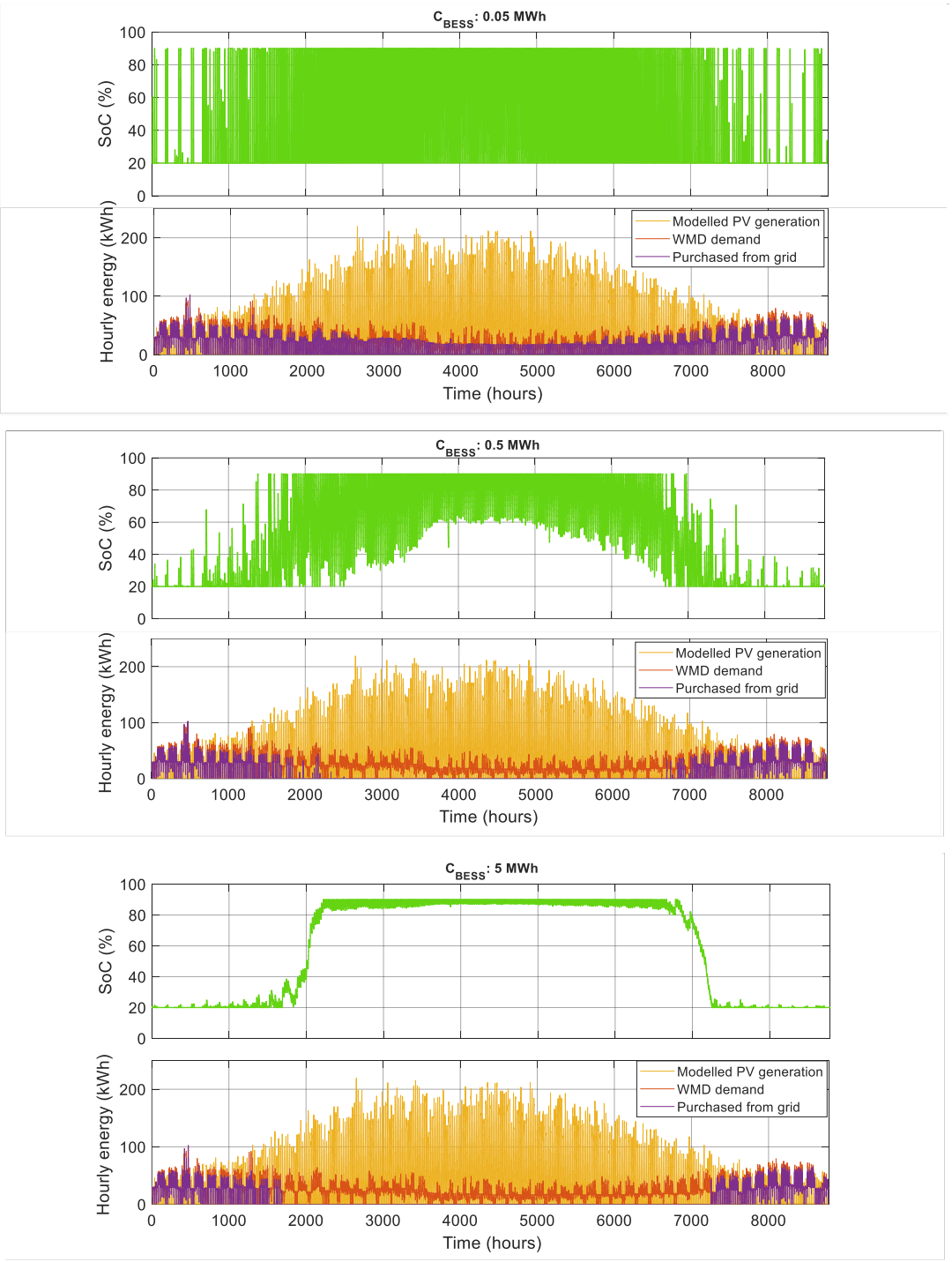

Figure 4.20. A comparison of the hourly energy flow at the BESS at CBESS of 0.05MWh, 0.5 MWh and 5MWh. It includes the State of Charge (SoC), modelled PV solar energy generation, energy demand from the WMD and energy purchased from the grid.

This trend changes for BESS with capacities from 0.5 MWh and 1 MWh. The BESS can store more surplus solar energy such that (i.e., summer months) the energy stored at the BESS is

higher than the energy demand from the WMD. Thus, the BESS is only partly discharged during this time.

The same tendency expands from spring to autumn for battery capacities equal to 5 MWh and 10 MWh. During this period, the BESS is almost fully charged all the time. It never completes a full charge/discharge cycle. The number of cycles in the BESS impacts directly its degradation, and the performance of the BESS. The higher the number of cycles in a BESS, the lower the system's lifetime. Battery degradation [307,308] has an important relevance to the total cost of the system and although it has not been considered as part of the economic analysis for this study, it should be considered as part of future research.

The percentage of energy demand covered by the grid at different battery capacities can be seen in Figure 4.21 through a purple line. A detailed breakdown is also shown in a pie chart for two BESS analysed before, 0.05 MWh and 0.5 MWh. The dark purple section of the pie chart represents the portion of the energy demand covered by the grid. The yellow section refers to the portion of the energy demand covered by instantaneous solar energy. The green section refers to the fraction of the energy demand covered by the BESS.

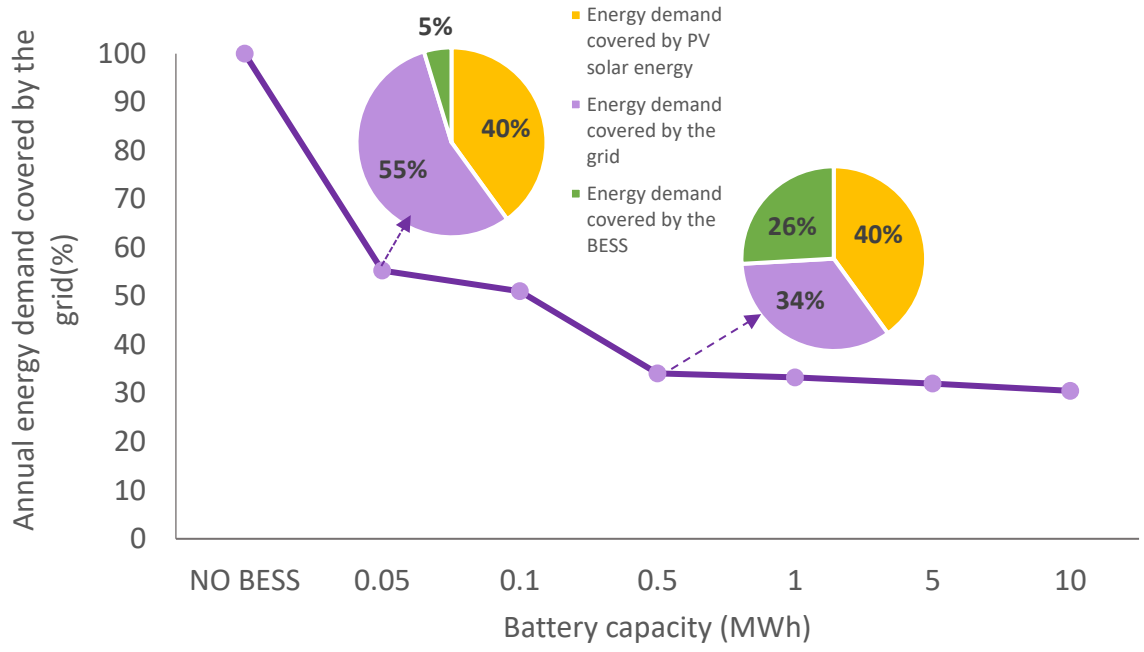

Figure 4.21. Breakdown of energy used at different CBESS for the WMD, either covered by PV solar energy, from the BESS or from the grid.

The bigger the BESS, the lower the percentage of energy purchased from the grid due to the use of PV surplus solar energy stored at the BESS. The highest percentage reduction of energy purchased from the grid is achieved by a BESS with a capacity of 10 MWh.

The system has been tested to estimate the lifetime cost at different BESS capacities. The results are depicted in Figure 4.22. Additionally, for analysis purposes, Figure 4.22 includes the outcomes obtained when there is no BESS nor PV panels in place (i.e. NO BESS). According to the results, a larger BESS capacity leads to a reduced energy cost. Introducing a BESS and PV panels would be justifiable to achieve cost reduction and decrease dependency on the grid.

However, when the cost of BESS, cost of PV panels, and network cost are included, some battery capacities cease being feasible for annual electricity cost reduction. As it can be seen in Figure 4.22, the potential reduction in electricity cost when using a BESS with capacities of 5 MWh to 10MWh is eclipsed by the costs of the BESS.

The BESS that achieved the highest reduction in total costs over the system lifetime corresponds to that of 0.5 MWh capacity. The total cost reduction when this BESS is used compared to the base case scenario (i.e. when BESS and PV panels are not installed) is £340,000.

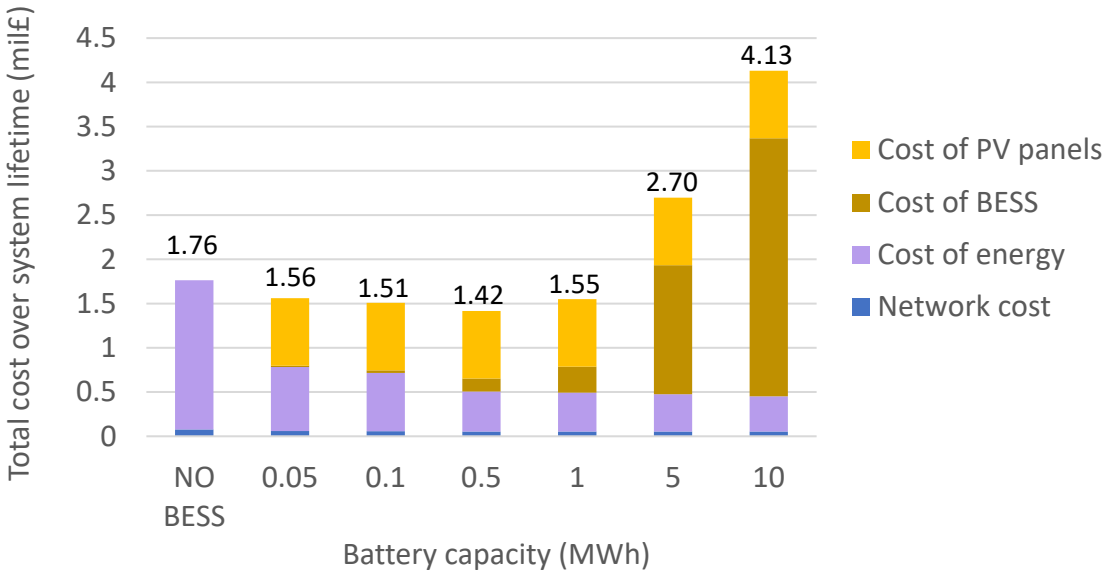

Figure 4.22. Total cost over system lifetime at different CBESS for WMD.

The system costs are itemised at different battery capacities (C_{BESS}) and can be seen in detail in Table 4.7.

Table 4.7. System cost at different battery capacities for the WMD. The values in £ are included in Appendix A.

Power connection capacity (MW)	BESS capacity (MWh)	Cost of energy per year (k£)	Surplus solar energy revenue per year (k£)	BESS capital cost (k£)	BESS O&M cost (k£)	PV capital cost (k£)	PV O&M cost (k£)	Network cost per year (k£)	Total cost over system lifetime (mil£)
0.15	NO BESS	112.4	0	0	0	0	0	5.2	1.76
	0.05	59.3	11.1	12.7	1.9	629.1	135.3	3.9	1.56
	0.1	54.5	10.6	25.4	3.8			3.8	1.51
	0.5	38.5	8.4	127.0	18.8			3.7	1.42
	1	37.6	8.3	254.0	37.5			3.7	1.55
	5	36.2	8.1	1,270.0	187.5			3.7	2.70
	10	34.5	7.9	2,540.0	375.5			3.6	4.13

For batteries with higher capacities (i.e. 5 MWh and 10 MWh), 54% and 70% of the total cost over system lifetime comes from the cost of the BESS. This includes the BESS capital cost and operating and maintenance (O&M) costs. The cost of the PV panels includes the PV panels capital costs and O&M cost, which especially for lower batteries represents between 48% and 53% of total costs over the system lifetime. The cost of energy storage technology has been decreasing over the last decade [309,310] and according to Cole *et al.* [300] cost projections indicate a further potential reduction in capital cost by 2030. On the other hand, the UK Government [311] expects reductions in levelised cost of energy (LCOE) for PV solar systems between 2025 (£44/MWh) and 2040 (£33/MWh). The cost reduction in both technologies is associated with an improvement in energy efficiency and it would be essential to reduce further the total costs of the system. Present costs have been used for this study and further research should be undertaken to investigate future cost scenarios. This work is beyond the scope of this project and will be considered as future work.

The network costs are presented in Table 4.7 as the addition of capacity charge, fixed charge, and consumption charge at each battery capacity. Network costs are reduced when the BESS is in place. As the BESS capacity increases, the network costs can be lowered. This reduction in network cost is linked to the consumption cost at different time bands and is presented in Table 4.8.

There are different time bands: amber, red, and green. The costliest time band is red and encompasses the times between 16:00h to 19:00h. The amber band covers the times from

07:00h-16:00h and 19:00h-21:00. The green band is the cheapest and it spans from 00:00h to 07:00h.

Table 4.8 Network costs itemised at different battery capacities for the WMD. The values in £ are included in Appendix A.

Power connection capacity (MW)	BESS capacity (MWh)	Capacity charge per year (k£)	Excess capacity charge per year (£)	Fixed charge per year (k£)	Consumption charge per year (£)			Total Network cost per year (k£)
					Red	Amber	Green	
0.15	NO BESS	1.8	0	1.1	1463	872	44	5.2
	0.05				803	265	40	3.9
	0.1				655	240	39	3.8
	0.5				579	211	20	3.7
	1				579	208	19	3.7
	5				574	202	18	3.6
	10				545	195	17	3.6

As illustrated in Figure 4.23, introducing a BESS has the largest cost saving potential at higher BESS capacities, particularly for reducing the consumption costs during red and amber consumption bands. These two bands are in place between 07:00h and 21:00h. During these times, PV solar energy is generated. A fraction of the solar energy is instantaneously used, otherwise it is stored at the BESS for later use. Outside these times, when solar energy is not generated, the energy stored in the BESS reduces the energy required from the grid and therefore, the consumption costs. The larger the BESS, the greater the surplus solar energy stored and the lower the consumption from the grid at those hours. For smaller battery capacities (i.e. 0.05 MWh and 0.1 MWh) the BESS is discharging for a maximum of three hours whereas if the capacity is equal or higher than 0.5 MWh the BESS is discharging for a longer period of time.

The consumption costs over the green band don’t change significantly when the BESS is in place. The green band takes place between 21:00h and 07:00h. The consumption costs can be reduced during these times if a BESS is used, with enough capacity to not be discharged before 21:00h. This is the case for BESS with 0.5 MWh to 10 MWh capacity.

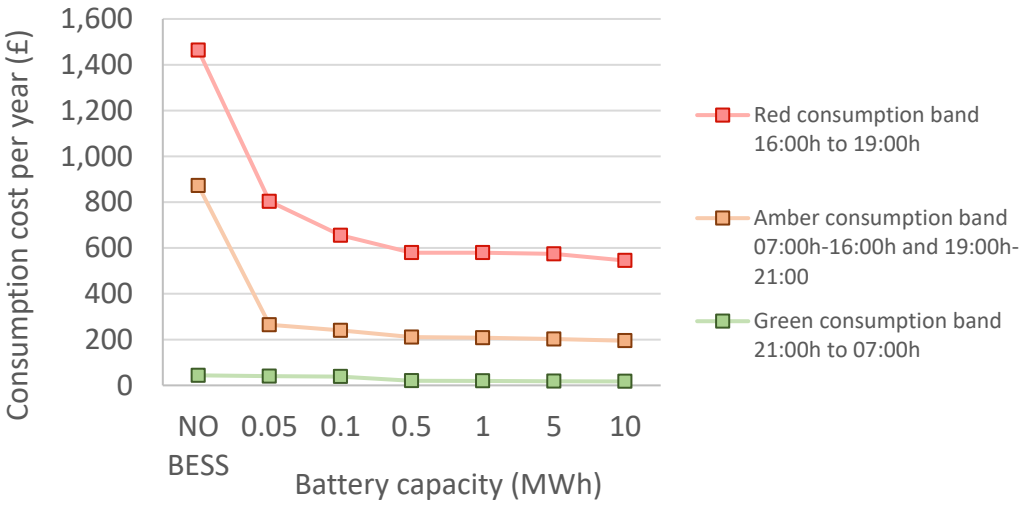

Figure 4.23. Network consumption cost for red, amber, and green bands at different CBESS.

One of the advantages of introducing a BESS in a system is that the power connection capacity on the site could be lowered without incurring in extra costs due to the excess capacity charges. For the WMD, the peak energy demand takes places somewhere in January for an approximated value of 102 kWh, as was shown in Figure 4.1. During the winter months, solar energy generation is at its lowest and the use of the BESS is limited. At higher BESS capacities, the system is independent from the grid for months at a time (see Figure 4.19).

Although the network costs represent only a fraction of the total costs over the system lifetime, it is one of the benefits of implementing a BESS system and worth exploring. The impact that lowering the power connection capacity would have in network costs is explored in the following section.

Impact of the power connection capacity ($Power_{capacity}$)

Different power connection capacities have been explored to evaluate their impact in the lifetime costs of the system. When the power connection capacity is changed, it has an impact on the network costs, precisely, in the capacity charge and the excess capacity charge. The installation of a BESS allows for the reduction of the power connection capacity and therefore a reduction in the costs. This is illustrated in Figure 4.24, where the power connection capacity is reduced in steps from 150 kW to 25 kW. When the power connection capacity ($Power_{capacity}$) is reduced, the excess capacity charge increases. However, the excess capacity charge is smaller when the system has a BESS (Figure 4.24b) compared to the base case scenario in which the BESS and the PV panels are not in place (Figure 4.24a).

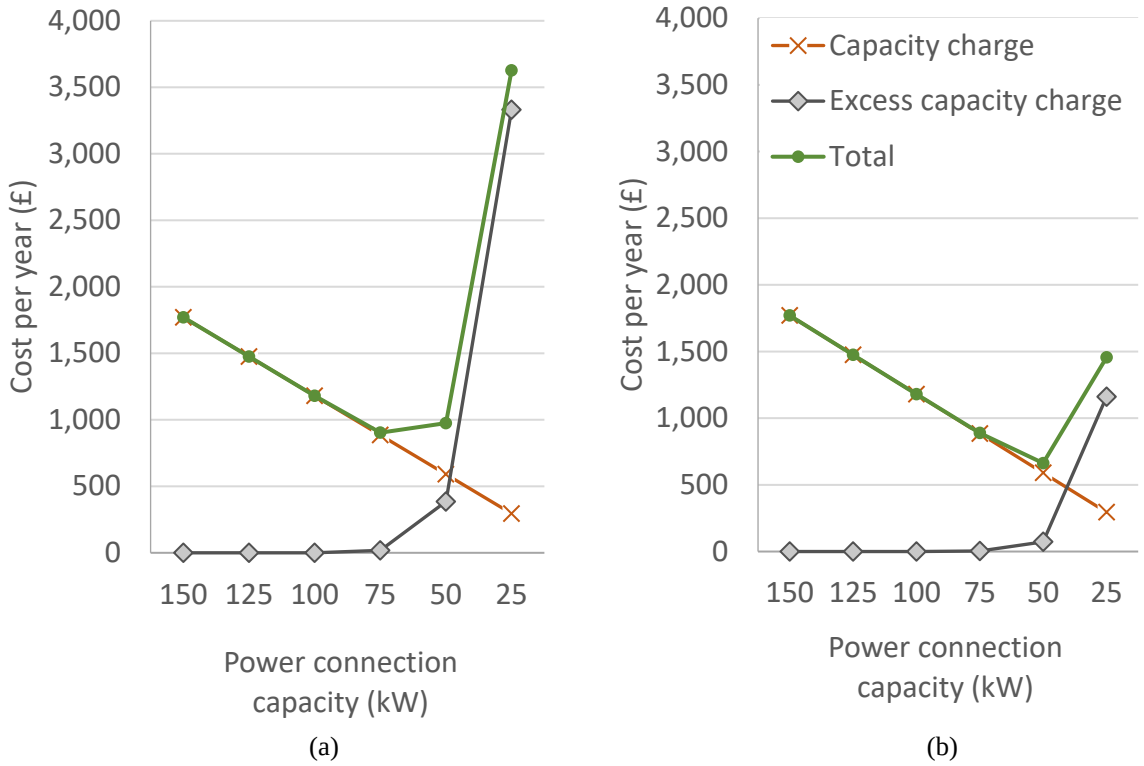

Figure 4.24. Capacity charge and excess capacity charge at different power connection capacities for (a) the base case scenario (system without BESS and PV panels) and (b) for a BESS with a capacity of 10 MWh

The total network costs in a year at different battery capacities can be seen in Figure 4.25. The power connection capacity used in Figure 4.25 corresponds to 25 kW. The most remarkable difference in total cost per year when the BESS is used if compared with the base case scenario corresponds to the power connection capacity of 25 kW. However, the declining trend in total network costs is similar for all the other power connection capacities. Between different BESS capacities, the network costs don't change significantly. The annual network costs for all the different $Power_{capacity}$ examined, at different battery capacities (C_{BESS}) can be seen in Table 4.9.

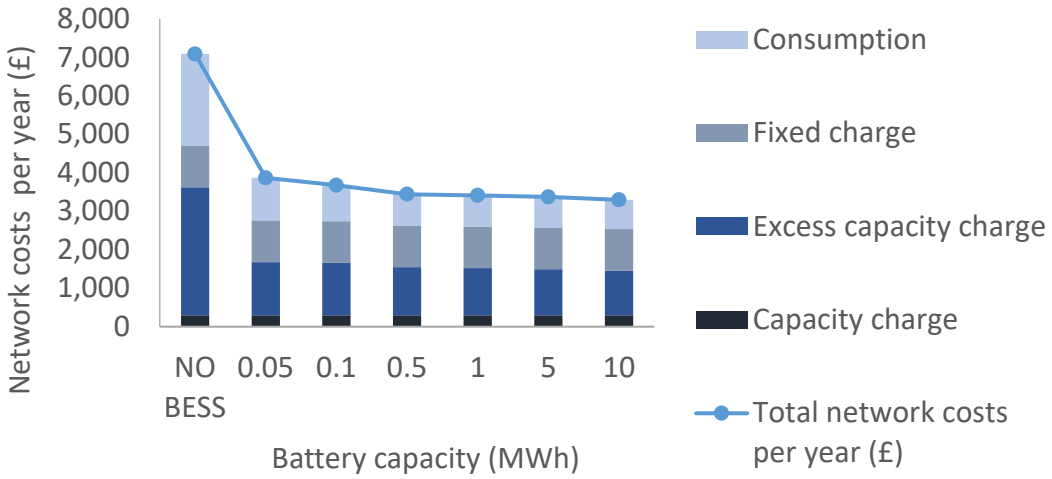

Figure 4.25. Network costs (£) per year at different CBESS for a power connection capacity of 25 kW.

According to the results shown in Table 4.9, network costs could be reduced from £5,234 (i.e. for the base case scenario) to £2,504 per year when the system has installed a BESS with a capacity of 10 MWh and the power connection capacity is set to 50 kW. Over the system lifetime the total network cost would be reduced by £40,950.

Table 4.9. Annual network costs (£) for all the power connection capacities at different battery capacities

		Power connection capacity (kW)					
		150	125	100	75	50	25
C_{BESS} (MWh)	NO BESS	5,234	4,939	4,644	4,367	4,438	7,090
	0.05	3,963	3,668	3,372	3,081	2,855	3,870
	0.1	3,788	3,493	3,198	2,907	2,681	3,677
	0.5	3,665	3,370	3,075	2,784	2,558	3,442
	1	3,661	3,366	3,071	2,780	2,554	3,413
	5	3,649	3,354	3,059	2,768	2,542	3,373
	10	3,612	3,317	3,022	2,730	2,504	3,297

Upon inclusion of all amortised expenses associated with each power connection capacity, a modest decrease in overall costs throughout the system's lifespan is observed. The biggest reduction in total costs over the system lifetime if the power capacity connection is reduced from 150 kW to 50 kW, when all amortised costs are included, is £20,000, as it is shown in Figure 4.26.

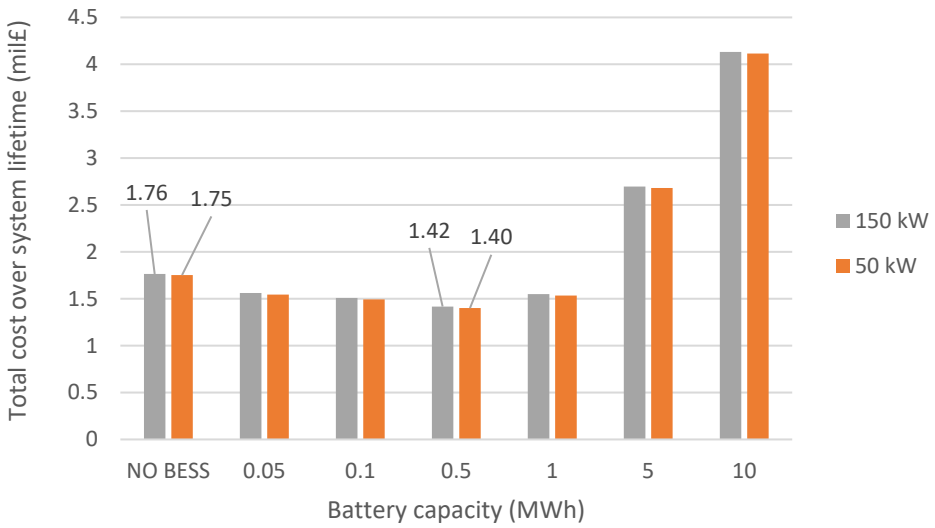

Figure 4.26. A comparison of the total cost over system lifetime between a power connection capacity of 150 kW (grey column) and 50 kW(orange column) at different battery capacities.

Additionally, Table 4.10 shows in detail all the costs associated at each power capacity connection and BESS size.

The impact on GHG emissions has been analysed and the results are shown in Figure 4.27. As was introduced in section 4.3.5, for the purpose of the study, the emissions associated with the WMD's energy consumption are considered. The GHG emissions have been estimated considering the impact of the energy purchased from the grid (purple column), the PV solar energy consumed instantaneously (yellow column) or used from the BESS (brown column) and displacing of energy from the grid mix with the sale of the surplus solar energy (green column). According to the results, the introduction of a BESS and PV panels into the system provide significant GHG savings. Moreover, the benefit from selling the surplus solar energy to the grid balances out the impact created from the energy consumed at the WMD. As it can be seen in Figure 4.27, the higher the BESS capacity, the lower the surplus solar energy available to be sold to the grid. Therefore, the biggest GHG savings are seen introducing a BESS of 0.05 MWh which reduces the GHG emissions by 41 tons CO_2 eq. per year.

Table 4.10. System cost at different power connection capacity for the WMD. The values in £ are included in Appendix A.

Power connection capacity (MW)	BESS capacity (MWh)	Cost of energy per year (k£)	Surplus solar energy revenue per year (k£)	BESS capital cost (k£)	BESS O&M cost (k£)	PV capital cost (k£)	PV O&M cost (k£)	Network cost per year (k£)	Total cost over system lifetime (mil£)
0.075	NO BESS	112.4	0	0	0	0	0	4.4	1.75
	0.05	59.3	11.1	12.7	1.9	629.1	135.3	3.1	1.55
	0.1	54.5	10.6	25.4	3.8			2.9	1.50
	0.5	38.5	8.4	127.0	18.8			2.8	1.40
	1	37.6	8.3	254.0	37.5			2.8	1.54
	5	36.2	8.1	1,270.0	187.5			2.8	2.68
	10	34.5	7.9	2,540.0	375.0			2.7	4.12
0.05	NO BESS	112.4	0	0	0	0	0	4.4	1.75
	0.05	59.3	11.1	12.7	1.9	629.1	135.3	2.9	1.54
	0.1	54.5	10.6	25.4	3.8			2.7	1.49
	0.5	38.5	8.4	127.0	18.8			2.6	1.40
	1	37.6	8.3	254.0	37.5			2.6	1.53
	5	36.2	8.1	1,270.0	187.5			2.6	2.68
	10	34.5	7.9	2,540.0	375.0			2.5	4.12
0.025	NO BESS	112.4	0	0	0	0	0	7.1	1.79
	0.05	59.3	11.1	12.7	1.9	629.1	135.3	3.9	1.56
	0.1	54.5	10.6	25.4	3.8			3.7	1.51
	0.5	38.5	8.4	127.0	18.8			3.4	1.41
	1	37.6	8.3	254.0	37.5			3.4	1.55
	5	36.2	8.1	1,270.0	187.5			3.4	2.69
	10	34.5	7.9	2,540.0	375.5			3.3	4.13

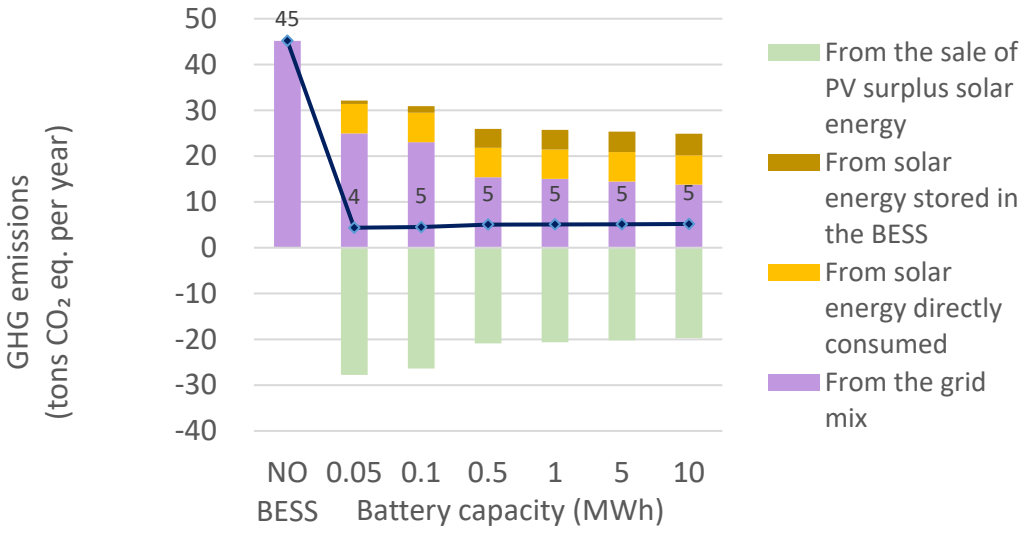

Figure 4.27. GHG emissions per year for the WMD at different CBESS.

4.4.2 M&S retail store

As discussed in section 4.3.1, there are significant differences in the PV solar energy generation and energy consumption between the WMD and the M&S retail store. The latter presents a higher energy demand and more stable consumption throughout the year than the WMD. On the other hand, the PV solar panels installed in the M&S retail store would generate more PV solar energy than those proposed for the WMD due to the location and the number of panels. Additionally, if PV solar panels were installed at the M&S retail store, 97% of the solar energy generated on-site would be used directly (without a BESS). However, the solar energy generated at M&S only meets approximately a third of the existing demand of the store.

Figure 4.28 shows the results corresponding to the hourly energy balance for the M&S retail store when the PV solar panels are in place but without a BESS. Each vertical line in Figure 4.28 marks the start of a new day. A week in January (Figure 4.28a) and a week in July (Figure 4.28b) have been plotted as an example. The M&S retail store relies on the energy supplied from the grid in the winter months. During a winter's day, only a few hours of sunlight allow the M&S retail store to reduce its energy consumption from the grid. In the summer, the energy supplied from the grid is still 100% required at night, but during the day, the grid load is considerably reduced due to the on-site PV solar generated energy.

The next section analyses the impact of adding a BESS to the M&S retail store. The energy management algorithm proposed is explored for batteries with varying capacities.

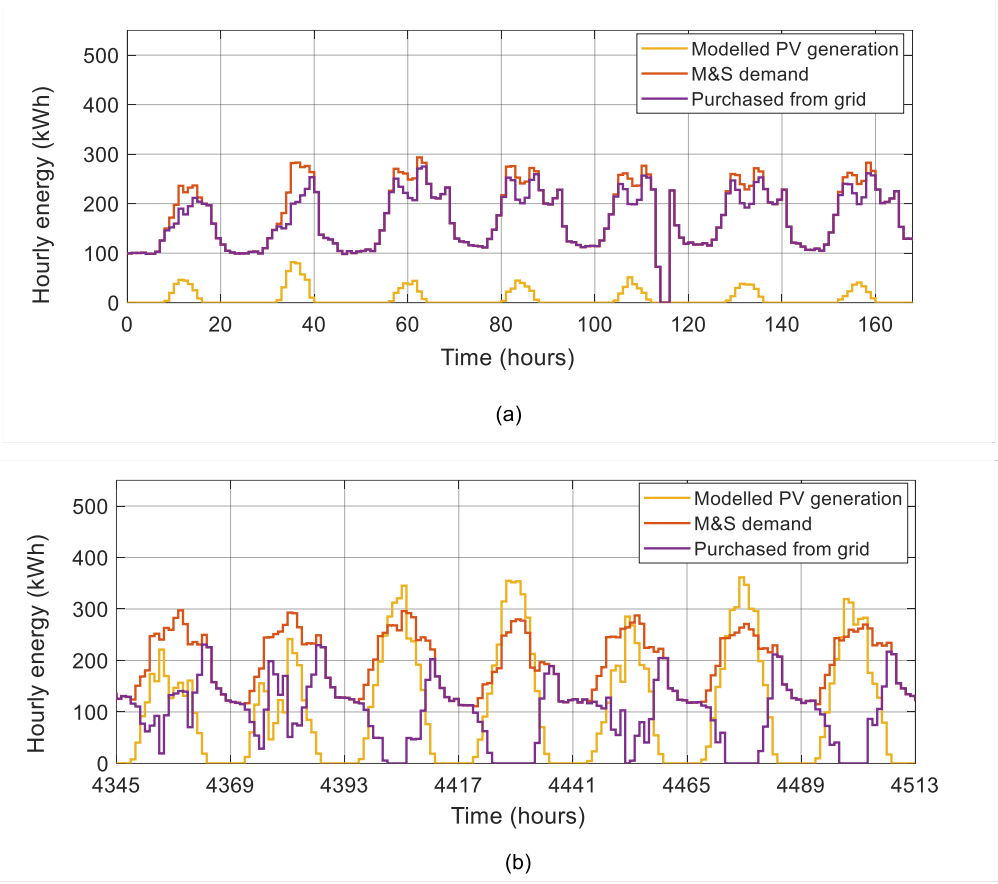

Figure 4.28. Simulation results for a week in (a) January and (b) July for the energy flow in the M&S retail store assuming the BESS is not installed.

Impact of the BESS capacity (C_{BESS})

The hourly energy results when a BESS of 0.5 MWh capacity is installed for a single day in January and July are shown in Figure 4.29. Over the winter months (Figure 4.29a), the modelled PV solar energy generation never surpasses the M&S retail store demand. Thus the impact of having a BESS cannot be justified to reduce the dependency on the grid. The PV solar energy generated is used instantaneously by the M&S retail store. However, the BESS can be used as a tool for the reduction in grid supply energy costs. The energy can then be purchased from the grid and stored in the BESS when the electricity price is below a certain threshold price (i.e., from 00:00h to 07:00h for a threshold price of 9 p/kWh) and used when the electricity price is above the threshold (i.e., from 08:00h to 23:00h). In this scenario the battery is fully charged quickly, in three hours, and fully discharged over two to three hours.

In the summer months (Figure 4.29b), when the PV solar energy is higher than the energy demand, the BESS is not only used as a tool to reduce the energy cost but also to store the surplus solar energy when it is available, lowering grid supply costs still further. The BESS is

charged at night at the lower electricity price and during the daytime when there is surplus solar energy (i.e. day 3, day 5, day 6 and day 7). Moreover, the energy purchase from the grid in the afternoon, when the energy demand is higher than the solar energy available, occurs between two to three hours later due to surplus solar energy that has been stored earlier in the day and is being discharged from the BESS. For example, Figure 4.28b and Figure 4.29b can be compared during the fourth day to reflect the displacement on the purchase from the grid when the BESS is in place. On the other hand, during summer (Figure 4.29b), the time it takes to discharge the BESS is longer than in winter (Figure 4.29a) due to the increase in PV solar energy generation/surplus.

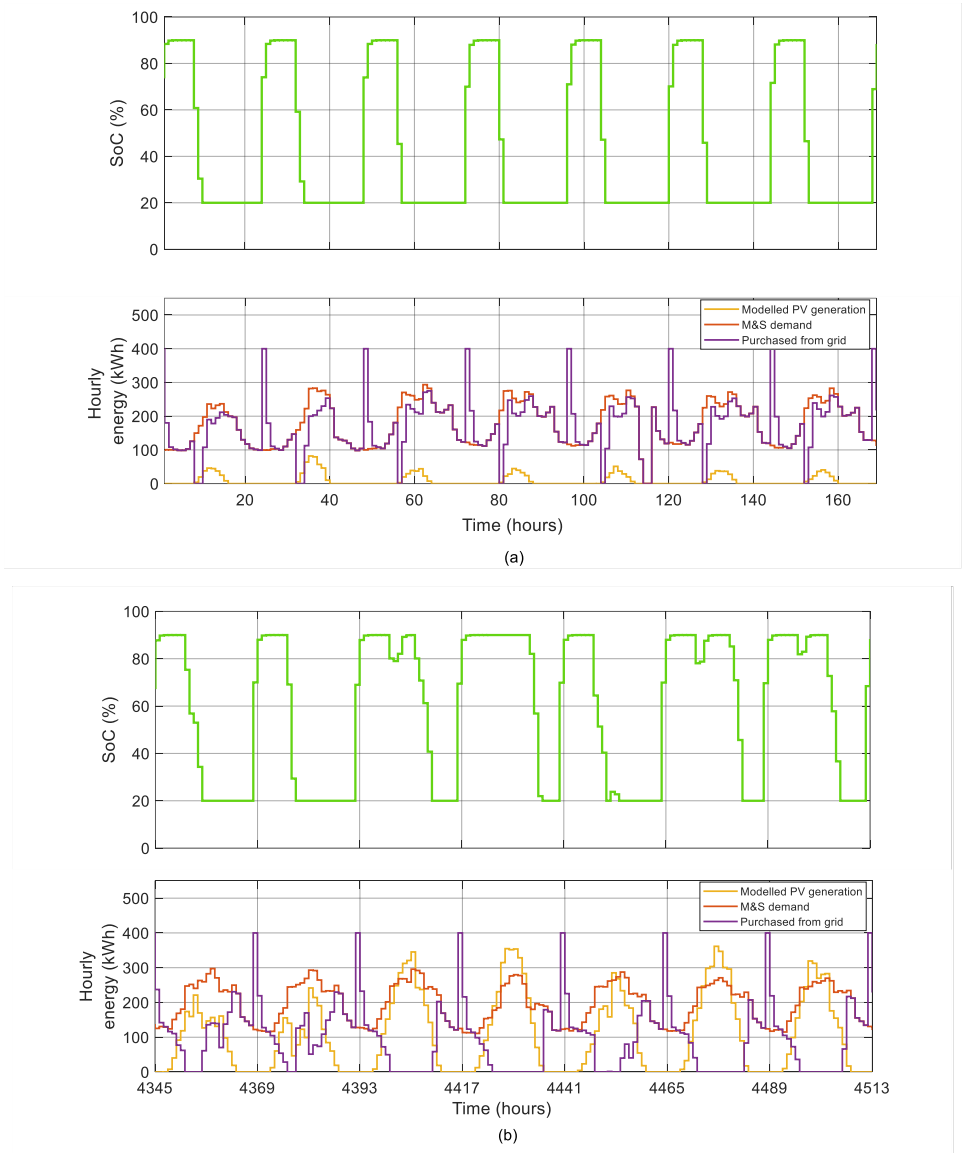

Figure 4.29. Simulation results when the energy management algorithm is applied in a week in (a) January and (b) July using a BESS with a capacity of 0.5 MWh for the M&S retail store.

The monthly results obtained when the energy management algorithm is applied to the M&S retail store can be seen in Figure 4.30 at different battery capacities (C_{BESS}). The positive values stand for energy consumption and BESS discharging mode, while the negatives indicate energy generation and charging of BESS. The energy purchased from the grid (i.e. purple coloured part of the bar) refers to the energy purchased from the grid to cover the demand directly. The energy "TO BESS" corresponds to the energy from the grid used to charge the BESS. The energy "FROM BESS" refers to the energy discharged from the BESS, which comes from the grid and the surplus solar energy. "Consumed from PV" refers to the solar energy that is used instantaneously to cover the demand.

As the BESS capacity increases, the energy purchased from the grid to cover the demand at a higher price is reduced (i.e. purple coloured part of the bar). In contrast, the energy purchased from the grid to charge the BESS at lower prices (i.e., "To BESS") increases. So, overall, the energy required from the grid is the same for all the BESS; however, a larger capacity allows for more energy to be drawn down from the grid and stored overnight when the prices are below the threshold. When the electricity price is above the threshold, energy stored at the BESS can be discharged, maximising the cost saving. This can be seen in detail in Figure 4.29b), Figure 4.32b) and Figure 4.33b).

From April to August, some surplus solar energy is not stored at the BESS (Figure 4.30). It happens some days because the BESS has already been fully charged from the grid by the time surplus solar energy is available. An example of this can be seen in Figure 4.29b during the fourth day of the week. This algorithm could be examined in future work to ensure capacity for excess solar in certain months. Moreover, it might reduce electricity costs, as less electricity would be bought from the grid.

Figure 4.30. Monthly energy distribution at the M&S retail store at different CBESS. The positives values stand for energy consumption and BESS discharging mode while the negatives indicate energy generation and charging of BESS.

The energy flow for battery capacities (C_{BESS}) equal to 0.05 MWh, 0.5MWh and 5MWh can be seen in detail in Figure 4.31 as an example.

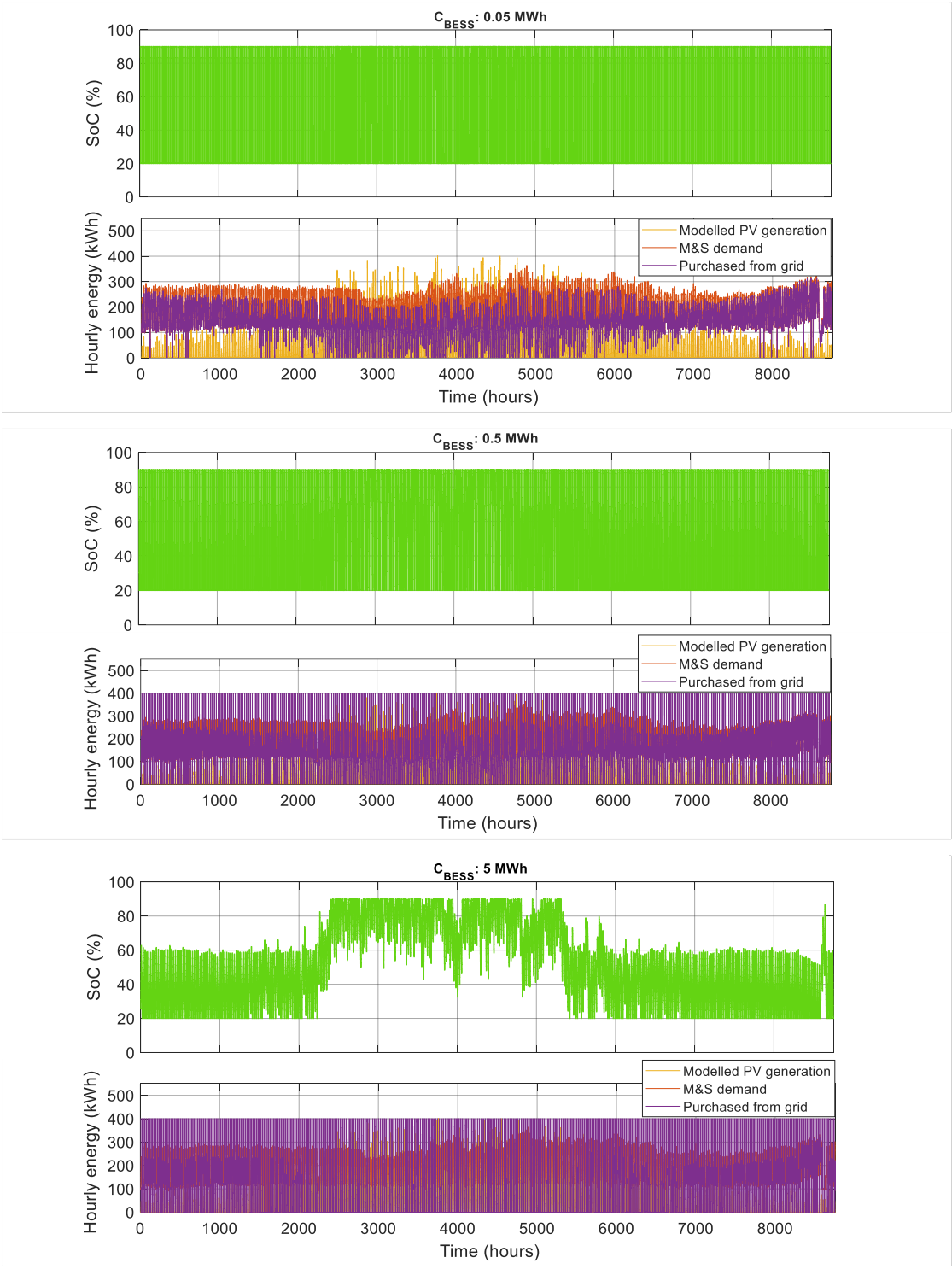

Figure 4.31. A comparison of the hourly energy flow at the BESS at different CBESS for the M&S retail store.

For smaller BESS with C_{BESS} of 0.05 MWh (see Figure 4.31) and 0.1 MWh, the power required to charge the battery is smaller when compared to a larger BESS. Moreover, at no time does the overall BESS + Store system fully utilise the 400kW grid connection available at the M&S retail store to charge the BESS and cover the demand. The energy flow is detailed in Figure 4.32 for a BESS with a C_{BESS} of 0.05 MWh as an example. However, the case for the BESS

with C_{BESS} of 0.1 MWh is very similar. Due to the deliberately limited capacity of the BESS, it takes up to three hours to fully charge it and just one hour to discharge in winter months (see Figure 4.32a) or up to two hours in summer months whilst supporting the store load. (See Figure 4.32b).

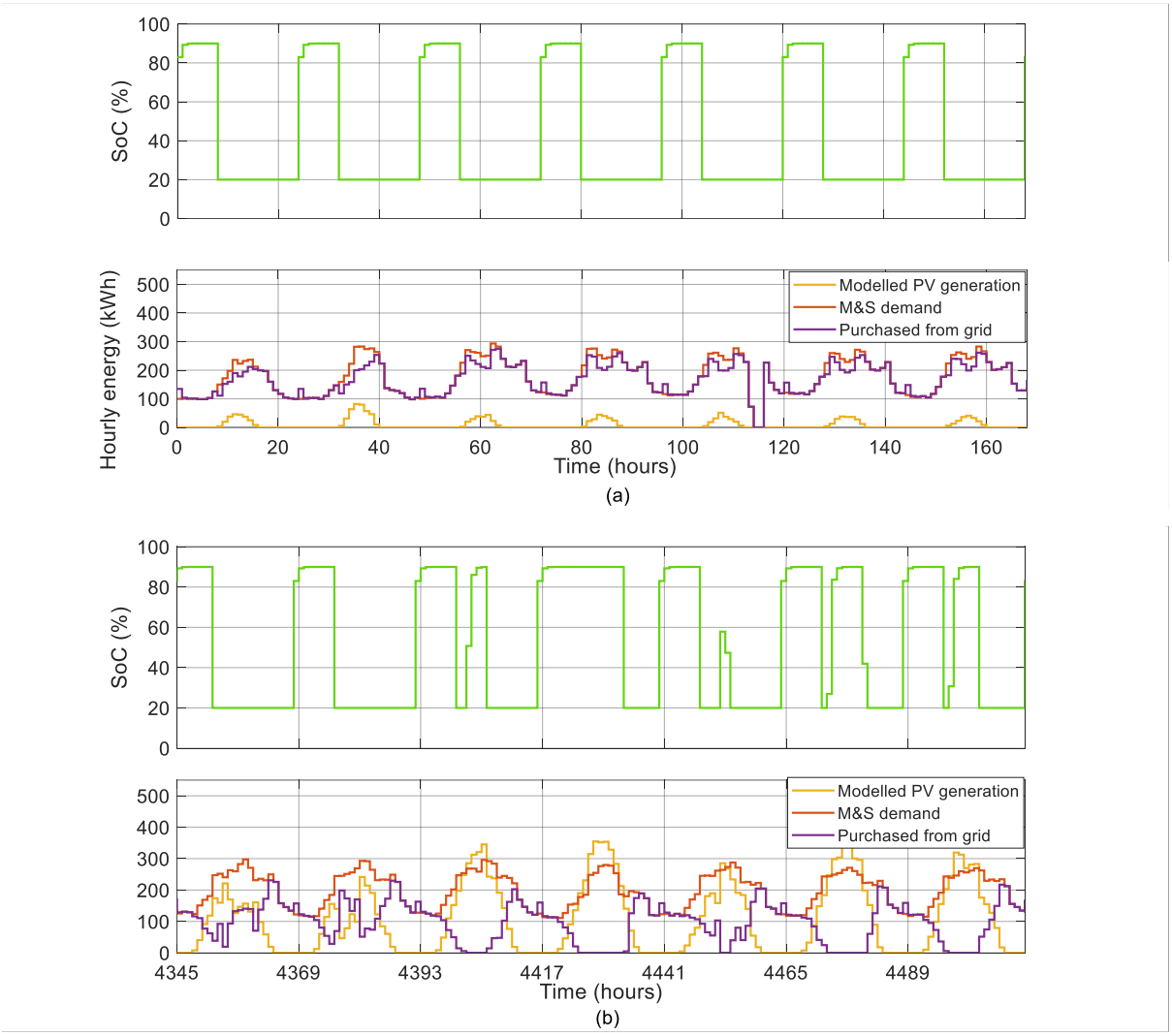

Figure 4.32. Simulation results when the energy management algorithm is applied in a week in (a) January and (b) July using a BESS with a capacity of 0.05 MWh for the M&S retail store.

When the BESS capacity is further increased to 5 MWh (see Figure 4.31) and 10 MWh, the BESS does not complete a cycle in the whole year. Between April and early August (from hours 2,100 to 5,200, approximately), when the PV solar energy generation is at its highest values, the grid is used most of the time to charge the BESS and the energy demand from the store is covered by the solar energy and the BESS. It can be seen in detail in Figure 4.33b for a BESS with a capacity of 5 MWh for a week in July. This is an advantage from the point of view of the grid network operator, as in times of peak demand, the M&S retail store is

completely independent of the grid and most of the energy drawn from the grid is done during lower demand periods. A trade-off is the time it takes to charge or discharge the battery, which has significantly increased compared to the smaller batteries analysed. However, this protects the battery and is an advantage regarding the BESS lifetime, as the battery completes significantly fewer full operation cycles, which contribute directly to the battery's ageing.

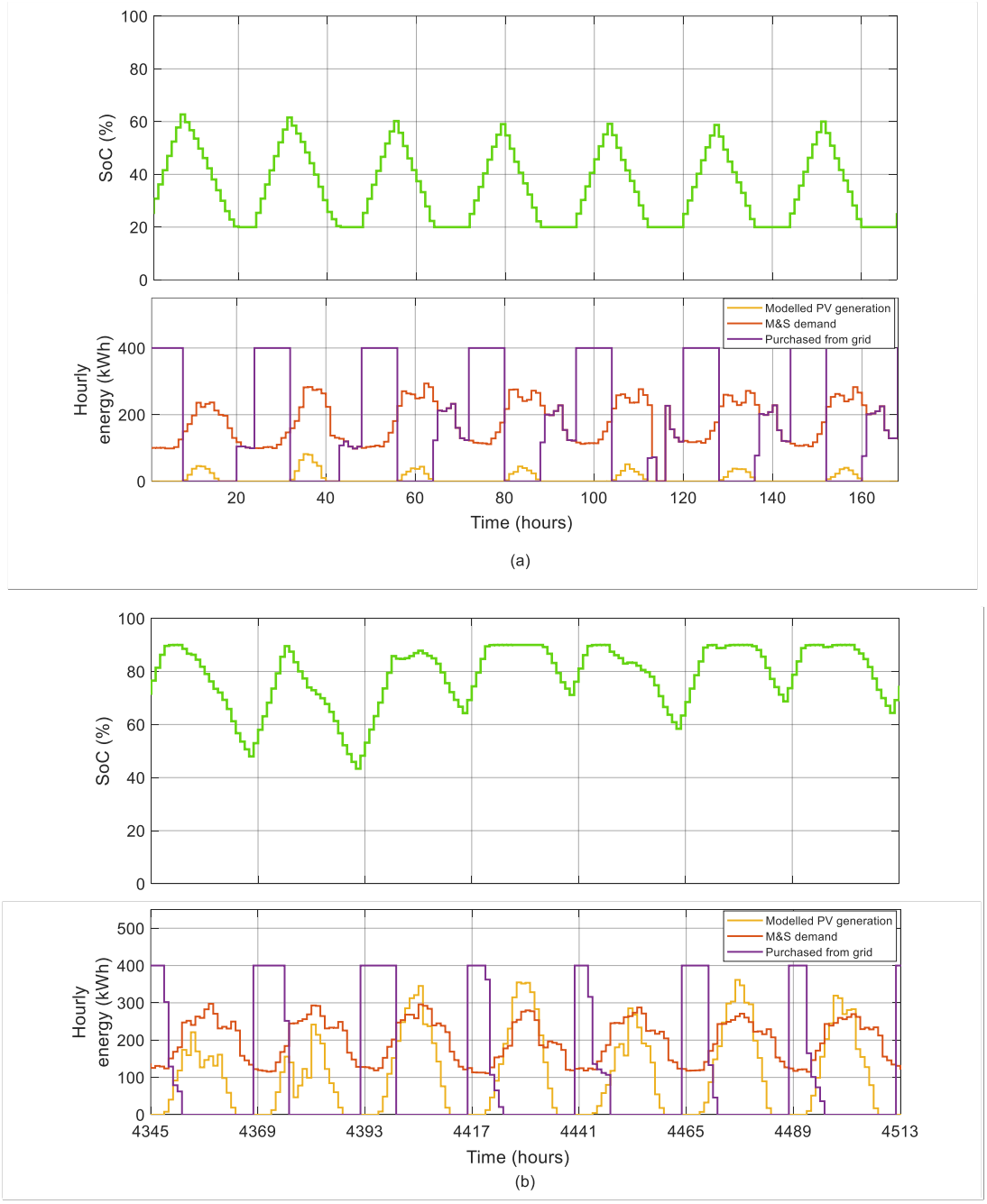

Figure 4.33. Simulation results when the energy management algorithm is applied in a week in (a) January and (b) July using a BESS with a capacity of 5 MWh for the M&S retail store.

The M&S retail store studied is currently 100% dependant on the grid, but if PV solar panels were installed, the dependency on the grid would be reduced by 28%.

The percentage of energy from the grid at different battery capacities is shown in Figure 4.34 through a purple line. A detailed breakdown is also shown in a pie chart for two BESS analysed before, 0.5 MWh and 5 MWh. The dark purple section of the pie chart represents the portion of the energy demand covered directly by the grid. The yellow section refers to the portion of the energy demand covered by instantaneous solar energy. The green section refers to the fraction of the energy demand covered by the BESS. Within the green section, the light purple fraction refers to the energy stored from the grid at a cheaper price, and the light yellow corresponds to the stored surplus solar energy.

As it is shown in Figure 4.34 and it was discussed previously, the energy purchased from the grid is the same for all the BESS capacities studied (i.e., light, and dark purple section of the pie charts). However, the amount paid for the energy differs due to the ability to time-shift supply and demand.

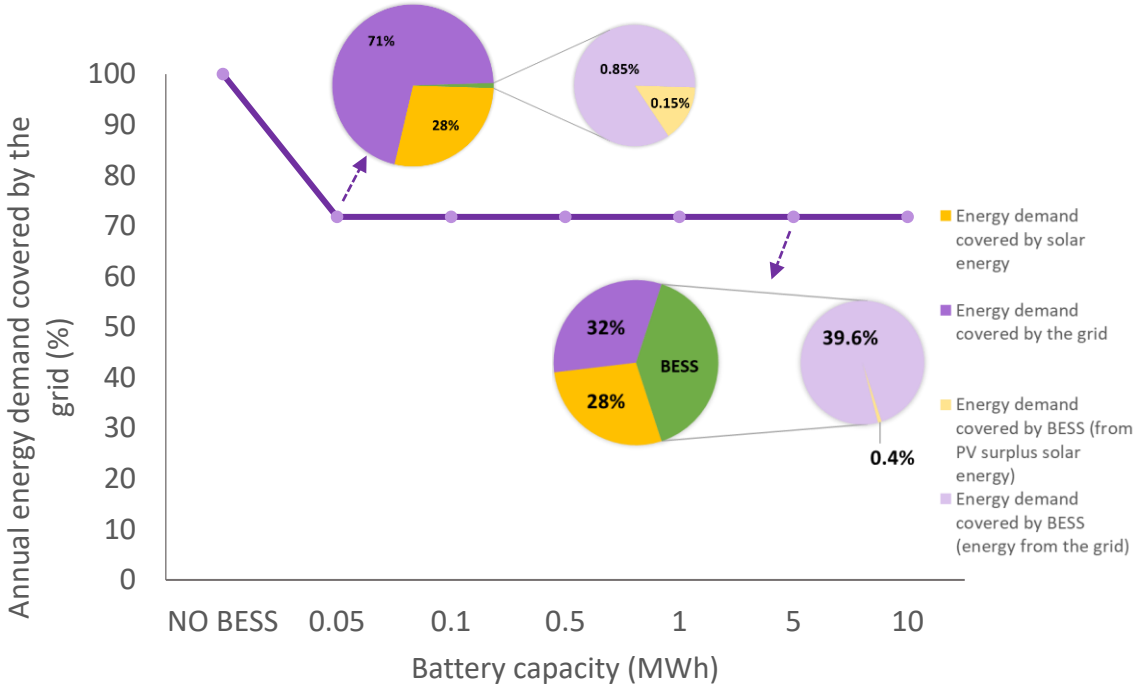

Figure 4.34. Percentage of energy used from the grid at different C_{BESS} for the M&S retail store (purple solid line). At 0.05 MWh and 5 MWh, the pie charts show the breakdown of energy covered by the grid, solar installation, and BESS (further broken down into energy stored from excess solar energy or the grid).

The system lifetime costs have been studied at different battery capacities. The results obtained can be seen in Figure 4.35. For the analysis, the system energy cost for the M&S retail store without PV solar panels and BESS is also included (i.e., NO BESS).

According to the results, system's lifetime total cost increases when the PV solar panels and a BESS are installed at the M&S retail store. The bigger the battery capacity, the higher the total cost of the system's lifetime.

The energy cost decreases as the BESS capacity increases, as this increases the ability to purchase energy at a cheaper rate. The total network costs (i.e., as introduced in section 4.3.4, these refer to the contracted power connection capacity costs and the use of the network distribution system that is charged by the energy supplier) follow a similar trend. However, the reduction in energy and network costs does not prevent the system from increasing the total cost when all the amortised costs are added (i.e. cost of BESS, cost of PV panels, and network cost). Therefore, under the assumptions considered, the decrease in energy and network costs wouldn't justify the adoption of BESS and PV solar panels.

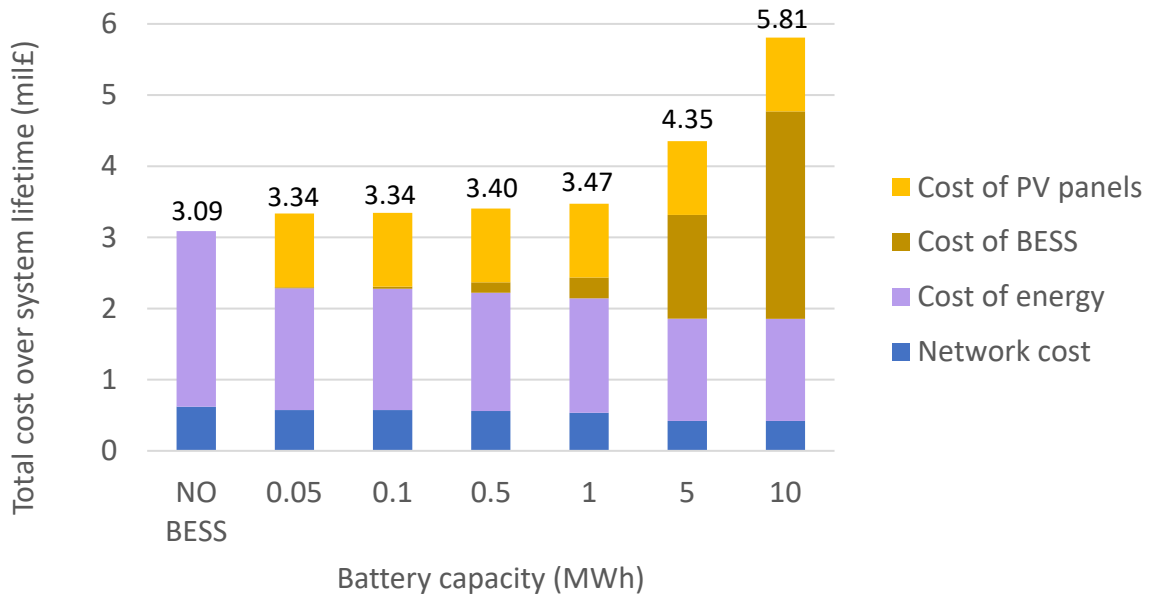

Figure 4.35. Total cost over system lifetime at different CBESS for M&S retail store.

This increase in total cost over the system lifetime can be seen in detail in Table 4.11 where the system costs are itemised at different battery capacities (C_{BESS}). For batteries with higher capacities (i.e. 5 MWh and 10 MWh), 33% and 50% of the total cost over system lifetime comes from the cost of the BESS (i.e. BESS capital cost and BESS O&M cost). On the

contrary, for smaller battery capacities, the percentage relative to the total cost is less than 8%. The cost of the PV panels (i.e. PV capital cost and PV O&M cost) has a stable contribution to the total costs and it decreases slightly as the BESS capacity increases. It decreases from 31% to 18% of the total costs for a BESS of 0.05 MWh and 10 MWh, respectively.

As opposite to the WMD, the cost of energy for the M&S retail store, especially for smaller BESS, has the most significant influence in the total costs. Precisely, between 52% and 46% of the total costs.

Table 4.11. System cost for M&S retail store. The values in £ are included in Appendix A.

Power connection capacity (MW)	BESS capacity (MWh)	Cost of energy (k£) per year	Surplus solar energy revenue (£) per year	BESS capital cost (k£)	BESS O&M cost (k£)	PV capital cost (k£)	PV O&M cost (k£)	Network cost (k£) per year	Total cost (mil£) over system lifetime
0.4	NO BESS	164.5	0	0	0	853.2	183.5	41.4	3.09
	0.05	114.7	637	12.7	1.9			38.2	3.34
	0.1	114.3	588	25.4	3.8			38.2	3.34
	0.5	111.4	569	127.0	18.8			37.3	3.40
	1	107.8	569	254.0	37.5			35.7	3.47
	5	96.4	547	1,270.0	187.5			28.0	4.35
	10	96.3	527	2,540.0	375.0			28.0	5.81

The benefits of including a BESS for the M&S store and commercial buildings alike will depend on the difference between the off-peak and peak electricity price. For the M&S retail store, these are 7.15 p/kWh and 10.76 p/kWh, respectively.

Figure 4.36 shows the results obtained when the gap between off-peak and peak electricity price increases (e.g., from 10.76 p/kWh to 15.76 p/kWh).

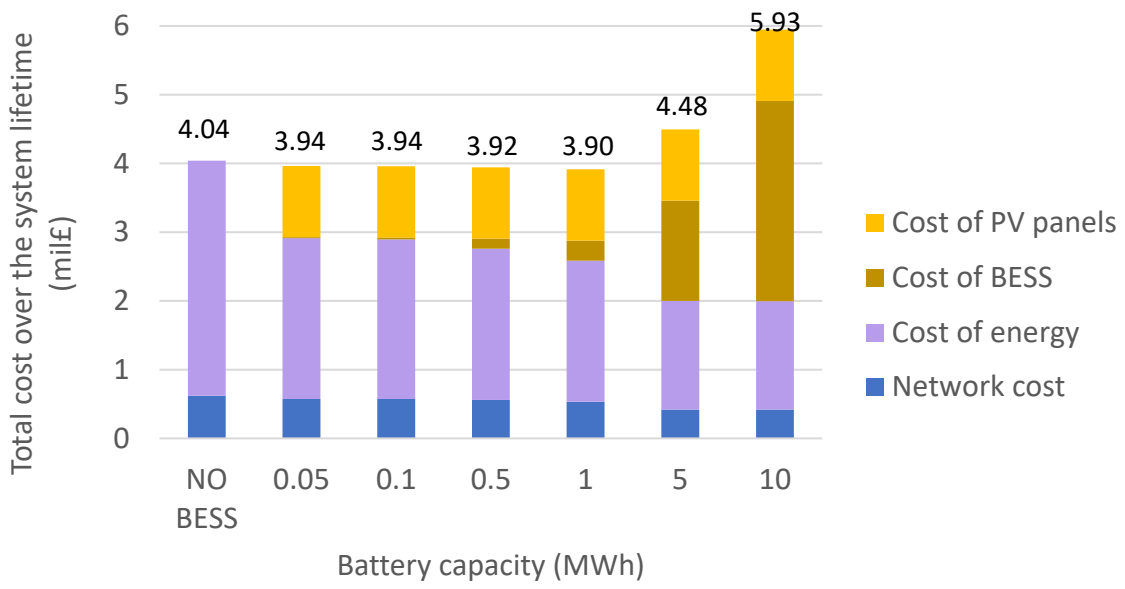

Figure 4.36. Total cost over system lifetime at different battery capacities for M&S retail store when the peak electricity price is increased.

As can be seen in Figure 4.36, system's lifetime total cost is reduced for certain battery capacities. As for the WMD, if all amortised costs are added (i.e. cost of BESS, cost of PV panels, and network cost), a BESS with a capacity higher than 5 MWh ceases being a feasible solution for annual electricity cost reduction. Here, the potential reduction in energy and network costs is eclipsed by the cost of BESS. The BESS that achieved the highest reduction in total costs over the system lifetime corresponds to 1 MWh capacity. The total cost reduction compared to the base case scenario (i.e. BESS and PV panels are not installed) is £140,000.

The network costs have a higher influence in the costs for the M&S retail store than for the WMD (Figure 4.22). The total network costs can be seen in Table 4.11 as the addition of capacity charge, fixed charge, and consumption charge at each battery capacity (C_{BESS}). As the BESS capacity increases, the network costs are reduced.

What influences the reduction of the total network costs at different BESS capacities is the consumption charge, shown in Table 4.12. As was previously explored, the BESS is charged at night when the electricity price is at its lowest value. This time coincides with the green consumption band. As the BESS capacity increases, and more energy is stored during this consumption band, the total charge per year for the green band increases. The consumption in the other bands, red and amber, is therefore reduced.

Table 4.12. Network costs for the M&S retail store

Power connection capacity (MW)	BESS capacity (MWh)	Capacity charge per year (£)	Excess capacity charge per year (£)	Fixed charge per year (£)	Consumption charge per year (£)			Total Network cost per year (k£)
					Red	Amber	Green	
0.4	NO BESS	7,203	0	17,220	14,982	1,889	110	41.4
	0.05				12,664	1,036	109	38.2
	0.1				12,628	1,010	113	38.2
	0.5				11,924	832	143	37.3
	1				10,464	636	179	35.7
	5				2,976	358	266	28.0
	10				2,952	359	266	28.0

The network consumption cost for red, amber, and green band at different battery capacities (C_{BESS}) for M&S retail store is shown in Figure 4.37. The energy purchased between 16:00h and 19:00h (i.e. red consumption band) is directly consumed by the M&S retail store because at this period of time, the electricity price is at its highest, and the BESS is not charged from the grid. The reduction in the red consumption charges when a BESS of 0.05 MWh is installed is related to the use of PV solar energy rather than any surplus energy stored in the BESS. From the end of spring until the end of summer, the PV panels generate enough solar energy to be used directly, thus reducing the energy purchased from the grid. The consumption charges for the red band continue decreasing slowly for batteries with capacities between 0.1 MWh and 1 MWh, as more surplus solar energy is stored, however limited. Regardless of the limited surplus solar energy, this has an impact on the cost of consumption charge, because the energy required from the grid is purchased closer to the evening and not in the middle of the day or early afternoon. When the BESS capacity reaches 5 MWh, the battery is large enough to store all the energy needed at night (i.e. 00:00h to 07:00h) and at the red consumption band the system does not use any energy from the grid in summer or just for a couple of hours in winter.

The costs associated with the consumption in the amber band also decreases as the BESS capacity increases, although the reduction is not that significant as it is for the red consumption band. The reduction in the amber consumption band is related to the direct use of PV solar energy by the M&S retail store. For this reason, the largest reduction in cost happens between the baseline scenario and the scenario in which the PV panels are installed together with a BESS of 0.05 MWh. The increase of BESS capacity has a minimal impact because the surplus solar energy is limited. For larger BESS, the difference in consumption cost is associated with

the energy stored at night thus although there is no surplus solar energy available, there is enough energy in the BESS to avoid purchasing it from the grid.

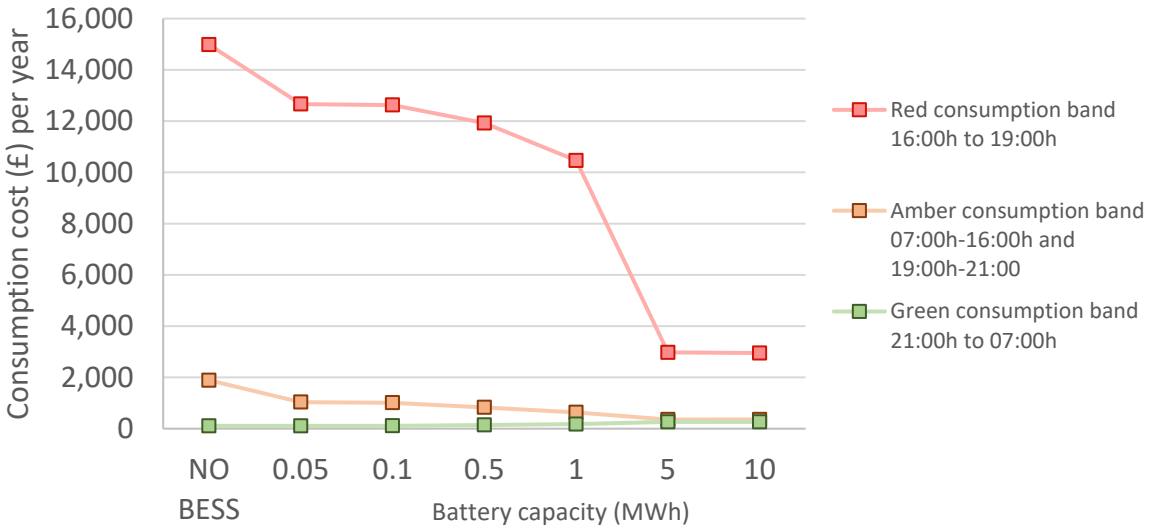

Figure 4.37. Network consumption cost for red, amber, and green band at different CBESS for M&S retail store.

As was discussed previously for the WMD, the network costs can be further reduced if the power capacity connection is lowered. This will be explored next.

Impact of the power connection capacity ($Power_{capacity}$)

In Figure 4.38, the capacity charge, the excess capacity charge and the total cost are shown for different power connection capacities ($Power_{capacity}$). The power connection capacity has been reduced in steps of 100 kW, from 400 kW. The analysis compared a baseline scenario without BESS or PV solar panels and a scenario in which a BESS of 10 MWh and PV solar panels would be installed.

When the power connection capacity is reduced, the excess capacity charge increases as the energy draw exceeds the purchased capacity, as can be seen in Figure 4.38. However, the excess capacity charge is smaller when the system has a BESS, and the total cost is also reduced. The introduction of a BESS, as happened for the WMD, allows for more flexibility when it comes to network costs associated with the $Power_{capacity}$ (i.e. capacity charge and excess capacity charge).

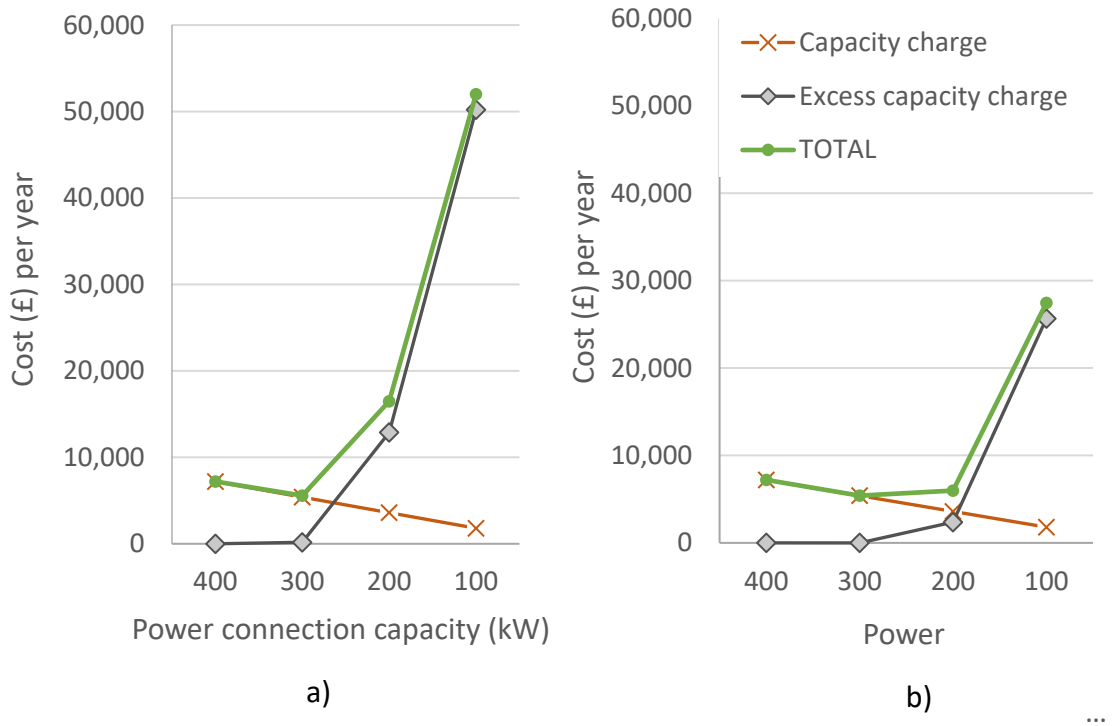

Figure 4.38. Capacity charge and excess capacity charge at different power connection capacities for (a) the base case scenario (system without BESS and PV panels) and (b) for a BESS with a capacity of 10 MWh for M&S retail store.

The power connection capacity has an impact on the consumption charge. When this is reduced, the available energy to be stored at the BESS at night is reduced as well. Figure 4.39, Figure 4.40, and Figure 4.41 show the results of consumption cost for the red, amber, and green bands, respectively, at different power connection capacities ($Power_{capacity}$) and battery capacity (C_{BESS}). The results obtained for the red (see Figure 4.39) and amber (see Figure 4.40) consumption bands follow the same trend; the consumption cost decreases as C_{BESS} and $Power_{capacity}$ increases. The opposite is true for the green consumption band (see Figure 4.41), as C_{BESS} and $Power_{capacity}$ increases, more energy is stored at the BESS at night, increasing the consumption during this band.

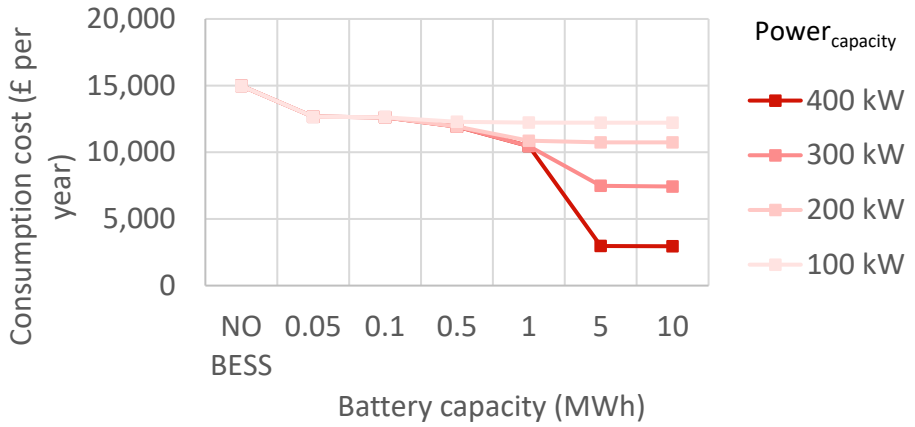

Figure 4.39. Consumption cost per year for the red band at different C_{BESS} and $Power_{capacity}$

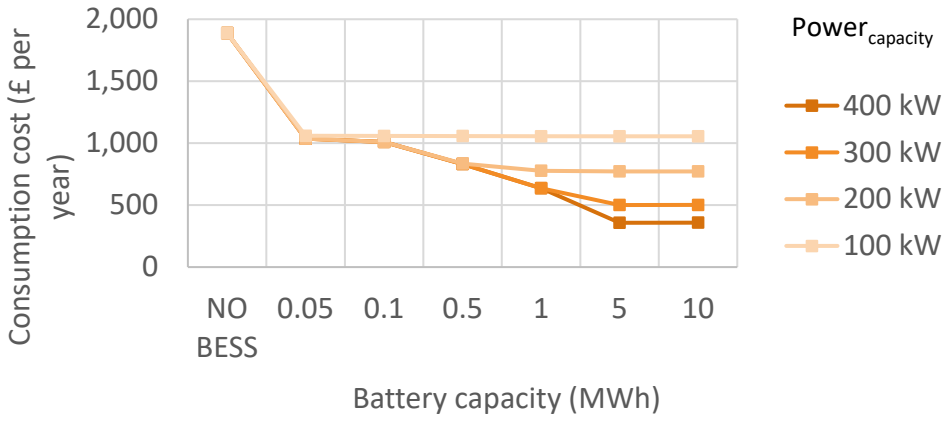

Figure 4.40. Consumption cost per year for the amber band at different C_{BESS} and $Power_{capacity}$

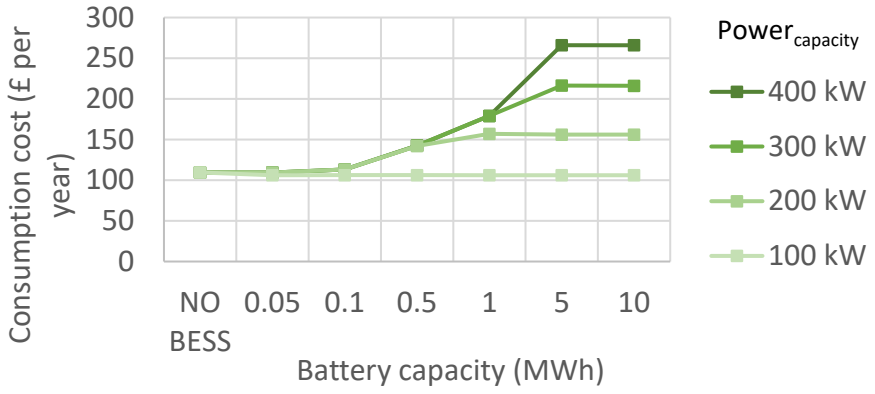

Figure 4.41. Consumption cost per year for the green band at different C_{BESS} and $Power_{capacity}$

The differences between the costs for the green consumption band (i.e. increased from £106 to £266) are smaller if compared to the differences corresponding to the amber band consumption (i.e. from £360 to £1,900) and red band (i.e. from £2,950 to £15,000). As a consequence, the

reduction in costs during the red band should be prioritised for reduction. The system cost at different $Power_{capacity}$ and C_{BESS} can be seen in Table 4.13.

When all the amortised cost are included, the reduction in the network costs from reducing the power connection capacity is no longer relevant, considering the total cost of the M&S retail store, as it is nowadays without PV panels nor BESS installed would be approximately £3.09m (Figure 4.35).

Table 4.13. System cost at different $Power_{capacity}$. The values in £ are included in Appendix A.

Power connection capacity (MW)	BESS capacity (MWh)	Cost of energy per year (k£)	Surplus solar energy revenue per year (£)	BESS capital cost (k£)	BESS O&M cost (k£)	PV capital cost (k£)	PV O&M cost £)	Network cost per year (k£)	Total cost over system lifetime (mil£)
0.3	NO BESS	164.5	0	0	0	0	0	39.8	3.06
	0.05	114.7	637	12.7	1.9	853	183.5	36.4	3.31
	0.1	114.3	588	25.4	3.8			36.4	3.32
	0.5	111.4	569	127.0	18.8			35.5	3.38
	1	107.8	569	254.0	37.5			33.9	3.44
	5	101.2	177	1,270.0	187.5			30.8	4.47
	10	100.9	53	2,540.0	375.0			30.8	5.93
0.2	NO BESS	164.5	0	0	0	0	0	50.7	3.23
	0.05	114.7	637	12.7	1.9	853	183.5	37.2	3.32
	0.1	114.3	588	25.4	3.8			37.2	3.33
	0.5	111.4	568	127.0	18.8			36.3	3.39
	1	109.2	508	254.0	37.5			35.0	3.48
	5	108.1	0	1,270.0	187.5			34.9	4.64
	10	108.1	0	2,540.0	375.0			34.9	6.10
0.1	NO BESS	164.5	0	0	0	0	0	86.2	3.76
	0.05	115.0	634	12.7	1.9	853	183.5	58.6	3.65
	0.1	114.8	569	25.4	3.8			58.6	3.66
	0.5	114.0	170	127.0	18.8			58.2	3.76
	1	113.7	22	254.0	37.5			58.1	3.90
	5	113.7	0	1,270.0	187.5			58.1	5.07
	10	113.7	0	2,540.0	375.0			58.1	6.53

The GHG emissions per year have also been estimated for the M&S retail store and are shown in Figure 4.42. The GHG emissions can be reduced from 321 tons CO_2 eq. to 261 tons CO_2 eq. per year. Over the system lifetime the reduction would be of 900 tons CO_2 eq. if any of the BESS capacities studied were added together with the PV solar installation. The GHG emissions do not decrease as the BESS increases because the energy purchased from the grid

and the PV solar energy consumed is the same no matter the size of the BESS, as it has been discussed before.

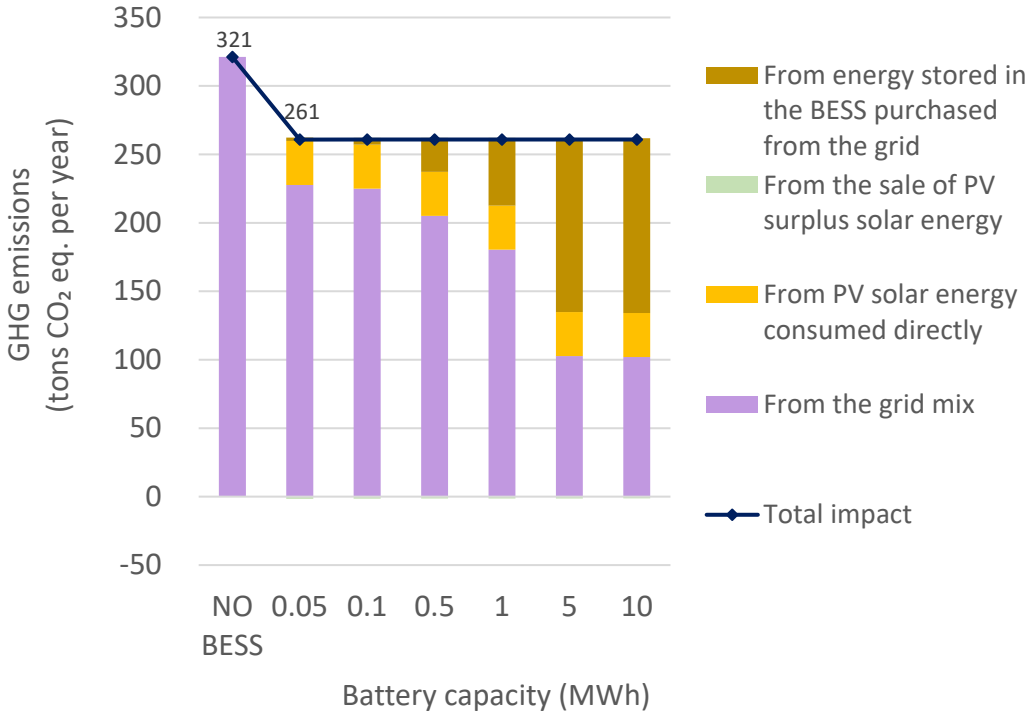

Figure 4.42. GHG emissions per year for the M&S retail store at different C_{BESS}.

Contrary to the WMD, the M&S retail store's introduction of PV panels and BESS is not economically feasible. Moreover, the on-site solar energy generated on M&S premises proves inadequate even for fulfilling their internal energy requirements. The economic benefit of installing a BESS under the M&S scenario depends on the gap between the off-peak and peak electricity price. The dependency on the grid under the M&S scenario is reduced thanks to the PV panels, as well as the GHG emissions.

4.5 Discussion

Based on the results shown in this chapter, the introduction of a BESS has a significant impact on overall costs, depending on the system under study and the use of the battery. The results obtained for the two different commercial sites are compared based on the three different variables studied:

1. Grid dependency: The grid dependency has been analysed to determine to what extent the system under study could be independent from the grid when a PV solar installation and a BESS are in place. The WMD achieved a reduction on grid dependency by up to 70% for the largest BESS (10MWh). The larger the BESS, the more grid independency

achieved. For the WMD, both the PV solar energy and the BESS play a key role in reducing grid dependency. On the other hand, for the M&S retail store, the potential grid dependency reduction with a BESS is not that significant if compared with the WMD. The maximum reduction achieved by the M&S retail store is equal to 29% regardless of the BESS capacity. In conclusion, in locations where PV solar energy is used to cover part of the energy demand, the dependency from the grid is reduced. In these locations, the use of BESS can maximise the potential reduction of grid dependency if there is a high amount of PV surplus solar energy to be stored.

2. Total cost: The total cost over system lifetime has been estimated at different BESS capacities and power connection capacities for both the WMD and the M&S retail store. According to the results, the WMD achieved a reduction in total cost over the system lifetime when the PV panels and certain BESS are in place, however this is not true for the M&S retail store based on the electricity prices provided (i.e., 7.15 p/kWh and 10.76 p/kWh). For the WMD, system's lifetime total cost can be reduced by up to 20% using a BESS with 0.5 MWh capacity, if compared to the base case scenario (i.e. no PV panels or BESS installed). For the WMD, the PV panel costs, and the BESS costs have the higher impact on total costs. Whereas for the M&S retail store, the cost of energy is the factor that contributes the most to the total costs over the system lifetime.
3. GHG emissions: The reduction in GHG emissions has also been explored for both premises. The WMD has the potential to reduce the GHG emissions by 91% when the PV solar system and BESS are in place. On the other hand, the M&S retail store only reduces the GHG emissions by 19%. The GHG emissions are not further reduced with larger BESS capacities at either site, so it can be concluded that the increase in BESS capacity does not further reduce the GHG emissions.

Depending on how the BESS is used, the outcomes obtained from the energy management algorithm are different. The results from the WMD show important reductions in total costs, grid dependency and GHG emissions. The difference between consumption and generation is relatively low for the WMD in comparison to the M&S retail store and it maximises the use of PV panels and BESS. On the contrary, for the M&S retail store, the economic benefits of installing a BESS are directly related to the difference in electricity price between peak and off-peak hours.

The installation of a BESS onsite gives more flexibility when it comes to the power connection capacity.

4.6 Summary

The impact of introducing a BESS has been explored in this chapter, considering two different types of premises. The reason for the selection of those two premises was to have a broader knowledge of how different factors such as energy demand, PV solar energy generation or other technical constraints impact on the outcomes achieved when a BESS is in place. The final aim of the thesis is to explore the feasibility of using PV solar energy generated on site and energy storage for EV fleet charging. Understanding how different commercial premises react to the introduction of a BESS regarding costs, grid dependency and GHG emissions is essential to progress with the study.

In order to achieve the aim of the chapter, an energy management model was developed. Throughout the review of existing literature, it was concluded that the modelling of the BESS is one of the most important components of the energy management system. Moreover, the approach used by many authors to describe the behaviour of the energy storage system as a function of the state of charge (SoC), has been proven to be an effective approach to assess the techno-economic aspects of a system formed by the energy storage, demand load and a renewable energy source. The same approach was followed in this study for the development of the energy management system.

The systems under study were described, and the energy management algorithm for each site was developed. The results obtained from the model were analysed considering the grid dependency, total costs and GHG emissions. It was found that the introduction of the BESS together with the PV solar system reduces the grid dependency, the total costs and the GHG emissions if compared to the base case scenario for the WMD. However, installing a BESS in premises similar to the M&S retail store is only economically justified for a certain gap between off-peak and peak electricity prices. Moreover, in premises like M&S, where the on-site solar energy generated proves inadequate even for fulfilling their internal energy requirements, justifying the use of solar energy for EV fleet charging seems challenging.

Following on from this study, the next chapter focuses on the impact of introducing an EV fleet into the WMD. The study explores the potential economic and environmental benefits of using PV panels and a BESS on site considering different fleet operational times and charging

patterns and it compares the outcome against a given base case scenario (i.e., the WMD does not have PV solar panels installed nor a BESS).

5 Electric fleet adoption

5.1 Introduction

The benefits of introducing a PV installation and a BESS into two different commercial premises, a waste management depot (WMD) and a M&S retail store, were studied in Chapter 4.

In this chapter, the impact of introducing a fleet of electric vehicles into the WMD, will be studied. A fleet of 19 electric refuse collection vehicles (eRCVs) will be introduced at the WMD. The WMD was chosen for this study, as opposed to the M&S retail store, due to the available data to perform the analysis, the energy requirements at both premises analysed in Chapter 4, and the inherently smaller requirement for a fleet of vehicles at a retail store. By the end of the chapter, the first three research question introduced in Chapter 2 will be answered:

- *What are the environmental and economic benefits of using solar energy and BESS to charge an electric freight fleet when logistic and operational constraints are considered?*
- *When using solar energy and BESS, what are the implications on the grid dependency and consequently GHG emissions, when different charging strategies are applied?*
- *Considering depot charging, would it be feasible to charge the EV fleet with solar energy assisted with energy storage systems, considering the operational and logistic constraints?*

For that purpose, the chapter explores the potential benefits, if any, of the integration of PV solar panels, a BESS and an eRCV fleet against a given base case scenario (BCS). The BCS refers to a hypothetical scenario in which the WMD does not have PV solar panels installed nor a BESS but wishes to switch its refuse collection vehicles to an electrically powered eRCV fleet. In this BCS, the eRCV fleet and the depot's demand are to be entirely covered from the grid mix. The energy flow of this system is assessed with the algorithm developed in Chapter 4 with additional modifications to add the eRCV fleet as an extra energy demand at specific hours in each day. The energy management algorithm described in this chapter has been

previously published in the Energies journal in 2023[10] [175]. The main function of the algorithm is the same, to prioritize the use of PV solar energy, with the support of the BESS, to cover as much of the energy demand as possible. Due to the scarcity of studies done with these 3 elements: PV solar energy, BESS and an eRCV fleet, the evaluation performed in this chapter considers different charging scenarios with the aim of providing a broader set of outcomes that could be applied considering different operational requirements and contributes to the novelty of the work through the inclusion of the fleet energy support. The results obtained from the algorithm are analysed at the end of the chapter considering not only the technical and economic aspects, but also the GHG emissions released.

5.2 Methodology

5.2.1 WMD fleet operational times and charging pattern.

The actual WMD refuse collection vehicle (RCV) fleet comprises 19 diesel vehicles with a total distance travelled and fuel consumed of approximately 23,000 miles and 19,500 litres of diesel per month respectively. At the time of this study, the RCV fleet collects general household waste every other week alternating with fortnightly household recycling collections, and garden or green waste collected fortnightly between March and December. In addition, approximately eight vehicles are anticipated to be used for weekly food waste collections in the future, although these have not been considered in the modelling.

For this study, it is considered that the whole RCV fleet is switched from diesel to electric. To estimate the total energy requirement of the fleet, the study uses the mileage data of the conventional RCV fleet and a conversion factor of 3.48 kWh/mile. The conversion factor was obtained by using the energy consumption model for eRCVs proposed by Zhao *et al.* [312] and is in line with the conversion factor published by other authors for similar eRCVs [313]. The assumed maximum battery capacity of each eRCV is 300 kWh, based on the average battery size of several eRCV manufacturer's prototypes. The model also assumes that the fleet operates Monday to Friday with a constant daily consumption of 185 kWh, therefore the potential

[10] Nunez Munoz M, Ballantyne EEF, Stone DA. Assessing the Economic Impact of Introducing Localised PV Solar Energy Generation and Energy Storage for Fleet Electrification. Energies 2023;16:3570. https://doi.org/10.3390/en16083570

disadvantages of short ranges applicable to other electric vehicle types or with other uses is not applicable in this case.

From Pelletier *et al.* [29], a company would commonly decide to have fewer chargers than vehicles. However, such assumption implies that there is always someone at the depot to unplug and move the eRCV when is fully charged to free the charging space for the other eRCVs that were not yet charged. For this study, the proposed number of chargers at the depot is varied according to the operational requirements, and the charging patterns are as follows:

Charging scenario 1: Charging starts at 16:00h, with 22 kW Level 2 chargers. Here, the eRCV fleet operates between 06:00h and 14:00h, and at this time the fleet returns to the depot to be charged. Assuming that each eRCV would arrive at slightly different times due to traffic, and slight route variations, this charging scenario provides a 2hr buffer for all vehicles to return to the depot prior to charging. The charging process therefore starts at 16:00h and lasts up to approximately 8.5 hours for the fleet to be fully charged. For this scenario, each eRCV will have its own charger (19 chargers in total), so the eRCVs are plugged into a charger on arrival and unplugged the next day just before leaving the depot for their collection route.

Charging scenario 2: Charging starts at 21:00h with 22 kW Level 2 chargers. Charging the fleet at 21:00h instead of 16:00h, enables the vehicles to be charged at a lower electricity price (post 21:00h is considered off-peak hours). Therefore, for this scenario the eRCV fleet operates between 06:00h and 14:00h and returns to the depot to wait until charging is scheduled from 21:00h. It is assumed that the eRCV fleet is fully charged at the end of the charging period for a total of approximately 8.5 hours. On account of overnight charging, having fewer chargers than eRCVs would require someone to physically stay at the depot at night to redistribute the eRCV around the lower number of chargers to make sure all the eRCVs are fully charged before the shift starts. To avoid this, it is assumed that the depot would have 19 chargers installed, as with scenario 1.

Charging scenario 3: Charging starts at 11:00h and 23:00h with 50 kW fast chargers. In this scenario, the charging process is split between two time windows. Here, 9 out of 19 eRCVs operate between 06:00h and 14:00h. On arrival back at the depot, the eRCVs are parked out of the charging slot because the charging process takes place from 23:00h. These 9 eRCVs require less than 4 hours to be fully charged due to the use of faster chargers. The other 10 eRCVs, operate between 06:00h and 10:00h, then return to the depot to be charged at 11:00h (the fleet

is fully charged in less than 4 hours) before returning on the road again from 18:00h until 22:00h. For this scenario, the maximum amount of eRCVs charging at the same time is 10, so the number of chargers required are fewer than from the previous charging scenarios. Precisely, 10 chargers are considered in this case. For the part of the fleet that is charged overnight, it wouldn't be necessary to have an extra worker there to move the eRCVs. For this, it is assumed that each of the 10 eRCVs drivers that return to the depot at 22:00h, will be in charge of moving one of the eRCVs parked from the other shift to the charging slot, before moving their own eRCV to the parking slot that is now free.

As a summary, the charging scenarios are shown in Table 5.1.

Table 5.1. Detailed information of each charging scenario.

Charging scenario	Operational time	Charging time	Number of chargers
1	06:00h – 14:00h	16:00 – 00:30h	19 Level 2 (22 kW)
2	06:00h – 14:00h	21:00h – 05:30h	19 Level 2 (22 kW)
3	06:00h – 14:00h 06:00h – 10:00h & 18:00h – 22:00h	23:00h – 03:00h 11:00h – 15:00h	10 Fast chargers (50 kW)

Crozier *et al.* [90] discussed the impact of charging large electric fleets on the grid supply network in the UK. For the WMD, the increase in electrical energy demand from switching from the conventional fleet to an electric fleet it is not an exception. The total demand of the site increases from 234 MWh to 914 MWh, approximately. Figure 5.1 shows the WMD total energy demand for each month when the fleet is powered by diesel (grey column) and when the fleet is electric (green column). From this figure it can be seen that the depot energy requirements are dominated by the fleet operation.

The monthly energy results depicted in Figure 5.1 assuming the fleet is electric, represent the combined energy consumption of the depot and the fleet of 19 eRCVs (green bars). However, when the WMD uses a diesel-powered fleet (grey bars), the energy consumption indicated by these grey bars corresponds solely to the energy demand of the depot. The energy demand represented by the grey bars follows a seasonal trend, with higher consumption during winter, and a decreased consumption during summer. This seasonal trend is not as apparent when the fleet is electrified, and there are a few peaks. Examining the months of January, April, June and October, the seasonal fluctuation in energy demand is still visible. However, some months,

such as March, May and August, peak against this pattern. These peaks are linked to the number of days that the fleet is operating. For instance, in February, the fleet operates for 20 days (Monday through Friday). In contrast, it increases to 23 operational days in March (due to there being more weekdays in March compared to the shorter month of February). The fleet's energy demand increase masks any seasonal fluctuation in energy demand by the depot during those months.

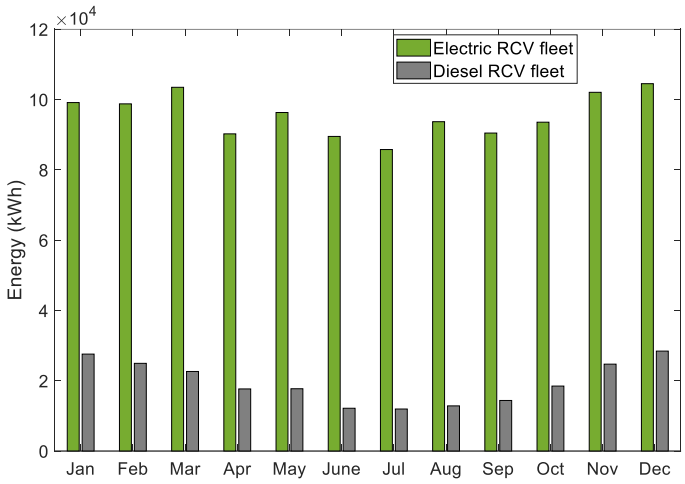

Figure 5.1. Total monthly energy consumption at the WMD with a diesel RCV fleet (grey column); and with an eRCV fleet (green column).

5.2.2 Scenarios

As discussed earlier, in order to assess the impact on grid dependency, total costs and GHG emissions when the fleet is electrified, two different energy supply scenarios have been selected, a base case scenario (BCS) and a scenario with local energy storage and generation (BESS scenario).

Base case scenario (BCS)

This refers to the WMD when there are no PV solar panels nor a BESS installed, but the fleet of RCVs has been already switched from conventional diesel to electric power. Therefore, the WMD is 100% dependent on the grid to cover the demand from both the building, and the eRCV fleet, as shown in Figure 5.2.

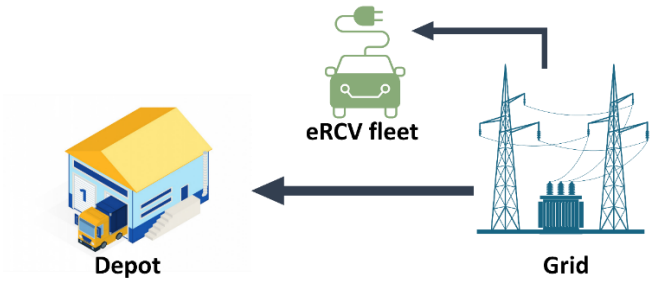

Figure 5.2. Energy flow diagram proposed for the BCS

BESS scenario

The BESS scenario assumes that the WMD has PV solar panels, a BESS, and the RCV fleet is electric. Six different BESS are considered, with capacities of 0.05 MWh, 0.1 MWh, 0.5 MWh, 1 MWh, 5 MWh and 10 MWh.

The results of this scenario are obtained using the energy management algorithm (EMA) developed for the WMD and introduced in chapter 4 (section 4.3.2) to which the eRCV fleet has been added. The proposed energy flow diagram is presented in Figure 5.3.

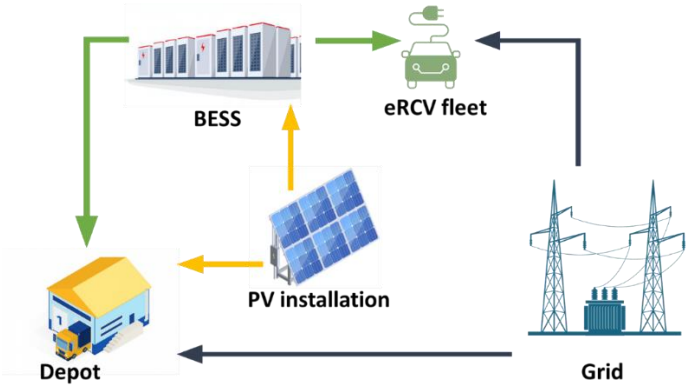

Figure 5.3. Energy flow diagram proposed for the BESS scenario.

The depot is assumed to be equipped with rooftop PV panels and a BESS (with a round-trip efficiency of 90% [146]). The depot's and the eRCV fleet energy demand are firstly supplied by solar energy followed by energy stored in the BESS, and lastly by the grid if needed. If, at any time, there is surplus solar energy after fulfilling the total energy demand, the excess is stored in the BESS for later use. For a detailed representation of the algorithm developed for the BESS scenario, please refer to Figure 5.4.

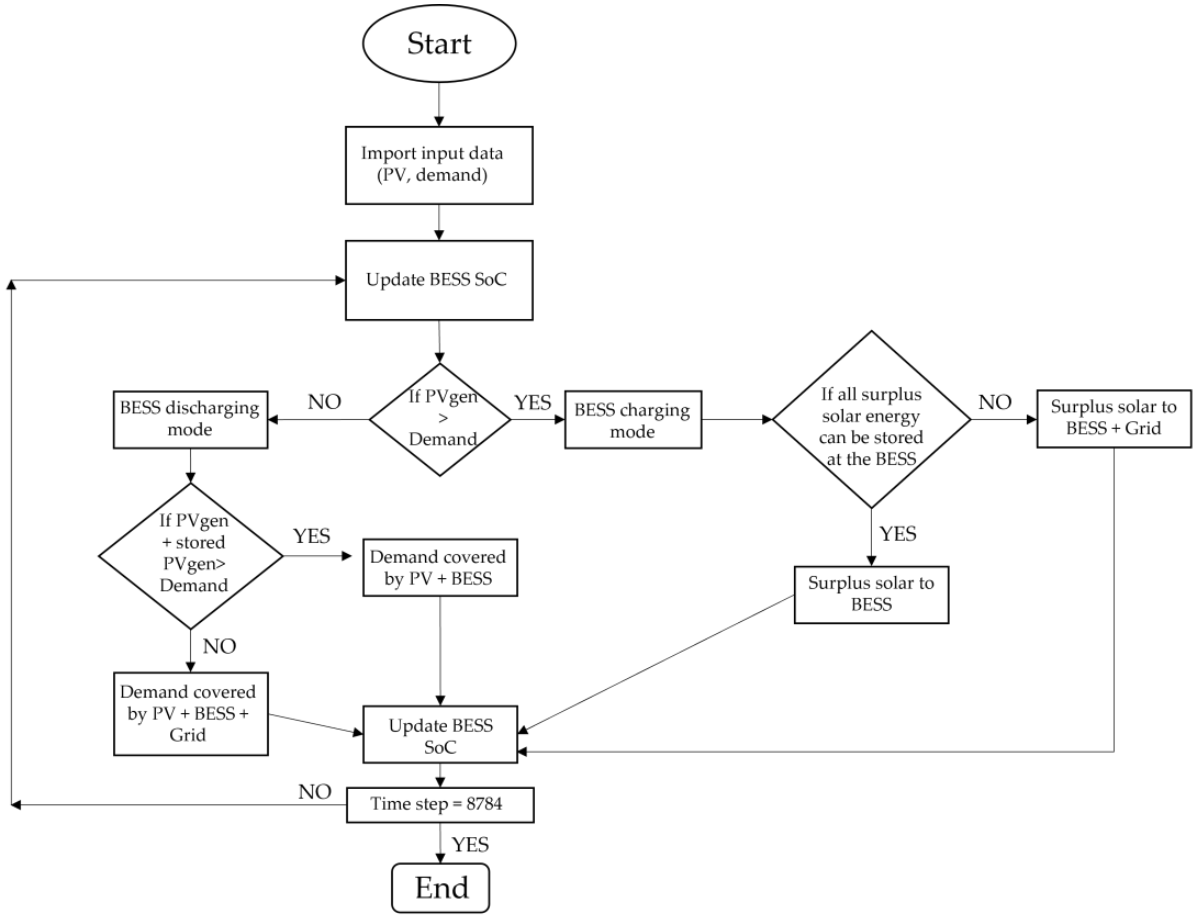

Figure 5.4. "Flow chart of the energy management algorithm developed for scenario 2" (Figure obtained from [175]).

In relation to the BESS, some constraints have been considered in the algorithm. Those constraints were introduced in Chapter 4 (section 4.3.2) and are summarised below.

1 The BESS is restricted to not being charged and discharged during the same hourly time step (t).

2 The BESS operates within a pre-set state of charge ($SoC_{(t)}$) range that is assumed to be 20% (SoC_{min}) and 90% (SoC_{max}) of the total battery capacity. These SoC limits were selected as reasonable values for typical battery system operations without being specific to any particular equipment [279].

3 The battery has a constraint for charging and discharging, limiting the maximum charging power to $2C_{BESS}$, where C_{BESS} is the capacity of the battery. This limitation aligns with the recommendations provided in various Lithium-based cell datasheets to prevent rapid cell degradation. As such, it is only advisable to operate up to $2C_{BESS}$.

4 The BESS is charged exclusively from the PV installation and is modelled assuming that any voltage or current change is achievable with changes in SoC [134]. As it was

previously discussed in Chapter 4, the SoC is the most frequent parameter used to evaluate the energy status of the battery [279]. According to Byrne *et al.* [278], this model is the most suitable for performing techno-economic analyses and operating within minutes to hours. Yang *et al.* [134], and Rosewater *et al.* [279], defined the charging/discharging process of the battery as in Equation 5.1:

$$C_{BESS} \cdot {}^{\partial SoC}/_{\partial t} = BESS_{rteff} \cdot {P_{BESS(t)}}^{+} + {P_{BESS(t)}}^{-}$$

Equation 5.1

Where $BESS_{rteff}$ is the battery round trip efficiency, ${}^{\partial SoC}/_{\partial t}$ is the rate of change of SoC and ${P_{BESS(t)}}^{+}$ and ${P_{BESS(t)}}^{-}$ are the charging/discharging power of the BESS, respectively.

5 The BESS is charged only when the PV solar energy generation surpasses the energy demands of both the WMD and eRCV fleet. The amount of surplus solar energy stored in the BESS is subject to the available capacity in the battery during the specific time step.

6 The BESS is discharged when there is insufficient PV solar energy to fulfil the energy demand for both the WMD and the eRCV fleet charging. Once the BESS reaches the minimum state of charge (SoC_{min}), the BESS cannot be discharged any further.

7 When the algorithm ends at time step 8784, the BESS energy balance must be 0. The energy balance is calculated following Equation 5.2. Total energy in and Total energy out is the sum of hourly values of energy coming in and out of the BESS for the whole year (i.e., from t=1 to t=8784), respectively. $\text{Energy}_{(t=0)}$ refers to the energy store at the BESS at t=0 (i.e., SoC_{min}) and $\text{Energy}_{(t=8784)}$ is the energy store at the BESS at t=8784.

$$\text{BESS energy balance (kWh)} = (\text{Total energy in} - \text{Total energy out}) - (\text{Energy}_{(t=0)} - \text{Energy}_{(t=8784)})$$

Equation 5.2

Considering the rise in peak energy demand due to switching to an electric RCV fleet, the energy management algorithm guarantees that the system never surpasses the peak power demand. However, it requires a network upgrade of the grid power connection capacity from

0.15 MW to 0.6 MW if the fleet is charged with 22kW chargers and, from 0.15 MW to 0.7 MW when the WMD uses fast chargers (i.e., 50 kW).

For each charging pattern discussed previously, the BCS and the BESS scenarios are simulated.

5.2.3 System cost analysis

The electricity price assumed corresponds to that introduced in chapter 4 for the WMD with an average value of 45.4 p/kWh. The maximum price is achieved at peak times (i.e., between 6am and 10am, and 4pm-8pm) and the minimum at off-peak times (i.e., from 9pm to 5am). Similarly, the economic analysis has been performed considering the costs introduced in chapter 4. These include the network charges, cost of energy, cost of BESS, cost of PV panels and the revenue from the sale of surplus solar energy. The system cost analysis is performed for the system lifetime, 15 years.

The capital cost associated with switching from a conventional fleet to electric fleet is not considered within the scope of this thesis. The objective here is to evaluate the impact of charging the fleet for the BCS and the BESS scenarios, assuming both would have an electric fleet, and not considering the costs of initially purchasing the electric vehicles.

The difference in costs incurred if fast chargers (i.e., 50KW) are installed instead of 22kW chargers will be considered. The objective being to reflect the difference in costs for each charging pattern. An average price for the EV chargers has been obtained from Furnari *et al.* [115] and is shown in Table 5.2.

Table 5.2. Initial costs associated with EV chargers.

	Level 2 charger (22kW)	**Rapid charger (50KW)**
Number of chargers	19	10
Cost per charger (£)	3,000	12,000

5.2.4 Greenhouse gas (GHG) emissions analysis

Whilst eRCVs achieve zero emissions at the tailpipe, the GHG emissions associated with the electricity consumed to charge the fleet have to be considered. Additionally, the emissions associated with the electricity consumed by the depot are included in the analysis. The calculations to obtain the GHG emissions follow the same procedure introduced in chapter 4.

5.3 Results

5.3.1 Grid dependency considering different charging strategies

The different charging scenarios have been analysed to evaluate grid dependency. Simulation results are plotted below for each charging scenario, for one example week in March and one in July. The results show two different BESS sizes, by way of example, highlighting BESS capacities of 0.5 MWh and 5MWh. The green line represents the SoC of the BESS, the blue line shows the eRCV fleet energy demand. The modelled PV generation, WMD energy demand and the energy purchased from the grid are displayed together at the bottom of each figure in yellow, orange, and purple colour, respectively.

Charging scenario 1:

The simulation results of the scenario where the eRCV fleet is charged at 16:00h can be seen in Figure 5.5 and Figure 5.6. As shown, the eRCV fleet (blue line) is charged from 16:00h to 00:30h, when the fleet is fully charged. A smaller BESS of 0.5 MWh is fully charged during winter months (Figure 5.5a) and discharges in just one hour when the fleet load is applied at 16.00. During summer months (Figure 5.5b), the BESS is not able to store all the solar energy generated and a significant amount must be sold to the grid as surplus solar energy. Due to the increase in sunlight hours and the availability of instantaneous solar energy, the BESS is discharged slowly during the first hours of the eRCV fleet charging period, starting at 16.00, as is seen in the graphs where the increased solar generation at the start of the fleet load application (16.00h) leads to it taking two time periods (hours) for the BESS to be fully discharged.

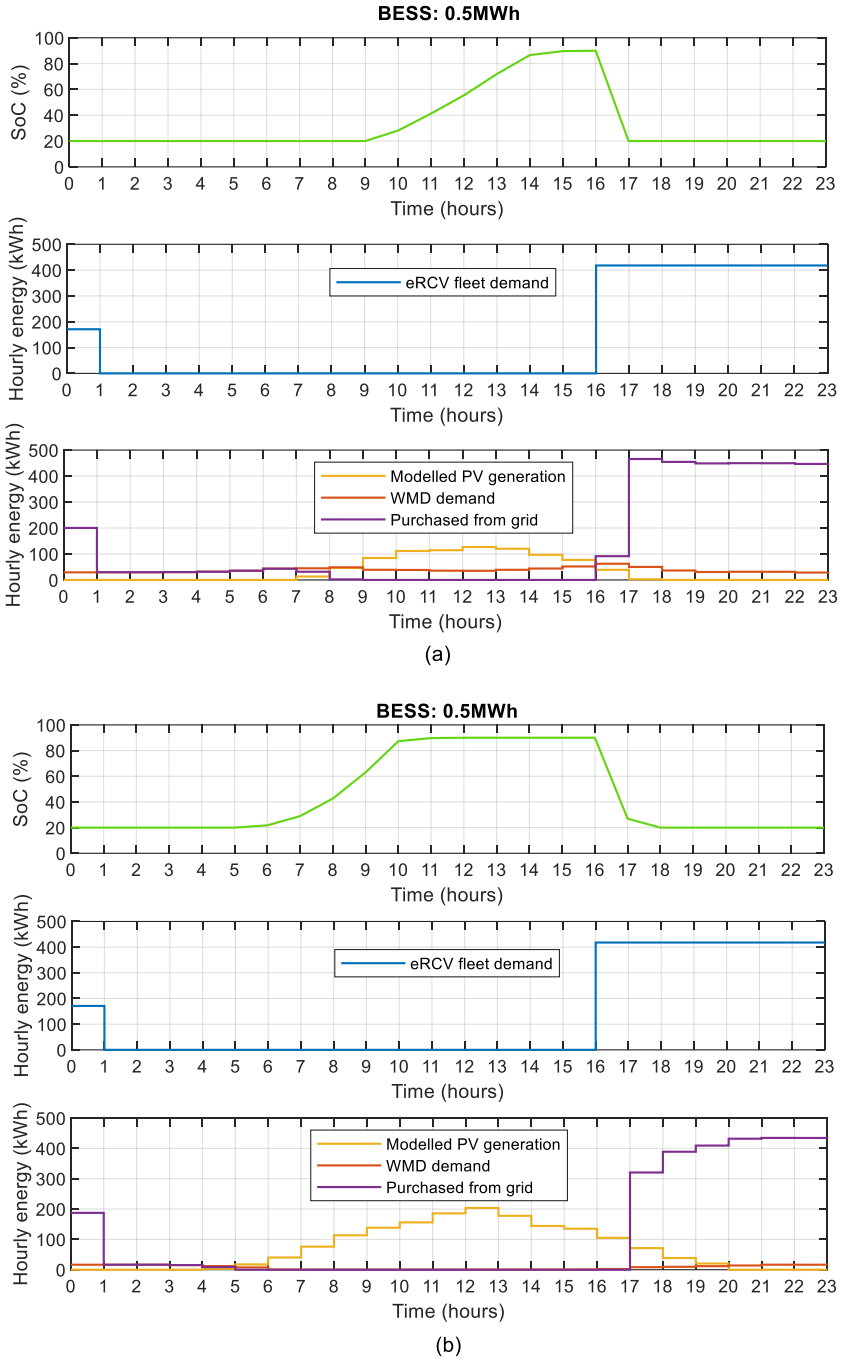

Figure 5.5. Simulation results when the eRCV fleet is charged at 16:00h for a day in (a) March and (b) July with a BESS of 0.5MWh.

If a larger BESS is in place, with a capacity of 5MWh (Figure 5.6), more solar energy can be stored, particularly during summer months (Figure 5.6b). This further reduces the dependency with the grid. In the winter months (Figure 5.6a), increasing the capacity of the BESS does not reduce the grid dependency any further, as the limiting factor is not the capacity of the BESS, but the availability of generated solar energy. However, during the summer months, when there is more solar energy generation, the larger BESS has a significant impact on the need for the

grid supply, delaying the requirement to purchase energy from the grid from 16.00h until 19.00h (Figure 5.5b).

In conclusion, when the fleet is charged in the afternoon (i.e., 16:00h) during the winter, a smaller BESS capacity is sufficient. However, in summer, a larger BESS is able to maximise the use of the solar energy and further reduce the grid dependency of the facility for fleet charging.

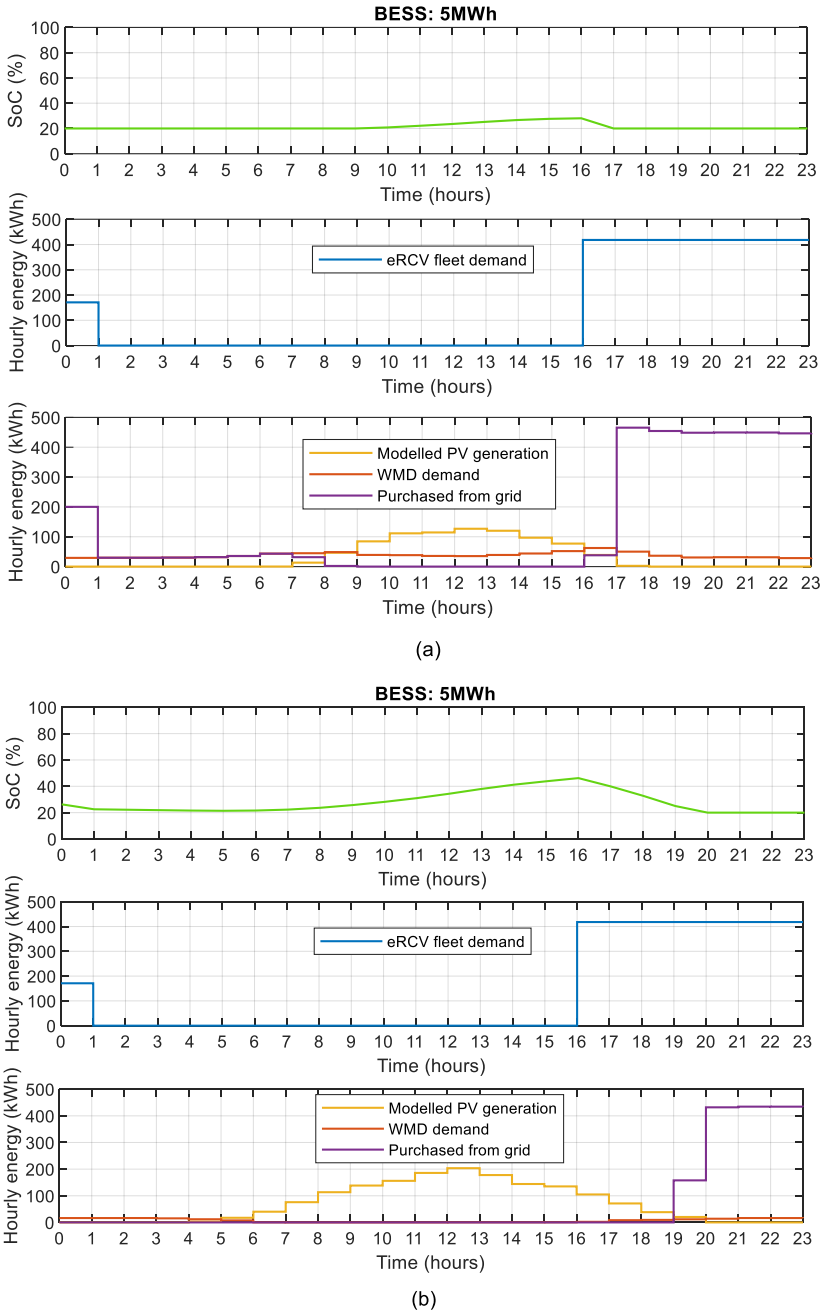

Figure 5.6. Simulation results when the eRCV fleet is charged at 16:00h for a day in (a) March and (b) July with a BESS of 5MWh.

Charging scenario 2:

Here, the simulation results for the scenario where the eRCV fleet is charged at 21:00h are discussed and can be seen in Figure 5.7 for a BESS with 0.5 MWh capacity and in Figure 5.8 for a BESS with 5 MWh capacity. The results are similar to those found in charging scenario 1. Increasing the BESS capacity in winter does not reduce the facilities dependency from the grid, as it can be seen in Figure 5.7a and, Figure 5.8a, as once again the limiting factor is the availability of solar energy generation, not the capacity to store it.

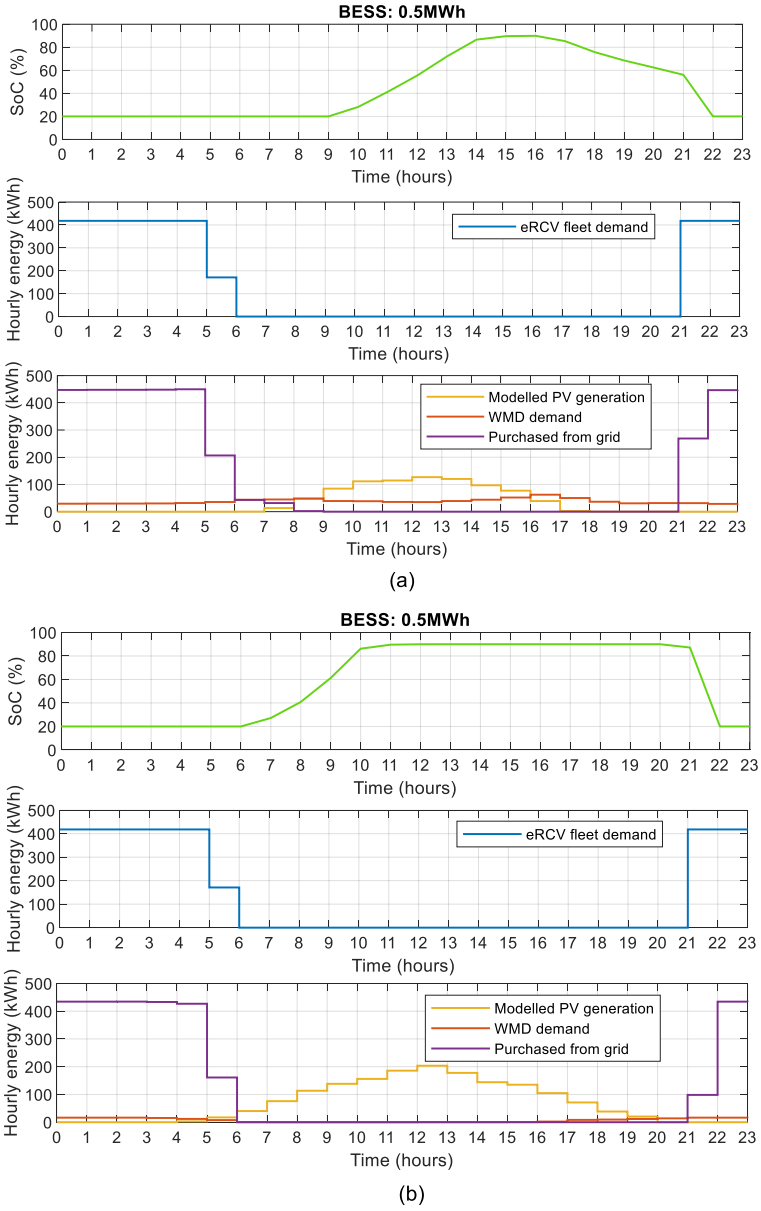

Figure 5.7. Simulation results when the eRCV fleet is charged overnight for a day in (a) March and (b) July with a BESS of 0.5MWh.

During summer months, once again the smaller BESS (Figure 5.7b) cannot store excess solar generation, and therefore effectively forces the system to sell a larger amount of surplus solar

energy to the grid. However, when a larger BESS is in place (Figure 5.8b), the grid consumption is almost zero, and the eRCV fleet is almost entirely charged from the generated solar energy, thus significantly lowering the energy bought from the grid, and therefore the operating costs of the fleet.

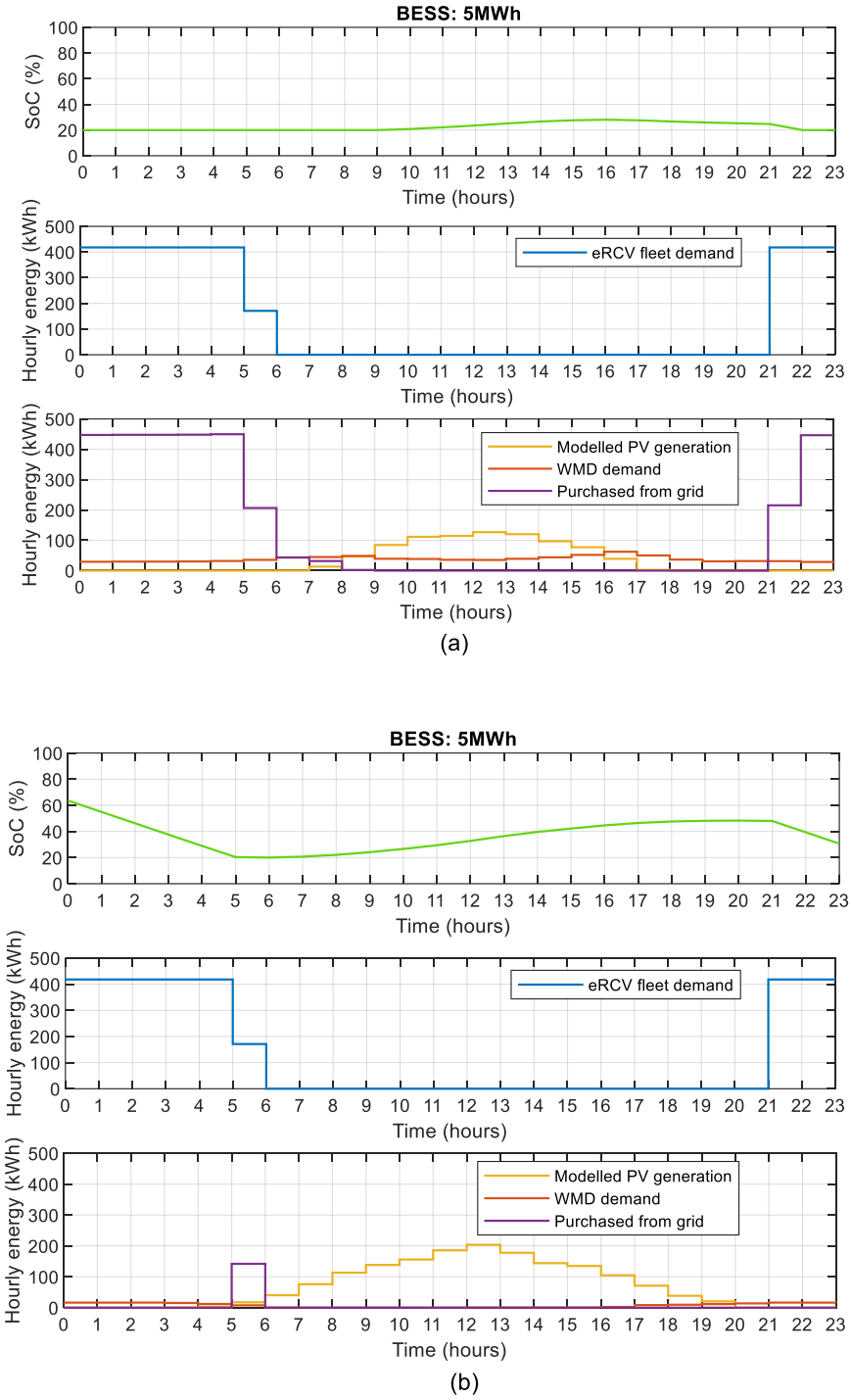

Figure 5.8. Simulation results when the eRCV fleet is charged overnight for a day in (a) March and (b) July with a BESS of 5MWh.

Charging scenario 3:

Now the simulation results when 10 eRCVs are charged at 11:00h and 9 eRCVs are charged at 23:00h are presented and can be seen in Figure 5.9 for a BESS with 0.5 MWh capacity and in Figure 5.10 for a BESS with 5MWh capacity. In this scenario, the use of solar energy is maximised with a smaller BESS (Figure 5.9). The eRCV demand coincides in time with the solar energy generation, and only surplus solar energy is required to be stored in the BESS (see Figure 5.9b compared with Figure 5.7b).

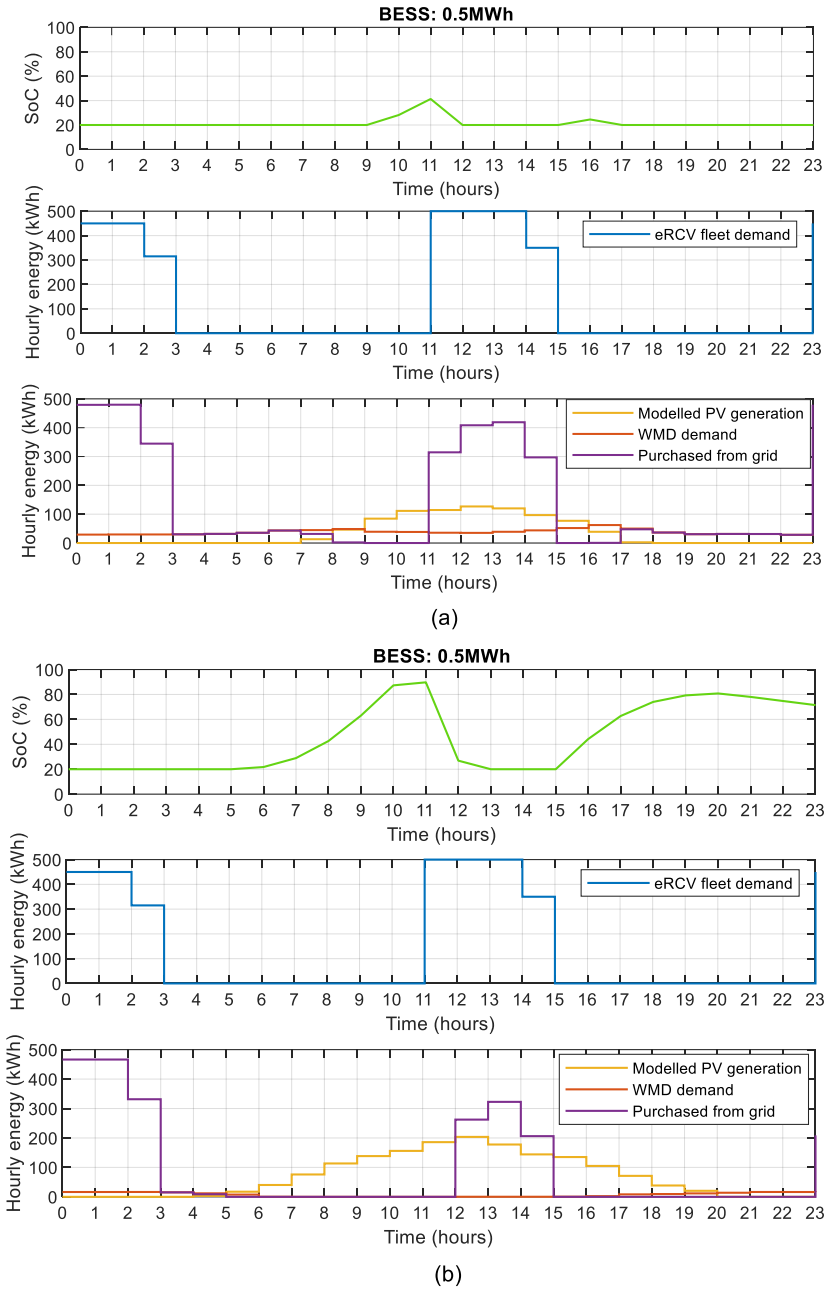

Figure 5.9. Simulation results when the eRCV fleet is charged at 11:00h and 23:00h for a day in (a) March and (b) July with a BESS of 0.5MWh.

As in the previous scenarios, the size of the BESS does not impact the energy used from the grid in winter, as can be seen by comparing Figure 5.9a and Figure 5.10a. During summer, the trend is the same as in previous scenarios. The larger the BESS, the lower the dependency of the facility on the grid.

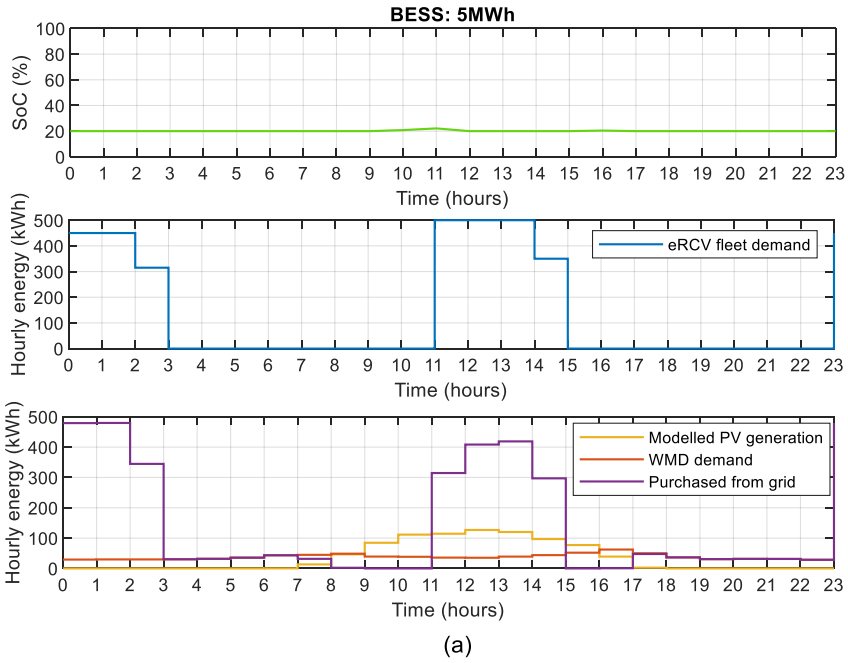

Figure 5.10. Simulation results when the eRCV fleet is charged at 11:00h and 23:00h for a day in (a) March and (b) July with a BESS of 5MWh.

The annual energy demand covered by the grid can be seen in Figure 5.11 as a comparison between a) charging scenario 1, b) charging scenario 2 and, c) charging scenario 3. As expected, the base case scenario (BCS) is 100% dependent on the grid irrespective of what charging scenario is in place, as no PV panels nor BESS are installed. When a BESS and PV is in place, the dependency on the grid is reduced as the BESS capacity increases. The energy demand covered by the grid, solar energy or the BESS has been included in a pie chart for a BESS of 0.5 MWh and 5 MWh as examples. In the figures, the energy demand covered by the BESS is actually excess solar generation stored by the BESS for use later in the day.

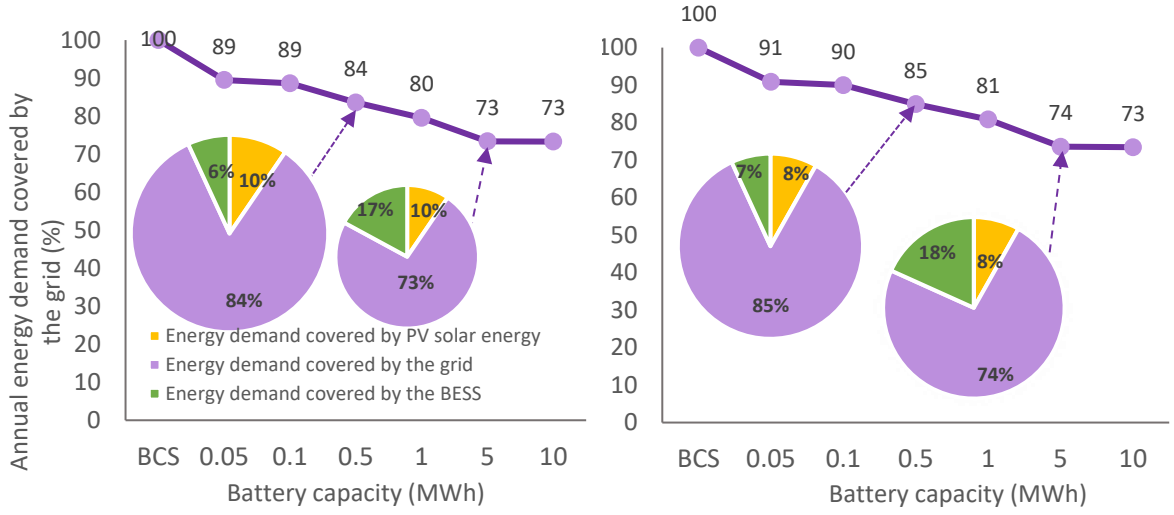

(a) (b)

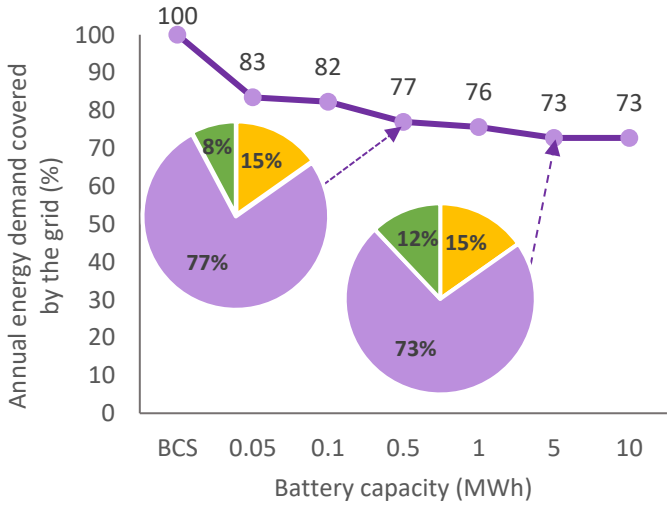

(c)

Figure 5.11. Energy demand covered by the grid, solar energy or by the BESS for a capacity of 0.5 MWh and 5MWh for (a) charging scenario 1, (b) charging scenario 2 and, (c) charging scenario 3.

For a smaller BESS capacity (i.e., 0.05 MWh), the grid dependency is reduced by approximately 17% when the eRCV is charged at 11:00h and 23:00h (Figure 5.11c, charging scenario 3), followed by charging the eRCV fleet at 16:00h (Figure 5.11a, charging scenario 1) that reduces the grid dependency by 11%. From these results, it is apparent that for sites considering the installation of a small BESS, charging scenarios 3 and 1 maximise the benefits of having a BESS installed. As previously discussed, the eRCV demand coincides in time with the solar energy generation for these two charging scenarios. Thus in the summer months, more capacity is available in the BESS to store surplus solar energy. As the BESS capacity increases, the dependency on the grid decreases for all the scenarios explored.

5.3.2 Total cost of ownership over the system lifetime

The total cost of ownership over the system lifetime (i.e., 15 years) has been analysed for each charging scenario, considering the BCS (i.e., the WMD does not have PV panels nor a BESS) and the BESS scenarios.

Charging scenario 1:

The total costs over the system lifetime when the eRCV fleet is charged at 16:00h, can be seen in Figure 5.12. Surprisingly, for this scenario only a BESS with a capacity equal to 1MWh reduces the total cost when compared to the BCS. Charging the eRCV fleet in the afternoon reduces the total costs by up to £150,000. This is because the fleet is charged not only when the electricity price is at its highest, but also when the network consumption red band is in place (please, refer to the network consumption band on chapter 4, section 4.3.4).

It is important to consider that when the PV solar installation and the BESS are in place, even for this charging scenario, the consumption from the grid is reduced and therefore the cost of energy is reduced. However, the benefits of having a BESS are minimised due to the high electricity and network prices making some of the BESS capacities uneconomic.

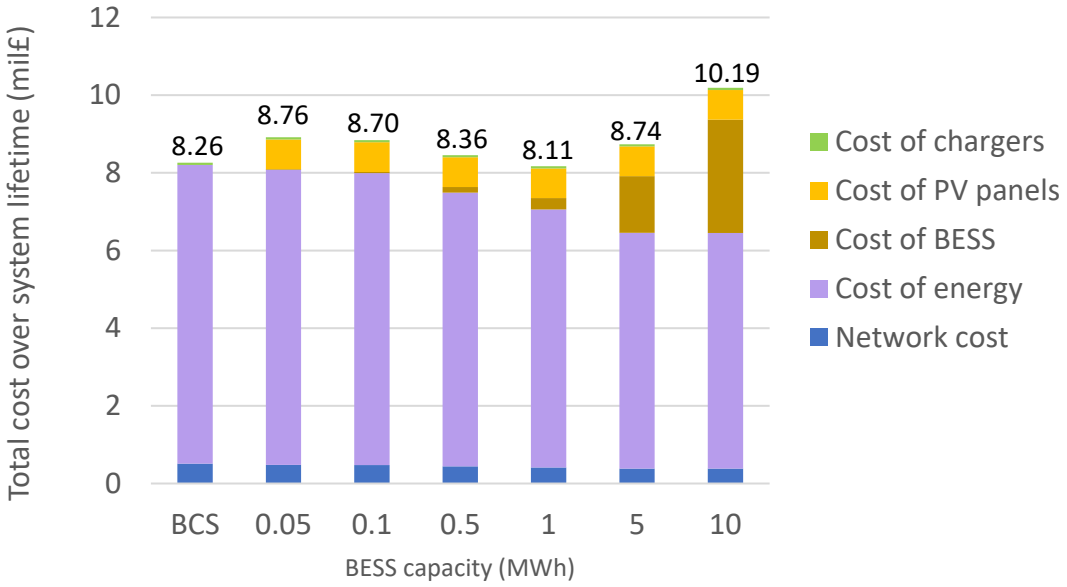

Figure 5.12. The total costs over the system lifetime for charging scenario 1.

Charging scenario 2:

The total costs over the system lifetime when the eRCV fleet is charged overnight, can be seen in Figure 5.13. From these results, it may be seen that the introduction of solar energy and BESS to support overnight charging reduces the total costs for BESS capacities smaller than 5 MWh. The maximum cost reduction is achieved using a BESS with a 1 MWh capacity, achieving approximately £530,000 reduction in costs.

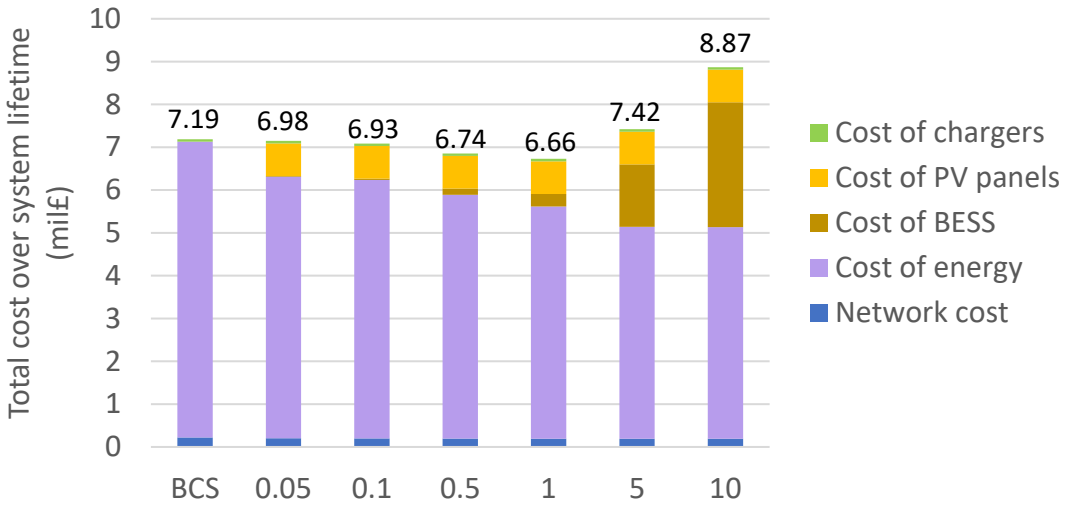

Figure 5.13. The total costs over the system lifetime for charging scenario 2.

Charging scenario 3:

The total costs over the lifetime for this scenario are shown in Figure 5.14. The trend in total costs is the same as the overnight charging trend (i.e., charging scenario 2). The introduction of PV panels and a BESS into the system reduces the total costs over the lifetime for a BESS smaller than 5 MWh, when compared with the base case scenario. However, for a larger BESS, the reduction in energy costs is overshadowed by the increase in BESS costs. The total costs can be reduced by up to £1M for a BESS with 0.5 MWh of capacity. This scenario provides the largest reduction in total costs of the 3 scenarios, compared to the base case.

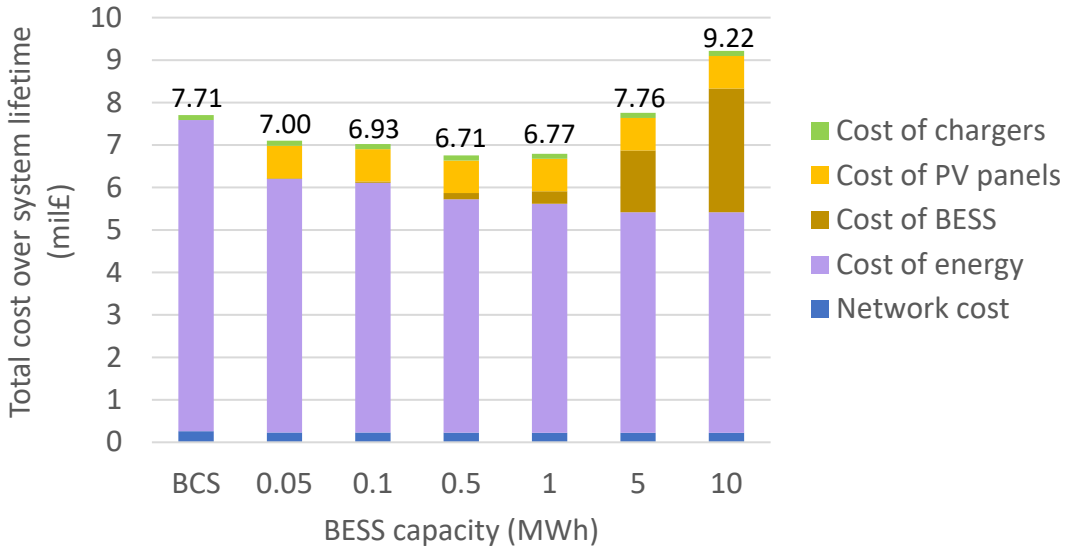

Figure 5.14. The total costs over the system lifetime for charging scenario 3.

Overall, the results confirm that overnight charging is the most economical solution for EV fleet charging when the system is 100% dependent on the grid (with no onsite solar energy generation). In fact, according to Furnari *et al.* [115], this is the option that many transport operators choose when it comes to fleet electrification for premises that do not have PV solar panels nor BESS installed on site, taking advantage of potential lower off-peak electricity prices for charging through the night. This charging pattern is also aligned with the operational requirements of many logistics companies, with fleets that operate in one shift during the day and are idle throughout the night. However, this could become problematic in cases where the fleet operates during the night or off-peak hours, for overnight / next day order fulfilment operations for example.

Additionally, the results show that having PV panels and BESS installed onsite reduces the total costs over the system lifetime when the BESS has a capacity below 5MWh, when compared to the BCS in this case. Under all the charging scenarios explored, overnight charging (i.e., charging scenario 2) is still an attractive option although it is not the most economic one. The highest reduction in total costs is achieved when the fleet is charged in two separate time slots (i.e., charging scenario 3). This scenario reduces the total costs by £1M. This charging pattern, however, is only compatible with certain fleets that can adapt their operation and working schedules to suit the optimal charging patterns. It would require a transformation that not all the logistic companies are able to follow, due to the operational requirements of the fleets and customers.

The least promising scenario is one in which the EV fleet is charged in the afternoon (i.e., charging scenario 1). As was discussed earlier, this period has the highest electricity and network charges, and therefore leads to the least impact in terms of cost savings.

Figure 5.15 shows the differences in network consumption band costs for the different scenarios. The consumption band cost is the price paid for using the network at certain hours over the day. The consumption band costs are divided into red, amber, and green, and operate as follows:

- The amber band rate is charged between 07:00h-16:00h and 19:00h-21:00.
- The red band rate spans from 16:00h to 19:00h.
- The green band rate is from 00:00h to 07:00h and from 21:00h to 24:00h.

When the eRCV fleet is charged at 16:00h (Figure 5.15a), the red band network consumption cost rises significantly.

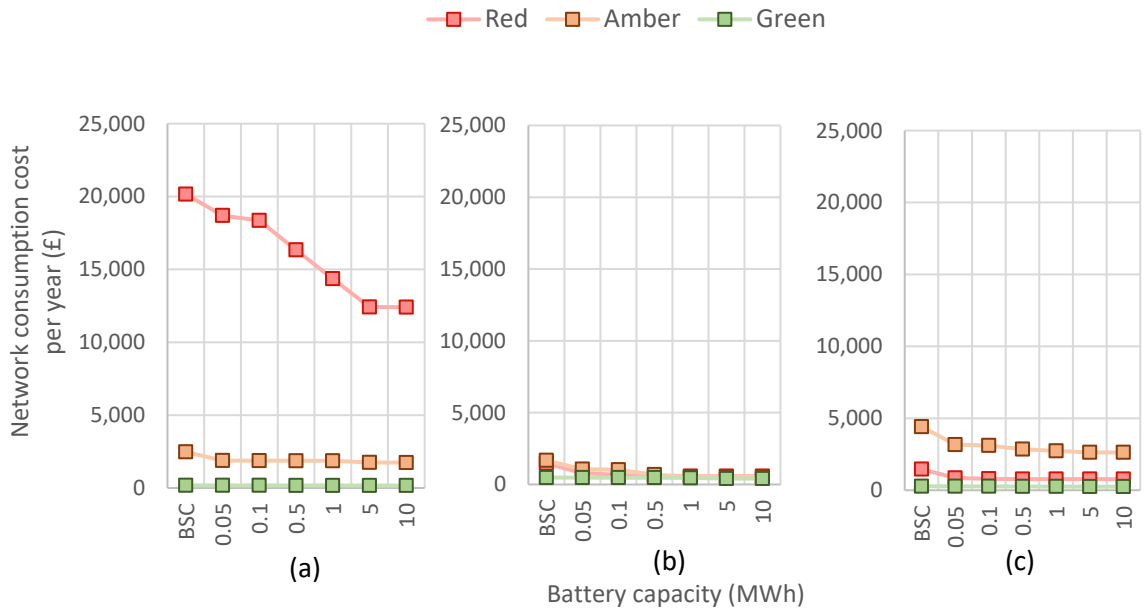

Figure 5.15. Consumption band cost per year when for (a) scenario 1, (b) scenario 2, (c) scenario 3

5.3.3 GHG emissions

The GHG emissions are now compared for all charging scenarios. Business and fleet operators whilst also looking to reduce operating costs, they are also incentivised by policy to reduce emissions as part of net zero targets and ambitions. Hence, comparing GHG emissions related to the charging scenarios studied, provides a useful analysis for business and operational decision making regarding the switch to EV fleets.

The analysis considers the emissions associated with the grid energy consumption by the depot and the eRCV fleet, emissions associated with the solar energy generation, and the emissions from the sale of surplus solar energy to the grid. The results are shown on an annual basis, considering 2023's grid mix in the UK. However, the grid GHG emissions will change as the grid is decarbonised, and so different results would be obtained if the simulation results are applied in a future, or past, scenario.

When looking at the GHG emissions from the whole system (i.e., as the sum of GHG emissions from WMD and from the eRCV fleet), the results are very similar between the different charging patterns as the overall energy consumed is the same but distributed differently over time. For this reason, the results on GHG emissions from the whole system are only presented for one of the charging scenarios (i.e., charging scenario 1) in Figure 5.16. The highest GHG

emissions per year are achieved for the BCS. When the WMD has PV panels and a BESS on site, regardless of the BESS capacity, the total GHG emissions are reduced compared to the base case scenario. The GHG emissions can be reduced by up to 41 tons CO_2 eq. per year with a BESS of 0.05 MWh. As the size of the BESS increases, more solar energy can be stored, and the amount of surplus solar energy available for sale is reduced. This reduces the GHG emission credit received by the system for selling energy back to the grid, and therefore increases the overall GHG emissions.

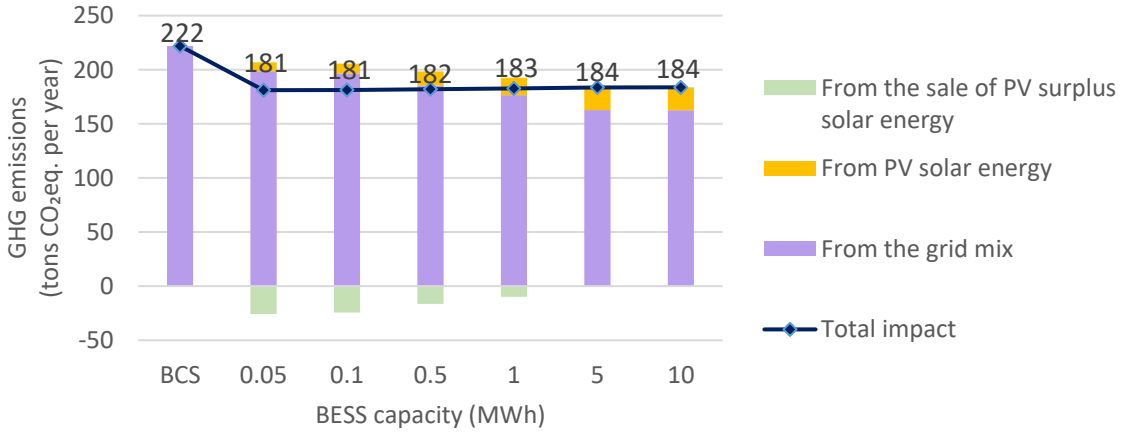

Figure 5.16. Total GHG emissions for scenario 1.

If only the results of the GHG emissions associated with charging the eRCV fleet are plotted (Figure 5.17), it can be seen that charging the eRCV at different times of the day impacts the eRCV fleet's GHG emissions. When the eRCV fleet is charged at night, most energy comes from the grid, especially for smaller BESS due to the capacity limitations to store surplus solar energy in summer months. Thus charging overnight increases the GHG emissions of an eRCV fleet. The differences between the three charging scenarios are minimised for a larger BESS (i.e., 5MWh and 10MWh), as they can store more significant amounts of surplus solar energy. The charging pattern that provides the most considerable reduction in GHG emissions corresponds to charging at 11:00h and 23:00h. In this charging scenario, more than half of the fleet is charged at 11 a.m. taking advantage of the peak solar energy generation.

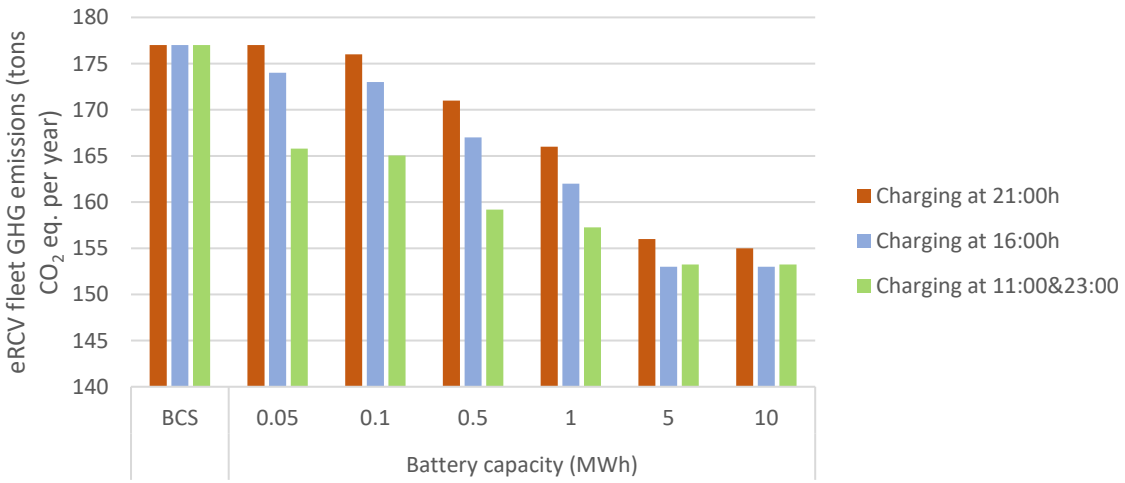

Figure 5.17. eRCV fleet GHG emissions per year for the different charging scenarios.

5.4 Discussion

Based on the results presented in this chapter, charging the eRCV fleet with solar energy supported by a BESS, reduces the overall grid dependency of the WMD facility, the costs over the system lifetime, and the GHG emissions when compared to the BCS.

1. Grid dependency: Integrating on-site solar energy generation for EV charging remains underutilised in the waste management sector, primarily due to the obstacles impeding its development and implementation. Specifically, solar energy, reliant on weather patterns, exhibits a constrained timeframe of peak power production, often concentrated around midday. As shown in Figure 5.11, the grid dependency is most reduced for smaller BESS capacities when the eRCV is charged around midday (scenario 3). This charging pattern maximises the benefits of having a BESS installed. For larger BESS capacities, the dependency on the grid is further reduced although there are no significant differences when all the charging scenarios are compared. The grid dependency can be reduced by up to 17% for the smallest BESS (i.e., 0.05MWh) when 10 eRCVs are charged at 11:00h and 9 eRCVs at 23:00h (i.e., scenario 3). For the largest BESS analysed (i.e., 10MWh) the grid dependency can be reduced by up to 27% independent of the charging scenario.

2. Total cost over the system lifetime: Charging the eRCV fleet at 16:00h (scenario 1) would be the least beneficial approach, for both the BCS and the proposed BESS systems, if compared with the other two charging patterns. As, at this time of the day, electricity prices and network consumption prices are at their highest values. However,

charging the eRCV fleet overnight (scenario 2) seems to be the most reasonable solution if the depot does not have PV solar panels or BESS on site (i.e., the BCS). Having PV solar panels and BESS installed on site reduces the total costs when the fleet is charged overnight or at 11:00h and 23:00h (scenario 3) for BESS smaller than 5MWh. The maximum cost reduction is achieved with a BESS of 0.5MWh when the eRCV fleet is split and charged at 11:00h and 23:00h. This provides savings of approximately £1M. If due to operational constraints the eRCV fleet has to be charged overnight, the maximum cost reduction would be £530,000 for a BESS of 1MWh over the system lifetime of 15 years.

3. GHG emissions: The different charging patterns impact the eRCV fleet GHG emissions when PV solar energy and BESS are installed on-site. For a smaller BESS, the GHG emissions are reduced the most when part of the fleet is charged at 11:00h and the rest of the eRCV fleet at 23:00h. Increasing the demand when the PV solar installation is generating energy maximises the instantaneous use of the solar energy. The scenario with the lowest GHG savings corresponds to overnight charging. For a larger BESS, the reduction in GHG emissions is similar for the three charging scenarios.

5.5 Summary

This chapter aims to answer research questions I and II:

- *What are the environmental and economic benefits of using solar energy and BESS to charge an electric freight fleet when logistic and operational constraints are considered?*
- *When using solar energy and BESS, what are the implications on the grid dependency and consequently GHG emissions, when different charging strategies are applied?*

In that regard, the electrification of a RCV fleet has been examined for a waste management depot (WMD). In order to have a broader knowledge of how the use of PV panels and a BESS could impact on fleet electrification, three different charging patterns were assessed. Understanding how feasible it would be to use renewable energy and a BESS to charge a fleet implies the necessity of considering the operational requirements of the fleet. Each logistics and commercial company has different constraints based on the operations required at the site, so it is important to reflect that into the charging utilisation.

For that purpose, each charging scenario was described and simulated following the energy management model developed in chapter 4. The results obtained from the simulations were analysed and compared against the base case scenario. In this chapter, the BCS stands for the hypothetical situation in which the WMD does not have PV panels nor BESS installed on site, and the RCV fleet is electric. The grid dependency, total cost over the system lifetime and the GHG emissions were then evaluated. It was found that the introduction of PV panels and a BESS reduces the grid dependency of the overall facility, system's lifetime total cost for certain BESS capacities and reduces the GHG emissions. Depending on the charging pattern, the benefits of having PV panels and a BESS on site can be further maximised. Overall, results conclude that it is economically feasible to use local solar energy generation and a BESS on site when a logistics or commercial company, similar to the characteristics of the WMD, decide to electrify their fleet.

Following on from this study, the next chapter considers a further constraint when it comes to fleet electrification, the grid power connection capacity. This is one of the most common barriers that logistics and commercial companies find when they wish to electrify the fleet and can be expensive and time-consuming to upgrade to support the fleet [89].

6 Technical assessment of EV fleet mass charging considering power capacity constraints

6.1 Introduction

The feasibility of adopting EV fleets into commercial depots was explored in Chapter 5 using locally generated PV solar energy and a BESS. The results demonstrated a reduction in total costs over system lifetime when the depot has installed PV solar panels and BESS to support the eRCV fleet charging, especially if the charging takes place overnight or if it is divided in two time slots (i.e., 11:00h and 23:00h).

Despite the encouraging results obtained in Chapter 5, it was assumed that the power connection to the depot could be upgraded due to increased energy demand. However, in reality, this assumption is only occasionally possible and often an issue that results in the delay of electric fleet adoption in logistic and commercial companies. Therefore, in this chapter, this potential power constraint is addressed, and a new algorithm is developed for that purpose. The chapter aims to evaluate a scenario of eRCV fleet charging in which the power connection capacity cannot be upgraded. In light of this issue, some solutions explored in the literature to date have focused on smart charging or load management. In Chapter 6, the author proposes energy storage as a complementary solution. By the end of the chapter, the final research question introduced in Chapter 2 will be answered: *To what extent solar energy and BESS can ease the power capacity constraints when it comes to EV fleet electrification?*

For that purpose, the algorithm keeps the power connection at the maximum allowed with the help of a BESS that is charged not only with PV surplus solar energy but also with energy from the grid mix. This is achieved at the expense of increasing the demand from the grid when the electricity and network prices are at their highest values. The simulations are carried out assuming the eRCV fleet is charged overnight (i.e., from 21:00h). The results are compared against those obtained for the overnight scenario explored in Chapter 5. The objective of making such a comparison is to determine, in cases where there is the option, what is the most feasible way forward, either to keep the power connection capacity at the same level as it was before the adoption of the eRCV fleet or upgrade the power connection to add more flexibility regarding the charging time and dependency from the grid at lower electricity and network

costs. The results presented in this chapter are part of previously published work in the Energies journal in 2023[11] [175].

6.2 Methodology

In this section, the scenarios studied are introduced and the energy management algorithm (EMA) developed is explained in detail.

6.2.1 Scenarios

For all the scenarios, it is assumed that the eRCV fleet operates between 06:00h and 14:00h and returns to the depot to wait until charging is scheduled from 21:00h. It is assumed that the eRCV fleet is fully charged at the end of the charging period for a total of approximately 8.5 hours. Three different scenarios have been considered to evaluate the impact of having PV panels and a BESS installed on site, shown diagrammatically in Figure 6.1.

Scenario 1

Scenario 1 (Figure 6.1a) assumes that the company does not have PV panels, nor a BESS installed, and that the site is fully dependent on the grid connection to cover both the existing depot load, and the eRCV fleet energy demand.

Scenario 2

Scenario 2 (Figure 6.1b) incorporates PV panels and a BESS at the WMD. The depot and the eRCV fleets energy demands are met by the grid and by the PV solar installation. An algorithm manages the energy flow for scenario 2, prioritising avoidance of grid usage during peak price periods, which requires upgrading the grid power connection. Owing to the heightened energy requirements following the integration of the eRCV fleet, it is assumed that the grid power connection capacity will be expanded from 0.15 MW to 0.6 MW. This scenario corresponds to the overnight scenario described in the chapter 5 (i.e., scenario 2).

[11] Part of this chapter has been used for publication at the Energies journal as "Nunez Munoz M, Ballantyne EEF, Stone DA. Assessing the Economic Impact of Introducing Localised PV Solar Energy Generation and Energy Storage for Fleet Electrification. Energies 2023;16:3570. https://doi.org/10.3390/en16083570 ."

Scenario 3

In Scenario 3 (Figure 6.1c), as in Scenario 2, PV panels and a BESS are installed at the WMD. However, the BESS in this scenario is charged from the PV solar installation and the grid. The primary aim of the algorithm in this context is to avert any necessity for an upgrade in the grid power connection, despite the surge in energy demand following the integration of the eRCV fleet at the WMD, at the expense of using the grid supplied energy at peak prices. Consequently, the power capacity connection remains at the pre-existing level of 0.15 MW.

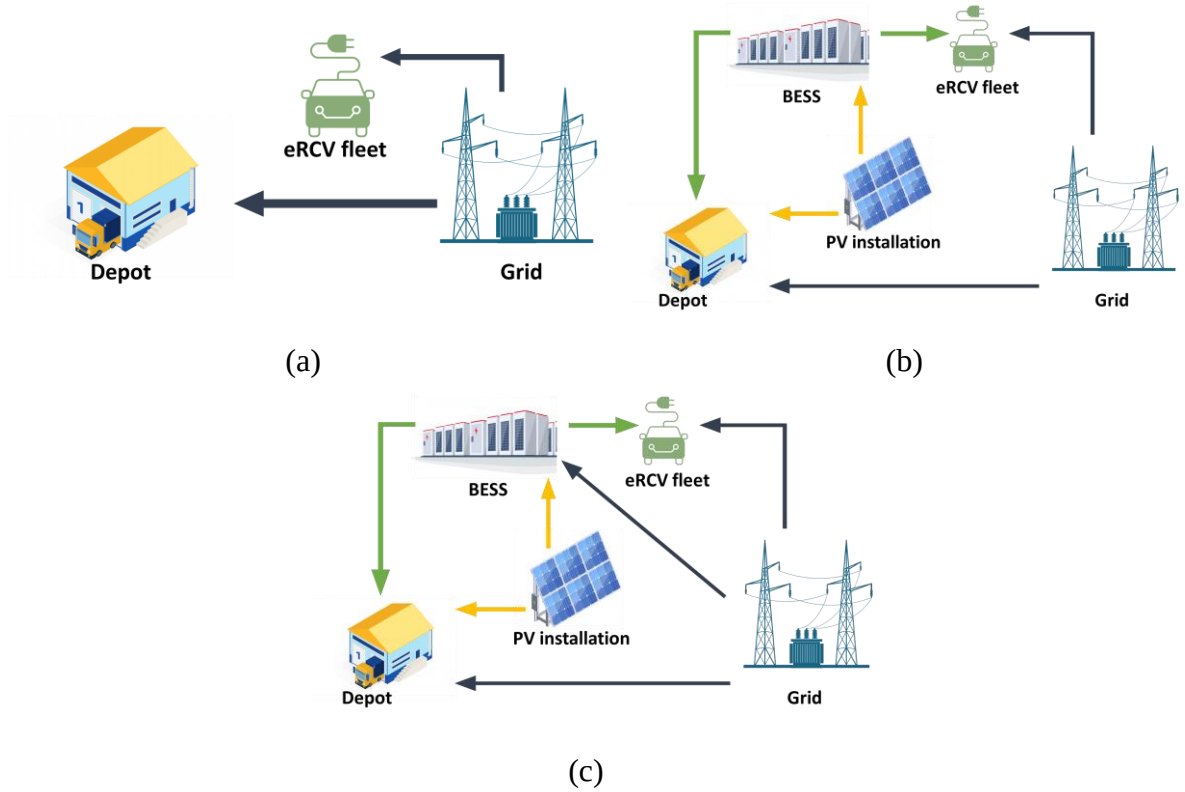

Figure 6.1. "Energy flow diagram for (a) scenario 1, (b) scenario 2 and, (c) scenario3" (Figure obtained from [175]).

To enable an economic comparison among the three scenarios, scenario 1 is performed considering both power connection capacities, 0.15 MW and 0.6 MW, as shown in Table 6.1.

Table 6.1. “Summary of the scenarios studied, and the approach used for the cost analysis” (Table obtained from [175]).

	Power connection capacity (0.15 MW)	Power connection capacity (0.6 MW)
Scenario 1	✓	✓
Scenario 2		✓
Scenario 3	✓	

6.2.2 Energy management algorithm

Two different energy management algorithms (EMA) have been modelled for evaluating the cost implications of fleet electrification for a company incorporating an on-site PV installation alongside a BESS.

Two priorities distinguish Scenario 2 and scenario 3. In Scenario 2, the algorithm focuses on decreasing reliance on the grid during peak price periods, even if it requires upgrading the power connection. On the other hand, in scenario 3 the algorithm avoids power connection upgrades, potentially resulting in excess capacity charges. Both algorithms were developed in Matlab Simulink.

The EMA designed for scenario 2: Prioritises grid consumption during off-peak electricity prices and network charges.

The primary goal of scenario 2 is to emphasise grid consumption during periods of lower network charges and electricity prices. To achieve this objective, the chosen energy management algorithm for scenario 2 aims to reduce the expense of purchasing electricity from the grid by prioritising the utilisation of PV solar energy whenever feasible, especially during peak network costs and high electricity price periods. Notably, two peak timeframes (between 6 am and 10 am, and 4 pm-8 pm) experience the highest electricity costs. In this regard, scenario 2 considers the overnight charging scenario that enables the vehicles to be charged at a lower electricity price (post 21:00h, is during off-peak hours). The EMA for scenario 2 was explained in detail in Chapter 5 (section 5.2.2) and assumes that the energy requirements of the depot and the eRCV fleet are met through a three-tier approach: primarily by solar energy, followed by energy sourced from the BESS, and as a final option, through the grid. During the day, when

the electricity and network costs are highest, the BESS is discharged when solar energy cannot meet the demand.

In Scenario 2, for the system to avoid exceeding the maximum capacity of the grid power connection during peak periods, an enhancement of the grid power connection is implemented, increasing it from 0.15 MW to 0.6 MW.

The EMA designed for scenario 3: Aims to prevent the need for a power connection capacity upgrade.

The main objective in creating the EMA for scenario 3 was to prevent any need for any potential power connection capacity upgrades resulting from transitioning from a conventional fleet to an electric one. For that purpose, the algorithm utilises a BESS that is charged from PV solar energy and also from the grid. The EMA effectively connects the system formed by the PV installation, the BESS, the EV fleet, and the depot with the grid (as illustrated earlier in Figure 6.1c).

As for the EMA developed for scenario 2, the BESS is assumed to have an efficiency of 90%. Due to the influence that different seasons have on solar energy generation, the energy flow for scenario 3 was managed differently in autumn/winter and spring/summer. Thus the EMA for scenario 3 is differentiated between the summer and winter seasons. In this regard, on weekends, the BESS is only charged from solar energy during summer, whereas in winter, energy from the grid is required as there is not enough solar energy to charge the BESS fully. A detailed diagram of the algorithm developed for scenario 3 can be seen in Figure 6.2.

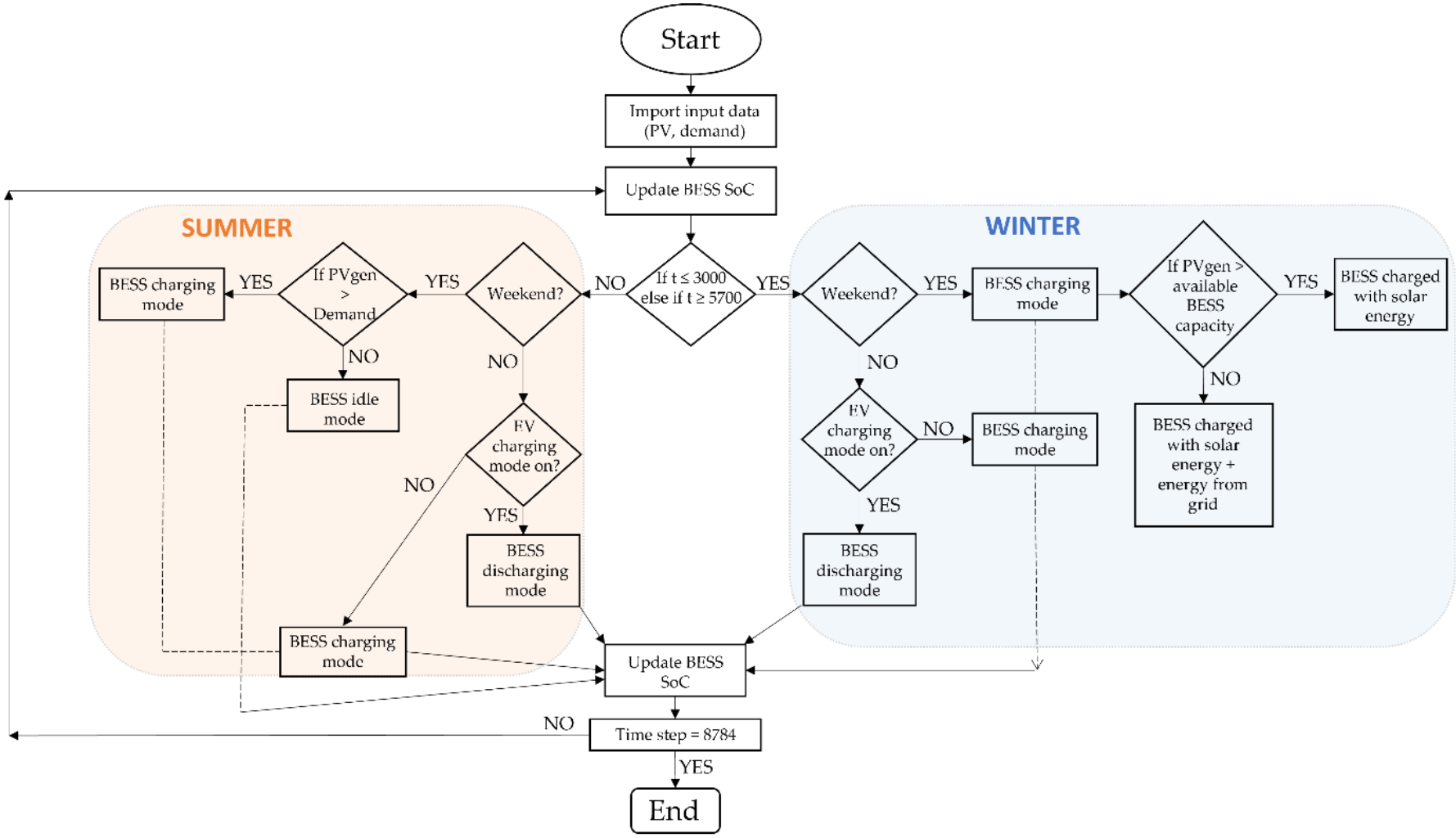

Figure 6.2. “Flow chart of the energy management algorithm developed for scenario 3” (Figure obtained from [175]).

In this algorithm for scenario 3, some constraints have been also applied. The constraints number 1, 2 and 3, previously introduced for the EMA developed for scenario 2 (see Chapter 5, section 5.2.2), are also applied here.

- The BESS is charged from the PV installation and from the grid. The BESS is modelled assuming that any voltage or current change is achievable with changes in SoC [134] following Equation 6.1.

$$C_{BESS} \cdot {}^{\partial SoC}/_{\partial t} = BESS_{rteff} \cdot {P_{BESS(t)}}^{+} + {P_{BESS(t)}}^{-}$$

Equation 6.1

- When the BESS is charged from the grid, the power required from the grid ($Power_{(t)}$) to charge the BESS can't be higher than the power connection capacity ($Power_{capacity}$), as in Equation 6.2.

$$Power_{(t)} < Power_{capacity}$$

Equation 6.2

- In autumn and winter, due to the scarcity of solar energy generation, the BESS is charged over the weekend from both the PV installation and from the grid. On weekdays, the BESS is only charged when the EV fleet charging mode is off.
- During spring and summer, the solar energy generation increases, and during the weekend, the BESS is only charged from the PV installation. On weekdays, the BESS is charged, when the EV fleet is not charging, from the PV installation and, if there is still available capacity, is charged from the grid.
- The BESS is discharged only on weekdays when the EV fleet charging mode is on throughout the whole year.
- As for the EMA developed for scenario 2, when the algorithm ends at time step 8784, the BESS energy balance must be 0.

Assuming the site can't upgrade the grid power connection network, the power connection capacity contracted at the site has to be the same as it was before switching the fleet to electric, 0.15 MW. This is done at the expense of storing energy from the grid, even during higher price periods as required.

6.2.3 System cost analysis

The system cost evaluation is performed for the three scenarios introduced in Table 6.1. namely, scenario 1, scenario 2, and scenario 3, for a system lifetime of 15 years. The total costs for Scenario 1 are estimated considering power connection capacities of 0.15 MW and 0.6 MW which facilitates its comparison with Scenario 2 (i.e., 0.6 MW) and Scenario 3 (i.e., 0.15 MW). The total costs for each scenario have been estimated following Equation 6.3

$$\text{Total costs over system lifetime} = \mathrm{E_c} + \mathrm{N_c} + \mathrm{BESS_c} + \mathrm{PV_c} - \mathrm{Rev_c}$$

Equation 6.3

Where ($\mathrm{E_c}$), is the energy from the grid, ($\mathrm{N_c}$) are the network costs, ($\mathrm{BESS_c}$) is the cost of the BESS, ($\mathrm{PV_c}$) is the cost of the PV installation and ($\mathrm{Rev_c}$) corresponds to the revenue obtained from the sale of surplus solar energy.

The detailed equations to estimate each parameter of Equation 6.3 have been introduced on Chapter 4.

The installation costs resulting from increasing the power connection capacity are also considered for the system cost analysis in this chapter for Scenario 1 and Scenario 2. The installation cost when the power connection capacity is upgraded from 0.15 MW to 0.6 MW (i.e., approximately 667 kVA considering a PF of 0.9) is assumed at £45,740. The value have been obtained according to the estimations from Energy UK [314], based on the approximate connection costs for an upgrade of between 200 kVA and 1,000 kVA which would be between £4,500 and £75,000.

Conversely, this study does not consider the eRCV fleet's purchase cost or the charging infrastructure expenses. The scenarios examined assume that the fleet at the WMD is already electric, making these costs outside the study's scope. Any potential new investment would pertain solely to the acquisition and installation of the PV and BESS. For all the three scenarios, the number of chargers is the same as the operational requirements of the fleet are equal for the three scenarios analysed.

6.3 Results

The section analyses the simulation results and then compares the outcomes of each scenario. This comparison aims to determine the relevance of installing PV panels and a BESS on-site. Ultimately, the section concludes by offering a comprehensive comparison and further discussion of all the studied scenarios.

6.3.1 Economic implications of integrating PV panels and a BESS to mitigate grid consumption during peak electricity and network prices.

The capacity of the BESS directly influences the extent to which the depot relies on the grid, thereby impacting energy and network expenses. This is shown in Figure 6.3, where two distinct BESS capacities are depicted: a 0.5 MWh BESS (Figure 6.3a) and a 5MWh BESS (Figure 6.3b). Figure 6.3 shows the monthly energy purchased from the grid, the monthly solar energy consumed directly from the PV panels ("consumed from PV"), the monthly solar energy stored at the BESS (stated as "to BESS" in the figure) for later use ("from BESS") and the solar surplus energy sold to the grid ("PV solar surplus").

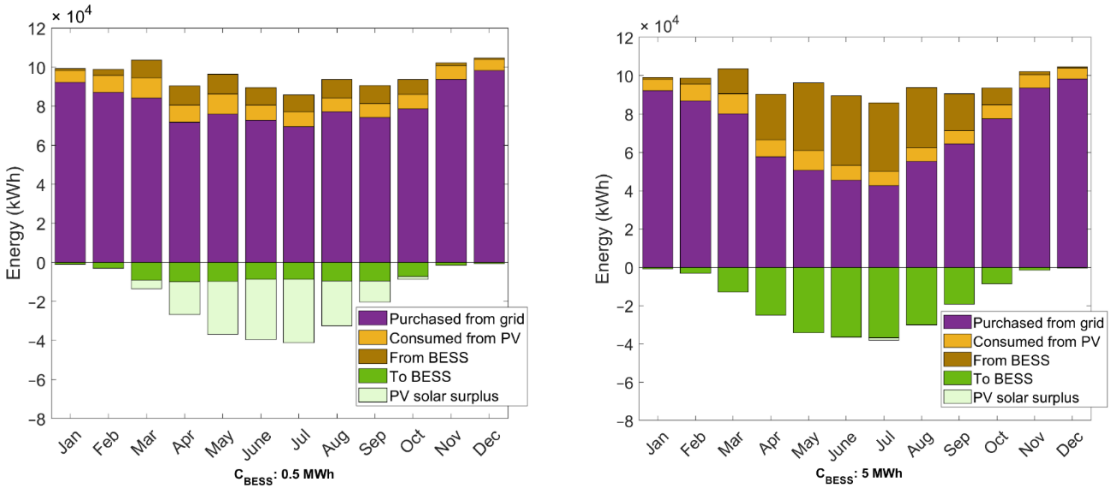

(a) (b)

Figure 6.3. "Monthly energy simulation results for scenario 2 using a BESS with a capacity of: (a) 0.5 MWh and (b) 5MWh. The positives values on each graph represent the energy consumption from the grid, from solar, either directly or via the BESS. The negative values indicate solar energy generation and energy storage in the BESS" (Figure obtained from [175]).

The use of a smaller BESS, such as the 0.5 MWh battery capacity, results in a lower portion of surplus solar energy being stored than in a larger BESS. In this case, the BESS can only store some of the generated excess solar energy, leading to a significant portion being sold back to

the grid, thereby failing to reduce grid dependency substantially. On the other hand, a larger BESS, like the battery with a capacity of 5 MWh, can store most of the surplus solar energy, reducing reliance on the grid. This is especially noticeable during the summer season when solar energy generation is at its peak, and the BESS capacity becomes the limiting factor. However, during winter months, when solar generation decreases, increasing the BESS size does not significantly reduce grid dependency. This is shown in more detail in Figure 6.5.

Figure 6.4 presents the annual energy demand drawn from the grid at different battery capacities. The analysis includes results for scenario 1 (No PV or BESS) for comparison with Scenario 2. As the BESS capacity increases, the energy drawn from the grid diminishes, as it can be seen by the declining purple line in the graph.

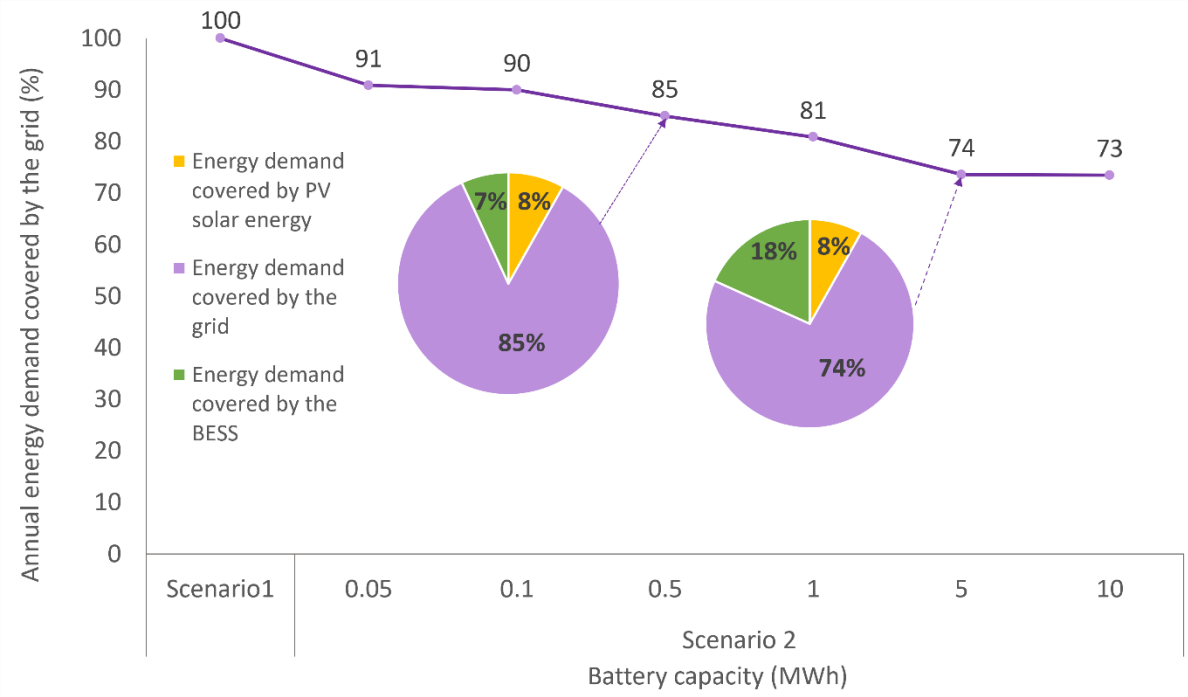

Figure 6.4. "Energy demand covered by the grid (purple line) for scenario 1 and scenario 2, and the breakdown of energy demand covered by the grid, by direct PV generation and by the solar via the BESS for C_{BESS} of 0.5 MWh and 5MWh as examples (pie charts)" (Figure obtained from [175]).

A comprehensive breakdown is provided for the two previously examined BESS capacities, namely 0.5 MWh and 5 MWh. At 0.5 MWh, there is a 15% reduction in energy demand from the grid. Specifically, the energy demand is distributed as follows: 85% is supplied by the grid, 8% is directly met through PV solar generation, and an additional 7% is fulfilled by the surplus solar energy stored within the BESS. In contrast, a 5 MWh BESS yields a more substantial 26% reduction in grid energy demand, with the following distribution: 74% of demand is met

by the grid, 8% is sourced directly from PV generation and a significant 18% is drawn from solar energy stored in the BESS. For a BESS with 10 MWh of capacity, a 27% reduction in grid supply is achievable, as it is constrained by the amount of PV generation rather than the size of the energy storage.

The hourly energy simulation outcomes for scenario 2 are depicted in Figure 6.5 illustrating a week in February (Figure 6.5a) and July (Figure 6.5b) with a BESS capacity of 5 MWh.

The BESS State of Charge (SoC) is displayed at the top of Figure 6.5 (indicated by the green line). In the middle, the energy consumption from the eRCV fleet is shown as a blue line. The bottom part of Figure 6.5 shows the hourly values of the modelled solar energy generation (in yellow), WMD energy demand (in orange), and energy purchased from the grid (in purple). The hours are denoted from "0", corresponding to the hour after 00:00h on Saturday morning, to "23", representing the last hour of the following Friday night. As it can be seen, the eRCV fleet is charged from Monday to Friday, aligning with the discussed usage patterns.

Taking Figure 6.5a as an illustration of a winter week, it becomes evident that the energy needed to fulfil the eRCV's requirements is entirely sourced from the grid. The benefits of incorporating on-site PV generation and a BESS are diminished compared to other seasons (as shown in Figure 6.5b), primarily due to significantly reduced PV generation in winter. However, in summer (Figure 6.5b), grid consumption decreases notably for the WMD building and the eRCV fleet. During weekends, the WMD operates independently from the grid, and the BESS becomes fully charged by storing surplus solar energy. As a result, the BESS accumulates enough energy to charge the fleet at night partially. On Mondays, the fleet's charging relies predominantly on the energy stored in the BESS from the PV generation over the weekend.

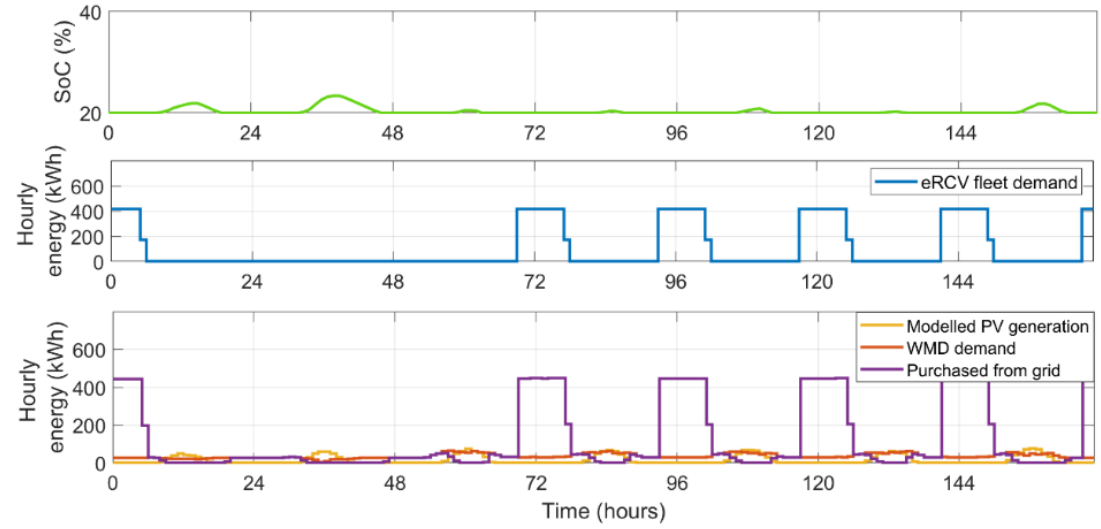

(a)

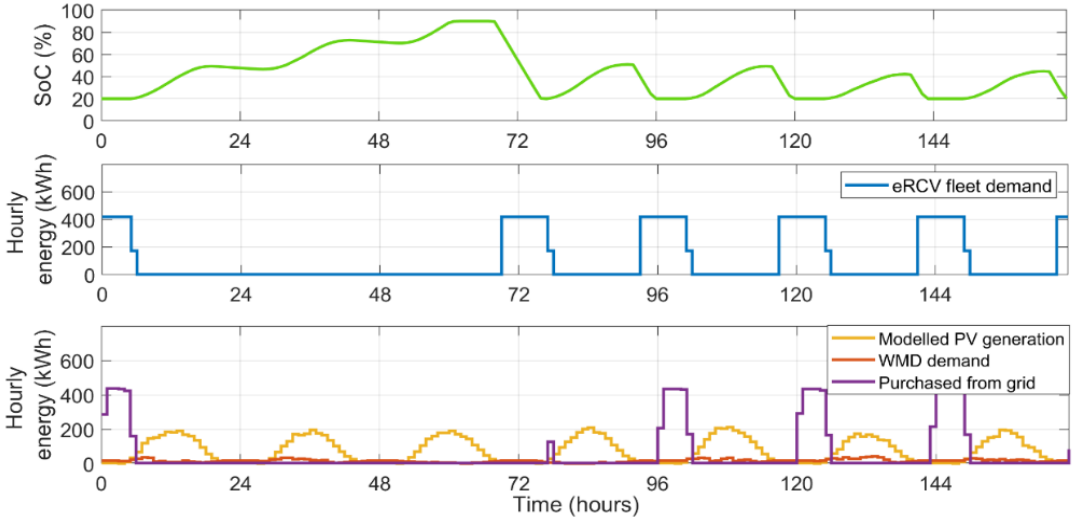

(b)

Figure 6.5. "Hourly energy distribution for scenario 2 with a BESS capacity of 5MWh in a week in (a); February and (b) July" (Figure obtained from [175]).

The lifetime costs for scenario 1, and for scenario 2 at different BESS capacities, have been calculated and are presented in Figure 6.6. The total costs are broken down into network costs, cost of energy, cost of BESS, and cost of PV panels. Additionally, for scenario 2, any surplus solar energy revenue has been deducted from the energy costs.

In Figure 6.6, the larger BESS capacities result in lower energy costs from the grid. Hence the introduction of a BESS and PV generation is justified to reduce the energy costs and grid dependency. However, when considering all amortized costs, including the BESS and PV panel costs, certain battery capacities are no longer economical for annual electricity cost reduction when compared to scenario 1.

Scenario 2 with a BESS of 1 MWh of capacity proves to be the most cost-effective, leading to a total cost reduction of £530,000 over the system's lifetime (i.e., 15 years) when compared to scenario 1.

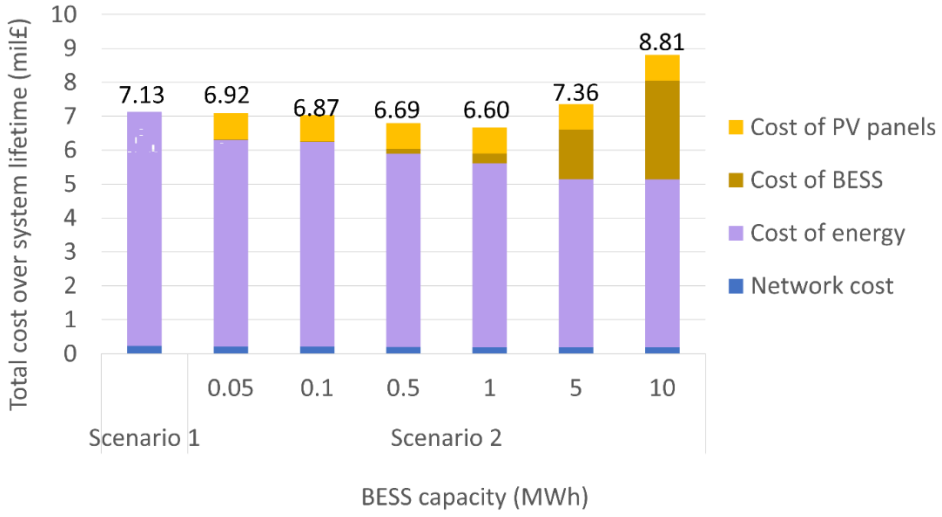

Figure 6.6. "Total cost over system lifetime for scenario 1 and scenario 2" (Figure obtained from [175]).

The detailed system costs for scenarios 1 and 2 at various battery capacities are presented in Table 6.2.

The energy cost, particularly for smaller BESS capacities, has the most significant impact on the total costs, ranging from 88% to 56%. For higher-capacity batteries (e.g., 5 MWh), the cost of the BESS (including capital cost and O&M cost) contributes between 20% and 33% to the total cost over the system's lifetime.

Table 6.2 also includes the network cost over the system's lifetime, encompassing all associated costs such as capacity, fixed, network upgrade, and consumption band costs. Exceeded capacity costs are excluded since the capacity connection is not exceeded in Scenario 1 or Scenario 2 for this specific case.

As can be seen in Table 6.2, the network cost decreases with increasing BESS capacity, with scenario 1 having the highest costs and scenario 2 with a 10 MWh BESS having the lowest. This reduction in network cost is due to the decrease in network consumption costs, as depicted in Figure 6.7.

Table 6.2. System cost at different battery capacities (C_{BESS}) for scenario 1 and scenario 2. The values in £ are included in Appendix B.

Power connection capacity (MW)	Scenarios		Cost of energy per year (k£)	Surplus solar energy revenue per year (k£)	BESS capital cost (k£)	BESS O&M cost (k£)	PV capital cost (k£)	PV O&M cost (k£)	Network cost over the system lifetime (k£)	Total cost over system lifetime (mil£)
0.6	Scenario1		460.4	0	0	0	0	0	222.4	7.13
	Scenario 2 (MWh)	0.05	407.2	11.1	12.7	1.9	629.1	135.3	203.4	6.92
		0.1	402.4	10.6	25.4	3.8			200.5	6.87
		0.5	379.5	7.3	127.0	18.8			194.2	6.69
		1	361.6	4.7	254.0	37.5			191.9	6.60
		5	330.0	0	1,270.0	187.5			191.2	7.36
		10	329.5	0	2,540.0	375.0			191.2	8.81

Figure 6.7 illustrates the network consumption cost per year for each consumption band in scenarios 1 and 2, for different BESS capacities. The contrast in red consumption band costs between scenario 1 and scenario 2, with a 0.05 MWh BESS capacity, is significant as the costs decrease by 43%. However, for BESS capacities larger than 0.5 MWh, the cost reduction for the red band consumption remains constant at 57%. Most of the decrease in the red band occurs during summer, when there is sufficient stored solar energy in the BESS to be used by the system during the red band period, eliminating the need for grid energy in this period. In contrast, insufficient PV generation in winter hinders any reduction in red band consumption, regardless of the BESS size.

The costs related to the amber band also decreased in scenario 2 compared to scenario 1. Larger BESS capacities exceeding 0.5 MWh can further reduce the costs associated with the amber band. This effect stems from the amber band occurring later in the day compared to the red band. Consequently, larger BESS capacities are particularly effective in prolonging the period during which excess solar energy is supplied to the system, resulting in a more significant reduction. The same holds for the costs linked to the green band, which only decrease with BESS capacities over 1 MWh, as these are capable of storing enough excess solar energy to meet the demand during the start of the evening period when the green band is active.

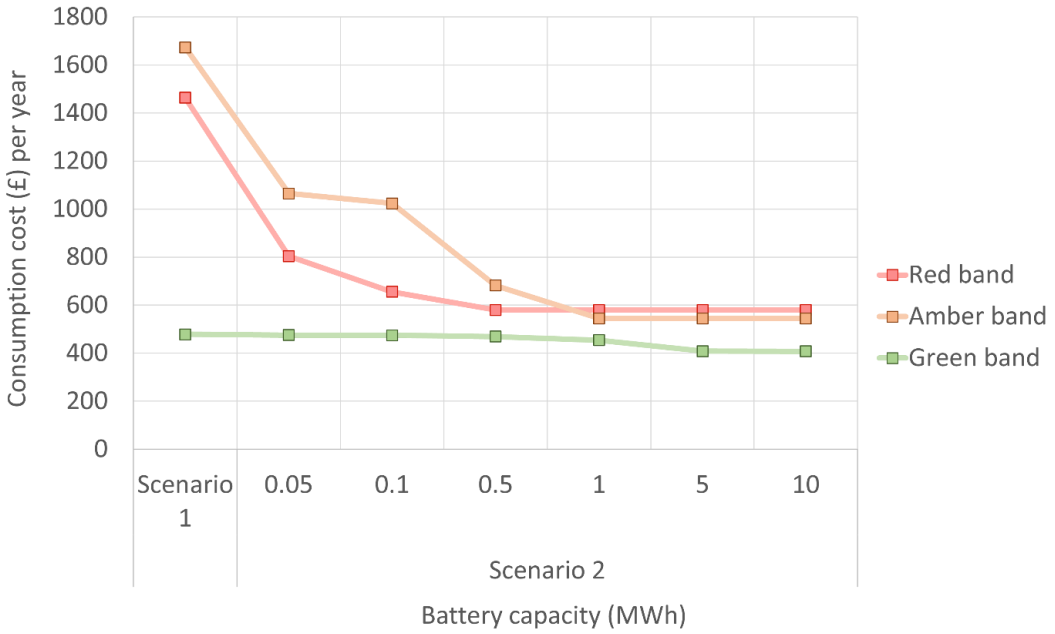

Figure 6.7. "Network consumption cost per year for scenario 1 and scenario 2" (Figure obtained from [175]).

In summary, the analysis conducted for scenarios 1 and 2 indicates that introducing PV panels and a BESS can yield economic benefits for logistics or commercial company when a fleet is electrified and consequently, the energy demand on site proportionately increases.

The algorithm applied in scenario 2 effectively fulfils its objective of reducing grid consumption during peak electricity and network price periods, leading to a total cost reduction of approximately £530,000 over the system's lifetime when PV panels and a BESS of 1 MWh are implemented, when compared to scenario 1.

Next, the study examines the outcomes for scenario 3 for comparison with scenario 1. Due to the constraint set on the algorithm developed for scenario 3 (the power capacity connection at the WMD cannot be upgraded upon electrification of the fleet, resulting in the grid connection remaining fixed at 0.15 MW), and in order to successfully compare this with scenario 1, the power connection for scenario 1 is also assumed to remain at 0.15 MW.

6.3.2 Economic implications of installing PV panels and BESS when there is a grid connection constraint.

This section is dedicated to examining a significant hurdle logistics, and commercial companies face when transitioning to an electrified fleet, namely the considerable increase in on-site energy demand coupled with a constrained grid power connection.

The hourly energy distribution for scenario 3, with a BESS capacity of 5 MWh, is depicted in Figure 6.8 for both a week in February (Figure 6.8a) and a week in July (Figure 6.8b). The figure illustrates the BESS State of Charge (SoC) at the top (green colour), the hourly energy consumption from the eRCV fleet below (blue line), and at the bottom, the hourly modelled PV generation, the WMD energy demand, and the energy purchased from the grid. As before, the first point in Figure 6.8 corresponds to a Saturday at 00:00h, and the last corresponds to a Friday at 23:00h.

Upon initial examination, it becomes apparent that the BESS with 5 MWh cannot maintain the power capacity connection within the initial constraint (i.e., 0.15 MW). This is evidenced in Figure 6.8a through the hourly energy purchased from the grid (purple line).

Throughout the winter months, the BESS gets fully charged from the grid on weekends (when the eRCV fleet does not operate) due to reduced PV generation at this time of the year. This ensures that the system avoids surpassing the power connection capacity during the initial days of the week (i.e., Monday to Wednesday). However, the BESS is not large enough to prevent exceeding the power connection capacity in order to successfully charge the eRCV fleet for the remaining days of the week.

During summer (as shown in Figure 6.8b) the system relies less on the grid to charge the BESS, and more importantly, the BESS can prevent exceeding the contracted power connection capacity with the grid network. At this time of the year, the PV solar energy generation is at its highest, and it maximises the potential of having PV panels and a BESS installed.

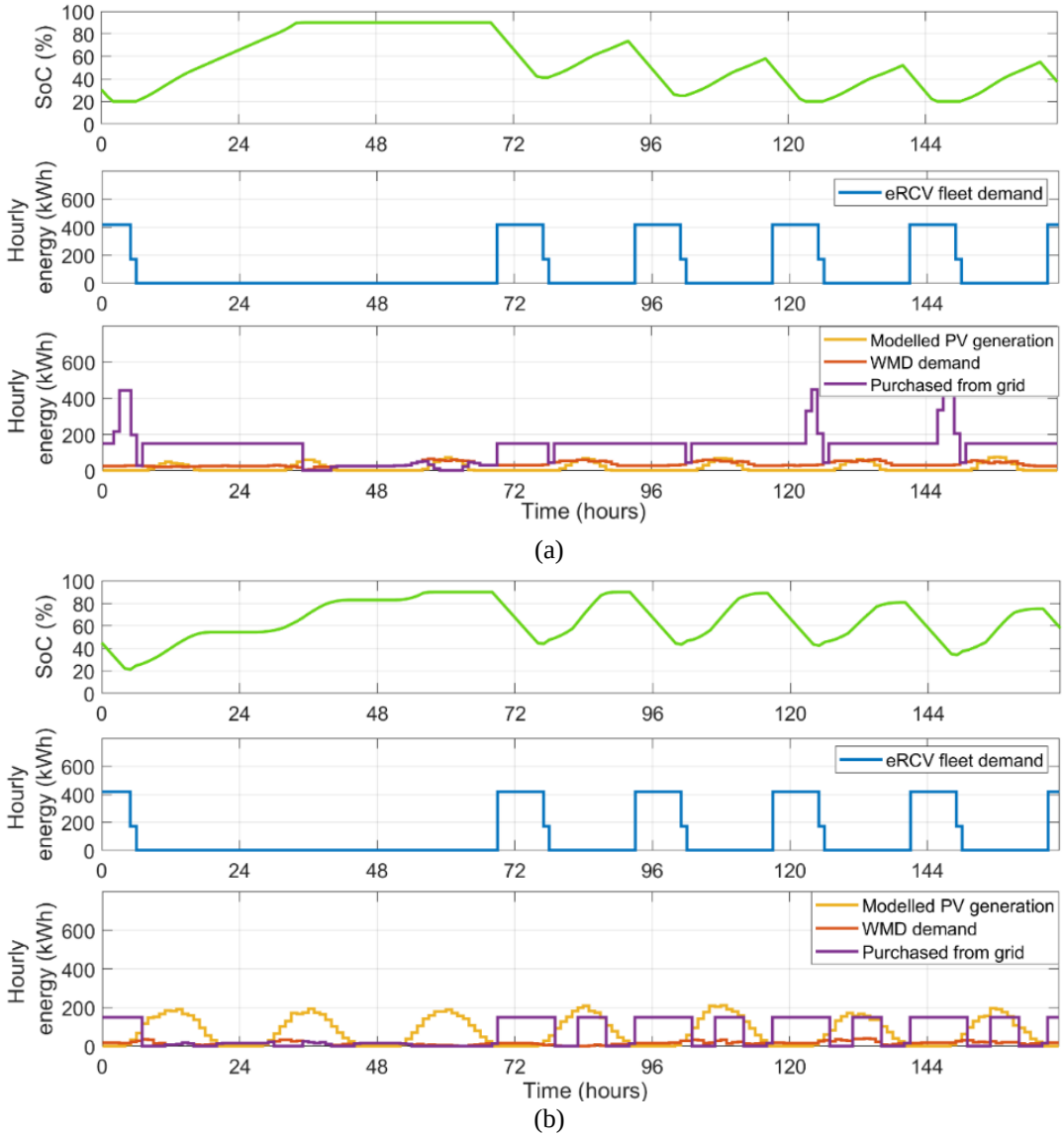

Figure 6.8. "Hourly energy distribution for scenario 3 with a BESS capacity of 5 MWh in a week in (a) February and (b) July" (Figure obtained from [175]).

Since the algorithm designed for scenario three did not meet the constraint set with a BESS of 5 MWh, a larger BESS of 10 MWh was analysed in the simulation. The outcomes are depicted in Figure 6.9. With a 10 MWh BESS, the system successfully maintains the power connection capacity within the contracted rating during winter (Figure 6.9a) and summer (Figure 6.9b).

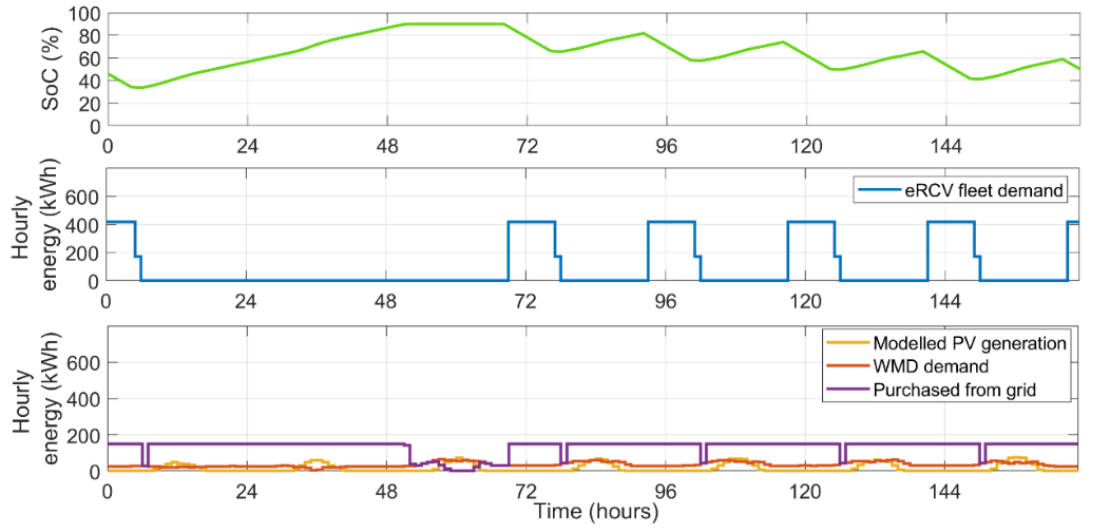

(a)

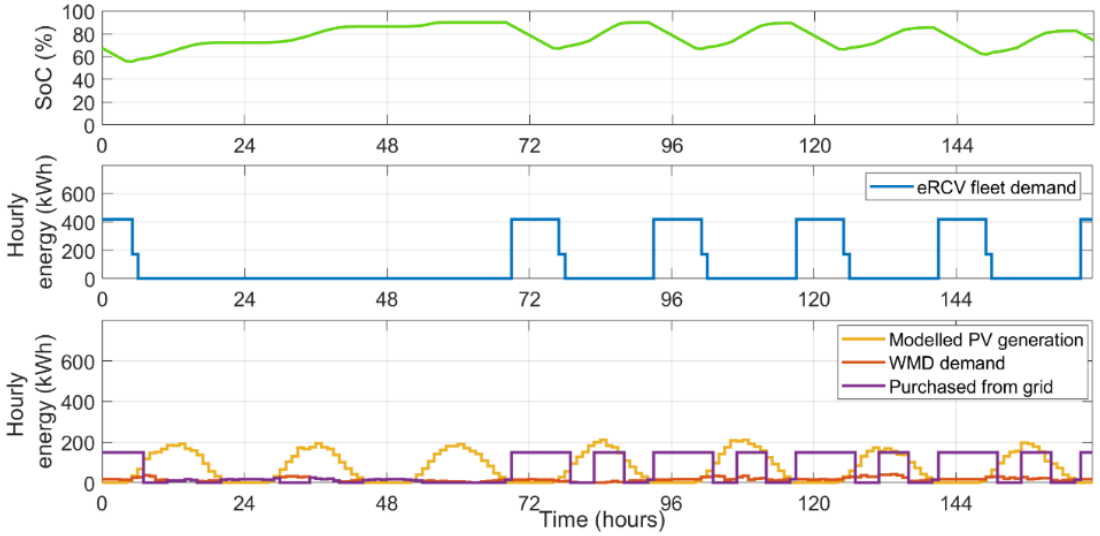

(b)

Figure 6.9. "Hourly energy distribution for scenario 3 with a BESS capacity of 10 MWh in a week in (a) February and (b) July" (Figure obtained from [175]).

In winter (Figure 6.9a), the BESS is fully charged over the weekend, storing higher energy than the smaller BESS. This stored energy is enough to supply the eRCV fleet throughout the week, eliminating the need for power connection upgrades. The BESS reaches full charge on Monday and is discharged to around 20% of its state of charge (SoC) by Friday. It is important to note that the system requires an almost continuous grid supply to achieve the algorithm's objective. On Saturday morning, the BESS is nearly fully discharged when the eRCV fleet has been completely recharged the previous night. Conversely, in summer (Figure 6.9b), the BESS starts the week almost fully charged, and it is only discharged to approximately 60% of its capacity by the end of the week.

Figure 6.9 illustrates certain limitations in the algorithm, which could be further improved and serve as potential future work. For example, the energy purchased from the grid in summer could be optimised considering the BESS is not discharged below 50% SoC. The algorithm is set to receive the energy from the grid at the maximum connection power capacity, but in summer, it can be reduced and by doing so, the cost of energy would also be reduced too. Furthermore, the simulation outcomes depicted in Figure 6.8b and Figure 6.9b highlight that some on-site solar energy generation remains untapped. Specifically, approximately 10% and 13% of PV energy generated is sold back to the grid with a BESS capacity of 5 MWh and 10 MWh, respectively. As can be seen in both figures, on Monday, when the PV installation starts to generate solar energy, the BESS is almost fully charged, and therefore the solar energy has to be sold to the grid.

Table 6.3 presents the estimated total cost over the system lifetime for Scenario 1 and Scenario 3. The results indicate that installing PV panels and a BESS reduces the energy cost compared to scenario 1. Additionally, network costs are significantly lower in scenario 3 compared to scenario 1. Specifically, with PV panels and a BESS of 5 MWh or 10 MWh on-site, network costs decrease by approximately 75% and 82%, respectively. This highlights one of the key benefits of using a BESS for fleet electrification: it enables increased energy demand without exceeding the grid connection power capacity and incurring additional associated costs. For this particular scenario, only a 10 MWh BESS can maintain the grid connection power capacity at its original value (i.e., 0.15 MW). However, it is essential to note that when considering all amortised costs, system's lifetime total cost does increase significantly when the BESS and the PV panels are installed.

Table 6.3. System cost for scenario 1 and scenario 3 (with a BESS of 10 MWh). The values in £ are included in Appendix B.

Power connection capacity (MW)	Scenarios		Cost of energy per year (k£)	Surplus solar energy revenue per year (k£)	BESS capital cost (k£)	BESS O&M cost (k£)	PV capital cost (k£)	PV O&M cost (k£)	Network cost over the system lifetime (k£)	Total cost over system lifetime (mil£)
0.15		Scenario1	460.4	0	0	0	0	0	908.9	7.8
	Scenario 3 (MWh)	5	421.8	2.1	1,270	187.5	629.1	135.3	231.9	8.8
		10	427.5	1.8	2,540	375.0			167.9	10.2

6.3.3 Feasibility assessment of PV panels and BESS implementation for electrifying freight fleet.

A comprehensive examination of the economic viability of integrating PV panels and a BESS into the freight fleet electrification process has been conducted between scenario 1, including power capacities of 0.15 MW and 0.6 MW, scenario 2 (i.e., 0.2 MW) and scenario 3 (i.e., 0.15 MW). For scenario 2, a BESS with 1 MWh capacity yielded the most significant cost reduction over the system's lifetime, so it has been the one considered for the analysis. Alternatively, a BESS of 10 MWh capacity has been chosen for the analysis to ensure compliance with the contracted grid connection power constraint.

Figure 6.10a compares total costs over the system lifetime for each scenario. As can be seen, Scenario 2, which involves PV panels and a BESS installation on site, emerges as the most viable option in terms of cost-effectiveness. The aim of scenario 2 is to reduce grid consumption during peak price periods, considering that the introduction of the electric fleet increases the electricity demand of the site considerably. When analysing Figure 6.10a, it becomes evident that upgrading the power connection is more cost-effective than investing in a larger BESS if the connection capacity is not constrained at the site.

However, if the upgrade of the power connection capacity is not an option for the logistics or commercial company (i.e., 0.15 MW), it would still be worth further exploring the potential benefits of introducing PV panels and a larger BESS. This ensures that the system can meet the increased energy demand without exceeding the power capacity of the grid connection. The comparison between scenario 1 and scenario 3 for the same power capacity (i.e., 0.15 MW) reveals the advantages of introducing a 10 MWh BESS in reducing the excess capacity charge incurred by the site from around £0.8M to zero (Figure 6.10b). Nonetheless, the economic feasibility of this option remains challenging due to the high cost of the large BESS as shown in Figure 6.10a (scenario 3). Despite the decreasing cost of energy storage technology in recent years [309,310] and with cost projections indicating a further potential reduction in capital cost by 2030 [300], BESS cost is still a major barrier to these systems.

If the logistics or commercial company has no intention of installing PV panels and a BESS (i.e., scenario 1), upgrading the power capacity connection could result in a considerable cost reduction of around £680,000 over the system's lifetime.

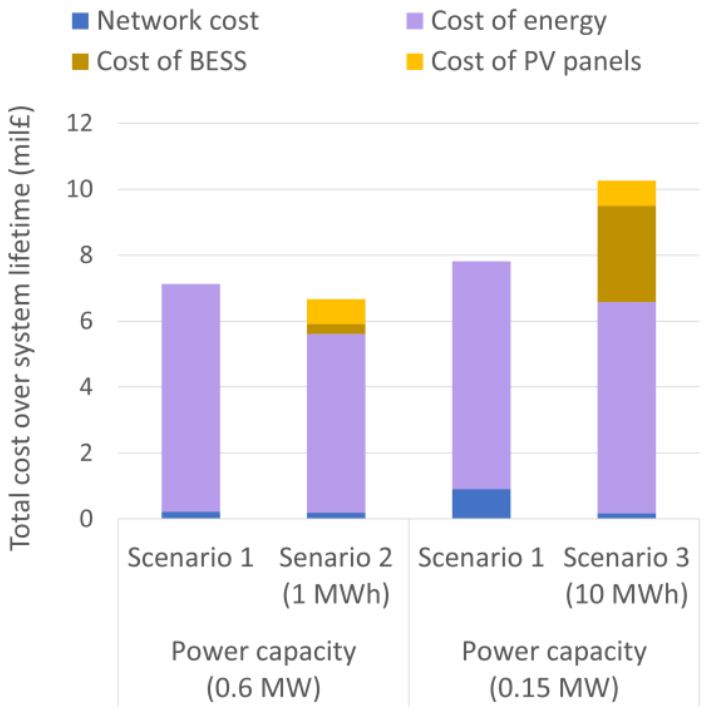

(a)

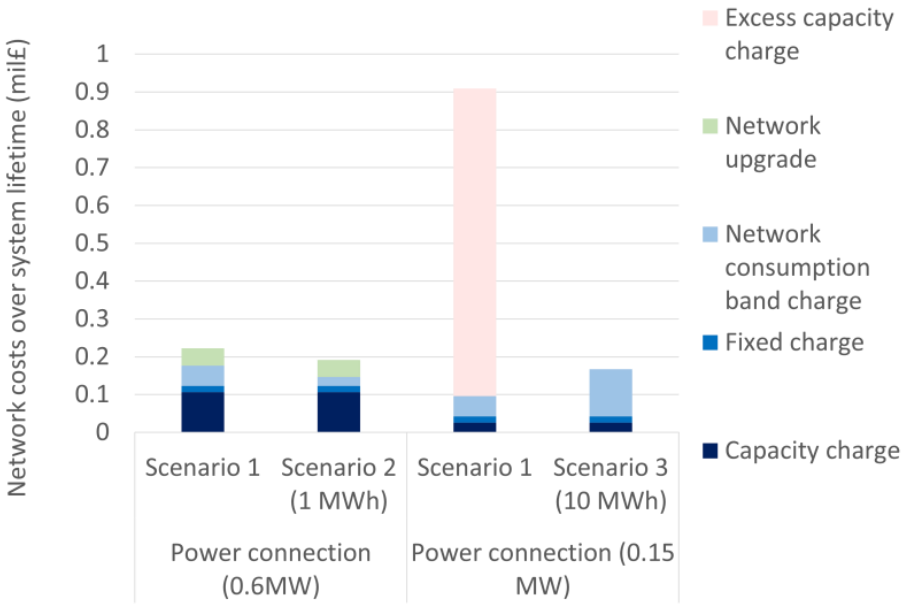

(b)

Figure 6.10. Top graph (a): Comparison of system's lifetime total cost between the three scenarios Bottom graph (b): Comparison of the network cost over system lifetime [175].

6.4 Summary

This chapter aims to answer the final research question: *To what extent, can solar energy and BESS ease the power capacity constraints when it comes to EV fleet electrification?*

There are not many references in literature addressing this challenge, together with renewable energy generation and a BESS. Moreover, publications tend to address the issue through charging schedule adjustments. However, in real life, this would imply a change in operational requirements, and may not be feasible in practical settings.

In that regard, the chapter aimed to assess cost impacts when a company electrifies its fleet, focusing on two priorities. The first is avoiding grid use during peak price periods necessitating power connection upgrading (Scenario 2). The second is avoiding power connection upgrades which may lead to excess capacity charges (Scenario 3). These priorities mirror real challenges logistics and commercial companies face during fleet electrification, influenced by operational needs or technical limitations.

For that purpose, this chapter evaluates three different scenarios. For all scenarios, it is assumed that the fleet has been electrified. Scenario 1 is characterised by being 100% dependent from the grid. In contrast, scenario 2 and scenario 3 have PV panels and a BESS installed. However, in scenario 3 a technical constraint prevents power capacity connection upgrades. The energy distribution for scenarios 2 and 3 is controlled by two rule-based energy management algorithms.

According to the findings, scenario 2 with a 1MWh BESS is the most cost-effective, resulting in a potential lifetime cost reduction of £530,000. It has been demonstrated that the presence of PV panels and a BESS on-site proves beneficial for all explored scenarios, regardless of whether the goal is to minimize grid dependency during peak times or avoid power connection upgrades.

At times, the upgrade of the power connection is not an option for different reasons outside the company's control (i.e., WMD in this case). Under these circumstances, if the grid connection power capacity is surpassed, the system incurs additional costs due to excess capacity charge. It has been demonstrated that under these circumstances, a 10 MWh BESS effectively fulfils energy requirements without surpassing the contracted grid connection power capacity. However, considering all amortized costs, using PV panels and the required 10 MWh BESS

becomes unfeasible, as the BESS cost outweighs the potential benefits. Further improvement is required for the algorithm developed under the grid connection power constraint, and forms part of future research. One area of improvement is optimising energy purchased from the grid during summer, where the BESS remains above 50% State of Charge (SoC). Adjusting the algorithm to reduce grid energy intake during summer can lower energy costs. Additionally, simulation results indicate that a portion of PV generation remains unused, with approximately 10% to 13% of PV energy being sold to the grid when a 5 MWh and 10 MWh BESS are installed, respectively. Finally, future research will consider the battery degradation in the economic cost analysis.

Having addressed all the research aims and research questions introduced previously in Chapter 1 and Chapter 2 respectively, the following final chapter will focus on highlighting the main findings of the thesis, as well as discussing future research opportunities.

7 Conclusions and Future work

The previous chapters of this thesis have developed and presented key insights on the feasibility of using locally generated solar energy, supported by a Battery Energy Storage System (BESS), for the adoption of EV fleets in commercial and logistics situations. This final chapter summarises the findings of the study and identifies potential limitations and areas for improvement, paving the way for future work and further research. By addressing the study's implications and outlining avenues for further explorations, this chapter sets the stage for continued progress and development in the subject of solar energy integration and BESS use, in both commercial and logistics operations, to support EV fleet adoption.

7.1 Overview of findings and discussions

To combat climate change, the UK aims for net-zero carbon emissions by 2050. In this context, the transport sector remains the primary source of GHG emissions in the UK, and hence its decarbonisation is required to achieve the UK’s legal pledge. Road freight transport has been proven to have negative environmental and air quality impacts. Furthermore, the efficiency measures adopted to date have shown limited impact on tackling GHG emission, and the sustainability of short-term alternatives to petroleum-based fuels is still being questioned. In the pursuit of decarbonising road freight transport, electrification emerges as a promising solution. In this regard, battery electric vehicles (BEVs) play an important role in eliminating tailpipe emissions and noise pollution and improving air quality. This is a mature technology that has been proven to be a feasible solution for the path towards a net-zero future. However, the benefits of road freight transport electrification can only be fully realised if the power grid successfully undergoes decarbonisation. Therefore, using renewable energies is crucial, and this was the subject of this thesis.

Unfortunately, the UK's power grid will not achieve complete decarbonisation until 2050. To this end, the main research question in this study was to investigate the feasibility of using on-site solar energy generation and energy storage for EV fleet charging at the depot, considering operational and technical constraints. This was achieved through an examination of the energy usage, and potential generation at two different commercial premises and a fleet of 19 electric refuse collection vehicles (eRCVs). Considering the pragmatic philosophical position adopted to overcome the main research question, the thesis proposed a methodology characterised by its practicality in real-life scenarios.

Initially, chapter 1 served as an introduction to contextualise the research problem and the motivation for undertaking the presented work. Above all the measures set to reduce the GHG emissions from road freight transport, electrification serves as a short-term solution and a potential alternative towards a net-zero emissions future. It was shown, however, that as long as the grid is not completely decarbonised, EVs have a significant impact on emissions resulting from charging with energy that is not generated from renewable sources.

Chapter 2 was dedicated to the review of the existing literature. In the beginning, a review of the GHG emissions from transportation worldwide, and more specifically from road freight transport in the United Kingdom, was conducted. Next, the literature review focused on the electrification of road freight transport, comparing past, present and future GHG emissions when the fleet is charged from the grid mix and renewable sources. Additionally, in Chapter 2, the state of the art of electric freight fleet charging has been looked at, along with the most known charging patterns and charging infrastructure used by road freight fleets. Moreover, a critical review was performed, examining the most recent publications concerning power and transport system integration. Finally, the literature review revealed that specific questions concerning the depot-based charging of freight fleets using renewable energy had yet to be answered. These are the following:

I. What are the environmental and economic benefits of using solar energy and BESS to charge an electric freight fleet when logistic and operational constraints are considered?
II. When using solar energy and BESS, what are the impacts on the grid network and consequently, GHG emissions, when different charging strategies are applied?
III. To what extent, solar energy and BESS can ease the power capacity constraints when it comes to EV fleet electrification?

In Chapter 3, a new solar model was developed. Throughout the development stage of the empirical solar model, it was necessary to create new empirical solar correlations based on solar radiation data measured close to the place where the simulation would be carried out. Considering this, three solar correlations were created for different locations in England. The model presented in this chapter aimed at providing accurate estimations of solar energy availability at specific sites within the UK. This model is considered essential in pursuing answers to all the research questions. The efficacy of the proposed solar model is demonstrated throughout result validation. In fact, the solar model is successfully implemented in a case study performed for a company in the manufacturing industry [43].

The other part of the proposed system to charge EV freight fleets with renewable energy corresponds to using a battery energy storage system (BESS). The use of a BESS supports on-site solar energy generation and maximises its benefits when it comes to EV freight fleet charging. In this regard, chapter 4 focused on evaluating the impact of introducing a BESS on the system's energy use. This has been achieved via an algorithm implemented in the MATLAB/Simulink environment. To that end, the approach has been demonstrated in two commercial premises, a waste management depot (WMD) and a M&S retail store. The intentions of selecting these two premises relied on having a broader knowledge of how different factors such as energy demand, PV solar energy generation, or other technical constraints impact the outcomes achieved when the BESS is in place. Therefore, understanding how different commercial premises react to introducing a BESS regarding costs, grid dependency, and GHG emissions was essential to progress with the study, more precisely to better understand how the system reacts to the adoption of EV fleets. The results from the WMD showed important reductions in total costs, grid dependency and GHG emissions. Contrary to the WMD, the M&S retail store's introduction of PV panels and BESS is not economically feasible. Moreover, the on-site solar energy generated on M&S premises proved inadequate even for fulfilling their internal energy requirements, which make the use of solar energy unfeasible to support EV fleet charging.

A fleet of 19 electric refuse collection vehicles (eRCVs) is explored for the WMD in Chapter 5, in a system governed by an energy management algorithm that prioritises the use of solar generated energy, with the support of the BESS, to cover as much of the energy demand as possible. The findings and results presented in this chapter answer research questions I and II. The operational constraints and the logistic aspects are considered for the three simulated charging strategies. The outcomes from the algorithm show that specific charging strategies maximise the use of solar energy. Thus it directly impacts the reduction of grid dependency, total cost of ownership and GHG emissions. Overall, results conclude that using local solar energy generation and a BESS on site is economically feasible when a logistics or commercial company electrifies their fleet, with similar characteristics as the WMD. This conclusion is supported by comparing the system proposed, characterised by the use of on-site solar energy generation supported by a BESS, against a hypothetical scenario in which the premises studied does not have PV solar panels installed nor a BESS but wishes to switch it’s refuse collection vehicles to an electrically powered eRCV fleet.

Chapter 6 analyses the feasibility of adopting EV fleets into commercial depots considering the use of solar energy supported by a BESS but considering one of the logistics and commercial companies' most claimed technical constraints, the power capacity connection. Therefore, the findings and results obtained from this chapter are focused on answering research question III. In order to address the power constraint issue, a new energy algorithm is developed. The algorithm aims to keep the power connection at the maximum allowed with the help of the BESS, charged not only with surplus solar energy but also with energy from the grid. The most common charging pattern used amongst logistics and commercial companies is chosen for the analysis, overnight charging. The results show that if the upgrade of the network power connection is not an option, a 10 MWh BESS, in this case, effectively fulfils energy requirements without surpassing the contracted grid connection power capacity. However, other strategies, such as smart charging, must be implemented with the BESS to make it an economically viable option. Few references in the literature address this challenge, and those published tend to solve the issue by modifying the charging schedule. Nevertheless, implementing such adjustments in practical scenarios could necessitate a shift in operational requirements, often proving unfeasible or undesirable.

7.2 Key findings and wider applicability

Overall, the findings presented in this thesis suggest that from an economic point of view, it is feasible to use local solar energy generation and a BESS on-site in various logistics or commercial settings to support fleet vehicle electrification, for example, the local authority WMD. Moreover, the modelling methodologies developed, and the findings obtained offer valuable guidance with regards to required solar energy generation and BESS capacity that is applicable to various types of EV fleets deployed in urban and commercial settings operating daily planned routes. Similar benefits can also be anticipated by extrapolating the principles of on-site solar energy generation and energy storage for EV fleet charging, as explored in this thesis, to different commercial EV fleets, such as electric bus fleets or short-haul road freight fleets that are growing in popularity.

The generation of on-site solar energy and the use of a BESS allows the system to reduce its dependency on the grid, to a greater or lesser extent depending on the charging strategy used, for all the scenarios analysed when the power connection capacity is not constrained. According to the results presented, using solar energy and BESS in a commercial or logistics company empowers businesses in multiple ways. It enables them to achieve energy

independence, reduce utility costs, and contribute to a greener future by minimizing their carbon footprint and promoting sustainable practices in their operations.

Additionally, this integration alleviates the strain on the grid infrastructure. Businesses mitigate the system's pressure and promote grid stability by reducing their reliance on the grid during peak demand periods. Consequently, the GHG emissions associated with the overall facility are reduced. This dual benefit highlights the significant role that solar energy and BESS play in enhancing both economic and environmental sustainability for commercial and logistics operations.

7.3 Future work

While the results presented in this thesis enhance the feasibility of incorporating solar energy supported by a BESS in the electrification of commercial and logistics company fleets, and its relevance towards a more sustainable present and future, numerous prospects for further research remain open. Potential future work could concentrate on refining the solar model and energy management systems proposed and delving deeper into the investigations described. Additionally, new concepts, such as Vehicle to Grid (V2G), could be introduced based on the presented findings, and further analysis could be conducted by comparing different fleets with different operational requirements to introduce greater intricacy into the evaluations. This opens avenues for optimising the existing framework and exploring innovative approaches to broaden the understanding of solar energy adoption and BESS implementations in commercial and logistics fleets.

7.3.1 Solar model

The solar model is based on empirical correlations to estimate the components of solar irradiation on inclined surfaces. The same approach is used for the development of programmes available online to estimate solar energy production. However, the particularity of the presented solar model is that it uses ground measurement data measured in different locations in the UK to create the empirical correlation. Thus, it adds extra accuracy to the estimations based on the UK. However, the solar model has been initially developed for commercial and logistics premises and therefore has some limitations.

First, the depots are placed on the city's outskirts and are rarely surrounded by buildings or vegetation close enough to create shadows on the rooftop. Other sites, such as private homes or city centre commercial buildings, may be more compromised, for which the solar model would require further development. Moreover, the depots are characterised by inclined roofs in which the PV panels are typically installed at the rooftop tilt angle to reduce installation costs. Such an arrangement avoids the generation of shadows between PV panels. Considering all those facts, the solar model developed in this thesis did not provide accurate estimations on shadowing. Instead, it assumes that 20% of the measured rooftop area is not available due to possible shadows, skylights, or more considerable hurdles such as, for example, AC units. Secondly, the solar model estimates hourly values of solar energy generation according to the periodicity of the input data measurements. Future work aims to reduce the time steps of the simulations and provide the model with tools to accurately estimate shadows or area spaces where PV panels cannot be installed.

7.3.2 Energy management algorithm

The energy management systems developed in the thesis are based on algorithms built in the form of “if”/”else” statements. This approach for developing algorithms is also commonly known as the rule-based approach. It is characterised for being simple to integrate [291] and it has been proven a successful approach when applied to PV+BESS systems previously by other authors [290,292,293] as discussed in Chapter 4. Moreover, the results obtained from each energy management system created in this thesis have served as a primary source of data for analysing the parameters explored.

Future work aims at implementing new strategies for more efficient energy distribution. The reason behind this is to reduce further the costs from the grid by maximising both the use of PV panels and BESS. For example, in Chapter 4, the algorithm developed for the M&S retail store connects the BESS with the PV installation and the grid. The store consumes significant amounts of energy, and most of the solar energy produced is directly consumed by the store. Since, in that scenario, the BESS would be empty most of the time because there is only a small quantity of solar surplus available, it is connected to the grid to benefit from lower energy prices. However, during certain months, particularly in summer, the small amount of solar surplus is not all stored because, by this time, the BESS has already been fully charged from the grid. The objective is to create a new strategy so that the BESS receives energy from the

grid only if no surplus solar is available. That way, the benefit of having solar energy produced on-site is maximised, and less electricity is bought from the grid. At the same time, the grid dependency can be further reduced.

Similarly, potential improvements are envisaged for the algorithm developed in Chapter 6 under the grid connection power constraint. In this case, the algorithm's main aim is to keep the power connection capacity below its maximum value, and that is achieved by the use of a BESS. However, future work aims at optimising the energy purchased from the grid in summer. During this time, the BESS is not discharged below 50% SoC. The algorithm is set to receive the energy from the grid at the maximum connection power capacity, but in summer, this could be reduced and by doing so, the cost of energy would also be reduced.

On the other hand, when the BESS is not connected to the grid, simulation results show that the BESS in winter is never fully charged due to the limiting factor of solar energy generation. In this situation, the system will benefit from an algorithm that, in winter periods or on days when there is no solar surplus, would be able to connect the BESS with the grid at lower energy prices, thus maximising the benefits of using cheaper energy when the prices are above the threshold.

This all requires certain modifications to the energy management algorithm that are worth exploring as future work, considering the benefits that could bring on the total cost of ownership, grid dependency and GHG emissions.

7.3.3 Other considerations

One of the constraints added to the algorithm when modelling the BESS accounts for the charging and discharging rate at maximum power. This limitation aligned with the recommendations provided in various Lithium-based cell datasheets to prevent rapid cell degradation. However, based on the calculation of the total cost of ownership, battery degradation was not considered in the economic analysis. Thus, future work aims at addressing the costs associated with battery degradation due to its relevance to the total cost of ownership.

On the other hand, the issue associated with the power capacity connection has been explored by considering purely overnight charging strategies. Future work could explore the issue when the EV fleet is charged with a different charging pattern. Moreover, according to cost

projections on BESS, future research could benefit for looking at smaller connection upgrades and different BESS sizes to find the best compromise. By doing so, it will be possible to construct a broader set of conclusions regarding the power connection issue considering commercial or logistics companies with different operating schedules.

Due to the characteristics of the eRCV fleet studied in the thesis, certain solutions have not been considered, such as V2G technology. This is incompatible with the operational requirements associated with the eRCV fleet, where all the eRCVs have to be charged simultaneously. Furthermore, due to technical constraints related to the size of their batteries, they require all of the available "off" time to recharge. Future work aims to consider V2G solutions in situations where the EV fleet may be available to support the grid during the high-use period by expanding the study to EV fleets that operate non- simultaneously.

8 References

[1] Committee on Climate Change. Sixth Carbon Budget - The UK's path to Net Zero 2020:1–448. https://www.theccc.org.uk/publication/sixth-carbon-budget/ (accessed April 13, 2023).

[2] UNFCCC. The Paris agreement 2015:492–505. https://unfccc.int/process-and-meetings/the-paris-agreement (accessed April 13, 2023).

[3] Great Britain. Climate Change Act 2008 (2050 Target Amendment) Order 2019 2008:1–104. https://www.legislation.gov.uk/ukpga/2008/27/introduction (accessed April 13, 2023).

[4] BEIS. 2021 UK Greenhouse Gas Emissions , Final Figures Statistical Release 2023. https://www.gov.uk/government/statistics/final-uk-greenhouse-gas-emissions-national-statistics-1990-to-2021 (accessed April 13, 2023).

[5] Department for Business Energy and Industrial Strategy, Department for Energy Security and Net Zero. "2021 UK greenhouse gas emissions: final figures - data tables." 2023.

[6] DfT. Data on energy and environment from transport. Statistical data set: Energy and environment (TSGB0308) 2022. https://www.gov.uk/government/statistical-data-sets/tsgb03.

[7] DfT. Transport and environment statistics 2022 2022. https://www.gov.uk/government/statistics/transport-and-environment-statistics-2022/transport-and-environment-statistics-2022 (accessed November 18, 2022).

[8] Transport & Environment. How to decarbonise the UK's freight sector by 2050. 2020.

[9] Ballantyne E, Heron G. Can transport operator schemes deliver regional sustainability benefits? The case of the UK Northern powerhouse region. Sustainability (Switzerland) 2020;12:1–14. https://doi.org/10.3390/su12041662.

[10] Leach F, Kalghatgi G, Stone R, Miles P. The scope for improving the efficiency and environmental impact of internal combustion engines. Transportation Engineering 2020;1:100005. https://doi.org/10.1016/j.treng.2020.100005.

[11] Woodburn AG. A logistical perspective on the potential for modal shift of freight from road to rail in Great Britain. International Journal of Transport Management 2003;1:237–45. https://doi.org/10.1016/j.ijtm.2004.05.001.

[12] Tob-Ogu A, Kumar N, Cullen J, Ballantyne EEF. Sustainability intervention mechanisms for managing road freight transport externalities: A systematic literature review. Sustainability (Switzerland) 2018;10. https://doi.org/10.3390/su10061923.

[13] Pan S, Ballot E, Fontane F. The reduction of greenhouse gas emissions from freight transport by pooling supply chains. Int J Prod Econ 2013;143:86–94. https://doi.org/10.1016/j.ijpe.2010.10.023.

[14] Madhusudhanan AK, Ainalis D, Na X, Garcia IV, Sutcliffe M, Cebon D. Effects of semi-trailer modifications on HGV fuel consumption. Transp Res D Transp Environ 2021;92:102717. https://doi.org/10.1016/j.trd.2021.102717.

[15] King Julia. The King review of low-carbon cars Pt. 1., The potential for CO2 reduction. 2007.

[16] European Environmental Agency -EEA. Reducing greenhouse gas emissions from heavy-duty vehicles in Europe. EEA Briefing No 15/2022 2022:1–11. https://www.eea.europa.eu/publications/co2-emissions-of-new-heavy (accessed April 13, 2023).

[17] Mckinnon A. Decarbonizing Logistics: Distributing goods in a low-carbon world. Kogan Page Limited; 2018.

[18] Rail Partners. Freight Expectations: How rail freight can support Britain’s economy and environment. 2023.

[19] Monios J. Integrating intermodal transport with logistics: a case study of the UK retail sector. Transportation Planning and Technology 2015;38:347–74. https://doi.org/10.1080/03081060.2015.1008798.

[20] DEFRA. Clean Air Strategy 2019 2019. https://www.gov.uk/government/publications/clean-air-strategy-2019 (accessed March 4, 2020).

[21] Department for Environment Food and Rural Affairs. Clean Air Zones - GOV.UK 2023. https://www.gov.uk/guidance/driving-in-a-clean-air-zone (accessed July 4, 2023).

[22] BEIS. Energy Consumption in the UK (ECUK) 1970 to 2021 2022. https://www.gov.uk/government/statistics/energy-consumption-in-the-uk-2022 (accessed April 15, 2023).

[23] Kollamthodi S, Norris J, Dun C, Brannigan C, Twisse F, Biedka M, et al. The role of natural gas and biomethane in the transport sector. Transport and Environment Report 2016:1–85. https://www.transportenvironment.org/sites/te/files/publications/2016_02_TE_Natural_Gas_Biomethane_Study_FINAL.pdf (accessed April 15, 2023).

[24] Langshaw L, Ainalis D, Acha S, Shah N, Stettler MEJ. Environmental and economic analysis of liquefied natural gas (LNG) for heavy goods vehicles in the UK: A Well-to-Wheel and total cost of ownership evaluation. Energy Policy 2020;137. https://doi.org/10.1016/j.enpol.2019.111161.

[25] Tong F, Jaramillo P, Azevedo IML. Comparison of Life Cycle Greenhouse Gases from Natural Gas Pathways for Medium and Heavy-Duty Vehicles. Environ Sci Technol 2015;49:7123–33. https://doi.org/10.1021/es5052759.

[26] Panoutsou C, Germer S, Karka P, Papadokostantakis S, Kroyan Y, Wojcieszyk M, et al. Advanced biofuels to decarbonise European transport by 2030: Markets, challenges, and policies that impact their successful market uptake. Energy Strategy Reviews 2021;34:100633. https://doi.org/10.1016/j.esr.2021.100633.

[27] Gray N, McDonagh S, O'Shea R, Smyth B, Murphy JD. Decarbonising ships, planes and trucks: An analysis of suitable low-carbon fuels for the maritime, aviation and haulage sectors. Advances in Applied Energy 2021;1:24. https://doi.org/10.1016/j.adapen.2021.100008.

[28] Rosenberg E, Espegren K, Danebergs J, Fridstrøm L, Beate Hovi I, Madslien A. Modelling the interaction between the energy system and road freight in Norway. Transp Res D Transp Environ 2023;114. https://doi.org/10.1016/j.trd.2022.103569.

[29] Pelletier S, Jabali O, Laporte G. Charge scheduling for electric freight vehicles. Transportation Research Part B: Methodological 2018;115:246–69. https://doi.org/10.1016/j.trb.2018.07.010.

[30] IEA. The Future of Hydrogen 2019. https://doi.org/10.1787/1e0514c4-en.

[31] Department for Energy Security and Net Zero. Hydrogen Net Zero Investment Roadmap 2023. https://www.gov.uk/government/publications/hydrogen-net-zero-investment-roadmap (accessed April 15, 2023).

[32] Bossel U. Does a hydrogen economy make sense? Proceedings of the IEEE 2006;94:1826–36. https://doi.org/10.1109/JPROC.2006.883715.

[33] Nicolaides D, Cebon D, Miles J. Prospects for Electrification of Road Freight. IEEE Syst J 2018;12:1838–49. https://doi.org/10.1109/JSYST.2017.2691408.

[34] Office for National Statistics. Climate change insights, business and transport, UK: February 2023 2023. https://www.ons.gov.uk/economy/environmentalaccounts/articles/climatechangeinsightsuk/february2023 (accessed April 13, 2023).

[35] Gustafsson M, Svensson N, Eklund M, Dahl Öberg J, Vehabovic A. Well-to-wheel greenhouse gas emissions of heavy-duty transports: Influence of electricity carbon intensity. Transp Res D Transp Environ 2021;93:102757. https://doi.org/10.1016/j.trd.2021.102757.

[36] Gray N, O'Shea R, Wall D, Smyth B, Lens PNL, Murphy JD. Batteries, fuel cells, or engines? A probabilistic economic and environmental assessment of electricity and electrofuels for heavy goods vehicles. Advances in Applied Energy 2022;8:100110. https://doi.org/10.1016/j.adapen.2022.100110.

[37] European Commision. Delivering the European Green Deal 2021. https://commission.europa.eu/strategy-and-policy/priorities-2019-2024/european-green-deal/delivering-european-green-deal_en (accessed April 20, 2023).

[38] BEIS. Net Zero Strategy: Build Back Greener. GOVUK 2021:368. https://www.gov.uk/government/publications/net-zero-strategy (accessed June 7, 2022).

[39] Johnson RB, Onwuegbuzie AJ. Mixed Methods Research: A Research Paradigm Whose Time Has Come. Educational Researcher 2004;33:14–26. https://doi.org/10.3102/0013189X033007014.

[40] Bryman A, Bell E. Business Research Methods. Oxford University Press; 2011.

[41] Saunders MNK, Lewis P, Thornhill A. Research methods for business students. Pearson Education Limited; 2019.

[42] Powerstar. Commercial Site Microgrids n.d. https://powerstar.com/microgrids/commercial-site-microgrids/ (accessed January 15, 2024).

[43] Nunez Munoz M, Ballantyne EEF, Stone DA. Understanding the solar power potential at a Sheffield manufacturing and engineering firm. A case study 2022. https://eprints.whiterose.ac.uk/185547/1/tufcot-case-study-indesign-doc-final.pdf (accessed July 31, 2023).

[44] IPCC. Climate change 2014 synthesis report summary Change. 2014.

[45] Clark PU, Shakun JD, Marcott SA, Mix AC, Eby M, Kulp S, et al. Consequences of twenty-first-century policy for multi-millennial climate and sea-level change. Nat Clim Chang 2016;6:360–9. https://doi.org/10.1038/nclimate2923.

[46] Crippa M, Guizzardi D, Banja M, Solazzo E, Muntean M, Schaaf E, et al. CO2 emissions of all world countries - 2022. Luxembourg: 2022. https://doi.org/10.2760/730164.

[47] IEA. CO2 Emissions in 2022 2023:19. https://www.iea.org/reports/co2-emissions-in-2022 (accessed April 27, 2023).

[48] Statista. Global transport CO_2 emissions by region 2021 2023. https://www.statista.com/statistics/1200745/regional-carbon-dioxide-emissions-transport-sector-worldwide/ (accessed April 26, 2023).

[49] Uherek E, Halenka T, Borken-Kleefeld J, Balkanski Y, Berntsen T, Borrego C, et al. Transport impacts on atmosphere and climate: Land transport. Atmos Environ 2010;44:4772–816. https://doi.org/10.1016/j.atmosenv.2010.01.002.

[50] European Environment Agency. Greenhouse gas emissions from transport in Europe 2022:1. https://www.eea.europa.eu/ims/greenhouse-gas-emissions-from-transport (accessed April 27, 2023).

[51] Du H, Chen Z, Peng B, Southworth F, Ma S, Wang Y. What drives CO2 emissions from the transport sector? A linkage analysis. Energy 2019;175:195–204. https://doi.org/10.1016/j.energy.2019.03.052.

[52] Carr D, Von Ehrenstein O, Weiland S, Wagner C, Wellie O, Nicolai T, et al. Modeling annual benzene, toluene, NO2, and soot concentrations on the basis of road traffic characteristics. Environ Res 2002;90:111–8. https://doi.org/10.1006/enrs.2002.4393.

[53] Rothengatter W. Climate change and the contribution of transport: Basic facts and the role of aviation. Transp Res D Transp Environ 2010;15:5–13. https://doi.org/10.1016/j.trd.2009.07.005.

[54] WHO. 9 out of 10 people worldwide breathe polluted air, but more countries are taking action 2018. https://www.who.int/news-room/detail/02-05-2018-9-out-of-10-people-worldwide-breathe-polluted-air-but-more-countries-are-taking-action (accessed May 23, 2020).

[55] European Commission. Transport in the European Union 2019:1–171. https://ec.europa.eu/transport/sites/transport/files/2019-transport-in-the-eu-current-trends-and-issues.pdf.

[56] DfT. Transport Statistics Great Britain 2021 2021. https://www.gov.uk/government/statistics/transport-statistics-great-britain-2021/transport-statistics-great-britain-2021#freight-transport (accessed April 27, 2023).

[57] Cruz C, Montenon A. Implementation and Impacts of Low Emission Zones on Freight Activities in Europe: Local Schemes Versus National Schemes. Transportation Research Procedia 2016;12:544–56. https://doi.org/10.1016/j.trpro.2016.02.010.

[58] Department for Transport (DfT). Domestic Road Freight Statistics, United Kingdom 2020. UK Department of Transport Statistical Release 2021:12. https://assets.publishing.service.gov.uk/government/uploads/system/uploads/attachment_data/file/1006792/domestic-road-freight-statistics-2020.pdf (accessed April 27, 2023).

[59] CCC. Reducing UK emissions - 2018 Progress Report to Parliament - Committee on Climate Change. Committee on Climate Change 2018.

[60] DfT. Road traffic statistics (TRA) - TRA0101 2022. https://www.gov.uk/government/statistical-data-sets/road-traffic-statistics-tra#traffic-volume-in-miles-tra01 (accessed April 28, 2023).

[61] BEIS. Digest of UK Energy Statistics - Electricity: commodity balances (DUKES Table_5.1) 2022. https://www.gov.uk/government/statistics/electricity-chapter-5-digest-of-united-kingdom-energy-statistics-dukes (accessed April 20, 2023).

[62] IEA. Global EV Outlook 2022 - Securing supplies for an electric future 2022:221. https://www.iea.org/reports/global-ev-outlook-2022 (accessed April 20, 2023).

[63] Schmidt M, Staudt P, Weinhardt C. 7. Transp Res D Transp Environ 2021;97. https://doi.org/10.1016/j.trd.2021.102894.

[64] Berkeley N, Bailey D, Jones A, Jarvis D. Assessing the transition towards Battery Electric Vehicles: A Multi-Level Perspective on drivers of, and barriers to, take up. Transp Res Part A Policy Pract 2017;106:320–32. https://doi.org/10.1016/j.tra.2017.10.004.

[65] Morganti E, Browne M. Technical and operational obstacles to the adoption of electric vans in France and the UK: An operator perspective. Transp Policy (Oxf) 2018;63:90–7. https://doi.org/10.1016/j.tranpol.2017.12.010.

[66] Department for Transport (DfT). Vehicle licensing statistics data tables - VEH0181. GOVUK 2022. https://www.gov.uk/government/statistical-data-sets/vehicle-licensing-statistics-data-tables#plug-in-vehicles (accessed April 28, 2023).

[67] Saber AY, Venayagamoorthy GK. Plug-in vehicles and renewable energy sources for cost and emission reductions. IEEE Transactions on Industrial Electronics 2011;58:1229–38. https://doi.org/10.1109/TIE.2010.2047828.

[68] Martins-Turner K, Grahle A, Nagel K, Göhlich D. Electrification of Urban Freight Transport - A Case Study of the Food Retailing Industry. Procedia Comput Sci, vol. 170, Elsevier B.V.; 2020, p. 757–63. https://doi.org/10.1016/j.procs.2020.03.159.

[69] Acha S, Green TC, Shah N. Optimal charging strategies of electric vehicles in the UK power market. ISGT 2011:1–8. https://doi.org/10.1109/ISGT.2011.5759128.

[70] Climate Change Committee. Delivering a reliable decarbonised power system 2023. https://www.theccc.org.uk/publication/delivering-a-reliable-decarbonised-power-system/ (accessed April 21, 2023).

[71] BEIS, Department for Energy Security and Net Zero. Greenhouse gas reporting: conversion factors 2022. https://www.gov.uk/government/publications/greenhouse-gas-reporting-conversion-factors-2022 (accessed April 21, 2023).

[72] Stamford L, Azapagic A. Environmental Impacts of Photovoltaics: The Effects of Technological Improvements and Transfer of Manufacturing from Europe to China. Energy Technology 2018;6:1148–60. https://doi.org/10.1002/ente.201800037.

[73] Sphera. GaBi LCA Database Documentation. GaBi Solutions 2021. https://gabi.sphera.com/support/gabi (accessed November 30, 2022).

[74] Nelson J, Gambhir A, Ekins-Daukes N. Solar power for CO2 mitigation 2014. https://www.imperial.ac.uk/media/imperial-college/grantham-institute/public/publications/briefing-papers/Solar-power-for-CO2-mitigation---Grantham-BP-11.pdf (accessed June 11, 2023).

[75] Brinkel NBG, Schram WL, AlSkaif TA, Lampropoulos I, van Sark WGJHM. Should we reinforce the grid? Cost and emission optimization of electric vehicle charging under

different transformer limits. Appl Energy 2020;276:13. https://doi.org/10.1016/j.apenergy.2020.115285.

[76] Danese A, Torsæter BN, Sumper A, Garau M. Planning of High-Power Charging Stations for Electric Vehicles: A Review. Applied Sciences (Switzerland) 2022;12:3214. https://doi.org/10.3390/app12073214.

[77] Borlaug B, Muratori M, Gilleran M, Woody D, Muston W, Canada T, et al. Heavy-duty truck electrification and the impacts of depot charging on electricity distribution systems. Nat Energy 2021;6:673–82. https://doi.org/10.1038/s41560-021-00855-0.

[78] Schiffer M, Klein PS, Laporte G, Walther G. Integrated planning for electric commercial vehicle fleets: A case study for retail mid-haul logistics networks. Eur J Oper Res 2021;291:944–60. https://doi.org/10.1016/j.ejor.2020.09.054.

[79] Whitehead J, Whitehead J, Kane M, Zheng Z. Exploring public charging infrastructure requirements for short-haul electric trucks. Int J Sustain Transp 2022;16:775–91. https://doi.org/10.1080/15568318.2021.1921888.

[80] Zemo Partnership, Electric Vehicle Energy Taskforce. Commercial EV Fleet Charging Requirements 2021. https://evenergytaskforce.com/reports/commercial-ev-fleet-charging/.

[81] Teoh T. Electric vehicle charging strategies for Urban freight transport: concept and typology. Transp Rev 2022;42:157–80. https://doi.org/10.1080/01441647.2021.1950233.

[82] Funke SÁ, Gnann T, Plötz P. Addressing the Different Needs for Charging Infrastructure: An Analysis of Some Criteria for Charging Infrastructure Set-up. In: Leal Filho W, Kotter R, editors. E-Mobility in Europe.Green Energy and Technology., Springer, Cham; 2015, p. 73–90. https://doi.org/10.1007/978-3-319-13194-8_4.

[83] San Román TG, Momber I, Abbad MR, Sánchez Miralles Á. Regulatory framework and business models for charging plug-in electric vehicles: Infrastructure, agents, and commercial relationships. Energy Policy 2011;39:6360–75. https://doi.org/10.1016/j.enpol.2011.07.037.

[84] Skippon S, Chappell J. Fleets' motivations for plug-in vehicle adoption and usage: U.K. case studies. Transp Res D Transp Environ 2019;71:67–84. https://doi.org/10.1016/j.trd.2018.12.009.

[85] Guo F, Yang J, Lu J. The battery charging station location problem: Impact of users' range anxiety and distance convenience. Transp Res E Logist Transp Rev 2018;114:1–18. https://doi.org/10.1016/j.tre.2018.03.014.

[86] De Socio M. Plugging into Amazon's fleet electrification strategy. GreenBiz 2020. https://www.greenbiz.com/article/plugging-amazons-fleet-electrification-strategy.

[87] Amazon. Shipment Zero 2019. https://sustainability.aboutamazon.com/environment/sustainable-operations/shipment-zero.

[88] Quak H, Nesterova N, Van Rooijen T, Dong Y. Zero Emission City Logistics: Current Practices in Freight Electromobility and Feasibility in the Near Future. Transportation Research Procedia, vol. 14, Elsevier B.V.; 2016, p. 1506–15. https://doi.org/10.1016/j.trpro.2016.05.115.

[89] UPS&GreenBiz. Curve Ahead: The future of Commercial Fleet Electrification 2018:1–19. https://sustainability.ups.com/media/UPS_GreenBiz_Whitepaper_v2.pdf.

[90] Crozier C, Morstyn T, McCulloch M. The opportunity for smart charging to mitigate the impact of electric vehicles on transmission and distribution systems. Appl Energy 2020;268. https://doi.org/10.1016/j.apenergy.2020.114973.

[91] Chen F, Chen Z, Dong H, Yin Z, Wang Y, Liu J. Research on the Influence of Electric Vehicle Multi-Factor Charging Load on a Regional Power Grid. Proceedings - 10th International Conference on Measuring Technology and Mechatronics Automation, ICMTMA 2018, vol. 2018- Janua, Institute of Electrical and Electronics Engineers Inc.; 2018, p. 163–6. https://doi.org/10.1109/ICMTMA.2018.00046.

[92] Pietracho R, Wenge C, Komarnicki P, Kasprzyk L. Multi-Criterial Assessment of Electric Vehicle Integration into the Commercial Sector—A Case Study. Energies (Basel) 2023;16. https://doi.org/10.3390/en16010462.

[93] Pelletier S, Jabali O, Laporte G. Goods distribution with electric vehicles: Review and research perspectives. Transportation Science 2016;50:3–22. https://doi.org/10.1287/trsc.2015.0646.

[94] Speth D, Plötz P, Funke S, Vallarella E. Public fast charging infrastructure for battery electric trucks—a model-based network for Germany. Environmental Research: Infrastructure and Sustainability 2022;2:025004. https://doi.org/10.1088/2634-4505/ac6442.

[95] Topsector Logistiek. Charging infrastructure for electric vehicles in urban logistics 2019. https://www.panteia.nl/nieuws/grote-kansen-elektrische-stadlogistiek/ (accessed April 22, 2023).

[96] European Automobile Manufacturers Association. European EV Charging Infrastructure Masterplan 2022:19–47. https://www.acea.auto/files/Research-Whitepaper-A-European-EV-Charging-Infrastructure-Masterplan.pdf (accessed June 11, 2023).

[97] Liimatainen H, van Vliet O, Aplyn D. The potential of electric trucks – An international commodity-level analysis. Appl Energy 2019;236:804–14. https://doi.org/10.1016/j.apenergy.2018.12.017.

[98] Powar V, Singh R. End-to-End Direct-Current-Based Extreme Fast Electric Vehicle Charging Infrastructure Using Lithium-Ion Battery Storage. Batteries 2023;9:169. https://doi.org/10.3390/batteries9030169.

[99] Felipe Á, Ortuño MT, Righini G, Tirado G. A heuristic approach for the green vehicle routing problem with multiple technologies and partial recharges. Transp Res E Logist Transp Rev 2014;71:111–28. https://doi.org/10.1016/j.tre.2014.09.003.

[100] Schneider M, Stenger A, Goeke D. The electric vehicle-routing problem with time windows and recharging stations. Transportation Science 2014;48:500–20. https://doi.org/10.1287/trsc.2013.0490.

[101] Goeke D, Schneider M. Routing a mixed fleet of electric and conventional vehicles. Eur J Oper Res 2015;245:81–99. https://doi.org/10.1016/j.ejor.2015.01.049.

[102] Hiermann G, Puchinger J, Ropke S, Hartl RF. The Electric Fleet Size and Mix Vehicle Routing Problem with Time Windows and Recharging Stations. Eur J Oper Res 2016;252:995–1018. https://doi.org/10.1016/j.ejor.2016.01.038.

[103] Montoya A, Guéret C, Mendoza JE, Villegas JG. The electric vehicle routing problem with nonlinear charging function. Transportation Research Part B: Methodological 2017;103:87–110. https://doi.org/10.1016/j.trb.2017.02.004.

[104] Pelletier S, Jabali O, Laporte G. The electric vehicle routing problem with energy consumption uncertainty. Transportation Research Part B: Methodological 2019;126:225–55. https://doi.org/10.1016/j.trb.2019.06.006.

[105] Raeesi R, Zografos KG. Coordinated routing of electric commercial vehicles with intra-route recharging and en-route battery swapping. Eur J Oper Res 2022;301:82–109. https://doi.org/10.1016/j.ejor.2021.09.037.

[106] Erdelić T, Carić T. Goods Delivery with Electric Vehicles: Electric Vehicle Routing Optimization with Time Windows and Partial or Full Recharge. Energies (Basel) 2022;15. https://doi.org/10.3390/en15010285.

[107] Betz J, Hann M, Jager B, Lienkamp M. Evaluation of the Potential of Integrating Battery Electric Vehicles into Commercial Companies on the Basis of Fleet Test Data. IEEE Vehicular Technology Conference 2017;2017-June. https://doi.org/10.1109/VTCSpring.2017.8108289.

[108] Betz J, Walther L, Lienkamp M. Analysis of the charging infrastructure for battery electric vehicles in commercial companies. IEEE Intelligent Vehicles Symposium, Proceedings, Institute of Electrical and Electronics Engineers Inc.; 2017, p. 1643–9. https://doi.org/10.1109/IVS.2017.7995945.

[109] Kin B, Hopman M, Quak H. Different Charging Strategies for Electric Vehicle Fleets in Urban Freight Transport. Sustainability (Switzerland) 2021;13. https://doi.org/10.3390/su132313080.

[110] Anosike A, Loomes H, Udokporo CK, Garza-Reyes JA. Exploring the challenges of electric vehicle adoption in final mile parcel delivery. International Journal of Logistics

Research and Applications 2021;1:25. https://doi.org/10.1080/13675567.2021.1978409.

[111] Ledna C, Muratori M, Brooker A, Wood E, Greene D. How to support EV adoption: Tradeoffs between charging infrastructure investments and vehicle subsidies in California. Energy Policy 2022;165:11. https://doi.org/10.1016/j.enpol.2022.112931.

[112] European Commision. Driving time and rest periods 2006. https://transport.ec.europa.eu/transport-modes/road/social-provisions/driving-time-and-rest-periods_en (accessed June 11, 2023).

[113] Schücking M, Jochem P, Fichtner W, Wollersheim O, Stella K. Charging strategies for economic operations of electric vehicles in commercial applications. Transp Res D Transp Environ 2017;51:173–89. https://doi.org/10.1016/j.trd.2016.11.032.

[114] Bradley L, Golestani N, Izumi K, Tanaka K, Yamakawa T. Charging Infrastructure Strategies: Maximizing the Deployment of Electric Drayage Trucks in Southern California. Los Angeles, CA, USA: 2019. https://doi.org/10.17610/T6BC7M.

[115] Enrico Furnari, Lionel Johnnes, Alexander Pfeiffer, Shivika Sahdev. Why most electric trucks will choose overnight charging. McKinsey 2020. https://www.mckinsey.com/industries/automotive-and-assembly/our-insights/why-most-etrucks-will-choose-overnight-charging (accessed March 19, 2023).

[116] Taefi TT, Stütz S, Fink A. Assessing the cost-optimal mileage of medium-duty electric vehicles with a numeric simulation approach. Transp Res D Transp Environ 2017;56:271–85. https://doi.org/10.1016/j.trd.2017.08.015.

[117] Mareev I, Becker J, Sauer DU. Battery dimensioning and life cycle costs analysis for a heavy-duty truck considering the requirements of long-haul transportation. Energies (Basel) 2018;11:55. https://doi.org/10.3390/en11010055.

[118] Çabukoglu E, Georges G, Küng L, Pareschi G, Boulouchos K. Battery electric propulsion: an option for heavy-duty vehicles? Results from a Swiss case-study. Transp Res Part C Emerg Technol 2018;88:107–23. https://doi.org/10.1016/j.trc.2018.01.013.

[119] García-Villalobos J, Zamora I, San Martín JI, Asensio FJ, Aperribay V. Plug-in electric vehicles in electric distribution networks: A review of smart charging approaches. Renewable and Sustainable Energy Reviews 2014;38:717–31. https://doi.org/10.1016/j.rser.2014.07.040.

[120] Blatiak A, Bellizio F, Badesa L, Strbac G. Value of optimal trip and charging scheduling of commercial electric vehicle fleets with Vehicle-to-Grid in future low inertia systems. Sustainable Energy, Grids and Networks 2022;31:100738. https://doi.org/10.1016/j.segan.2022.100738.

[121] Quirós-Tortós J, Ochoa L, Butler T. How electric vehicles and the grid work together: Lessons learned from one of the largest electric vehicle trials in the world. IEEE Power and Energy Magazine 2018;16:64–76. https://doi.org/10.1109/MPE.2018.2863060.

[122] Dallinger D, Wietschel M. Grid integration of intermittent renewable energy sources using price-responsive plug-in electric vehicles. Renewable and Sustainable Energy Reviews 2012;16:3370–82. https://doi.org/10.1016/j.rser.2012.02.019.

[123] Rahbari O, Vafaeipour M, Omar N, Rosen MA, Hegazy O, Timmermans JM, et al. An optimal versatile control approach for plug-in electric vehicles to integrate renewable energy sources and smart grids. Energy 2017;134:1053–67. https://doi.org/10.1016/j.energy.2017.06.007.

[124] Di Giorgio A, Liberati F, Canale S. Electric vehicles charging control in a smart grid: A model predictive control approach. Control Eng Pract 2014;22:147–62. https://doi.org/10.1016/j.conengprac.2013.10.005.

[125] Tang Y, Zhang Q, Wen Z, Bunn D, Nieto Martin J. Optimal analysis for facility configuration and energy management on electric light commercial vehicle charging. Energy 2022;246. https://doi.org/10.1016/j.energy.2022.123363.

[126] Hoehne CG, Chester M V. Optimizing plug-in electric vehicle and vehicle-to-grid charge scheduling to minimize carbon emissions. Energy 2016;115:646–57. https://doi.org/10.1016/j.energy.2016.09.057.

[127] Dogan A, Alci M. Heuristic optimization of EV charging schedule considering battery degradation cost. Elektronika Ir Elektrotechnika 2018;24:15–20. https://doi.org/10.5755/j01.eie.24.6.22283.

[128] Datta U, Kalam A, Shi J. Smart control of BESS in PV integrated EV charging station for reducing transformer overloading and providing battery-to-grid service. J Energy Storage 2020;28. https://doi.org/10.1016/j.est.2020.101224.

[129] Powell S, Cezar GV, Min L, Azevedo IML, Rajagopal R. Charging infrastructure access and operation to reduce the grid impacts of deep electric vehicle adoption. Nat Energy 2022;7:932–45. https://doi.org/10.1038/s41560-022-01105-7.

[130] Nguyen VL, Tran-Quoc T, Bacha S, Nguyen B. Charging strategies to minimize the peak load for an electric vehicle fleet. IECON Proceedings (Industrial Electronics Conference), 2014, p. 3522–8. https://doi.org/10.1109/IECON.2014.7049022.

[131] Toniato E, Mehta P, Marinkovic S, Tiefenbeck V. Peak load minimization of an e-bus depot: impacts of user-set conditions in optimization algorithms. Energy Informatics 2021;4. https://doi.org/10.1186/s42162-021-00174-4.

[132] Houbbadi A, Trigui R, Pelissier S, Redondo-Iglesias E, Bouton T. A quadratic programming based optimisation to manage electric bus fleet charging. International Journal of Electric and Hybrid Vehicles 2019;11:289–307. https://doi.org/10.1504/IJEHV.2019.102862.

[133] Tang W, Zhang YJ. A Model Predictive Control Approach for Low-Complexity Electric Vehicle Charging Scheduling: Optimality and Scalability. IEEE Transactions on Power Systems 2017;32:1050–63. https://doi.org/10.1109/TPWRS.2016.2585202.

[134] Yang Y, Bremner S, Menictas C, Kay M. Modelling and optimal energy management for battery energy storage systems in renewable energy systems: A review. Renewable and Sustainable Energy Reviews 2022;167. https://doi.org/10.1016/j.rser.2022.112671.

[135] Jain R, Veda S, Becker W, Ketring S, Ganger D. Application of Site Controllers for Electrification of Commercial Fleet Vehicles. Proceedings of the IEEE Power Engineering Society Transmission and Distribution Conference, vol. 2020- Octob,

Institute of Electrical and Electronics Engineers Inc.; 2020. https://doi.org/10.1109/TD39804.2020.9300038.

[136] Anglani N, Oriti G, Colombini M. Optimized energy management system to reduce fuel consumption in remote military microgrids. IEEE Trans Ind Appl 2017;53:5777–85. https://doi.org/10.1109/TIA.2017.2734045.

[137] Divshali PH, Choi BJ, Liang H. Multi-agent transactive energy management system considering high levels of renewable energy source and electric vehicles. IET Generation, Transmission and Distribution 2017;11:3713–21. https://doi.org/10.1049/IET-GTD.2016.1916.

[138] Alam MS, Arefifar SA. Energy Management in Power Distribution Systems: Review, Classification, Limitations and Challenges. IEEE Access 2019;7:92979–3001. https://doi.org/10.1109/ACCESS.2019.2927303.

[139] Moradi H, Esfahanian M, Abtahi A, Zilouchian A. Optimization and energy management of a standalone hybrid microgrid in the presence of battery storage system. Energy 2018;147:226–38. https://doi.org/10.1016/j.energy.2018.01.016.

[140] UK Power Network Services. UPS - Facilitating large fleet operators to go electric | UK Power Networks Services 2022. https://www.ukpowernetworksservices.co.uk/case-studies/ups-facilitating-large-fleet-operators-to-go-electric/ (accessed February 23, 2023).

[141] Simolin T, Rauma K, Viri R, Mäkinen J, Rautiainen A, Järventausta P. Charging powers of the electric vehicle fleet: Evolution and implications at commercial charging sites. Appl Energy 2021;303:117651. https://doi.org/10.1016/j.apenergy.2021.117651.

[142] Amann G, Bermúdez V, Boscov Kovacs E, Gallego S, Giannelos S, Iliceto A, et al. E-mobility deployment and impact on grids: Impact of EV and charging infrastructure on European T&D grids - Innovation needs 2022. https://smart-networks-energy-transition.ec.europa.eu/system/files/2022-11/ETIP SNET E-Mobility White Paper_pdf.pdf (accessed June 18, 2023).

[143] European Commission. REPowerEU: affordable, secure and sustainable energy for Europe. European Commission - European Commission 2022.

https://commission.europa.eu/strategy-and-policy/priorities-2019-2024/european-green-deal/repowereu-affordable-secure-and-sustainable-energy-europe_en#documents (accessed June 18, 2023).

[144] HM Government. British Energy Security Strategy: Secure, clean and affordable British energy for the long term. 2022.

[145] IEA. World Energy Outlook 2022. 2022.

[146] Das CK, Bass O, Kothapalli G, Mahmoud TS, Habibi D. Overview of energy storage systems in distribution networks: Placement, sizing, operation, and power quality. Renewable and Sustainable Energy Reviews 2018;91:1205–30. https://doi.org/10.1016/j.rser.2018.03.068.

[147] Moghaddam Z, Ahmad I, Habibi D, Masoum MAS. A coordinated dynamic pricing model for electric vehicle charging stations. IEEE Transactions on Transportation Electrification 2019;5:226–38. https://doi.org/10.1109/TTE.2019.2897087.

[148] Tulpule PJ, Marano V, Yurkovich S, Rizzoni G. Economic and environmental impacts of a PV powered workplace parking garage charging station. Appl Energy 2013;108:323–32. https://doi.org/10.1016/j.apenergy.2013.02.068.

[149] Chaouachi A, Bompard E, Fulli G, Masera M, De Gennaro M, Paffumi E. Assessment framework for EV and PV synergies in emerging distribution systems. Renewable and Sustainable Energy Reviews 2016;55:719–28. https://doi.org/10.1016/j.rser.2015.09.093.

[150] Braam F, Groß A, Mierau M, Kohrs R, Wittwer C. Coordinated charge management for battery electric vehicles. Computer Science - Research and Development 2017;32:183–93. https://doi.org/10.1007/s00450-016-0307-6.

[151] Seddig K, Jochem P, Fichtner W. Integrating renewable energy sources by electric vehicle fleets under uncertainty. Energy 2017;141:2145–53. https://doi.org/10.554/IR/1000077130.

[152] Hoarau Q, Perez Y. Interactions between electric mobility and photovoltaic generation: A review. Renewable and Sustainable Energy Reviews 2018;94:510–22. https://doi.org/10.1016/j.rser.2018.06.039.

[153] Zhang TZ, Chen TD. Smart charging management for shared autonomous electric vehicle fleets: A Puget Sound case study. Transp Res D Transp Environ 2020;78. https://doi.org/10.1016/j.trd.2019.11.013.

[154] Alvaro-Hermana R, Fraile-Ardanuy J, Fuentes M. Feasibility Study of an Electric Shuttle Fleet Fed by Solar Power. Procedia Comput Sci 2016;83:799–806. https://doi.org/10.1016/j.procs.2016.04.169.

[155] Mouli GRC, Bauer P, Zeman M. System design for a solar powered electric vehicle charging station for workplaces. Appl Energy 2016;168:434–43. https://doi.org/10.1016/j.apenergy.2016.01.110.

[156] Bhatti AR, Salam Z, Aziz MJBA, Yee KP, Ashique RH. Electric vehicles charging using photovoltaic: Status and technological review. Renewable and Sustainable Energy Reviews 2016;54:34–47. https://doi.org/10.1016/j.rser.2015.09.091.

[157] Bhatti AR, Salam Z, Aziz MJBA, Yee KP. A critical review of electric vehicle charging using solar photovoltaic. Int J Energy Res 2016;40:439–61. https://doi.org/10.1002/er.

[158] Clairand JM, Rodríguez-García J, Álvarez-Bel C. Electric vehicle charging strategy for isolated systems with high penetration of renewable generation. Energies (Basel) 2018;11:3188. https://doi.org/10.3390/en11113188.

[159] Domínguez-Navarro JA, Dufo-López R, Yusta-Loyo JM, Artal-Sevil JS, Bernal-Agustín JL. Design of an electric vehicle fast-charging station with integration of renewable energy and storage systems. International Journal of Electrical Power and Energy Systems 2019;105:46–58. https://doi.org/10.1016/j.ijepes.2018.08.001.

[160] Environmental Protection Act 1990 c.43, Part II, Section 45 n.d. https://www.legislation.gov.uk/ukpga/1990/43/section/45 (accessed January 27, 2024).

[161] Smith L. Constituency casework. Household waste collection in England and Wales: FAQs. House of Commons Library 2023.

https://commonslibrary.parliament.uk/household-waste-collection-in-england-and-wales/ (accessed January 27, 2024).

[162] McLeod FN, Cherrett TJ. Appraisal of waste collection routeing and scheduling. Proceedings of Institution of Civil Engineers: Waste and Resource Management 2011;164:97–104. https://doi.org/10.1680/WARM.900022.

[163] McLeod F, Cherrett T. Quantifying the transport impacts of domestic waste collection strategies. Waste Management 2008;28:2271–8. https://doi.org/10.1016/j.wasman.2007.09.041.

[164] Anghinolfi D, Paolucci M, Robba M, Taramasso AC. A dynamic optimization model for solid waste recycling. Waste Management 2013;33:287–96. https://doi.org/10.1016/J.WASMAN.2012.10.006.

[165] Erdem M. Optimisation of sustainable urban recycling waste collection and routing with heterogeneous electric vehicles. Sustain Cities Soc 2022;80:103785. https://doi.org/10.1016/J.SCS.2022.103785.

[166] Ewert R, Grahle A, Martins-Turner K, Syré AM, Nagel K, Göhlich D. Electrification of Urban Waste Collection: Introducing a Simulation-Based Methodology for Technical Feasibility, Impact and Cost Analysis. World Electric Vehicle Journal 2021, Vol 12, Page 122 2021;12:122. https://doi.org/10.3390/WEVJ12030122.

[167] Amine Masmoudi M, Coelho LC, Demir E. Plug-in hybrid electric refuse vehicle routing problem for waste collection. Transp Res E Logist Transp Rev 2022;166:102875. https://doi.org/10.1016/J.TRE.2022.102875.

[168] Nowakowski P, Wala M. Electric waste collection vehicles in Poland: A challenge or burden for local communities? Sustain Chem Pharm 2024;38:101452. https://doi.org/10.1016/J.SCP.2024.101452.

[169] Zhao R, Stincescu T, Ballantyne EEF, Stone DA. Sustainable city: Energy usage prediction method for electrified refuse collection vehicles. Smart Cities 2020;3:1100–16. https://doi.org/10.3390/smartcities3030054.

[170] Climate Change Committee. Delivering a reliable decarbonised power system 2023. https://www.theccc.org.uk/publication/delivering-a-reliable-decarbonised-power-system/ (accessed April 21, 2023).

[171] Mohamad F, Teh J, Lai CM. Optimum allocation of battery energy storage systems for power grid enhanced with solar energy. Energy 2021;223. https://doi.org/10.1016/j.energy.2021.120105.

[172] Ugirumurera J, Haas ZJ. Optimal Capacity Sizing for Completely Green Charging Systems for Electric Vehicles. IEEE Transactions on Transportation Electrification 2017;3:565–77. https://doi.org/10.1109/TTE.2017.2713098.

[173] Nunez Munoz M, Ballantyne EEF, Stone DA. Using locally generated renewable energy to charge depot based electric freight fleets. World Conference on Transport Research (WCTR), 2023.

[174] Nunez Munoz M, Ballantyne EEF, Stone DA. Development and evaluation of empirical models for the estimation of hourly horizontal diffuse solar irradiance in the United Kingdom. Energy 2022;241. https://doi.org/10.1016/j.energy.2021.122820.

[175] Nunez Munoz M, Ballantyne EEF, Stone DA. Assessing the Economic Impact of Introducing Localised PV Solar Energy Generation and Energy Storage for Fleet Electrification. Energies (Basel) 2023;16:3570. https://doi.org/10.3390/en16083570.

[176] Berrizbeitia SE, Gago EJ, Muneer T. Empirical models for the estimation of solar sky-diffuse radiation. A review and experimental analysis. Energies (Basel) 2020;13. https://doi.org/10.3390/en13030701.

[177] Burnett D, Barbour E, Harrison GP. The UK solar energy resource and the impact of climate change. Renew Energy 2014;71:333–43. https://doi.org/10.1016/j.renene.2014.05.034.

[178] Vignola F, Harlan P, Perez R, Kmiecik M. Analysis of satellite derived beam and global solar radiation data. Solar Energy 2007;81:768–72. https://doi.org/10.1016/j.solener.2006.10.003.

[179] Polo J, Wilbert S, Ruiz-Arias JA, Meyer R, Gueymard C, Súri M, et al. Preliminary survey on site-adaptation techniques for satellite-derived and reanalysis solar radiation datasets. Solar Energy 2016;132:25–37. https://doi.org/10.1016/j.solener.2016.03.001.

[180] Lave M, Weekley A. Comparison of high-frequency solar irradiance: Ground measured vs. satellite-derived. 2017 IEEE 44th Photovoltaic Specialist Conference, PVSC 2017 2017:1–6. https://doi.org/10.1109/PVSC.2017.8366211.

[181] Ruiz-Arias JA, Alsamamra H, Tovar-Pescador J, Pozo-Vázquez D. Proposal of a regressive model for the hourly diffuse solar radiation under all sky conditions. Energy Convers Manag 2010;51:881–93. https://doi.org/10.1016/j.enconman.2009.11.024.

[182] Muneer T, Etxebarria S, Gago EJ. Monthly averaged-hourly solar diffuse radiation model for the UK. Building Services Engineering Research and Technology 2014;35:573–84. https://doi.org/10.1177/0143624414522639.

[183] Despotovic M, Nedic V, Despotovic D, Cvetanovic S. Evaluation of empirical models for predicting monthly mean horizontal diffuse solar radiation. Renewable and Sustainable Energy Reviews 2016;56:246–60. https://doi.org/10.1016/j.rser.2015.11.058.

[184] Bashahu M. Statistical comparison of models for estimating the monthly average daily diffuse radiation at a subtropical African site. Solar Energy 2003;75:43–51. https://doi.org/10.1016/S0038-092X(03)00213-5.

[185] Gouda SG, Hussein Z, Luo S, Yuan Q. Review of empirical solar radiation models for estimating global solar radiation of various climate zones of China. Prog Phys Geogr 2020;44:168–88. https://doi.org/10.1177/0309133319867213.

[186] Muneer T, Gueymard C, Kambezidis H. Solar radiation and daylight models. 2004th ed. Oxford: Elsevier Butterworth Heinemann.; 2004.

[187] De Simón-Martín M, Díez-Mediavilla M, Alonso-Tristán C. Modelling solar data: Reasons, main methods and applications. Renewable Energy and Power Quality Journal 2013;1:767–71. https://doi.org/10.24084/repqj11.440.

[188] Noia M, Ratto CF, Festa R. Solar irradiance estimation from geostationary satellite data: II. Physical models. Solar Energy 1993;51:449–56. https://doi.org/10.1016/0038-092X(93)90130-G.

[189] Noia M, Ratto CF, Festa R. Solar irradiance estimation from geostationary satellite data: I. Statistical models. Solar Energy 1993;51:449–56. https://doi.org/10.1016/0038-092X(93)90130-G.

[190] Hay JE. Calculating solar radiation for horizontal surfaces- I. Theoretically based approaches. Renew Energy 1993;3:357–64.

[191] Hay JE. Calculating solar radiation for horizontal surfaces-II. Empirically based approaches. Renew Energy 1993;3:365–72. https://doi.org/10.1016/0960-1481(93)90103-N.

[192] Voyant C, Notton G, Kalogirou S, Nivet ML, Paoli C, Motte F, et al. Machine learning methods for solar radiation forecasting: A review. Renew Energy 2017;105:569–82. https://doi.org/10.1016/j.renene.2016.12.095.

[193] Lai JP, Chang YM, Chen CH, Pai PF. A survey of machine learning models in renewable energy predictions. Applied Sciences (Switzerland) 2020;10. https://doi.org/10.3390/app10175975.

[194] Mellit A, Pavan AM, Ogliari E, Leva S, Lughi V. Advanced methods for photovoltaic output power forecasting: A review. Applied Sciences (Switzerland) 2020;10. https://doi.org/10.3390/app10020487.

[195] Martín L, Zarzalejo LF, Polo J, Navarro A, Marchante R, Cony M. Prediction of global solar irradiance based on time series analysis: Application to solar thermal power plants energy production planning. Solar Energy 2010;84:1772–81. https://doi.org/10.1016/j.solener.2010.07.002.

[196] Lou S, Li DHW, Lam JC, Chan WWH. Prediction of diffuse solar irradiance using machine learning and multivariable regression. Appl Energy 2016;181:367–74. https://doi.org/10.1016/j.apenergy.2016.08.093.

[197] Amrouche B, Le Pivert X. Artificial neural network based daily local forecasting for global solar radiation. Appl Energy 2014;130:333–41. https://doi.org/10.1016/j.apenergy.2014.05.055.

[198] Alzahrani A, Kimball JW, Dagli C. Predicting solar irradiance using time series neural networks. Procedia Comput Sci, vol. 36, Elsevier B.V.; 2014, p. 623–8. https://doi.org/10.1016/j.procs.2014.09.065.

[199] Behrang MA, Assareh E, Ghanbarzadeh A, Noghrehabadi AR. The potential of different artificial neural network (ANN) techniques in daily global solar radiation modeling based on meteorological data. Solar Energy 2010;84:1468–80. https://doi.org/10.1016/j.solener.2010.05.009.

[200] Khatib T, Mohamed A, Sopian K. A review of solar energy modeling techniques. Renewable and Sustainable Energy Reviews 2012;16:2864–9. https://doi.org/10.1016/j.rser.2012.01.064.

[201] Salhi H, Lazhar Belkhiri ·, Tiri · Ammar. Evaluation of diffuse fraction and diffusion coefficient using statistical analysis 2020;10:133. https://doi.org/10.1007/s13201-020-01216-0.

[202] Li H, Bu X, Long Z, Zhao L, Ma W. Calculating the diffuse solar radiation in regions without solar radiation measurements. Energy 2012;44:611–5. https://doi.org/10.1016/j.energy.2012.05.033.

[203] Pandey CK, Katiyar AK. Solar Radiation: Models and Measurement Techniques. Journal of Energy 2013;2013:1–8. https://doi.org/10.1155/2013/305207.

[204] Maleki SAM, Hizam H, Gomes C. Estimation of hourly, daily and monthly global solar radiation on inclined surfaces: Models re-visited. Energies (Basel) 2017;10. https://doi.org/10.3390/en10010134.

[205] Iqbal M. Correlation of average diffuse and beam radiation with hours of bright sunshine. Solar Energy 1979;23:169–73. https://doi.org/10.1016/0038-092X(79)90118-X.

[206] Hussain M. Estimation of global and diffuse irradiation from sunshine duration and atmospheric water vapour content. Solar Energy 1984;33:217–20. https://doi.org/10.1016/0038-092X(84)90240-8.

[207] Coppolino S. A simple model for computing diffuse solar radiation. Solar Energy 1989;43:385–9. https://doi.org/10.1016/0038-092X(89)90111-4.

[208] Li H, Ma W, Wang X, Lian Y. Estimating monthly average daily diffuse solar radiation with multiple predictors: A case study. Renew Energy 2011;36:1944–8. https://doi.org/10.1016/j.renene.2011.01.006.

[209] Tapakis R, Michaelides S, Charalambides AG. Computations of diffuse fraction of global irradiance: Part 1 – Analytical modelling. Solar Energy 2016;139:723–32. https://doi.org/10.1016/j.solener.2015.12.042.

[210] Liu BYH, Jordan RC. The interrelationship and characteristic distribution of direct, diffuse and total solar radiation. Solar Energy 1960;4:1–19. https://doi.org/10.1016/0038-092X(60)90062-1.

[211] Liu BYH, Jordan RC. The interrelationship and characteristic distribution of direct, diffuse and total solar radiation. Solar Energy 1960;4:1–19. https://doi.org/10.1016/0038-092X(60)90062-1.

[212] Erbs DG, Klein SA, Duffie JA. Estimation of the diffuse radiation fraction for hourly, daily and monthly-average global radiation. Solar Energy 1982;28:293–302. https://doi.org/10.1016/0038-092X(82)90302-4.

[213] Reindl DT, Beckman WA, Duffie JA. Diffuse fraction correlations. Solar Energy 1990;45:1–7.

[214] De Miguel A, Bilbao J, Aguiar R, Kambezidis H, Negro E. Diffuse solar irradiation model evaluation in the North Mediterranean Belt area. Solar Energy 2001;70:143–53. https://doi.org/10.1016/S0038-092X(00)00135-3.

[215] Muneer T, Saluja GS. Correlation between hourly diffuse and global solar irradiation for the UK. Building Services Engineering Research & Technology 1986;7:37–43. https://doi.org/10.1177/014362448600700106.

[216] Muneer T, Munawwar S. Improved accuracy models for hourly diffuse solar radiation. Journal of Solar Energy Engineering, Transactions of the ASME 2006;128:104–17. https://doi.org/10.1115/1.2148972.

[217] Gopinathan KK, Soler A. The determination of monthly mean hourly diffuse radiation on horizontal surfaces using equations based on hourly clearness index, sunshine fraction and solar elevation. International Journal of Solar Energy 1996;18:115–24. https://doi.org/10.1080/01425919608914310.

[218] Vazquez M, Ruiz V, Perez R. The roles of scattering, absorption, and air mass on the diffuse-to-global correlations. Solar Energy 1991;47:181–8. https://doi.org/10.1016/0038-092X(91)90077-A.

[219] Bailek N, Bouchouicha K, Al-Mostafa Z, El-Shimy M, Aoun N, Slimani A, et al. A new empirical model for forecasting the diffuse solar radiation over Sahara in the Algerian Big South. Renew Energy 2018;117:530–7. https://doi.org/10.1016/j.renene.2017.10.081.

[220] Torres JL, De Blas M, García A, de Francisco A. Comparative study of various models in estimating hourly diffuse solar irradiance. Renew Energy 2010;35:1325–32. https://doi.org/10.1016/j.renene.2009.11.025.

[221] Muneer T, Younes S, Munawwar S. Discourses on solar radiation modeling. Renewable and Sustainable Energy Reviews 2007;11:551–602. https://doi.org/10.1016/j.rser.2005.05.006.

[222] CEDA. CEDA Archive 2017. https://www.ceda.ac.uk/services/ceda-archive/ (accessed March 16, 2021).

[223] Met Office. MIDAS Open: UK hourly solar radiation data, v202007. Centre for Environmental Data Analysis 2020. https://doi.org/10.5285/1dc8578eb7434a7d8a661744d53eedf9.

[224] Gueymard C. Prediction and performance assessment of mean hourly global radiation. Solar Energy 2000;68:285–303. https://doi.org/10.1016/S0038-092X(99)00070-5.

[225] Met Office. UK regional climates - Met Office. MetOffice 2016:1. https://www.metoffice.gov.uk/research/climate/maps-and-data/regional-climates/index (accessed September 21, 2021).

[226] Muneer T, Fairooz F. Quality control of solar radiation and sunshine measurements - lessons learnt from processing worldwide databases. Building Services Engineering Research and Technology 2002;23:151–66. https://doi.org/10.1191/0143624402bt038oa.

[227] Duffie JA, Beckman WA. Solar Radiation. Solar Engineering of Thermal Processes. 4th ed., John Wiley & Sons, Incorporated; 2013.

[228] Kittler R, Darula S. Determination of time and sun position system. Solar Energy 2013;93:72–9. https://doi.org/10.1016/j.solener.2013.03.021.

[229] Cooper PI. The Absorption of Solar Radiation in Solar Stills. Solar Energy 1969;12:333–46. https://doi.org/10.1016/0038-092X(69)90047-4.

[230] Sunter M. MIDAS Data User Guide for UK Land Observations. 2021.

[231] Brownson JRS. Sun-Earth Geometry. Solar Energy Conversion Systems, Elsevier Science & Technology, Saint Louis; 2014.

[232] Younes S, Claywell R, Muneer T. Quality control of solar radiation data: Present status and proposed new approaches. Energy 2005;30:1533–49. https://doi.org/10.1016/j.energy.2004.04.031.

[233] Chaâbane M, Masmoudi M, Medhioub K. Determination of Linke turbidity factor from solar radiation measurement in northern Tunisia. Renew Energy 2004;29:2065–76. https://doi.org/10.1016/j.renene.2004.03.002.

[234] Remund J, Wald L, Lefèvre M, Ranchin T, Page J. Worldwide Linke Turbdidity Information. Ises 2003 2003;41.

[235] Huang KT. Identifying a suitable hourly solar diffuse fraction model to generate the typical meteorological year for building energy simulation application. Renew Energy 2020;157:1102–15. https://doi.org/10.1016/j.renene.2020.05.094.

[236] Khorasanizadeh H, Mohammadi K, Goudarzi N. Prediction of horizontal diffuse solar radiation using clearness index based empirical models; A case study. Int J Hydrogen Energy 2016;41:21888–98. https://doi.org/10.1016/j.ijhydene.2016.09.198.

[237] Hofmann M, Seckmeyer G. A new model for estimating the diffuse fraction of solar irradiance for photovoltaic system simulations. Energies (Basel) 2017;10. https://doi.org/10.3390/en10020248.

[238] Yao W, Zhang C, Wang X, Sheng J, Zhu Y, Zhang S. The research of new daily diffuse solar radiation models modified by air quality index (AQI) in the region with heavy fog and haze. Energy Convers Manag 2017;139:140–50. https://doi.org/10.1016/j.enconman.2017.02.041.

[239] Pelland S, Remund J, Kleissl J, Oozeki T, De Brabandere K. Photovoltaic and Solar Forecasting : State of the Art. 2013.

[240] Mahajan B, Namrata K. Performance evaluation of developed empirical models for predicting global solar radiation in western region of India. International Journal of Renewable Energy Research 2019;9:1135–43.

[241] Jiang Y. Estimation of monthly mean daily diffuse radiation in China. Appl Energy 2009;86:1458–64. https://doi.org/10.1016/j.apenergy.2009.01.002.

[242] David M, Diagne HM, Lauret P. Outputs and error indicators for solar forecasting models. World Renewable Energy Forum, WREF 2012, Including World Renewable Energy Congress XII and Colorado Renewable Energy Society (CRES) Annual Conferen 2012;2:831–6.

[243] Notton G, Voyant C. Forecasting of Intermittent Solar Energy Resource. In: Yahyaoui I, editor. Advances in Renewable Energies and Power Technologies, Elsevier; 2018, p. 77–114. https://doi.org/10.1016/B978-0-12-812959-3.00003-4.

[244] Theristis M, Venizelou V, Makrides G, Georghiou GE. Energy Yield in Photovoltaic Systems. In: Kalogirou SA, editor. McEvoy's Handbook of Photovoltaics, Elsevier; 2018, p. 671–713. https://doi.org/10.1016/B978-0-12-809921-6.00017-3.

[245] Kambezidis HD. The Solar Resource. In: Sayigh A, editor. Comprehensive Renewable Energy, Elsevier; 2012, p. 27–84. https://doi.org/10.1016/B978-0-08-087872-0.00302-4.

[246] Hoff TE, Perez R, Kleissl J, Renne D, Stein J. Reporting of irradiance modeling relative prediction errors. Progress in Photovoltaics: Research and Applications 2013;21:1514–9. https://doi.org/10.1002/pip.2225.

[247] Demain C, Journée M, Bertrand C. Evaluation of different models to estimate the global solar radiation on inclined surfaces. Renew Energy 2013;50:710–21. https://doi.org/10.1016/j.renene.2012.07.031.

[248] Mcevoy A, Markvart T, Castaner L. Practical Handbook of Photovoltaics: Fundamentals and Applications. Elsevier Science & Technology, London; 2011.

[249] Soulayman S. Comments on solar azimuth angle. Renew Energy 2018;123:294–300. https://doi.org/10.1016/j.renene.2018.02.063.

[250] Liu BYH, Jordan RC. The long-term average performance of flat-plate solar-energy collectors. Solar Energy 1963;7:53–74. https://doi.org/10.1016/0038-092x(63)90006-9.

[251] Gul M, Kotak Y, Muneer T, Ivanova S. Enhancement of albedo for solar energy gain with particular emphasis on overcast skies. Energies (Basel) 2018;11:1–17. https://doi.org/10.3390/en11112881.

[252] Demain C, Journée M, Bertrand C. Evaluation of different models to estimate the global solar radiation on inclined surfaces. Renew Energy 2013;50:710–21. https://doi.org/10.1016/j.renene.2012.07.031.

[253] Shukla KN, Rangnekar S, Sudhakar K. Comparative study of isotropic and anisotropic sky models to estimate solar radiation incident on tilted surface: A case study for Bhopal, India. Energy Reports 2015;1:96–103. https://doi.org/10.1016/j.egyr.2015.03.003.

[254] Noorian AM, Moradi I, Kamali GA. Evaluation of 12 models to estimate hourly diffuse irradiation on inclined surfaces. Renew Energy 2008;33:1406–12. https://doi.org/10.1016/j.renene.2007.06.027.

[255] Reindl DT, Beckman WA, Duffie JA. Evaluation of hourly tilted surface radiation models. Solar Energy 1990;45:9–17. https://doi.org/10.1016/0038-092X(90)90061-G.

[256] El-Sebaii AA, Al-Hazmi FS, Al-Ghamdi AA, Yaghmour SJ. Global, direct and diffuse solar radiation on horizontal and tilted surfaces in Jeddah, Saudi Arabia. Appl Energy 2010;87:568–76. https://doi.org/10.1016/j.apenergy.2009.06.032.

[257] Hay JE. Calculation of monthly mean solar radiation for horizontal and inclined surfaces. Solar Energy 1979;23:301–7. https://doi.org/10.1016/0038-092X(79)90123-3.

[258] Willmott CJ. On the climatic optimization of the tilt and azimuth of flat-plate solar collectors. Solar Energy 1982;28:205–16. https://doi.org/10.1016/0038-092X(82)90159-1.

[259] Appelbaum J, Massalha Y, Aronescu A. Corrections to anisotropic diffuse radiation model. Solar Energy 2019;193:523–8. https://doi.org/10.1016/j.solener.2019.09.090.

[260] Ghaleb B, Asif M. Application of solar PV in commercial buildings: Utilizability of rooftops. Energy Build 2022;257. https://doi.org/10.1016/j.enbuild.2021.111774.

[261] Ofgem. Smart Export Guarantee: Guidance for Generators. 2019.

[262] BEIS. The future for small-scale low-carbon generation. 2019.

[263] BEIS. Greenhouse gas reporting: conversion factors 2020 2020.

[264] SunWatts. PV panel and inverter price 2021. https://sunwatts.com/ (accessed May 11, 2021).

[265] GreenMatch. Installation Cost of Solar Panels (2021) 2021. https://www.greenmatch.co.uk/blog/2014/08/what-is-the-installation-cost-for-solar-panels (accessed May 11, 2021).

[266] The eco experts. Solar Panel Cleaning 2020. https://www.theecoexperts.co.uk/solar-panels/cleaning (accessed May 11, 2021).

[267] Solar-Wind.co.uk. Solar PV Panel Mounting Frames 2021. https://www.solar-wind.co.uk/solar-pv-panel-mounting-support-frameworks-brackets (accessed May 11, 2021).

[268] Harari D. Economic update: Ukraine crisis adds to inflationary pressures. House of Commons Library 2022.

[269] Kanchev H, Colas F, Lazarov V, Francois B. Emission reduction and economical optimization of an urban microgrid operation including dispatched PV-based active generators. IEEE Trans Sustain Energy 2014;5:1397–405. https://doi.org/10.1109/TSTE.2014.2331712.

[270] Solanki B V., Bhattacharya K, Canizares CA. A Sustainable Energy Management System for Isolated Microgrids. IEEE Trans Sustain Energy 2017;8:1507–17. https://doi.org/10.1109/TSTE.2017.2692754.

[271] Taha MS, Abdeltawab HH, Mohamed YARI. An online energy management system for a grid-connected hybrid energy source. IEEE J Emerg Sel Top Power Electron 2018;6:2015–30. https://doi.org/10.1109/JESTPE.2018.2828803.

[272] Zhang N, Hu Z, Dai D, Dang S, Yao M, Zhou Y. Unit commitment model in smart grid environment considering carbon emissions trading. IEEE Trans Smart Grid 2016;7:420–7. https://doi.org/10.1109/TSG.2015.2401337.

[273] Tziovani L, Hadjidemetriou L, Kolios P, Astolfi A, Kyriakides E, Timotheou S. Energy Management and Control of Photovoltaic and Storage Systems in Active Distribution Grids. IEEE Transactions on Power Systems 2022;37:1956–68. https://doi.org/10.1109/TPWRS.2021.3118785.

[274] Chakir A, Tabaa M, Moutaouakkil F, Medromi H, Julien-Salame M, Dandache A, et al. Optimal energy management for a grid connected PV-battery system. Energy Reports, vol. 6, 2020, p. 218–31. https://doi.org/10.1016/j.egyr.2019.10.040.

[275] Iliadis P, Ntomalis S, Atsonios K, Nesiadis A, Nikolopoulos N, Grammelis P. Energy management and techno-economic assessment of a predictive battery storage system applying a load levelling operational strategy in island systems. Int J Energy Res 2021;45:2709–27. https://doi.org/10.1002/er.5963.

[276] Ahmad Khan A, Naeem M, Iqbal M, Qaisar S, Anpalagan A. A compendium of optimization objectives, constraints, tools and algorithms for energy management in

microgrids. Renewable and Sustainable Energy Reviews 2016;58:1664–83. https://doi.org/10.1016/j.rser.2015.12.259.

[277] Ul Ain Binte Wasif Ali J, Kazmi SAA, Altamimi A, Khan ZA, Alrumayh O, Mahad Malik M. Smart Energy Management in Virtual Power Plant Paradigm with a New Improved Multilevel Optimization Based Approach. IEEE Access 2022;10:50062–77. https://doi.org/10.1109/ACCESS.2022.3169707.

[278] Byrne RH, Nguyen TA, Copp DA, Chalamala BR, Gyuk I. Energy Management and Optimization Methods for Grid Energy Storage Systems. IEEE Access 2017;6:13231–60. https://doi.org/10.1109/ACCESS.2017.2741578.

[279] Rosewater DM, Copp DA, Nguyen TA, Byrne RH, Santoso S. Battery Energy Storage Models for Optimal Control. IEEE Access 2019;7:178357–91. https://doi.org/10.1109/ACCESS.2019.2957698.

[280] Carli R, Dotoli M, Jantzen J, Kristensen M, Ben Othman S. Energy scheduling of a smart microgrid with shared photovoltaic panels and storage: The case of the Ballen marina in Samsø. Energy 2020;198:117188. https://doi.org/10.1016/j.energy.2020.117188.

[281] Babacan O, Ratnam EL, Disfani VR, Kleissl J. Distributed energy storage system scheduling considering tariff structure, energy arbitrage and solar PV penetration. Appl Energy 2017;205:1384–93. https://doi.org/10.1016/j.apenergy.2017.08.025.

[282] Puranen P, Kosonen A, Ahola J. Technical feasibility evaluation of a solar PV based off-grid domestic energy system with battery and hydrogen energy storage in northern climates. Solar Energy 2021;213:246–59. https://doi.org/10.1016/j.solener.2020.10.089.

[283] Berrueta A, Soto A, Marcos J, De La Parra I, Sanchis P, Ursua A. Identification of Critical Parameters for the Design of Energy Management Algorithms for Li-Ion Batteries Operating in PV Power Plants. IEEE Trans Ind Appl 2020;56:4670–8. https://doi.org/10.1109/TIA.2020.3003562.

[284] Chakir A, Tabaa M, Moutaouakkil F, Medromi H, Alami K. Smart multi-level energy management algorithm for grid-connected hybrid renewable energy systems in a micro-

grid context. Journal of Renewable and Sustainable Energy 2020;12:55301. https://doi.org/10.1063/5.0015639.

[285] Chapaloglou S, Nesiadis A, Iliadis P, Atsonios K, Nikolopoulos N, Grammelis P, et al. Smart energy management algorithm for load smoothing and peak shaving based on load forecasting of an island's power system. Appl Energy 2019;238:627–42. https://doi.org/10.1016/j.apenergy.2019.01.102.

[286] Mbungu NT, Bansal RC, Naidoo R, Miranda V, Bipath M. An optimal energy management system for a commercial building with renewable energy generation under real-time electricity prices. Sustain Cities Soc 2018;41:392–404. https://doi.org/10.1016/j.scs.2018.05.049.

[287] Tiemann PH, Bensmann A, Stuke V, Hanke-Rauschenbach R. Electrical energy storage for industrial grid fee reduction – A large scale analysis. Energy Convers Manag 2020;208:112539. https://doi.org/10.1016/j.enconman.2020.112539.

[288] Sepúlveda-Mora SB, Hegedus S. Making the case for time-of-use electric rates to boost the value of battery storage in commercial buildings with grid connected PV systems. Energy 2021;218:119447. https://doi.org/10.1016/j.energy.2020.119447.

[289] McLaren J, Laws N, Anderson K, DiOrio N, Miller H. Solar-plus-storage economics: What works where, and why? Electricity Journal 2019;32:28–46. https://doi.org/10.1016/j.tej.2019.01.006.

[290] Bukar AL, Tan CW, Yiew LK, Ayop R, Tan WS. A rule-based energy management scheme for long-term optimal capacity planning of grid-independent microgrid optimized by multi-objective grasshopper optimization algorithm. Energy Convers Manag 2020;221:113161. https://doi.org/10.1016/j.enconman.2020.113161.

[291] Coraddu A, Gil A, Akhmetov B, Yang L, Romagnoli A, Ritari A, et al. Energy storage on ships. Sustainable Energy Systems on Ships: Novel Technologies for Low Carbon Shipping, Elsevier; 2022, p. 197–232. https://doi.org/10.1016/B978-0-12-824471-5.00012-8.

[292] Arfeen ZA, Abdullah MP, Sheikh UU, Siddique A, Raheem A, Kausar M. Efficient energy flow criteria of hybrid solar battery packs grid for electric vehicle rapid-charging

facility. International Journal of Ambient Energy 2023. https://doi.org/10.1080/01430750.2022.2162963.

[293] Jafari M, Malekjamshidi Z. Optimal energy management of a residential-based hybrid renewable energy system using rule-based real-time control and 2D dynamic programming optimization method. Renew Energy 2020;146:254–66. https://doi.org/10.1016/j.renene.2019.06.123.

[294] Luthander R, Widén J, Nilsson D, Palm J. Photovoltaic self-consumption in buildings: A review. Appl Energy 2015;142:80–94. https://doi.org/10.1016/j.apenergy.2014.12.028.

[295] BEIS. Gas and electricity prices in the non-domestic sector - GOV.UK 2022. https://www.gov.uk/government/statistical-data-sets/gas-and-electricity-prices-in-the-non-domestic-sector (accessed June 1, 2022).

[296] Bolton P, Stewart I. Domestic energy prices- House of Commons. 2022.

[297] Ofgem. Latest energy price cap announced by Ofgem | Ofgem 2022. https://www.ofgem.gov.uk/publications/latest-energy-price-cap-announced-ofgem (accessed January 11, 2023).

[298] Nord Pool. Market Data | Nord Pool UK 2022. https://www.nordpoolgroup.com/en/ (accessed June 1, 2022).

[299] Western Power Distribution. Western Power Distribution - Charging Statements 2022. https://www.westernpower.co.uk/our-network/use-of-system-charges/charging-statements (accessed June 1, 2022).

[300] Cole W, Frazier AW, Augistine C. Cost Projections for Utility-Scale Battery Storage: 2021 Update. 2021.

[301] Kebede AA, Kalogiannis T, Van Mierlo J, Berecibar M. A comprehensive review of stationary energy storage devices for large scale renewable energy sources grid integration. Renewable and Sustainable Energy Reviews 2022;159. https://doi.org/10.1016/j.rser.2022.112213.

[302] Vignesh Ramasamy, David Feldman, Jal Desai, Robert Margolis. U.S. Solar Photovoltaic System and Energy Storage Cost Benchmarks: Q1 2021. 2021.

[303] British Gas. Smart Export Guarantee | British Gas 2023. https://www.britishgas.co.uk/energy/smart-export-guarantee.html (accessed June 29, 2023).

[304] Octopus energy. Smart Export Guarantee | Octopus Energy 2023. https://octopus.energy/smart/smart-export-guarantee/ (accessed June 29, 2023).

[305] Scottish Power. Smart Export Guarantee | ScottishPower 2022. https://www.scottishpower.co.uk/smart-export-guarantee (accessed June 29, 2023).

[306] BEIS. Greenhouse gas reporting: conversion factors 2022 - GOV.UK. Conversion Factors 2021: Full Set (for Advanced Users) 2022:1. https://www.gov.uk/government/publications/greenhouse-gas-reporting-conversion-factors-2022 (accessed November 20, 2022).

[307] Gailani A, Al-Greer M, Short M, Crosbie T. Degradation cost analysis of Li-Ion batteries in the capacity market with different degradation models. Electronics (Switzerland) 2020;9. https://doi.org/10.3390/electronics9010090.

[308] García-Miguel PLC, Alonso-Martínez J, Arnaltes Gómez S, García Plaza M, Asensio AP. A Review on the Degradation Implementation for the Operation of Battery Energy Storage Systems. Batteries 2022;8. https://doi.org/10.3390/batteries8090110.

[309] Kichou S, Markvart T, Wolf P, Silvestre S, Chouder A. A simple and effective methodology for sizing electrical energy storage (EES) systems based on energy balance. J Energy Storage 2022;49:104085. https://doi.org/10.1016/j.est.2022.104085.

[310] Zhu K, Li X, Campana PE, Li H, Yan J. Techno-economic feasibility of integrating energy storage systems in refrigerated warehouses. Appl Energy 2018;216:348–57. https://doi.org/10.1016/j.apenergy.2018.01.079.

[311] BEIS. Electricity generation costs 2020. 2020.

[312] Zhao R, Stincescu T, Ballantyne EEF, Stone DA. Sustainable city: Energy usage prediction method for electrified refuse collection vehicles. Smart Cities 2020;3:1100–16. https://doi.org/10.3390/smartcities3030054.

[313] Gao Z, Lin Z, Davis SC, Birky AK. Quantitative evaluation of MD/HD vehicle electrification using statistical data. Transp Res Rec 2018;2672:109–21. https://doi.org/10.1177/0361198118792329/FORMAT/EPUB.

[314] Energy UK. Connecting Your Fleet: A guide for businesses in Greater London. 2020.

9 Appendix A

This appendix includes the full cost analysis tables from Chapter 4.

Table 9.1. System cost at different battery capacities for the WMD.

Power connection capacity (MW)	BESS capacity (MWh)	Cost of energy per year (£)	Surplus solar energy revenue per year (£)	BESS capital cost (£)	BESS O&M cost (£)	PV capital cost (£)	PV O&M cost (£)	Network cost per year (£)	Total cost over system lifetime (mil£)
0.15	NO BESS	112,389	0	0	0	0	0	5,234	1.76
	0.05	59,317	11,127	12,700	1,875	629,100	135,282	3,963	1.56
	0.1	54,496	10,574	25,400	3,750			3,788	1.51
	0.5	38,498	8,375	127,000	18,750			3,665	1.42
	1	37,568	8,270	254,000	37,500			3,661	1.55
	5	36,154	8,104	1,270,000	187,500			3,649	2.70
	10	34,487	7,909	2,540,000	375,000			3,612	4.13

Table 9.2 Network costs itemised at different battery capacities for the WMD.

Power connection capacity (MW)	BESS capacity (MWh)	Capacity charge per year (£)	Excess capacity charge per year (£)	Fixed charge per year (£)	Consumption charge per year (£)			Total Network cost per year (£)
					Red	Amber	Green	
0.15	NO BESS	1,770	0	1,084	1463	872	44	5,234
	0.05				803	265	40	3,963
	0.1				655	240	39	3,788
	0.5				579	211	20	3,665
	1				579	208	19	3,661
	5				574	202	18	3,649
	10				545	195	17	3,612

Table 9.3. System cost at different power connection capacity for the WMD.

Power connection capacity (MW)	BESS capacity (MWh)	Cost of energy per year (£)	Surplus solar energy revenue per year (£)	BESS capital cost (£)	BESS O&M cost (£)	PV capital cost (£)	PV O&M cost (£)	Network cost per year (£)	Total cost over system lifetime (mil£)
0.075	NO BESS	112,389	0	0	0	0	0	4,367	1.75
	0.05	59,317	11,127	12,700	1,875	629,100	135,282	3,081	1.55
	0.1	54,496	10,574	25,400	3,750			2,907	1.50
	0.5	38,498	8,375	127,000	18,750			2,784	1.40
	1	37,568	8,270	254,000	37,500			2,780	1.54
	5	36,154	8,104	1,270,000	187,500			2,768	2.68
	10	34,487	7,909	2,540,000	375,000			2,730	4.12
0.05	NO BESS	112,389	0	0	0	0	0	4,438	1.75
	0.05	59,317	11,127	12,700	1,875	629,100	135,282	2,855	1.54
	0.1	54,496	10,574	25,400	3,750			2,681	1.49
	0.5	38,498	8,375	127,000	18,750			2,558	1.40
	1	37,568	8,270	254,000	37,500			2,554	1.53
	5	36,154	8,104	1,270,000	187,500			2,542	2.68
	10	34,487	7,909	2,540,000	375,000			2,504	4.12
0.025	NO BESS	112,389	0	0	0	0	0	7,090	1.79
	0.05	59,317	11,127	12,700	1,875	629,100	135,282	3,870	1.56
	0.1	54,496	10,574	25,400	3,750			3,677	1.51
	0.5	38,498	8,375	127,000	18,750			3,442	1.41
	1	37,568	8,270	254,000	37,500			3,413	1.55
	5	36,154	8,104	1,270,000	187,500			3,373	2.69
	10	34,487	7,909	2,540,000	375,000			3,297	4.13

Table 9.4. System cost for M&S retail store.

Power connection capacity (MW)	BESS capacity (MWh)	Cost of energy (£) per year	Surplus solar energy revenue (£) per year	BESS capital cost (£)	BESS O&M cost (£)	PV capital cost (£)	PV O&M cost (£)	Network cost (£) per year	Total cost (mil£) over system lifetime
0.4	NO BESS	164,519	0	0	0	853,200	183,472	41,404	3.09
	0.05	114,740	637	12,700	1,875			38,233	3.34
	0.1	114,285	588	25,400	3,750			38,174	3.34
	0.5	111,372	569	127,000	18,750			37,322	3.40
	1	107,777	569	254,000	37,500			35,702	3.47
	5	96,421	547	1,270,000	187,500			28,022	4.35
	10	96,295	527	2,540,000	375,000			28,000	5.81

Table 9.5. System cost at different $Power_{capacity}$.

Power connection capacity (MW)	BESS capacity (MWh)	Cost of energy per year (£)	Surplus solar energy revenue per year (£)	BESS capital cost (£)	BESS O&M cost (£)	PV capital cost (£)	PV O&M cost (£)	Network cost per year (£)	Total cost over system lifetime (mil£)
0.3	NO BESS	164,519	0	0	0	0	0	39,775	3.06
	0.05	114,740	637	12,700	1,875	853,000	183,472	36,437	3.31
	0.1	114,285	588	25,400	3,750			36,378	3.32
	0.5	111,372	569	127,000	18,750			35,525	3.38
	1	107,777	569	254,000	37,500			33,906	3.44
	5	101,243	177	1,270,000	187,500			30,831	4.47
	10	100,910	53	2,540,000	375,000			30,778	5.93
0.2	NO BESS	164,519	0	0	0	0	0	50,678	3.23
	0.05	114,740	637	12,700	1,875	853,000	183,472	37,230	3.32
	0.1	114,285	588	25,400	3,750			37,171	3.33
	0.5	111,404	568	127,000	18,750			36,267	3.39
	1	109,189	508	254,000	37,500			35,009	3.48
	5	108,132	0	1,270,000	187,500			34,864	4.64
	10	108,132	0	2,540,000	375,000			34,864	6.10
0.1	NO BESS	164,519	0	0	0	0	0	86,201	3.76
	0.05	115,005	634	12,700	1,875	853,000	183,472	58,588	3.65
	0.1	114,829	569	25,400	3,750			58,550	3.66
	0.5	114,020	170	127,000	18,750			58,168	3.76
	1	113,733	22	254,000	37,500			58,067	3.90
	5	113,691	0	1,270,000	187,500			58,054	5.07
	10	113,691	0	2,540,000	375,000			58,054	6.53

10 Appendix B

This appendix includes the full cost analysis tables from Chapter 6.

Table 10.1. "System cost at different battery capacities (C_{BESS}) for scenario 1 and scenario 2" (Table obtained from [175])..

Power connection capacity (MW)	Scenarios		Cost of energy per year (£)	Surplus solar energy revenue per year (£)	BESS capital cost (£)	BESS O&M cost (£)	PV capital cost (£)	PV O&M cost (£)	Network cost over the system lifetime (£)	Total cost over system lifetime (mil£)
0.6		Scenario1	460,405	0	0	0	0	0	222,443	7.13
	Scenario 2 (MWh)	0.05	407,211	11,111	12,700	1,875	629,100	135,282	203,362	6.92
		0.1	402,385	10,558	25,400	3,750			200,510	6.87
		0.5	379,530	7,332	127,000	18,750			194,168	6.69
		1	361,592	4,719	254,000	37,500			191,882	6.60
		5	329,997	76	1,270,000	187,500			191,205	7.36
		10	329,479	0	2,540,000	375,000			191,194	8.81

Table 10.2. "System cost for scenario 1 and scenario 3 (with a BESS of 10 MWh)" (Table obtained from [175]).

Power connection capacity (MW)	Scenarios		Cost of energy per year (£)	Surplus solar energy revenue per year (£)	BESS capital cost (£)	BESS O&M cost (£)	PV capital cost (£)	PV O&M cost (£)	Network cost over the system lifetime (£)	Total cost over system lifetime (mil£)
0.15		Scenario1	460,405	0	0	0	0	0	908,840	7.81
	Scenario 3 (MWh)	5	421,791	2,098	1,270,000	187,500	629,100	135,282	231,878	8.75
		10	427,450	1,790	2,540,000	375,000			167,849	10.23